



UNIL | Université de Lausanne

Unicentre

CH-1015 Lausanne

<http://serval.unil.ch>

Year : 2020

Post-transcriptional mechanisms that regulate cancer stem cell maintenance

Waszyk Patricia

Waszyk Patricia, 2020, Post-transcriptional mechanisms that regulate cancer stem cell maintenance

Originally published at : Thesis, University of Lausanne

Posted at the University of Lausanne Open Archive <http://serval.unil.ch>

Document URN : urn:nbn:ch:serval-BIB_B423B55B9DEF5

Droits d'auteur

L'Université de Lausanne attire expressément l'attention des utilisateurs sur le fait que tous les documents publiés dans l'Archive SERVAL sont protégés par le droit d'auteur, conformément à la loi fédérale sur le droit d'auteur et les droits voisins (LDA). A ce titre, il est indispensable d'obtenir le consentement préalable de l'auteur et/ou de l'éditeur avant toute utilisation d'une oeuvre ou d'une partie d'une oeuvre ne relevant pas d'une utilisation à des fins personnelles au sens de la LDA (art. 19, al. 1 lettre a). A défaut, tout contrevenant s'expose aux sanctions prévues par cette loi. Nous déclinons toute responsabilité en la matière.

Copyright

The University of Lausanne expressly draws the attention of users to the fact that all documents published in the SERVAL Archive are protected by copyright in accordance with federal law on copyright and similar rights (LDA). Accordingly it is indispensable to obtain prior consent from the author and/or publisher before any use of a work or part of a work for purposes other than personal use within the meaning of LDA (art. 19, para. 1 letter a). Failure to do so will expose offenders to the sanctions laid down by this law. We accept no liability in this respect.



UNIL | Université de Lausanne

Faculté de biologie
et de médecine

Département de la Formation et de la Recherche

**Post-transcriptional mechanisms that regulate
cancer stem cell maintenance**

Thèse de doctorat en médecine et ès sciences (MD-PhD)

Présentée à la

Faculté de biologie et de médecine
de l'Université de Lausanne

par

Patricia WASZYK

Médecin diplômée de la Confédération Helvétique

Jury

Prof. Lorenz Hirt, président et répondant MD-PhD

Prof. Ivan Stamenkovic, directeur de thèse

Prof. Tatiana Petrova, experte

Prof. Andrea Superti-Furga, expert

Prof. Douglas Hanahan, expert

Lausanne 2020

Imprimatur

Vu le rapport présenté par le jury d'examen, composé de

Président·e	Monsieur Prof. Lorenz	Hirt
Directeur·trice de thèse	Monsieur Prof. Ivan	Stamenkovic
Répondant·e	Monsieur Prof. Lorenz	Hirt
Expert·e·s	Madame Prof. Tatiana	Petrova
	Monsieur Prof. Andrea	Superti-Furga
	Monsieur Prof. Douglas	Hanahan

le Conseil de Faculté autorise l'impression de la thèse de

Madame Patricia WASZYK

Maîtrise universitaire en médecine Université de lausanne

intitulée

**Post-transcriptional mechanisms that regulate
cancer stem cell maintenance**

Lausanne, le 20 mars 2020

pour Le Doyen
de la Faculté de biologie et de médecine



Prof. John PRIOR
Vice-Director of the Doctoral School

Contents

Summary	5
Résumé	7
List of Abbreviations	11
List of Figures	13
List of Tables	15
1 Introduction	17
1.1 Cancer: definition and hallmarks	18
1.2 Tumor heterogeneity	20
1.2.1 The stochastic and cancer stem cell models	20
1.2.2 CSC plasticity	23
1.2.3 The role of the CSC niche	25
1.2.4 CSC resistance to therapy	26
1.3 Epigenetic regulation of cellular plasticity	28
1.3.1 MicroRNAs	30
1.3.2 Long non-coding RNAs	33
1.4 RNA binding proteins	36
1.4.1 The LIN28 paralogs	38
1.4.2 The IMP family of RBPs	41
1.5 Aim of the study	45

2	Glioblastoma	47
2.1	Introduction	47
2.1.1	Characteristics of GBM	47
2.1.2	Glioma stem cells	49
2.1.3	GBM heterogeneity	50
2.1.4	The GBM cell of origin	54
2.1.5	<i>In vivo</i> models of GBM	54
2.1.6	Non-coding RNAs in GBM	56
2.2	Targeting glioma stem cells using a small molecule	58
2.2.1	Background	58
2.2.2	Results	59
2.2.3	Discussion	65
2.3	The role of long-non-coding RNA H19 in GBM	67
2.3.1	Background	67
2.3.2	Results	69
2.3.3	Discussion	74
2.4	Materials and Methods	78
3	Ewing Sarcoma	85
3.1	Introduction	85
3.1.1	Pediatric malignancies: a challenging field	85
3.1.2	Sarcomas: a heterogeneous group of tumors	88
3.1.3	Ewing sarcoma clinical presentation and diagnosis	90
3.1.4	The fusion protein EWS-FLI1	91
3.1.5	EWS-FLI1 and tumorigenesis of EwS	94
3.1.6	The cell of origin of EwS	96
3.1.7	<i>In vivo</i> models of EwS	97
3.2	LIN28 and IMP RNA-binding proteins in EwS	98
3.3	Results	101
3.4	Discussion and future perspectives	109
3.5	Materials and Methods	115

<i>CONTENTS</i>	3
4 Conclusion	121
5 Supplementary Material	127
5.1 Glioblastoma	127
5.2 Ewing Sarcoma	130
6 Publications	133
1 Manuscript I: LIN28B control of EWS-FLI1 stability	133
2 Manuscript II: Targeting Haspin for cancer therapy	135
Acknowledgements	137
References	139

Summary

Within a tumor, a subpopulation of cells, namely the cancer stem cells (CSCs), can self-renew, generate more differentiated progeny, and replicate the tumor of origin *in vivo*, thereby sustaining and promoting tumor growth. Importantly, these cells are often quiescent and resistant to treatment, so that efforts should be put into finding novel ways to target CSCs to improve patient survival. While genetic mutations participate in creating a CSC phenotype, epigenetic mechanisms play an equally important role in transformation. Among these, microRNAs (miRNAs) and long non-coding RNAs (lncRNAs) modulate the expression of a large network of genes.

Let-7 miRNAs induce differentiation, but are often repressed in cancer. Here, we attempted to enhance miRNA maturation and restore their function in glioblastoma (GBM), a highly aggressive primary brain malignancy with an exceedingly poor prognosis, using the small molecule enoxacin, which has been shown to stimulate miRNA maturation in other settings. We injected primary patient-derived GBM cells in mice and treated them with enoxacin and temozolomide (an alkylating agent used in GBM treatment), alone or in combination. Enoxacin did not impair tumor formation, suggesting that miRNA maturation cannot be further stimulated in GBM. Subsequently, we looked at lncRNAs expressed in GBM that may be involved in CSC maintenance and focused on H19. Expression of H19 correlated with poor patient outcome, and H19 binds IMP2, an RNA-binding protein (RBP) essential for CSC maintenance in GBM. Although we could not reach clear conclusions as to its role in GBM due to technical issues, we believe that H19 may be involved in GBM tumorigenesis, and its function requires further investigation.

In addition to non-coding RNAs, RBPs are essential regulators of gene expression, as they are involved in every step of mRNA life. Among RBPs involved in cancer, LIN28B, an oncofetal RBP that inhibits let-7 maturation, is necessary for CSC survival in a subset of highly aggressive Ewing sarcomas (EwS). EwS is the second most common primary bone cancer in children and adolescents, and harbors the t(11;22) translocation leading to the chimeric transcription factor EWS-FLI1. Of note, LIN28B stabilizes EWS-FLI1 transcripts, and mediates CSC maintenance. We explored the biological relevance of IMPs for EwS CSCs. IMPs are RBPs known to inhibit the let-7 pathway. However, silencing IMP paralogs failed to affect CSC tumorigenicity. Therefore, our results further support the role of LIN28B for CSC maintenance. Because LIN28B affects translation of targets, we will further investigate the role of LIN28B in EwS by comparing whole

RNA and proteomic data of LIN28B⁺ EwS. In doing so, we will identify pathways regulated by LIN28B independently of let-7 and EWS-FLI1, that increase the aggressiveness of a subset of EwS. Moreover, these pathways may be applicable to other LIN28B⁺ childhood cancers driven by a fusion protein.

Résumé

Dans une tumeur, les cellules souches cancéreuses (CSC) sont capables de se renouveler, générer des cellules plus différenciées, et répliquer la tumeur d'origine *in vivo*. Ces cellules sont notamment souvent quiescentes et résistantes aux traitements, faisant d'une priorité l'identification de nouvelles méthodes pour cibler les CSC afin d'augmenter la survie du patient. Alors que les mutations génétiques favorisent l'acquisition d'un phénotype de CSC, les mécanismes épigénétiques jouent un rôle tout aussi prépondérant dans la transformation tumorale. Parmi eux, les microARN (miRNA) et longs ARN non-codants (long non-coding RNAs, lncRNA) peuvent influencer l'expression d'un vaste réseau de gènes.

Les miRNA let-7 sont exprimés dans les cellules différenciées mais sont souvent réprimés dans les cancers. Ici, nous avons tenté d'accroître leur expression et rétablir leurs fonctions dans le glioblastome (GBM), une tumeur primaire cérébrale hautement agressive, en utilisant la molécule d'énoxacine qui stimule la maturation de miRNA. Nous avons injecté des organoïdes de GBM dérivés de tumeurs de patients dans des souris que nous avons traitées avec l'énoxacine et/ou du temozolomide (l'agent de chimiothérapie couramment utilisé pour le traitement des GBM), seuls ou en combinaison. L'énoxacine n'a pas diminué la formation de tumeurs, suggérant que la maturation de miRNA ne peut pas être stimulée dans les GBM. Nous avons donc cherché les lncRNA exprimés dans les GBM qui pourraient être impliqués dans le maintien des CSC. Nous avons identifié H19, dont l'expression corrèle avec un mauvais pronostic. H19 peut se lier à IMP2, une protéine liant les ARN (RNA-binding proteins, RBP) essentielle au maintien des CSC dans les GBM. Bien que nous n'ayons pas pu atteindre de conclusions en raison de difficultés techniques, il semble que H19 soit impliqué dans la tumorigénèse des GBM, et sa fonction dans ce contexte mérite d'être explorée.

Les RBP sont des régulateurs essentiels de l'expression génique, car impliqués dans chaque étape de la vie de l'ARN messager. LIN28B, une RBP oncofoetale capable d'inhiber la maturation des miRNA let-7, est requise pour la survie des CSC dans une partie des sarcomes d'Ewing (SE), le deuxième cancer primaire de l'os le plus fréquent chez les enfants et adolescents, caractérisé par la translocation t(11;22), formant la protéine de fusion EWS-FLI1. Nous avons étudié le rôle de la famille de RBP IMP, comprenant trois paralogues partiellement redondants et capables de réprimer la cascade de signalisation des let-7. Le knockdown de chacun des trois IMPs n'a

pas réduit la tumorigenicité des CSC. Nos résultats renforcent donc la position de LIN28B pour le maintien des CSC. Sachant que LIN28B affecte la traduction d'ARN cibles, nous souhaitons investiguer son rôle dans le SE en comparant les données des ARN et du protéome totaux des SE LIN28B⁺. Ainsi, nous pourrions identifier des circuits régulés par LIN28B indépendamment des let-7 et d'EWS-FLI1 qui contribuent au phénotype agressif d'une partie des SE. De plus, ces circuits pourraient être impliqués dans d'autres cancers pédiatriques LIN28B⁺ présentant une protéine de fusion.

List of Abbreviations

ABC	ATP binding cassette
Akt	AKT serine/threonine kinase 1
ALL	acute lymphoblastic leukemia
ANOVA	analysis of variance
ATA	amino terminal transactivation domain
BBB	blood brain barrier
bFGF	basic fibroblast growth factor
c-MYC	MYC proto-oncogene
C/EBP-β	CCAAT/enhancer binding protein β
Cas9	CRISPR-associated endonuclease 9
CCS	clear cell sarcoma of soft tissue
ChIP-seq	chromatin immunoprecipitation sequencing
ChIRP-seq	chromatin isolation by RNA purification sequencing
CLIP-seq	UV crosslinking and immunoprecipitation sequencing
CLL	chronic lymphoblastic leukemia
CML	chronic myeloid leukemia
CRISPR	clustered regularly interspaced short palindromic repeats
CRISPRi	CRISPR-intermediated interference
CSC	cancer stem cell
CSD	cold shock domain
DMSO	dimethyl sulfoxide
DSRCT	desmoplastic small round cell tumor
EGF	epidermal growth factor
EGFR	epidermal growth factor receptor
EMT	epithelial-to-mesenchymal transition
eRIC	enhanced RNA interactome capture
ESFT	Ewing sarcoma family of tumors
ETS	erythroblastosis transforming virus 1
EwS	Ewing sarcoma
EWSR1	Ewing sarcoma breakpoint region 1
EZH2	enhancer of zest homolog 2
FACS	fluorescence-activated cell sorting
FBS	fetal bovine serum
FISH	fluorescent <i>in situ</i> hybridization
FLI1	Friend leukemia virus integration 1 transcription factor
FLS	FLI1 specific domain
FUS	fused in sarcoma

GAPDH	glyceraldehyde 3-phosphate dehydrogenase
GBM	Glioblastoma Multiforme
gRNA	guide RNA
GSC	glioma stem cell
HIF	hypoxia inducible factor
HMGA	High Mobility Group AT-Hook
hpMSC	human pediatric mesenchymal stem cell
HSC	hematopoietic stem cell
IDH1	isocitrate dehydrogenase 1
IFN-1	type-I interferon
IGF1	insulin-like growth factor 1
IGF2	insulin-like growth factor 2
IGF2BP	IGF2 mRNA binding protein
iPSC	induced pluripotent stem cell
ITH	intratumoral heterogeneity
KH	K-homology
KLF4	Krüppel-like factor 4
KRAB	Krüppel associated box
LIN28B	Lin-28 homolog B
LIP	liver-enriched inhibitory protein
lncRNA	long non-coding RNA
MEF	mouse embryonic fibroblast
MET	mesenchymal-to-epithelial transition
MGMT	O ⁶ -methylguanine-DNA methyltransferase
miRNA	microRNA
MRE	miRNA recognition element
MRI	magnetic resonance imaging
mRNP	messenger ribonucleoparticle
MSC	mesenchymal stem cell
NANOG	Nanog homeobox
ncRNA	non-coding RNA
NCSC	neural crest stem cell
NHEJ	non-homologous end-joining
NSC	neural stem cell
OCT3/4	octamer-binding transcription factor 3-4
OLIG2	oligodendrocyte transcription factor 2
ORF	open reading frame
PAM	protospacer-adjacent motif
PAR-CLIP	photoactivatable ribonucleoside-enhanced crosslinking and immunoprecipitation
PBS	phosphate-buffered saline
PDX	patient-derived xenograft
PI3K	phosphoinositide 3-kinase
PNET	peripheral primitive neuroectodermal tumor
POU3F2	POU class 3 homeobox 2
PRC2	Polycomb repressive complex 2

Rb	retinoblastoma-associated protein
RBP	RNA binding protein
RHA	RNA helicase A
RIP	RNA immunoprecipitation
RISC	RNA-induced silencing complex
RNA Pol II	RNA polymerase II
RRM	RNA recognition motif
RRM2	ribonucleoside-diphosphate reductase subunit M2
rRNA	ribosomal RNA
RTK	receptor tyrosine kinase
SALL2	Spalt-like transcription factor 2
SD	standard deviation
SDS-PAGE	sodium dodecyl sulfate polyacrylamide gel electrophoresis
SOX2	SRY-Box transcription factor 2
SVZ	subventricular zone
TAF15	TATA-box associated transcription factor 15
TBP	TATA box binding protein
TBST	tris-buffered saline with Tween 20
TCGA	The Cancer Genome Atlas
TF	transcription factor
TGF-β	transforming growth factor beta
TLS	translocated in liposarcoma
TMZ	temozolomide
TRBP2	trans-activation responsive RNA-binding protein 2
tRNA	transfer RNA
TSS	transcription start site
VEGF	vascular endothelial growth factor
ZKD	zinc knuckle domain

List of Figures

Introduction	17
1.1 The Hallmarks of Cancer	19
1.2 Tumor heterogeneity and CSCs	21
1.3 The canonical miRNA biogenesis pathway	32
1.4 Representation of various functions of lncRNAs	35
1.5 RBPs are involved in mRNA fate	37
1.6 LIN28 structure and mechanisms of action	40
1.7 IMPs structure and mechanisms of action	43
Glioblastoma	47
2.1 Macroscopic and microscopic morphology of GBM	48
2.2 Genomic alterations underlying glioblastoma tumorigenesis	52
2.3 Gene expression and genomic alterations across the four glioblastoma subtypes	53
2.4 Dysregulated miRNAs and targeted pathways in GBM	57
2.5 Effects of enoxacin on GBM organoids <i>in vitro</i>	61
2.6 Experimental design for <i>in vivo</i> drug testing	62
2.7 Effects of enoxacin on primary GBM organoids <i>in vivo</i>	64
2.8 Toxicity of enoxacin <i>in vitro</i> in organoids versus adherent GBM-derived cells	65
2.9 The various mechanisms of action of H19	68
2.10 H19 is correlated with poor prognosis and is expressed in GSCs	71
2.11 H19 overexpression in MGH4S	73
2.12 Infection efficiency in 293T and in GBM samples	75

Ewing Sarcoma	85
3.1 Epidemiological and genome-wide data of childhood cancer	86
3.2 Recurrent translocations found in malignant sarcomas	88
3.3 Clinical presentation of Ewing sarcoma	91
3.4 Structural features of TET proteins and FLI1, and the EWS-FLI1 fusion protein	93
3.5 EWS-FLI1 modulates chromatin conformation and transcriptional profile in EwS	96
3.6 The roles of LIN28 and IMPs in EwS CSCs	101
3.7 IMP3 correlates with poor prognosis and high LIN28B expression	102
3.8 IMP expression and CRISPR-mediated knockdown	104
3.9 Effect of IMP downregulation on proliferation	105
3.10 IMP knockdown does not impair tumorigenicity <i>in vivo</i>	107
3.11 Combined knockdown of IMP2 and IMP3 in EwS1 organoids	108
3.12 LIN28B expression and knockdown in EwS cell lines	110
3.13 Identifying EWS-FLI1 independent genes regulated by LIN28B	113
Supplementary Material	127
S1.1 H19 overexpression in GBM cell lines	128
S2.1 Western blot of EwS2 xenografts	130

List of Tables

Ewing Sarcoma	85
3.1 Chromosomal translocations in sarcomas	89
Supplementary Material	127
S1.1 Properties of primary GBM samples	127
S1.2 Upregulated let-7 target genes in high H19 expression GBM	128
S1.3 Oligos used for CRISPRi genome editing	129
S2.1 Characteristics of Ewing sarcoma samples	130
S2.2 Oligos used for CRISPR-Cas9 genome editing	131
S2.3 List of primers used for qRT-PCR	132

Chapter 1

Introduction

Cancer is currently the second most common cause of death worldwide, and has recently replaced cardiovascular diseases as the first cause of death in high-income countries. The same is predicted to occur in middle- and low-income countries, as cancer may progressively become the leading cause of mortality worldwide during the next decades (Dagenais et al., 2019). Importantly, despite multimodal therapeutic approaches, considerable advances in patient management and the never-ending efforts in the field of research, cancer still bears a somber prognosis. Drastic improvement in patient survival for some forms of cancer over the last half-century remains overshadowed by other cancer types that invariably represent a death sentence for the patient at the moment of diagnosis. Thus, as the global cancer burden is increasing, much research is still warranted to better understand tumors, so that they can be better prevented, identified earlier, and treated more efficiently by adopting more specific and personalised therapeutic approaches.

Major advancements in cellular profiling during the last decades have provided extensive insight into the individual particularities of the cells composing the tumor bulk, and have shed light onto the extensive cellular plasticity within the tumor, as well as onto the role of cellular permissiveness for malignant transformation. Thus, increasing effort is being put into characterizing the regulatory pathways that shape the cell tumorigenicity.

In this context, the goal of my work was to identify, characterize, dissect and target the mechanisms that shape the cancerous cell to maintain and promote its malignant behavior.

The main body of this manuscript is divided into four chapters:

- 1) General introduction: first, we start by defining cancer and look into the different post-transcriptional epigenetic regulation mechanisms that are of particular interest in this work.
- 2) Part 1: here, we focus on Glioblastoma Multiforme (GBM), in which we introduce key aspects of this aggressive tumor and present the results and discussions from two projects that I worked on, focusing on targeting a key regulatory pathway in malignant cells, and on identifying a potential actor responsible for malignant transformation.
- 3) Part 2: this part focuses on Ewing sarcoma (EwS), after introducing some key points to consider in pediatric malignancies. The molecular pathology of this subclass of sarcomas is presented, followed by the results from the main project of this thesis, which is still ongoing, where I explored the roles of two families of RNA binding proteins in promoting and preserving cancer stem cells in EwS.
- 4) Conclusion: we finish by putting our findings in perspective and discussing future axes, based on the results from the previous chapters.

1.1 Cancer: definition and hallmarks

Cancer encompasses over a hundred highly complex and dynamic diseases that are unified by common denominative features. Indeed, a tumor can arise in most tissues, from virtually any cell type, and at any stage of life. This variable constellation of conditions will grant the tumor with particular traits, specific degrees of differentiation and a singular behavior based on when, where and how it develops. Accordingly, cell transformation in the epithelium, mesenchyme or bone marrow will lead to the development of carcinoma, sarcoma or hematologic malignancies, respectively.

Despite a large degree of heterogeneity, cancers display shared characteristics. The principle unifying cancer is rather straightforward and can be succinctly described as a cell escaping homeostatic regulation and developing in an uncontrolled manner. Following a succession of genetic alterations and epigenetic modifications, the transformed cell acquires proliferative advantage over neighboring cells, leading to the formation of a tumor mass that disrupts the societal rules of cells. The features developed by cancer cells to sustain tumor growth were first defined in

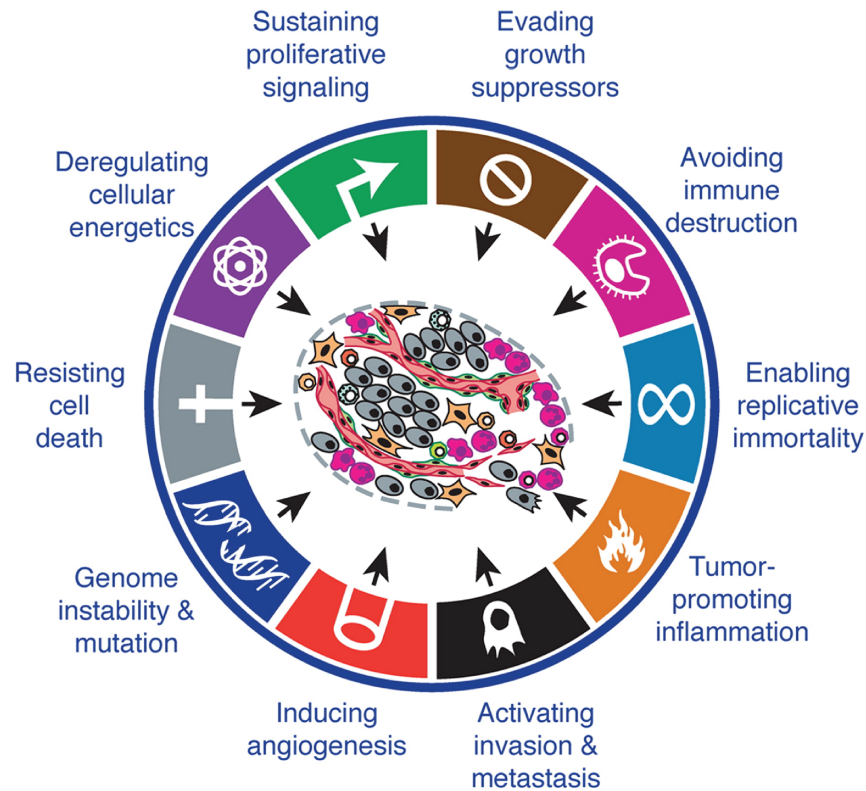


Figure 1.1: The Hallmarks of Cancer. Adapted from Hanahan and Weinberg (2011).

2000 and listed as the hallmarks of cancer (Hanahan and Weinberg, 2000), later expanded with the addition of two supplementary properties (Hanahan and Weinberg, 2011) (Figure 1.1).

Properties of cancer cells include: 1) sustaining proliferative growth; 2) evading growth suppressors; 3) avoiding immune destruction; 4) enabling replicative immortality; 5) stimulating tumor promoting inflammation; 6) activating invasion and metastasis; 7) inducing angiogenesis; 8) genome instability; 9) resisting cell death; 10) deregulating cellular genetics.

Taken together, these hallmarks define cancer as a unique entity capable of using the microenvironment to its advantage and constantly adapting to increase its chances of survival and propagation. Therefore, each of the hallmarks of cancer must be explored so that we become more familiar with the enemy and identify potential weaknesses in this complex system, requiring a detailed understanding of the crucial mechanisms behind tumor growth and maintenance of its driving force.

My research focused on identifying and understanding some of the regulators essential for cellular proliferation and survival, with the goal to find ways of targeting such mechanisms. More specifically, I concentrated my work on exploring ways of targeting the main driving force of the tumor, namely the cancer stem cells (CSCs). In the experimental applications presented,

I focused on some of the fundamental biological properties of CSCs: their proliferative potential, their capacity to form tumors *in vivo*, expression of stemness markers, and the role of epigenetic regulators that mediate CSC plasticity.

1.2 Tumor heterogeneity

1.2.1 The stochastic and cancer stem cell models

At first, tumors were thought to be made out of uniform and undifferentiated cells. However, about a century ago, it was noted that tumor histology is not homogeneous. Cells that constitute the tumor bulk are heterogeneous, and can be distinguished as diverse subpopulations with distinct proliferation kinetics, cell markers, genetic anomalies, therapeutic response and tumorigenic potential (Kreso and Dick, 2014). This led to the notion that one of the subpopulations may provide the driving force of the tumor and possibly give rise to the other subpopulations. Two models have since been suggested to explain the heterogeneity observed within a tumor.

First, the stochastic model proposes that an initial tumor cell can give rise to a progeny after a first oncogenic event. This event creates genetic instability, resulting in the accumulation of additional mutations over time. Some mutations may provide no survival advantage, causing the cells to die, while others may confer cells with selective advantage. As a result, this cell subpopulation takes over and becomes the dominant clone within the tumor. This leads to the development of a bulk of heterogeneously mutated cells, some of which become increasingly aggressive and preserve tumor initiating capacity (Nowell, 1976). Intrinsic (genetic instability and epigenetic changes) as well as extrinsic (immune and environmental) factors all contribute to ongoing stochastic cellular changes, thereby erasing any possible hierarchical structure within the tumor (Figure 1.2 A, left panel).

However, this concept was challenged a little over 20 years ago with the emergence of the CSC theory, first evidenced in leukemias (Bonnet and Dick, 1997) and subsequently in solid tumors, including breast (Al-Hajj et al., 2003), brain (Singh et al., 2003), colon (O'Brien et al., 2007) and sarcoma (Wu et al., 2007; Suvà et al., 2009), among others. New evidence supported the notion that a tumor initiating cell acquires self-renewal capacity through genetic mutations and epigenetic modifications, which provide it with the ability to maintain the tumor source indefinitely (Figure 1.2 A, right panel). Similar to normal embryonic stem cells that self-renew and generate a differentiated progeny within a normal tissue through asymmetrical division, CSCs

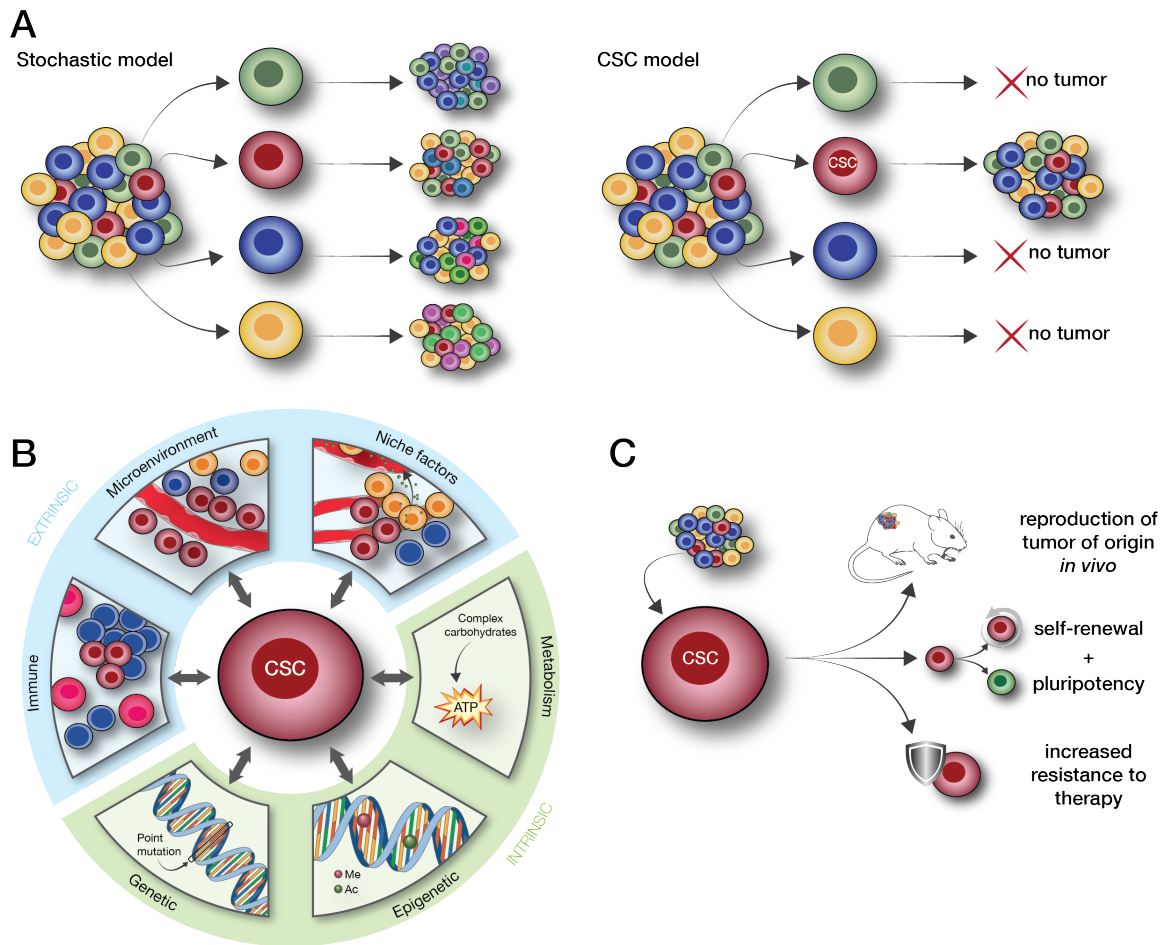


Figure 1.2: Tumor heterogeneity and CSCs. (A) *Left*, the stochastic model: each cell within the tumor bulk can reproduce a tumor following genomic instability and random mutations. *Right*, the CSC model: the tumor bulk consists of heterogeneous subpopulations of cells, of which the CSCs are the only ones that maintain a tumorigenic potential and reproduce the tumor of origin following successful isolation. (B) Mechanisms that regulate CSCs state. Key intrinsic regulators include genetic, epigenetic, and metabolic processes, and extrinsic regulators include interactions with the microenvironment, including niche factors and the immune system. Adapted from Lathia et al. (2015). (C) Some key characteristics of CSCs.

behave as drivers of tumor growth and progression, ensuring indefinite self-renewal and fuelling the bulk with heterogeneous tumor progenitor cells and more differentiated subpopulations exhibiting limited proliferative potential. This creates a hierarchical model, at the apex of which is a small population of CSCs. Isolation of a small proportion of cells that express restricted, although not specific, cell surface markers, notably CD133 and CD44 (Visvader and Lindeman, 2008), provided evidence to support the CSC model. Upon xenotransplantation, isolated CSCs successfully reproduced the initial tumor phenotype, thereby giving birth to heterogeneous cell subpopulations, composed of CSCs and more differentiated progeny, most of which lack tumorigenic potential. CSCs are regulated by both intrinsic (genetic, epigenetic and metabolic) and extrinsic (microenvironmental, immune and niche) factors (Figure 1.2 B). Some of these aspects, such as epigenetic events and niche cues, are discussed hereafter.

The question remains open as to the nature of the cell of origin of CSCs. Care must be taken not to misinterpret the name “cancer stem cell”, as it does not imply that CSCs necessarily arise from a normal stem cell. Instead, the name merely refers to the CSCs sharing many common properties with normal stem cells, such as self-renewal and the ability to generate a more differentiated progeny (Figure 1.2C). Also, much like normal stem cells, CSCs typically remain in a quiescent state with slow proliferative kinetics, which, among other mechanisms, protects them from conventional chemotherapy targeted at actively dividing cells (Kreso et al., 2013). The question regarding the cell of origin of CSCs remains a highly debated topic and the answer varies depending on the cancer type. This will be discussed in more details later, specifically for GBM and EwS.

Tumors harbor an average of 4.6 driver mutations in protein-coding genes or, less frequently, in non-coding genes, that mainly affect three essential processes: cell fate, cell survival and genome maintenance (Vogelstein et al., 2013; Campbell et al., 2020; Rheinbay et al., 2020). Moreover, genome sequencing of a variety of tumors has revealed an additional level of complexity: within one tumor type, a multitude of driver mutations have been described, while the same single driver mutation can be found in multiple cancer types (Alexandrov et al., 2013; Campbell et al., 2020). Indeed, cancer progression follows an evolutionary multistage process consisting of acquisition of mutations and subsequent selection, and each subclone can behave differently to those mutations (Burrell et al., 2013).

Extensive intratumoral heterogeneity (ITH) has been reported in a variety of solid and hematologic neoplasms (Rosenthal et al., 2017). Numerous parameters collectively act on the tumor bulk and mediate the resulting heterogeneity. The trigger driver mutations may initially appear slowly (Merlo et al., 2006), or result from catastrophic events (chromothripsis, chromoplexy or kataegis) that may directly shift the cell to an aggressive phenotype (Campbell et al., 2010). Subsequently, mutations produce fitter subclones that expand under the selective pressures from microenvironmental, immune or therapeutic cues (Rosenthal et al., 2017), and it is possible for multiple CSC populations to coexist (Anderson et al., 2011). In addition, clone populations may compete for substrates (Marusyk and Polyak, 2010), while some subclones may provide a crosstalk with the dominant population and further support its growth (Calbo et al., 2011). In parallel, neutral evolution also occurs during tumor progression, resulting in the existence of passenger mutations, which do not necessarily confer advantage to the cells but are maintained as the clonal population grows (Hess et al., 2019). In line with this, the order in which mutations

are acquired can affect transformation and response to therapy (Ortmann et al., 2015), suggesting that a permissive environment may provide proliferative advantage and an optimal context to further support malignant progression following additional mutations. Consistent with this notion, premalignant leukemic precursor cells are detected in the blood of healthy individuals, but may either disappear, remain quiescent, or further transform into overt leukemic cells years later as a result of intrinsic or extrinsic factors (Rodríguez-Hernández et al., 2017). Thus, acquisition of mutations and/or genomic aberrations combined with selective pressure lead to ITH, contributing to tumor progression following a complex hierarchy.

Importantly, tumors with high ITH, in which higher numbers of distinct clonal populations are detected, have been linked to poorer outcome (Mroz et al., 2015; Morris et al., 2016; Andor et al., 2016), and could potentially predict the metastatic potential and clinical course of the tumor (Iacobuzio-Donahue et al., 2020). Moreover, the clinical significance of ITH translates into additional challenges for CSC targeting. Particularly, therapy of the initial tumor using cytotoxic agents can select or even generate resistant clones and ease their outgrowth, which provides an explanation as to why the molecular profile of recurrent tumors may differ from that of the original lesion (Sharma et al., 2010).

Taken together, adult cancers result from a multistage process, and a single mutation is rather unlikely to constitute the defining trait of a single tumor type, and each tumor may respond differently to this mutational event. In childhood cancers, in contrast, a single mutation may suffice to trigger transformation. Nonetheless, cancer cells behave differently as a result of additional mutations or epigenetic changes, as we will discuss later. Furthermore, as distinct driver and passenger mutations may coexist in cell clones, whether a genomic alteration has biological relevance must be tested and functionally confirmed. Thus, with so many degrees of heterogeneity, each tumor requires detailed characterization to obtain a precise landscape of its cellular profiles. This has become possible in recent years with high-throughput sequencing and single-cell profiling on cells within various tumor types (Garraway and Lander, 2013), and has highlighted the ability of tumors to adapt and change over time via cellular plasticity.

1.2.2 CSC plasticity

The CSC theory does not completely abrogate the stochastic model. These two apparently separate notions can be unified by observing cellular plasticity. Indeed, random mutations, gene expression deregulation and a certain degree of genomic instability are required for initial

CSC emergence. More precisely, there are two accepted principles behind this process: 1) a normal stem cell becomes a CSC following transforming genetic mutations; and 2) accumulated mutations and epigenetic changes reprogram cells to create a permissive environment for them to revert from their differentiated state into stem-like pluripotent cells (Reya et al., 2001; Frank and Nowak, 2003). This creates a conundrum, in which we may eradicate CSCs but as long as there may still be a subset of plastic cells with the ability to dedifferentiate, in the light of clonal evolution and selective pressure, they may recreate a new subpopulation of CSCs. Inflammation is also believed to participate in emergence of CSCs (Iliopoulos et al., 2011). Furthermore, the effects of a stochastic event will cause variable responses depending on the cell undergoing this change (Kreso and Dick, 2014).

For carcinomas to be able to metastasize, cancerous epithelial cells need to acquire mobility. This is rendered possible by the epithelial-to-mesenchymal transition (EMT) process. EMT is a physiological process in the context of development and wound healing. Upon environmental cues, such as hypoxia and secretion of transforming growth factor beta (TGF- β), or internal mutations, an epithelial cell loses cell-to-cell adhesion and apical-basal polarity, thereby acquiring a mesenchymal-like phenotype (Lamouille et al., 2014). Importantly, the EMT process is not strictly dichotomous with either pure epithelial or mesenchymal phenotypes. Rather, EMT includes the intermediate spectrum ranging between these two extremes, as the current terminology “transition” instead of “transformation” adequately implies. Hence, partial EMT refers to the particular magnitude of phenotypic changes acquired by the cell toward a mesenchymal-like state. In cancer, *de novo* expression of stemness genes grants invasion and motility to a transformed cell, a first step toward metastasis. The cell escapes the primary tumor in order to join the blood or lymphatic circulation and reach distal organs (Nieto et al., 2016). Despite some data challenging the central role of EMT in metastasis, EMT should not be ruled out as a key process in tumor invasion, as partial activation of EMT associated traits are widely found in carcinoma and CSCs, at least to a certain degree, and facilitates their dissemination as single cells or in clusters (Nieto et al., 2016; Batlle and Clevers, 2017; Derynck and Weinberg, 2019). Moreover, EMT is believed to be reversible, with cells reacquiring an epithelial phenotype during this mesenchymal-to-epithelial transition (MET), a process that could be involved in the metastatic process as the cells settle in a distant site after migration (Thiery, 2002; Yang and Weinberg, 2008; Mani et al., 2008).

The plasticity observed in non-tumor initiating cells further fueled the idea of engineering

induced pluripotent stem cells (iPSCs) by reprogramming differentiated cells to acquire stem-like properties. Succeeding in doing so would provide sensitive information to identify the key molecular players in the transformation and maintenance of CSCs. By combining the expression of a panel of stem-cell associated transcription factors (TFs), a panel of four TFs, namely OCT3/4, SOX2, c-MYC and KLF4, permitted to obtain iPSCs from differentiated fibroblasts (Takahashi and Yamanaka, 2006). Shortly thereafter, another group identified another set of four TFs capable of reprogramming human fibroblasts: OCT4, SOX2, NANOG and LIN28 (Yu et al., 2007). Similarly, four core TFs necessary for tumor propagation were identified in GBM cells, that include POU3F2, SOX2, SALL2, and OLIG2, allowing to reprogram differentiated glioma cells back into a CSC-like state (Suvà et al., 2014). Identifying TFs essential for pluripotency is a key step toward better understanding the mechanisms behind tumor initiation.

The hierarchy of normal stem cells has been shown to be more plastic than previously expected, as findings reported that pluripotent cells, and even lineage-committed cells, can re-enter a stem-like state in a specific environment (Tata et al., 2013; Batlle and Clevers, 2017). This phenomenon was also observed in breast cancer, where particular environmental stimuli could cause cells from various phenotypes to acquire tumorigenic properties (Gupta et al., 2011). This observation suggests that the hierarchy may not always be so rigid and that the cancer environment is yet another critical determinant of cellular plasticity in the tumor. Based on this, efforts to target CSCs should be combined with therapies that target the more differentiated progeny to increase the chances of completely eradicating the tumor by preventing the reversible transition of differentiated cells to CSCs.

1.2.3 The role of the CSC niche

Tumors cannot be simplified as closed-up organisms acting independently of their surroundings. Rather, tumors are constantly exchanging information and acting upon their environment through a bidirectional regulation (Quail and Joyce, 2013). Normal stem cells proliferate and sustain their population within a specific microenvironment called a niche. These niches consist of stromal cells, comprising mesenchymal and immune cells, vascular endothelial cells, soluble factors secreted by the different actors, and components of the extracellular matrix, that are exploited toward promoting cancer progression by providing CSCs with the most favorable conditions for growth. Indeed, the niche can drive the stem state of the tumor cells and sustain their stemness features (Scadden, 2014). Niches have been thoroughly studied and particularly well

described in colorectal cancer, underlining their role in sustaining local inflammation and tumor progression (Borovski et al., 2011). Gliomas offer another good example of the importance of the niche for tumor growth, as CSCs rely tightly on the surrounding vasculature and the signals from the endothelial cells for tumor maintenance (Borovski et al., 2011).

Interestingly, different tumor types have the propensity to follow specific organ-selectivity and kinetics for metastatic spread. For instance, prostate cancer tends to metastasize mainly to the bones following a prolonged latency, whereas lung adenocarcinoma will generally present with multi-organ metastasis after a shorter latency period (Nguyen et al., 2009). This is in part due to the organ specific barrier, which will be more or less permissive for cell extravasation. As a result, a cell is more likely to colonize an organ with a more complex barrier, such as the brain, if it is already equipped with the necessary tools and properties to successfully invade locally. Such functions may be intrinsically acquired at the initial site through random mutations, or result from the influence of the CSC niche (Obenauf and Massagué, 2015). In addition, an adequate environment is essential for the malignant cells to proliferate at the metastatic destination. Indeed, only about 0.01 % of circulating tumor cells successfully home and colonize an organ and eventually produce visible metastases (Chambers et al., 2002). According to the “seed and soil” paradigm, the development of a metastasis strongly depends on an appropriate microenvironment that sustains the tumor growth, in a comparable manner as in the primary site (Valastyan and Weinberg, 2011).

Furthermore, niches can also create a protective environment for tumor cells at a secondary site, such as in the bone marrow, and constitutes one of the many pathways behind CSC resistance to therapy (Nguyen et al., 2009; Obenauf and Massagué, 2015).

1.2.4 CSC resistance to therapy

Most chemotherapies and radiotherapies developed in the last century focus on targeting the fast-dividing non-CSCs by inducing DNA damage in actively replicating cells. As mentioned before, CSCs are often dormant and therefore may escape conventional therapies (Chen et al., 2012; Qin et al., 2012; Vanner et al., 2014). Reduced sensitivity of CSCs compared to non-CSCs has been extensively described in many tumors, and implicate various mechanisms, ranging from activation of DNA repair pathways (Bao et al., 2006) to remodeling of the chromatin (Sharma et al., 2010; Liao et al., 2017). Additionally, cytotoxic agents used in chemotherapies can induce mutations in the cells. Depending on the mutation caused in surviving cells, this process stochastically

confers the cells increased fitness and may be a vector of selection for CSCs with improved survival (Greaves and Maley, 2012). Regardless of the mechanism, the CSC model explains why relapse can occur despite the virtual disappearance of cancer cells after therapy, and underlines the need for targeted approaches specifically designed for dormant CSCs.

Unfortunately, some new treatments targeted at the CSCs that show encouraging initial response can be later followed by relapse as a result of newly acquired resistance of CSCs (Dagogo-Jack and Shaw, 2018). Detection of fusion genes as the main mutational drivers for a variety of cancers, including leukemia or EwS, bore major promises. Rightfully so, it seemed plausible that targeting the fusion protein would single handedly stop tumor progression and ensure CSCs eradication. The $t(9;22)(q34;q11)$ translocation in a hematopoietic stem cell has been identified as the principal initiating event for chronic myeloid leukemia (CML) in more than 95% of patients, and leads to the formation of the constitutively activated BCR-ABL tyrosine kinase (Goldman and Melo, 2003). Significant effort was put into finding a functional tyrosine kinase inhibitor and clinical trials quickly started after identification of imatinib (Gleevec) as a potential candidate, with very encouraging results (Druker, 2002). However, the system is not perfect and analysis of refractory patients revealed various mechanisms responsible for drug resistance: 1) imatinib may fail to inhibit BCR-ABL following oncogene amplification or reduced binding capacity resulting from amino acid changes (target-dependent resistance); 2) the cell may have already adapted and acquired additional pathways, making BCR-ABL less essential for survival (target-independent resistance); 3) expression of drug efflux pumps such as ATP binding cassettes (ABCs) increase the efflux of imatinib from the cell, decreasing its intracellular availability (drug-dependent resistance) (Henkes et al., 2008). CML and the use of imatinib illustrate well the challenges encountered while developing CSC targeted therapies, and each of the resistance strategies listed above have been described in other tumor types (Gottesman et al., 2002). Overall, targeting of many promising candidate pathways eventually show rather mixed results upon clinical testing and fail to significantly improve patient survival (Adorno-Cruz et al., 2015).

Identification of pathways and distinct signatures proper to CSCs, and understanding the mechanisms behind drug resistance could help predict how these cells can be targeted to enhance patient outcome. Currently, much effort is being put into building systems to efficiently predict patient response based on the patient's tumor characteristics, linking clinical and genomic data. GBM represents a sadly excellent example of a particularly challenging and complex refractory tumor, as a result of extensive inter- and intratumoral heterogeneity and cellular plasticity.

Localized sampling is therefore rarely representative of the extent of the tumor mass and cells are largely prone to adapting to the treatment by off-target alterations (Eder and Kalman, 2014). The genetic profile of GBM has been extensively well defined, with considerable data regarding its mutational landscape. As we will review in Chapter 2, although some molecular subtypes are associated with better prognosis, much effort is still warranted to identify a specific pathway whose targeting will prove truly beneficial for GBM patients in the long-term.

1.3 Epigenetic regulation of cellular plasticity

Epigenetics refer to all the various heritable processes that lead to changes in the transcriptome without altering the primary DNA sequence. Indeed, all the cells in an organism carry the same genetic information encoded in their DNA. Yet, organs, tissues, as well as cells within a given tissue, can vary considerably in morphology, function and behavior. Tight regulation of cell fate is critical to ensure homeostasis of the body, and is controlled by dynamic epigenetic modulation, which permits the orchestration of the expression of specific genes through various mechanisms.

The most common and best characterized epigenetic alterations include:

- 1) DNA methylation, which can repress gene transcription at the promoter site;
- 2) histone modifications that underlie chromatin remodeling and modulate access to DNA for transcription;
- 3) post-transcriptional changes of gene expression via non-coding RNAs (ncRNAs) that constitute the main focus of this work.

Although cancer is basically a genetic disease, it is becoming increasingly apparent that epigenetic modifications play an equally important and sometimes even dominant role in carcinogenesis compared to genetic events (Kreso and Dick, 2014). A single oncogenic event, such as a point mutation, may initiate transformation. However, in the majority of adult cancers, this single event is not sufficient to generate the series of following events leading to proliferation and tumorigenesis. This suggests that a first event leads to a permissive cell state that may allow other events to occur, which could in their turn cause the cell to acquire tumorigenicity. To support this, efficiency of cellular reprogramming into iPSCs varies considerably based on the initial differentiation state of the manipulated cell. Thus, compared to fibroblasts, mouse-derived neural stem cells can be reprogrammed more efficiently and require induction of only two TFs,

namely in combination with KLF4 or c-MYC (Kim et al., 2008). Furthermore, epigenetics is also involved in response to therapy. For example, various cancer cells displayed modified chromatin conformation following exposure to drug, rendering them resistant to treatment (Sharma et al., 2010). Therefore, exploring the epigenetic landscape of CSCs, including the impact of ncRNAs on post-transcriptional gene expression regulation, can provide key elements to identify therapeutic approaches that augment patient remission and, in at least some tumor types, possibly lead to cure (Baylin and Jones, 2011).

The former approach to biology long focused on a clear sequence of events initiated by DNA transcription into an RNA strand, subsequently translated into a protein that permits the ultimate expression of the genetic information into a specific phenotype. According to this view, RNA serves merely as an intermediary messenger for protein expression. This principle has progressively been challenged, as new types of RNA were identified, such as ribosomal RNA (rRNA) and transfer RNA (tRNA), both involved in protein translation. Finally, with the development of whole genome sequencing technologies 20 to 30 years ago, it could be demonstrated that about 70% of the genome is transcribed, while only 2% of the transcriptomic output encodes proteins (Dunham et al., 2012). Deep-sequencing of the genome revealed pervasive DNA transcription that produces stable RNAs of various lengths and lacking any protein-coding potential (Carninci et al., 2005; Kapranov et al., 2007). While these transcripts were first viewed as random noise, it became clearer that this “dark matter” required further investigation, as the number of identified non-coding transcripts kept on growing, and it remained to be established whether they were inert or had functional biological relevance (Johnson et al., 2005). When looking at a typical eukaryotic cell, rRNAs, tRNAs and mRNAs represent up to 99% of the total RNA mass, with up to 10^7 copies in total. In contrast, other ncRNAs compose less than 1% of the RNA mass and their molecules are much less abundant, by two to three orders of magnitude (Palazzo and Lee, 2015). If these ncRNAs are so scarce in the cell in comparison to mRNA and the translation machinery, it can be assumed that their function can only be very limited. However, findings demonstrating the presence of binding sites around protein-coding and non-protein coding genes suggest otherwise, showing that ncRNA expression can be regulated by transcription factors, implying a function that needs to be neatly monitored for cellular homeostasis (Cawley et al., 2004). Furthermore, comparison of the murine and human genomes underscores high sequence conservation outside coding-frames on chromosome 21, further supporting a potentially important role of non-coding elements in the genome (Dermitzakis et al., 2002).

Altogether, these observations reinforce the notion that epigenetic events and regulatory elements may play an increasingly important role in regulation of both normal cell fate and tumorigenesis. Studying the biogenesis and functions of ncRNAs may provide essential insight into potentially targetable epigenetic pathways maintained in CSCs. The ncRNAs involved in epigenetic regulation include microRNAs (miRNAs), long non-coding RNAs (lncRNAs), short interfering RNAs (siRNAs), and piwi-interacting RNAs (piRNAs). Here, we will focus on miRNAs and lncRNAs.

1.3.1 MicroRNAs

miRNAs were initially discovered in 1993 in *C. elegans*, where the gene *LIN-14* had to be downregulated for normal larval development by *lin-4*, a short RNA sequence that did not encode a protein (Lee et al., 1993). Remarkably, many other short ncRNAs were later found to be highly conserved across species, including the let-7 family (Pasquinelli et al., 2000), highlighting a potentially essential role of these short transcripts in cell development and control of gene expression.

miRNAs are short ncRNA sequences, generally 22 nucleotide-long, and act mainly as post-transcriptional gene repressors by binding the 3'-UTR of target mRNAs and repressing their translation or targeting them for degradation (Melo and Esteller, 2011), thereby promoting cell differentiation (Bartel, 2009; Martinez and Gregory, 2010), proliferation (Brennecke et al., 2003; Hatfield et al., 2005) and apoptosis (Xu et al., 2003). In embryonic stem cells, a limited repertoire of miRNAs is expressed, that is absent or expressed at very low levels in differentiated cells. Therefore, miRNA clusters are differentially involved and tightly regulated depending on their effect on promoting or repressing the cell cycle (Martinez and Gregory, 2010).

Expression of the mature forms of miRNAs follows a specific pattern, highly dependent on the tissue and cell state, and is under the control of tissue-, developmental- and cell-specific signalling (Kim et al., 2009b). About half of the miRNAs are found in clusters and are transcribed from a common promoter. They can be localized at protein-coding loci, most often in intronic regions, or in non-protein coding areas. Transcription of miRNA genes is regulated by the recruitment of transcription factors, including p53 and c-MYC, and can also be epigenetically modulated, for instance as a result of changes in the DNA methylation state and histone marks (Kim et al., 2009b; Peng and Croce, 2016).

The canonical biogenesis of miRNAs begins in the nucleus with transcription of the DNA

sequence into a primary-miRNA (pri-miRNA), which is then cleaved by DROSHA in association with dsRNA-binding protein DGCR8 (DiGeorge syndrome critical region gene 8), into a hairpin RNA, namely the premature-miRNA (pre-miRNA) (step 1 in Figure 1.3). Following exportation from the nucleus into the cytoplasm, mediated by XPO5 (Exportin 5) in association with the GTPase Ran (step 2 in Figure 1.3), the pre-miRNA strand is converted into a mature duplex by the RNase III endonuclease DICER1, and cleaved into the miRNA/miRNA* duplex (step 3 in Figure 1.3), consisting of the passenger strand destined for degradation (miRNA*) and the leading strand (miRNA) (step 4 in Figure 1.3). Trans-activation responsive RNA-binding protein 2 (TRBP2) functions as a guide to determine which of the RNA strands constitutes the leading miRNA strand to be further processed and loaded on an Argonaute RNase (AGO1-4). Together, DICER1, Argonaute, TRBP2 and the leading miRNA strand form the RNA-induced silencing complex (RISC), also known as miRNA loading complex (miRLC). Finally, RISC binds the 3'-UTR of target mRNA transcripts for translation inhibition or mRNA degradation (step 5 in Figure 1.3) (Melo and Esteller, 2011). In addition, direct pathway activation by miRNAs acting as ligands of Toll-like receptors (TLR) has been described (Fabbri et al., 2012; Fabbri, 2012). Alternatively, some miRNAs follow the non-canonical pathway, which involves splicing of their mRNA precursor. In this case, the hairpin sequence, called mirton, bypasses DROSHA to be processed by a spliceosome instead, and is available for export from the nucleus to the cytoplasm where it undergoes the subsequent steps of maturation (Winter et al., 2009).

The main mechanism for miRNA binding involves the nucleotides in positions 2 to 7 at the 5'-end of the mature miRNA strand, referred to as the seed region (Lewis et al., 2003, 2005), and follows simple Watson-Crick base pairing. This sequence is essential for target recognition at the canonical sites, which are conserved binding sites found across a broad range of mRNA transcripts (Agarwal et al., 2015), leading to significant changes in the proteome (Selbach et al., 2008). With each miRNA capable of targeting hundreds of mRNA, miRNAs have the power to affect large molecular networks (Thomas et al., 2010).

Shortly after miRNAs were discovered and their presence confirmed in mammalian cells (Lagos-Quintana et al., 2001), scientists postulated and investigated miRNA implication in cellular deregulation and cancer pathways. This was first clearly demonstrated in adult chronic lymphoblastic leukemia (CLL), in which loss of the chromosomal region 13q14 had already been described but was not associated with the loss of a key gene in this context. By more accurately identifying the critical lost chromosomal region, miR-15a and miR-16-1 were found to be signifi-

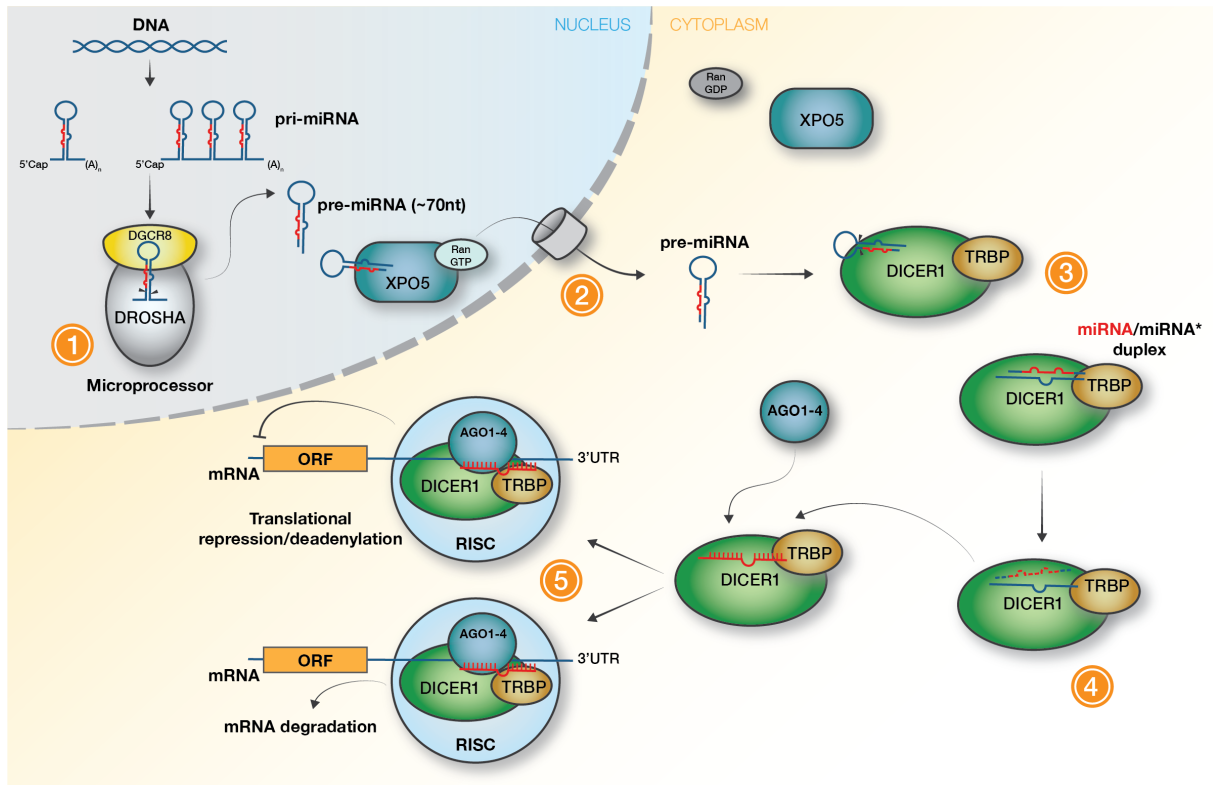


Figure 1.3: The canonical miRNA biogenesis pathway. Adapted from Melo and Esteller (2011).

cantly downregulated in a majority of CLL patients (Calin et al., 2002). Several studies followed showing that miRNAs can act either as tumor suppressors or as oncogenes (Kent and Mendell, 2006; Ventura and Jacks, 2009).

Therefore, the perturbed miRNA signature found in cancerous cells is the result of a dysregulation of miRNA expression and can occur at several levels (Peng and Croce, 2016):

- chromosomal aberration may lead to duplication or loss of genomic region containing miRNA loci;
- miRNA transcription may be modulated by changes in DNA methylation and histone marks, or affected by the expression of specific transcription factors that activate miRNA transcription;
- miRNA maturation may be impaired at various levels, based on the activity or expression of proteins implicated in the biogenesis pathway. Indeed, expression of certain miRNAs in tumors remain low, although the levels of pre- and pri-miRNA are maintained, suggesting impaired miRNA maturation as a key component in oncogenesis (Thomson et al., 2006);
- post-transcriptionally, miRNAs can be bound by proteins or other RNAs that repress miRNA function, as is the case of LIN28B, which we discuss later.

The let-7 family of highly conserved miRNA, consisting of 13 members that are partially functionally redundant, is absent in embryonic stages, but strongly expressed in differentiated cells, and its downregulation is known to promote transformation (Kumar et al., 2007). Furthermore, decreased expression levels of let-7 have been seen in various malignant tumors, including lung, hepatocellular, skin, breast, ovarian and urothelial cancers, as well as hematopoietic malignancies (Viswanathan et al., 2009; Croce, 2009). Their repressed target genes include the oncogene *c-MYC* (Kim et al., 2009a), the cell cycle regulator *Cyclin D1* (Li et al., 2012), *HMGA2*, involved in motility and self-renewal (Lee and Dutta, 2007), *IMP2*, involved in CSC metabolism (Degrauwe et al., 2016a), and *RRM2*, involved in DNA synthesis in dividing cells (Bhutia et al., 2013), among others. The let-7 miRNAs are usually repressed in embryonic stem cells and CSCs by the RNA binding protein (RBP) LIN28B, thus contributing to maintenance of cell pluripotency (Viswanathan and Daley, 2010).

1.3.2 Long non-coding RNAs

While smaller ncRNAs have been thoroughly investigated, lncRNAs represent a subgroup of transcripts that remain largely enigmatic. lncRNAs are defined as transcripts that are greater than 200 nucleotides long, have no clear open reading frames (ORFs) and lack protein-coding potential (Angrand et al., 2015). Like mRNAs, lncRNAs are transcribed by RNA Polymerase II and can undergo splicing and polyadenylation (Quinn and Chang, 2016). However, they display poor cross-species conservation (Derrien et al., 2012). Whereas they were first believed to represent junk RNA, subsequent findings progressively demonstrated their diverse roles in the cell (Figure 1.4). Some data show that several lncRNAs can actually give rise to small functional peptides, for instance in the skeletal muscle (Anderson et al., 2015), but ribosome profiling confirms lncRNAs as mainly untranslated transcripts (Guttman et al., 2013). They now appear to be significant regulators of various processes, including cell pluripotency and tumorigenesis, either as tumor suppressors or as oncogenes, by interactions with other molecules (Fatica and Bozzoni, 2014; Wapinski and Chang, 2011; Yan et al., 2015; Schmitt and Chang, 2016).

The first reported lncRNA, H19, was identified in mouse embryogenesis (Pachnis et al., 1988) and consists of a 2.3 kbp-long transcript. Further investigation confirmed that the H19 transcript undergoes splicing and polyadenylation but is not translated into a protein (Brannan et al., 1990). Since then, thousands of lncRNAs have been reported, but biological activity has been defined in only about a handful of them (Ponting et al., 2009). LncRNAs can be subdivided

in five categories that define their genomic organization, based on their position relative to a neighboring protein-coding gene:

- 1) Sense: the lncRNA locus overlaps one or more exons of another transcript;
- 2) Antisense: the lncRNA locus overlaps one or more exons of another transcript in the opposite direction;
- 3) Bidirectional or divergent: the lncRNA is under the control of a promoter that also initiates transcription of a coding gene in the opposite direction;
- 4) Intronic: the lncRNA corresponds to the intron of another transcript;
- 5) Intergenic: the lncRNA is produced from a transcription unit located between two protein coding genes.

This classification, however, is based solely on the lncRNA sequence location in the genome, and does not necessarily correlate with their expression or function. As mentioned earlier, lncRNA expression is largely dependent on the cell type and state, and will vary in the context of disease. Regulation of lncRNA transcription thus relies on the control of highly conserved promoters. However, it is unclear if lncRNA activation is the cause or the result of its expression in certain cellular contexts. Transcription of lncRNAs require an open chromatin with promoters enriched in active histone modifications. Some studies, however, have shown that lncRNAs may be regulated not individually, but rather as a class, as their global expression is significantly downregulated upon knockdown of DICER1 and depends on c-MYC expression (Zheng et al., 2014). Furthermore, as listed above, many lncRNAs result from the antisense transcription of a protein-coding gene under the control of a bidirectional promoter. This phenomenon, called divergent transcription, suggests that antisense transcripts may be under specific regulation independent of their mRNA counterparts (Quinn and Chang, 2016).

Understanding the mechanisms underlying lncRNA function is required to determine their putative utility in cancer treatment. Due to their length, lncRNA transcripts can fold and contain several binding sites for other molecules, so that the secondary structure is an important factor for their function. Whether located in the nucleus or in the cytoplasm, lncRNAs can regulate gene expression through various mechanisms, based on interactions with different cellular macromolecules: 1) direct binding of lncRNAs to chromatin, changing its conformation or recruiting other regulatory molecules to specific loci, 2) binding of lncRNA to proteins, leading

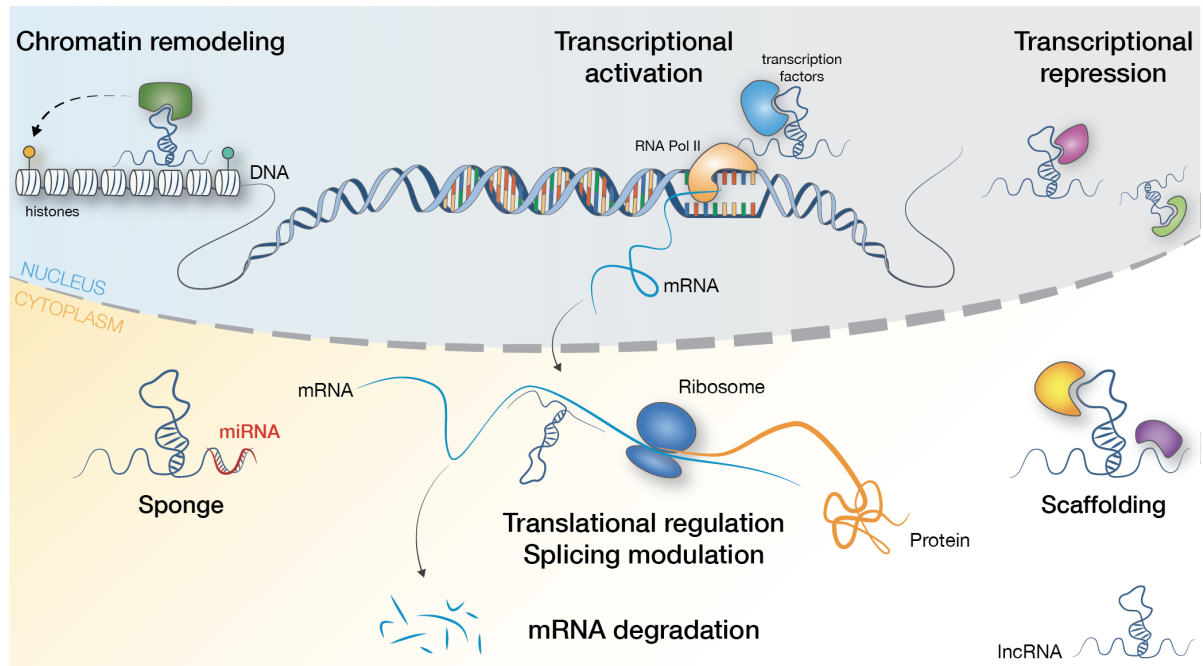


Figure 1.4: Representation of various functions of lncRNAs. Inside the nucleus, lncRNAs can recruit chromatin remodelling proteins to change chromatin conformation, and positively or negatively regulate gene transcription by binding TFs. In the cytoplasm, lncRNAs can act as sponges and sequester miRNAs and regulate translational activity, splicing, as well as RNA degradation. By binding several partners, lncRNAs can act as scaffolds.

to formation of protein complexes or inhibiting protein-protein interactions, 3) interaction with mRNA causing recruitment of proteins and affecting splicing, stability or translation, or interaction with miRNAs leading to their sequestration and loss of function (Wang and Chang, 2011; Angrand et al., 2015; Bergmann and Spector, 2014).

Furthermore, lncRNAs can affect both proximal (*cis*-acting) and distal (*trans*-acting) genes (Kopp and Mendell, 2018). On a *cis*-acting level, a lncRNA can regulate the transcription of a neighboring gene by recruiting the necessary transcriptional machinery for regulated transcription. This mechanism is employed by *Xist* to silence almost all of the inactivated X chromosome, by extensively repressing chromatin. Alternatively, DNA regulatory elements found within the lncRNA locus may impact transcription of the neighboring protein-coding gene. Another mechanism of action is independent of the mature lncRNA sequence but relies on transcription of the antisense lncRNA to interfere with transcription of the protein-coding gene. Similarly, splicing of a nearby lncRNA locus can affect gene transcription (Kopp and Mendell, 2018). Functions of lncRNAs in *trans* include chromatin state reprogramming, as exemplified by *HOTAIR*, whose expression is increased in breast cancer and is associated with an invasive phenotype, as a result of Polycomb repressive complex 2 (PRC2) redistribution across the genome (Gupta et al., 2010). Other lncRNAs may reorganize nuclear structure, by acting as scaffolds linking distal areas of actively transcribed DNA together. Additionally, lncRNAs may bind specific RBPs or sequester

other RNAs, thereby limiting their availability in the cell (Kopp and Mendell, 2018). Lastly, lncRNAs may be precursors of miRNAs, as evidenced by *H19*. Indeed, miR-675 is found within the first intron of *H19*. Interestingly, expression levels of *H19* and miR-675 are neither equal nor stable across tissues, suggesting that processing into miRNA may be regulated based on the local function of the lncRNA (Dey et al., 2014).

Altogether, the term lncRNA as used to define a single subclass is rather elusive, as it currently encompasses largely heterogeneous transcripts that can exert a broad spectrum of relevant cellular functions. Further characterization of these long transcripts is warranted to better subdivide them based on their biological properties. As their expression pattern varies in a tissue and cancer specific manner, lncRNAs are interesting candidate biomarkers to predict tumor prognosis and response to therapy (Schmitt and Chang, 2016).

1.4 RNA binding proteins

Investigations on the post-transcriptional fate of mRNA have brought to light a wide range of regulatory processes implicated in all levels of mRNA metabolism, from the birth of a nascent mRNA to its decay (Figure 1.5). Indeed, transcripts do not circulate inside the cells as naked nucleotide strands. Rather, they form messenger ribonucleoparticles (mRNPs) in combination with a dynamic assembly of proteins bound to the transcript, involved in all steps of mRNA fate, including transcription, splicing, 3'-end and 5'-end processing, transportation, translation, as well as mRNA stability and decay (Glisovic et al., 2008). RBPs are involved as much in transport and localization as in maturation of mRNA, either directly or by recruiting additional proteins. It is believed that each RBP can individually target hundreds of transcripts, which can in turn bind a multitude RBPs, thus creating a complexly entangled network (Müller-McNicoll and Neugebauer, 2013). The identification of more than a thousand RBPs (Sundararaman et al., 2016; Trendel et al., 2019), as well as their striking conservation across species (Gerstberger et al., 2014), indicate that post-transcriptional regulation is an essential component of gene expression. In addition to mRNAs, RBPs can also synergize with or antagonize ncRNAs to affect gene expression, either by competitive binding to target mRNAs, recruitment of RISC, or facilitating miRNA binding through changes of mRNA conformation (Mitchell and Parker, 2014; Degrauwe et al., 2016b).

Thus, RBPs increase the diversity of the regulatory network that controls cell fate. Indeed,

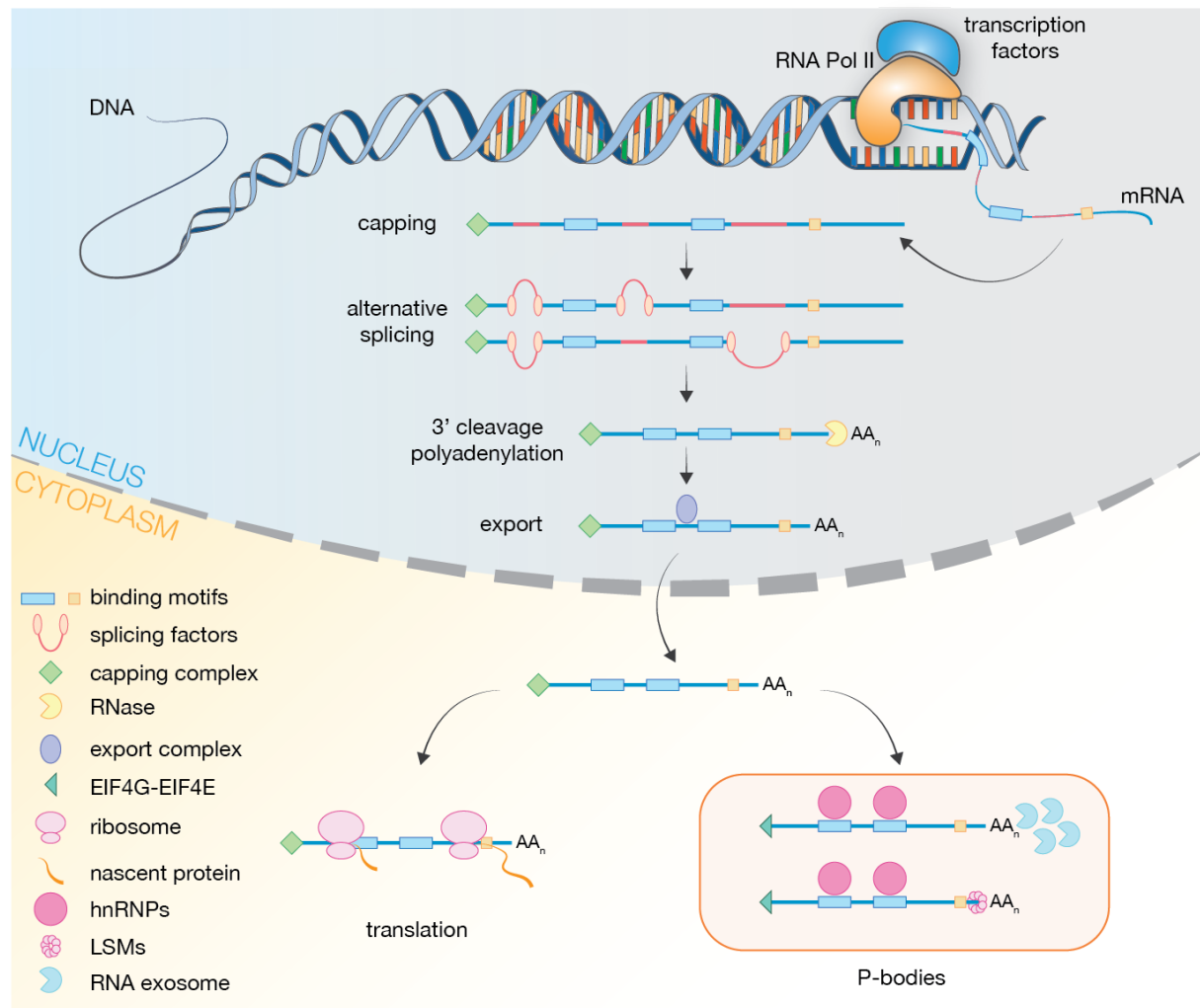


Figure 1.5: RBPs are involved in mRNA fate. RNA transcripts are bound by changing complexes of multiple RBPs, which are involved in maturation, modification, splicing, export of mRNAs and transport to specific sites. Following delivery to site, mRNA is either translated or stocked in P-bodies until further processing or degradation. AA_n , polyadenylation; hnRNPs, heterogeneous nuclear ribonucleoproteins; P-bodies, processing-bodies. Adapted from Marchese et al. (2016).

post-transcriptional regulation provides a faster response in comparison to transcriptional control. Also, it gives a chance for the environment to directly influence the transcriptome through signalling cues from the cellular niche. By having an effect independently of the gene expression levels, an additional regulatory dimension allows more precise fine-tuning of the cell identity.

With the development of more stringent and selective technologies, such as photoactivatable ribonucleoside-enhanced crosslinking and immunoprecipitation (PAR-CLIP) (Hafner et al., 2010) and enhanced RNA interactome capture (eRIC) (Perez-Perri et al., 2018), studies have started unmasking the identity and function of RBPs with more precision. These technologies have also started shedding light onto the so-called “enigmRBPs”, a group of proteins without previously recognized RNA binding domains, identified as RBPs in yeast and human proteomes (Beckmann et al., 2015). Moreover, while a panel of protein-RNA binding motifs have been described,

such as the RNA recognition motif (RRM) and the K-homology (KH), more non-canonical sites are progressively being uncovered thanks to these new methods, highlighting the complexity of RNA-protein interactions (Castello et al., 2012, 2016).

Alterations in the correct assembly of mRNPs and impaired function of such regulatory pathways can negatively impact the cellular balance and trigger a large panel of diseases, ranging from degenerative disorders to cancer (Ramaswami et al., 2013; Lukong et al., 2008). Among the RBPs that have been associated with cancer, the LIN28 paralogs are involved in the let-7 miRNA maturation pathway and normally expressed during embryogenesis (Viswanathan et al., 2009). Additionally, the IMP family of highly conserved oncofetal RBPs, also termed IGF2 mRNA binding proteins (IGF2BPs), is known to be highly expressed in developing tissues, important for cell growth and cell migration during embryogenesis (Mueller-Pillasch et al., 1999), and is believed to be a key player in the process of stemness maintenance.

1.4.1 The LIN28 paralogs

LIN28 was first described in *C. elegans*, where its differential regulation at early larval stages is critical for developmental timing (Ambros and Horvitz, 1984). Later, LIN28 was found to be highly conserved across species and expressed exclusively during development (Moss and Tang, 2003). In mammals, two paralogs have been identified, LIN28A and LIN28B (here, we use “LIN28” to refer to the two paralogs together). Both paralogs share 73% amino acid identity across a unique combination of two RNA binding regions, namely one cold shock domain (CSD) and one zinc knuckle domain (ZKD), composed of two CCHC zinc fingers (Figure 1.6 A). Interestingly, phylogenetic studies found that LIN28A and LIN28B are more closely related individually across species than to one another within the same species. Furthermore, LIN28 in *C. elegans* is similarly related to both paralogs (Figure 1.6 B). This suggests that LIN28B may have resulted from a duplication event in an ancestral gene, and that LIN28A/B may possess distinct properties (Guo et al., 2006). Indeed, LIN28B contains a nuclear and a nucleolar localization signal (Figure 1.6 A), causing LIN28B to be recruited to the nucleus, while LIN28A is primarily located in the cytoplasm (Piskounova et al., 2011)

LIN28 paralogs are typically expressed during normal embryogenesis, where they control the critical balance between pluripotency and differentiation, and regulate the stem cell metabolism (Zhang et al., 2016a). Notably, LIN28B participates in cellular dedifferentiation and reprogramming of somatic cells (Yu et al., 2007). The potential role of LIN28 in tumorigenesis was

uncovered by using NIH3T3 cells, in which overexpression of LIN28 was sufficient for tumors to form *in vivo* (Viswanathan et al., 2009). Furthermore, reactivation of LIN28B has been reported in various tumor types, where it is linked to malignant transformation and correlates with cancer aggressiveness, leading to its classification as an oncofetal protein (Viswanathan et al., 2009; Balzeau et al., 2017). Most interestingly, among all tumors that express LIN28, 25 % are childhood malignancies (Carmel-Gross et al., 2015), and include various cancer types, such as Wilms tumor (Urbach et al., 2014), neuroblastoma (Hennchen et al., 2015; Powers et al., 2016) and primitive neuro-ectodermal brain tumors (Choi et al., 2016; Picard et al., 2012).

Most of the work on LIN28 has focused on the interactions between the LIN28 paralogs and the let-7 miRNAs. Early on, LIN28 was early found to be negatively regulated by let-7 during nematode development, as the 3'-UTR of LIN28 contains several let-7 binding sites (Pasquinelli et al., 2000). Later, observations demonstrated that LIN28 can repress let-7 biogenesis. Indeed, disparities observed respectively high and low levels of precursor and mature let-7 transcripts during development helped uncover mechanisms of post-transcriptional regulation of ncRNAs. Among these, LIN28 was shown to bind the GGAG loop in let-7 miRNAs and affect their maturation process (Heo et al., 2008; Viswanathan et al., 2008). As a result of the different locations of the LIN28 paralogs, distinct mechanisms participate in let-7 miRNA silencing. LIN28A, primarily located in the cytoplasm, binds a conserved let-7 loop and recruits the TUTase Zcchc11 (TUT4), which uridylylates the 3'-end of let-7 precursors, leading to transcript degradation by the nuclease DIS3L2 (Heo et al., 2008). In contrast, LIN28B, found in the nucleus, blocks let-7 maturation by recruiting precursor transcripts to nucleoli devoid of the microprocessor machinery and preventing further maturation (Piskounova et al., 2011) (Figure 1.6 C). Given that LIN28 is expressed during early development, whereas let-7 miRNAs appear at later stages, this negative feedback loop is central in maintaining the balance between stem and differentiated cell states (Figure 1.6 D). As a result, aberrant reactivation of LIN28 negatively regulates let-7 expression, reverses the cell to a stem-like state, and hence participates in tumorigenesis. To further appreciate the impact of LIN28 expression, a recent study demonstrated that depletion of mature let-7 frees Argonaute proteins from let-7 miRNAs, and RISC complexes become more available to bind other miRNAs, thus shifting the miRNome and the resulting transcriptome (Tan et al., 2019).

Nevertheless, there is increasing evidence that LIN28 function is not limited to let-7 downregulation. Transgenic mouse experiments showed that varying levels of LIN28 affect glucose uptake

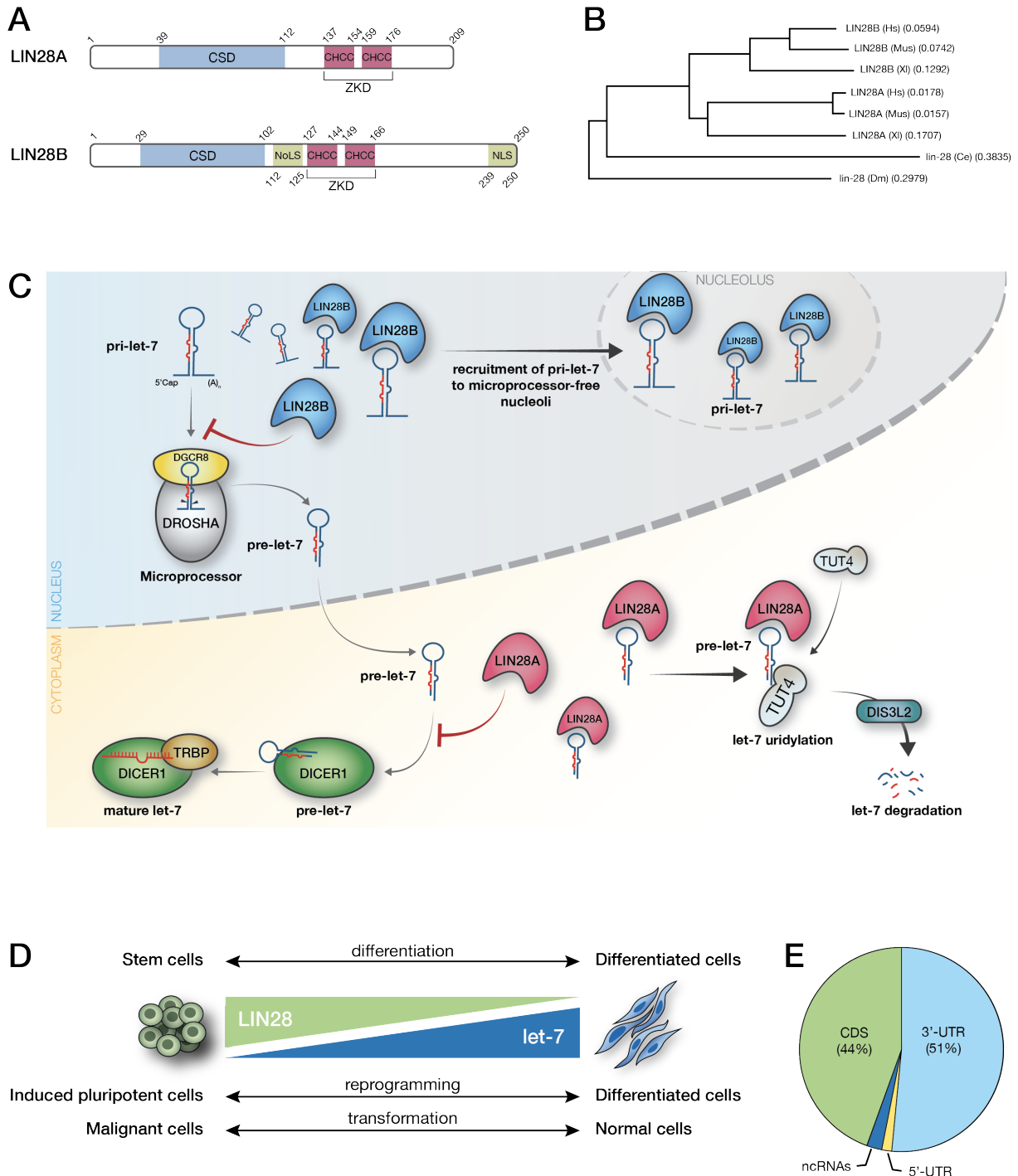


Figure 1.6: LIN28 structure and mechanisms of action. (A) Schematic representation of the human LIN28 paralogs structure with their domains. CSD, cold shock domain; CCHC, Cys-Cys-His-Cys zinc finger; ZKD, zinc knuckle domain; NoLS, nucleolar localization signal; NLS, nuclear localization signal. Adapted from Thornton and Gregory (2012). (B) Phylogenetic tree representing sequence alignments of the LIN28 paralogs. The number in parentheses after the gene name correspond to the calculated evolutionary distance. *Hs*, Homo sapiens; *Mm*, *Mus musculus*; *Xl*, *Xenopus laevis*; *Dm*, *Drosophila melanogaster*; *Ce*, *Caenorhabditis elegans*. Adapted from Guo et al. (2006). (C) LIN28A/B regulation of let-7 maturation. In the nucleus, LIN28B binds and sequesters pri-let-7 to nucleoli and prevents maturation by the microprocessor DGCR8/DROSHA. In the cytoplasm, LIN28A binds pre-let-7 transcripts and recruits TUT4, which adds a short polyU tail to pre-let-7, which is no longer a DICER1 substrate, resulting in degradation of pre-let-7 by DIS3L2. (D) Biological consequence of the LIN28-let-7 balance. High LIN28 expression in undifferentiated cells blocks biogenesis of let-7 miRNAs. As differentiation progresses, LIN28 expression is lost, resulting in production of mature let-7 that can negatively regulate LIN28. In the generation of iPSCs and in tumorigenesis, LIN28 helps drive pluripotency, self-renewal, de-differentiation, and/or cellular transformation to a malignant phenotype. Adapted from Balzeau et al. (2017). (E) Distribution of LIN28B binding sites in conservative sequence clusters to non-coding RNAs and different transcript regions (5'-UTR, CDS and 3'-UTR) of protein-coding genes. Adapted from Graf et al. (2013).

and insulin sensitivity whereas mature let-7 transcripts remain stable (Zhu et al., 2011). Moreover, LIN28 promotes proliferation of embryonic stem cells by binding to mRNAs encoding cell cycle regulators and enhancing their translation into the final protein product, suggesting a role in post-transcriptional gene regulation independent of let-7 miRNAs (Peng et al., 2011). Recently, UV crosslinking and immunoprecipitation sequencing (CLIP-seq) and PAR-CLIP analyses have identified thousands of transcripts bound by LIN28A and LIN28B at a loop motif containing GGAGA and RGGSWG sequences, respectively, and have shown that targets consist mainly of 3'-UTR and protein-coding sequences in addition to the let-7 precursors (Figure 1.6 E). Some identified transcripts bound to LIN28B include IGF2 (Polesskaya et al., 2007), (Qiu et al., 2009), Cyclins and CDK4 (Xu et al., 2009a), HMGA1 (Peng et al., 2011), and LIN28B itself (Graf et al., 2013; Hafner et al., 2013). Notably, most binding transcripts encoded RNA transcriptional regulators, as well as RNA processing and splicing factors, and are positively regulated when bound to LIN28 (Wilbert et al., 2012; Graf et al., 2013; Hafner et al., 2013). Furthermore, LIN28 interaction with RNA helicase A (RHA) supports a function in translational regulation in association with ribosomes (Balzer and Moss, 2007; Peng et al., 2011; Jin et al., 2011). As a result, LIN28 paralogs can bind a plethora of targets and affect their abundance and translation, and it may be expected that the binding partners involved in transformation are specific to the cellular context in which LIN28 is expressed.

Based on these studies, it appears that the role of the RBPs LIN28 in tumorigenesis is not limited to their interaction with let-7 miRNA precursors and further investigation of their implication in cancer requires the inclusion of the post-transcriptional effects of the paralogs on bound protein-coding transcripts.

1.4.2 The IMP family of RBPs

The IMP family of RBPs is composed of three members, namely IMP1, IMP2 and IMP3. All three IMPs share a similar structure, composed of two RRM domains at the N-terminal end and four KH domains in the C-terminal region, a similarity that is translated into shared functions of these three RBPs (Nielsen et al., 1999). IMP1 and IMP3 share the highest homology in the family, with 73% amino acid sequence identity. KH3/4 seem to regulate mRNA recognition, whereas KH1/2 and the RRM domains contribute to stabilize mRNA binding (Bell et al., 2013). In addition, the presence of repeated KH binding sites increases binding affinity and specificity, as the KH domains allow recognition of only short segments of mRNA (Chao et al., 2010). Recently,

KH domains in IMPs were reported to identify the N⁶-methyladenosine (m⁶A) modification in mRNA, one of the most abundant post-transcriptional mRNA modifications (Huang et al., 2018).

The prolonged half-life of IMP-mRNA complexes reflects important binding affinity and stability, and suggests an essential role of IMPs in stocking or long-distance transport of target transcripts (Nielsen et al., 2004). Despite a similar structure, KH3/4 domains in IMPs recognize and bind distinct RNA consensus sequences (Schneider et al., 2019; Biswas et al., 2019). Nevertheless, enhanced CLIP analyses showed overlap in identified IMP targets (Conway et al., 2016). Moreover, knockdown of IMP1 in this study did not show dramatic changes of the transcriptional profile, suggesting a redundancy between IMPs. Altogether, IMPs appear to be involved in the regulation of many steps of mRNA maturation by forming mRNPs that control mRNA stability, export and fate and the large repertoire of targets places IMPs in the control of a large and complex mRNA network.

IMP1 is known to be strongly involved in localization of transcripts and regulates neural stem cell (NSC) differentiation and function (Nishino et al., 2013). In human pluripotent stem cells, IMP1 promotes cell survival and adhesion (Conway et al., 2016). Furthermore, IMP1 appears to be involved in metabolism and stem cell maintenance, as IMP1-deficient mice are smaller than normal littermates and display significantly impaired and delayed gut development (Hansen et al., 2004). Mechanistically, IMP1 can prevent miRNA silencing by sequestering target mRNAs in RISC-free granules, thus protecting transcripts from miRNA-mediated degradation, and participates in the transport of transcripts to their appropriate destination for translation initiation (Weidensdorfer et al., 2009; Müller et al., 2018). By preventing miRNA silencing of target transcripts, IMP1 may participate in the maintenance of an undifferentiated cell state.

IMP2 has been less deeply investigated than the other two paralogs, probably due to the fact that it is still detected in adult tissues, making its reexpression less likely to cause transformation. However, recent work has revealed that IMP2 may also function as an oncogene. Whereas IMP2 is involved in muscle cell motility (Boudoukha et al., 2010) and in brain development, where it is essential for the neural progenitor cell population (Degrauwe et al., 2016a), it is also required for CSC maintenance in GBM, where it regulates key metabolic pathways (Janiszewska et al., 2012). Implication of IMP2 in cellular metabolism is further supported by observations of IMP2-deficient mice. Homozygous deletion of IMP2 leads to a smaller phenotype, a decrease in adipocyte precursors, and resistance to obesity (Dai et al., 2015). Importantly, IMP2 binds to miRNA recognition elements (MREs) and consequently protects a wide range of transcripts

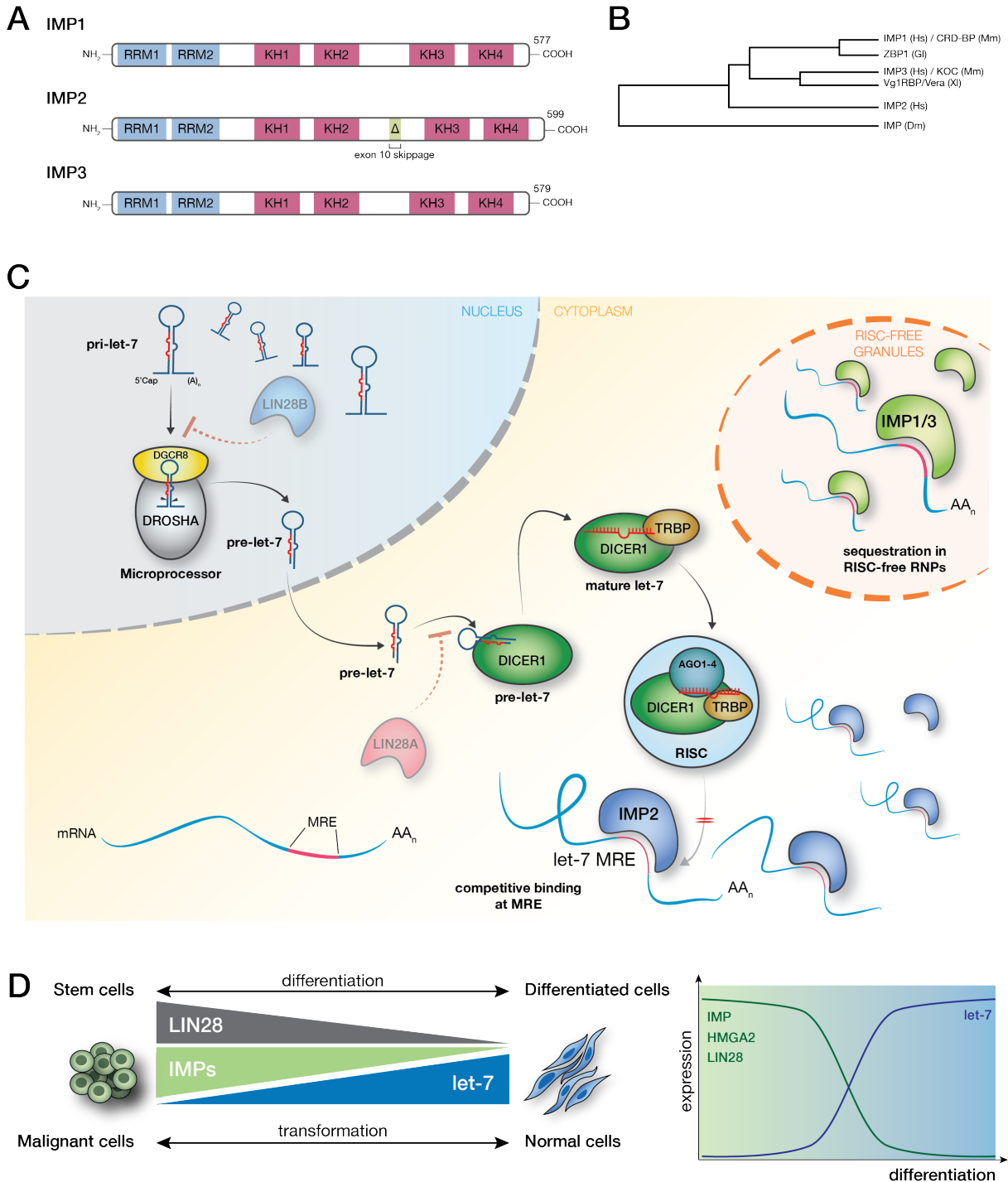


Figure 1.7: IMPs structure and mechanisms of action. (A) Schematic representation of the human IMP paralogs structure with two RRM domains followed by two pairs of KH domains. In IMP2, a splice variant where exon 10 is skipped generates an isoform named p62. The affected area is shown in green. Adapted from Bell et al. (2013). (B) Phylogenetic tree representing sequence homology of the IMP paralogs across species. Human IMP1 and IMP3 are most closely related, whereas no ortholog has been described for IMP2. *Hs*, Homo sapiens; *Mm*, *Mus musculus*; *XI*, *Xenopus laevis*; *Dm*, *Drosophila melanogaster*; *Gf*, *Gallus gallus*. Adapted from Christiansen et al. (2009). (C) Schematic representation of mechanisms of action of IMPs. IMP1 and IMP3 can recruit target transcripts inside RISC-free mRNPs, whereas IMP2 can competitively bind the let-7 miRNA recognition elements (MRE) in the 3'-UTR of target transcripts. Both mechanisms prevent let-7-mediated target degradation. LIN28A/B are included in the image, as they also regulate the let-7 pathway by inhibiting the let-7 maturation process. (D) Biological consequence of the IMP-let-7 balance. High IMP expression in undifferentiated cells prevents let-7-mediated decay, thereby conserving the expression of target transcripts, such as LIN28. As differentiation progresses, loss of IMPs restores let-7 activity, resulting in downregulation of IMPs and its targets, including LIN28 and HMGA2. In tumorigenesis, IMPs participate in driving cellular transformation to a malignant phenotype.

from let-7 mediated decay (Degrauwe et al., 2016a). Thus, IMP2 uses diverse mechanisms to promote and maintain a stem-like cell state.

In contrast, IMP3 has been widely studied in cancer (Bell et al., 2013). Similarly to IMP1, IMP3 was shown to sequester mRNA targets in RISC-free mRNP granules, thereby safeguarding mRNAs from degradation (Jønson et al., 2014). Evidence strongly suggests that IMP3 is implicated in increased tumor aggressiveness across many malignancies, including pancreatic, renal, urothelial, colorectal and hepatic cancers (Jeng et al., 2008; Schaeffer et al., 2010; Gong et al., 2014; Lederer et al., 2014). Consistent with this notion, IMP3 synergized with IMP1 to promote mesenchymal features and increase cell invasion (Lederer et al., 2014).

In physiological conditions, IMP1 and IMP3 are expressed exclusively in embryonic tissues. In contrast, IMP2 expression levels are high during development and further maintained into adulthood in some tissues (Degrauwe et al., 2016b). Despite distinct targets, all IMPs are involved in the control of mRNA turnover and transport. The implication of IMPs in the promotion of a stemness phenotype was proven in various malignancies, including breast, colorectal and hepatic carcinomas, as well as GBM (Degrauwe et al., 2016b) and is strongly supported by their ability to interfere with normal miRNA-mediated silencing. Particularly, IMPs protect their own transcripts from let-7 degradation, thereby forming a positive feedback loop that further potentiates IMP expression. While it is not yet clear if IMPs act coordinately or individually, their reactivation may underlie a key pathway essential for CSC maintenance.

1.5 Aim of the study

Our laboratory recently found that IMP2 preserves CSCs in GBM by protecting transcripts from let-7 degradation (Degrauwe et al., 2016a). To further explore the roles of IMP2 and let-7 pathways in GBM, I first attempted to reverse the CSC phenotype by re-establishing proper let-7 function. Additionally, PAR-CLIP data on CSC provided an extensive landscape of IMP2 targets. From this, we identified the lncRNA H19 as a potential candidate and we attempted to define its functional role in CSC maintenance. Lastly, given that LIN28 is often re-expressed in childhood cancers, that LIN28 and IMPs are commonly expressed together in tumor cells, and that both RBP families converge to regulate the let-7 miRNA pathway, I assessed possible redundancy between these various players in the pediatric context of EwS, in which dysregulation of let-7 miRNAs has been previously described and effectively targeted (De Vito et al., 2011, 2012; Cornaz-Buros et al., 2014).

Chapter 2

Glioblastoma

2.1 Introduction

2.1.1 Characteristics of GBM

Glioblastoma Multiforme (GBM) is the most common form of primary brain malignancy in adults, with an incidence of about 3 newly diagnosed cases per 100'000 per year and discrete male predominance. Prognosis for GBM is particularly dismal, as the median survival is 15 months with treatment and 3 months if left untreated, with a 5-year survival rate below 5% (Thakkar et al., 2014). Most cases of GBM occur between the ages 45 and 70. Typically, GBM patients present with neurological signs, including local neurological deficits, headache, and/or seizures, depending on the location and size of the tumor. Symptoms develop rather rapidly, appearing over a couple of days to a few weeks before diagnosis (Gladson et al., 2010). The clinical presentation of GBM is similar to that of any brain tumor or brain metastasis, prompting the patient to undergo brain magnetic resonance imaging (MRI) to identify the underlying lesion, followed by definite diagnosis based on analysis of tumor tissue obtained during surgical resection, or from localized brain biopsy (Figure 2.1).

The current standard of care includes maximal safe surgical resection as the first step in the management of high-grade gliomas. At this stage, brain MRI should be repeated to assess the extent of the resection, as GBM is a notoriously invasive tumor. Subsequently, the patient receives radiation therapy and chemotherapy, most commonly with temozolomide (TMZ), an alkylating agent that readily crosses the blood brain barrier (BBB). However, despite advances in treatment strategies and maintenance protocols, virtually all cases of GBM relapse, making this cancer largely incurable to this date. This is due to its strong invasive proclivity into the

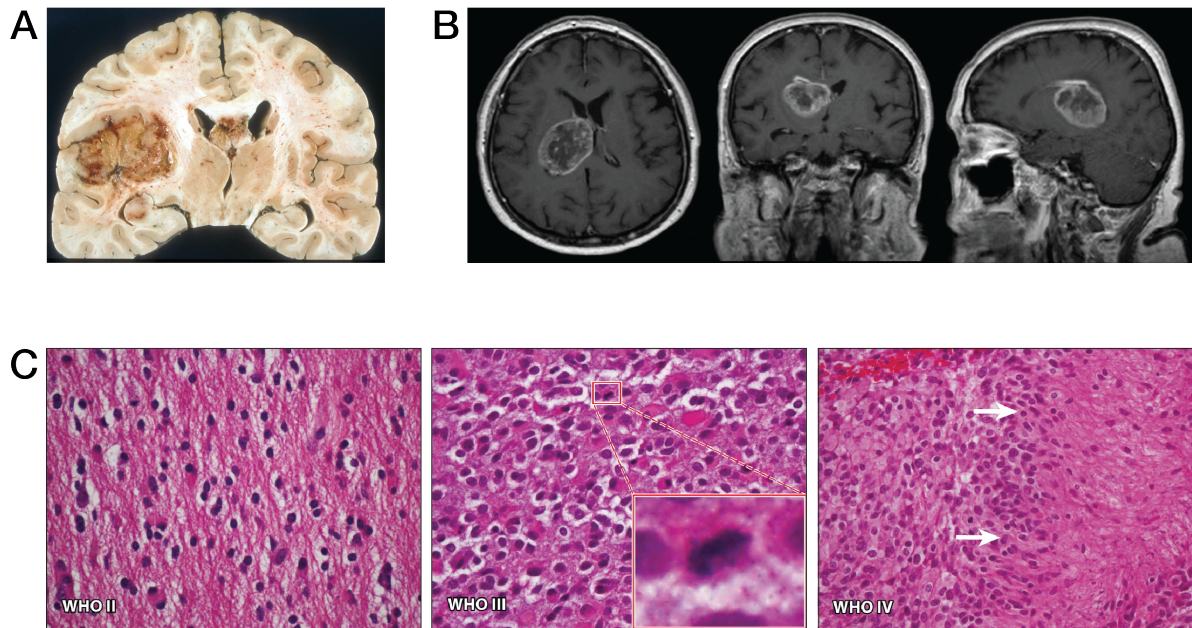


Figure 2.1: Macroscopic and microscopic morphology of GBM. (A) Gross appearance of GBM showing a hemorrhagic, necrotic and infiltrating mass. Image adapted from Wikimedia Commons under a CC BY-SA 4.0 license. (B) T1 MRI of the brain with contrast, showing a tumor in the right hemisphere with right lateral ventricle involvement, later confirmed as GBM by histopathology. From left to right: axial, coronal and sagittal views. Image adapted from Wikimedia Commons under a CC BY-SA 3.0 license. (C) Micrographs of gliomas grades II to IV. Increased mitotic activity is found in WHO Grade III gliomas (insert) and WHO grade IV/GBM tumors display pseudopalisading necrosis, the signature feature of GBM (arrows). Magnification x40. Adapted from Huse et al. (2013).

brain tissue, extensive ITH, and persistence of tumor-initiating cells (Auffinger et al., 2015).

GBM is the most aggressive form of astrocytoma, a family of tumors subdivided into four WHO grades, based on histological features, with increasing degrees of malignancy: grade I, pilocytic astrocytoma; grade II, diffuse astrocytoma; grade III, anaplastic astrocytoma; grade IV, GBM. In most cases (90-95%), GBM arises *de novo*, typically in patients aged 60 or more, and is therefore called primary GBM. Alternatively, in around 5% of cases, GBM can result from pre-existing grade II/III gliomas that transform into a more aggressive phenotype, and is thus termed secondary GBM, mainly in younger patients (Gladson et al., 2010). Although the age-adjusted prognosis is similar in primary and secondary onset GBM, this distinction bears considerable clinical significance for therapy, as it implies that different mechanisms govern GBM development, and, as a result, primary and secondary GBM display distinct molecular profiles (Ohgaki and Kleihues, 2005). The majority of GBMs involve the brain hemispheres, and, less commonly, secondary GBM can be found in the brain stem or the spinal cord.

Grade I gliomas are most common in children and bear a good prognosis due to their benign nature. Grade II gliomas are associated with a median survival of 5 to 8 years and display increased cellularity with nuclear atypia. Grade III gliomas display higher hypercellularity and atypia, increased mitosis, and bear a worse prognosis, with a 3-year median survival. The major

hallmarks that distinguish Grade IV GBM from lower-grade gliomas include the presence of extensive pseudopalisading necrosis within the tumor tissue and/or marked endothelial proliferation (Gladson et al., 2010) (Figure 2.1 C).

2.1.2 Glioma stem cells

The genetic heterogeneity of GBM has been long established (Shapiro et al., 1981), and the identification of a subpopulation of tumor-initiating cells in leukemia launched the quest for such cells in solid tumors, including the highly heterogeneous GBM. In 2003, Singh et al. identified a small subset of cells in pediatric brain tumors that shared some of the expected characteristics of CSCs, in that they mimicked the NSC phenotype, expressed stemness markers, namely CD133 and nestin, and were crucial for proliferation of the tumor *in vitro*. Final confirmation of the CSC model in brain tumors shortly followed, as the same group later confirmed reproduction of the tumor *in vivo* upon xenotransplantation of as few as 100 CD133⁺ cells, whereas as many as 10⁵ injected CD133⁻ cells failed to form a tumor (Singh et al., 2004). In parallel, another study further characterized tumor-initiating cells isolated from primary GBM samples and confirmed their ability to differentiate, proliferate and reproduce the tumor of origin after serial xenotransplantation (Galli et al., 2004). In GBM, the cells displaying CSC features are termed glioma stem cells (GSCs).

Successful identification of GSCs allows to better understand and determine potential key pathways that govern their emergence and maintenance, and that could potentially be targeted. Indeed, GSCs are known to be involved in the various processes that lead to therapeutic resistance and the resulting poor GBM prognosis: GSCs promote resistance to radiation (Bao et al., 2006) as well as chemoresistance and recurrence (Chen et al., 2012), in addition to neovascularization (Cheng et al., 2013) and invasion (Wakimoto et al., 2009). Thus, eradication of GSCs appears as an inevitable strategy toward achieving GBM cure. Efforts to better identify and permit robust isolation of GSCs to study these cells have been challenged by the lack of a unique cell surface marker specific for GSCs. Thus, using a combination of several surface markers to isolate GSCs seems to be the only alternative. This panel now includes CD133, SSEA1 and CD44 (Singh et al., 2004; Son et al., 2009; Anido et al., 2010), although their expression is heterogeneous among patients and can change as a result of microenvironmental cues (Dirkse et al., 2019). In addition to surface markers, detection of intracellular proteins offers a supplementary means to identify GSCs, as they express stemness genes such as *SOX2*, *OLIG2* and nestin, many of which

are also expressed in normal NSCs (Gimple et al., 2019).

In situ, GSCs have been identified in specialized GBM niches, all highly dependent on specific vascularization patterns. Brain tumor niches can present in three different constellations. First, the perivascular niches stimulate CSC proliferation around abnormal capillaries in the brain, where specific angiogenic signals are produced by CSCs, mainly VEGF, and survival factors are in turn produced by endothelial cell, thus promoting CSCs propagation (Calabrese et al., 2007). Furthermore, increased capillary leakiness facilitates entry of immune cells, including tumor-infiltrating macrophages, monocytes, and neutrophils, that globally participate in immune-suppressive functions and facilitate tumor propagation (Hambardzumyan and Bergers, 2015). Second, GSCs also reside in hypoxic niches. Indeed, poor perfusion is a characteristic trait of GBM and confers supplementary stemness traits to GSCs, via induction of hypoxia inducible factors (HIFs) (Heddleston et al., 2009; Auffinger et al., 2015). These areas of hypoxia further develop into necrotic regions surrounded by pseudopalisading tumor cells, the signature histological feature of GBM. These cells migrate, resulting in extension of necrosis and of inflammation. Third, the invasive niche implicates a dialog between GSCs and the available surrounding astrocytes and microglia to actively invade the normal brain parenchyma along normal vascular highways, with activation of the EMT-like program within the GSCs (Hambardzumyan and Bergers, 2015). These observations reveal the multiplicity and divergence on which GSCs can rely for their survival and progression. Moreover, the tumor environment can substantially reshape the cells and is also responsible for GSC heterogeneity and plasticity (Dirkse et al., 2019).

2.1.3 GBM heterogeneity

As the name “Glioblastoma Multiforme” implies, Bailey and Cushing (1926) noticed early on already that this aggressive brain tumor can take various shapes. That this heterogeneity is in addition extensively encountered at the molecular level could not have been predicted, and has been largely reported since. Precisely characterising and understanding the mutational landscape of GBM increases the likelihood of finding culprit pathways crucial for GSC maintenance, and whose targeting may represent efficient therapeutic strategies. Thanks to large-scale DNA and RNA analyses, many recurrent genetic alterations, such as point mutations, genomic copy number alterations, epigenetic modifications, as well as commonly disrupted pathways, have been identified in GBM during the last two decades. Particularly, highly prevalent mutations or copy number alterations of *TP53*, *PTEN*, *RB1*, *EGFR* and *PI3K*, among others, helped highlight three

main pathways that are deregulated in virtually all GBM cases, namely the RTK/RAS/PI3K pathway, alongside the p53 and the Rb tumor suppressors pathways (The Cancer Genome Atlas Research Network et al., 2008; Parsons et al., 2008) (Figure 2.2 A).

Moreover, distinct sets of mutations are found in primary GBM and secondary GBM, based on the knowledge collected from sequencing of lower-grade gliomas. Indeed, although they likely originate from the same progenitor cell, a NSC, their transformation processes follow different pathways (Figure 2.2 B). By sequencing a greater number of genes in a smaller pool of GBM samples, Parsons et al. (2008) found recurrent mutations in *IDH1*, a gene involved in isocitrate oxidation. Whereas approximately 10% of primary GBM harbor mutated *IDH1*, a striking majority of secondary GBM carry a *IDH1* mutant. This is also the case in many grade II and III gliomas (Dunn et al., 2012), and survival analysis revealed that mutated *IDH1* is associated with improved prognosis (Parsons et al., 2008; Yan et al., 2009). Consequently, GBM is characterized as either *IDH1*-wild-type or *IDH1*-mutant, a feature now included in the routine diagnostic evaluation of GBM (Louis et al., 2016).

Among epigenetic alterations found in a subset of GBM, the methylation status of O⁶-methylguanine-DNA methyltransferase (*MGMT*), which encodes a DNA repair enzyme that removes alkyl groups from guanine bases in DNA, constitutes an essential prognostic factor. TMZ is a widely used alkylating agent in GBM chemotherapy that causes DNA damage leading to apoptosis. Methylation of the *MGMT* promoter, found in about half of GBM patients, represses *MGMT* transcription, thereby preventing the target cell from removing TMZ-established alkyl groups and repairing DNA. This ultimately leads to apoptotic cell death, as DNA repair is hindered, and improves patient response to treatment. The methylation status of the *MGMT* promoter has therefore become a key prediction marker for patient response to alkylating agents. As a result, a methylated status identifies the patients who benefit most from TMZ therapy regimens and correlates with better survival rates (Hegi et al., 2005).

The accumulated data from comprehensive tumor profiling has prompted researchers to implement a new taxonomy to subdivide GBM, that integrates the nature and frequency of genetic alterations across samples. In a pivotal paper, using information from 200 sequenced tumors taken from The Cancer Genome Atlas (TCGA) database, Verhaak et al. (2010) proposed four new categories based on the mutational profiles of GBM samples and named in accordance with previously identified transcriptional signatures (Phillips et al., 2006): classical, mesenchymal, proneural and neural. This subclassification was strengthened with further support from

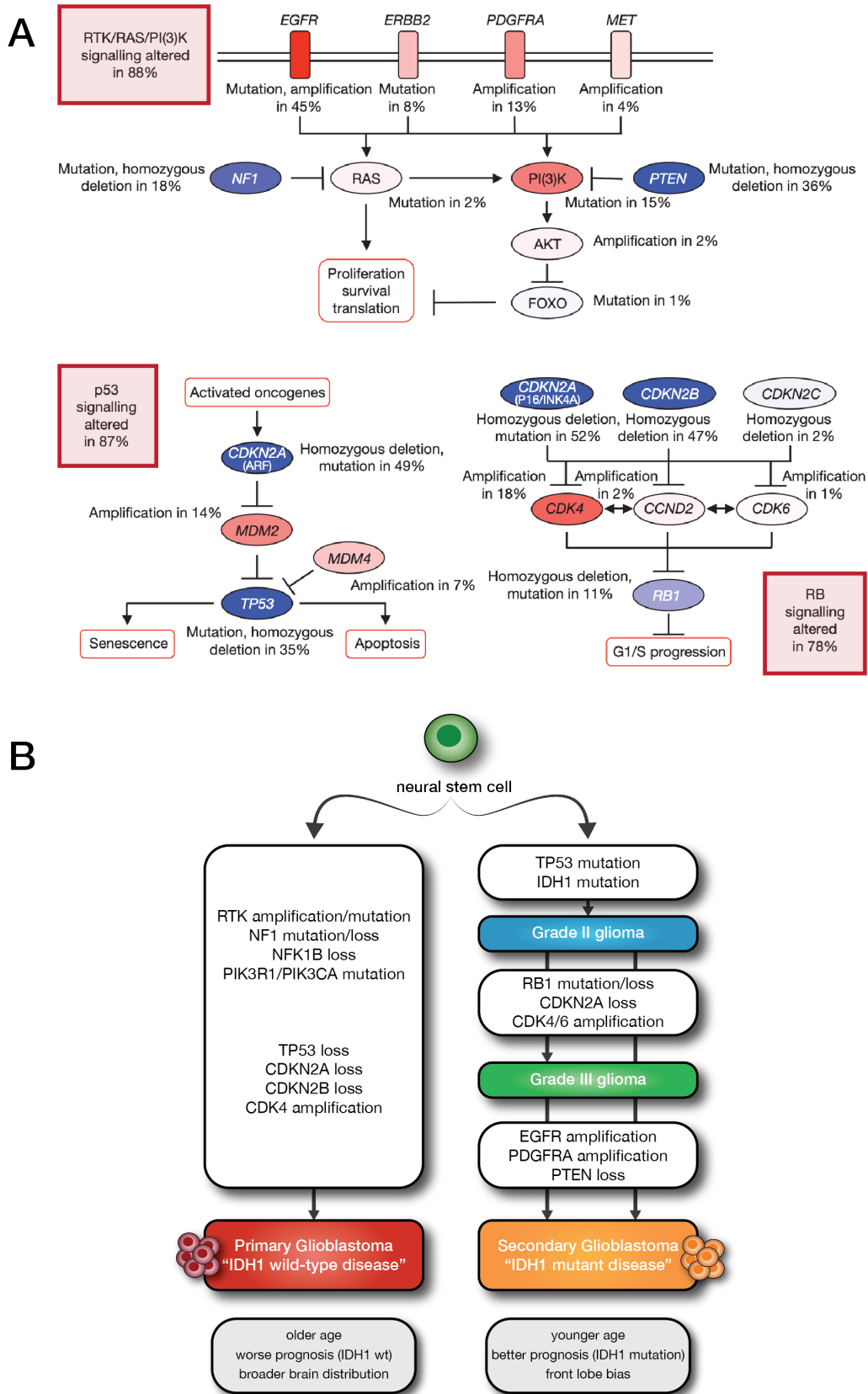


Figure 2.2: Genomic alterations underlying glioblastoma tumorigenesis. (A) Critical altered pathways in GBM and the frequency of mutation or amplification. Adapted from The Cancer Genome Atlas Research Network et al. (2008). (B) Common alterations found in primary or secondary onset GBM. Primary onset GBM is mainly associated with a IDH1 wild-type phenotype, and poorer prognosis (95% of cases). On the other hand, secondary GBM develops from lower grade GBM, either from grade II progressing to grade III glioma, or directly from grade II glioma, with accumulation of genetic aberrations. It is associated with mutated IDH1 and bears a better prognosis (5% of cases). Adapted from Dunn et al. (2012).

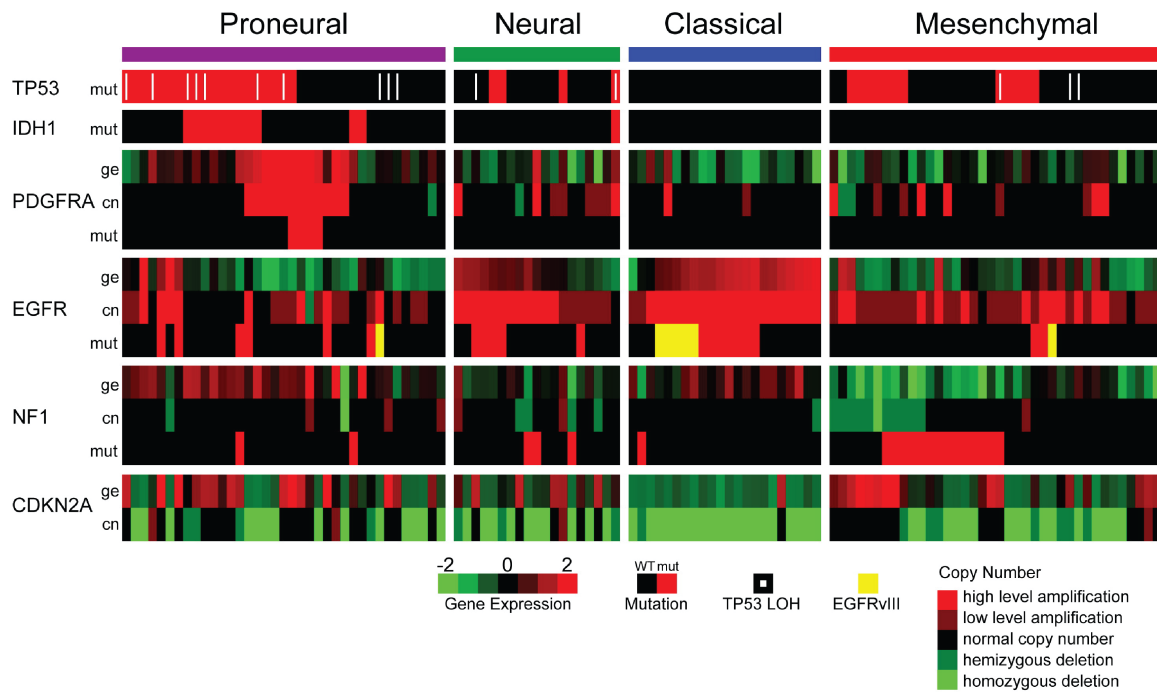


Figure 2.3: Gene expression and genomic alterations across the four glioblastoma subtypes. Gene expression data (202 samples) and mutation and copy number data (116 samples) from the TCGA dataset for frequently mutated genes. ge, gene expression; cn, copy numbers; mut, mutations. Reproduced from Verhaak et al. (2010).

publicly available independent GBM datasets. Each subtype harbors specific signature genetic alterations (Figure 2.3), and correlates with patient survival: proneural tumors have the best prognosis, with an expression profile that resembles that of normal brain cells and differentiating neurons, as opposed to the mesenchymal subtype, which displays similarities to mesenchymal tissue and is associated with a more severe prognosis.

Recently, single-cell sequencing has revealed additional heterogeneity within the tumor itself, as subpopulations of cells with different expression profiles can co-exist within the tumor bulk (Patel et al., 2014). GSCs, particularly, primarily cluster to the proneural and mesenchymal subtypes. Interestingly, the majority of recurrent GBM cases display a change in phenotype with a shift toward a mesenchymal signature (Phillips et al., 2006; Verhaak et al., 2010), which is supported by the identification of C/EBP β and STAT3 transcription factors as major mediators of the mesenchymal phenotype and of tumor aggressiveness (Carro et al., 2010). In line with this, proneural GSCs have a propensity to shift toward a mesenchymal signature, and subsequently gain resistance and other aggressive features (Bhat et al., 2013; Minata et al., 2019). Moreover, analysis of initial and recurrent GBM showed that the tumors are not closely related, but share a rather distant ancestor: relapsed tumors display a distinct set of mutations (Wang et al., 2016), and initial TMZ treatment may set the grounds for clonal evolution, by inducing new mutations and applying selective pressure on GSCs (Johnson et al., 2014).

Still, deeper single-cell approaches noted that GBM cells share four main transcriptional signatures and can transition from one signature to the other, under the influence of some of the mutated genes shown in Figure 2.3 (Neftel et al., 2019). Another study showed that in spite of distinct inter- and intratumoral mutational profiles among GBM cells, the infiltrating cells on the tumor front share the expression of common signature genes (Darmanis et al., 2017). Thus, while the complexity of GBM relies on extensively heterogeneous cell populations, profiling and clustering of cells has revealed additional signatures in the most aggressive cells. Hypothetically, because such signatures appear in the most invasive cells following exhaustive treatment attempts, they may reflect the ideal profile acquired by an optimally aggressive cell under the strongest selective pressures, to which malignant GBM cells may ultimately converge, as hypothesized and modelled in breast cancer (Lloyd et al., 2016).

2.1.4 The GBM cell of origin

Debate surrounding the cell of origin of GBM long opposed the notions of GBM arising from deregulated NSCs or from a transformed dedifferentiated astrocyte. In the last decade, a significant body of evidence has advocated NSCs as the cell of origin of GBM, mainly based on observations from engineered mouse models. Indeed, the various known GBM genetic mutations successfully produced GBM-like tumors *in vivo* when expressed in neural progenitor cells, but not in mesenchymal cells (Gimple et al., 2019). More compellingly, in about half of the patients, NSCs situated in the subventricular zone (SVZ) of GBM patients share common mutations with the matching tumor tissue, thus providing strong support for NSCs as the GBM cell of origin (Lee et al., 2018).

2.1.5 *In vivo* models of GBM

Since the identification of GSCs, various approaches have been used to study these cells, both *in vitro* and *in vivo*. Three types of *in vivo* models have been developed for neuro-oncology research: chemically induced, genetically engineered, including via viral induction, and xenograft models.

Chemically induced models, mainly in rats, rely on administration of a carcinogen locally into the brain, intravenously, orally, or through the placenta of pregnant rats. However, this approach may seem too artificial, as human cases of GBM are generally not associated with exposure to chemical agents. Another drawback is the inconsistency of tumor production in different species, suggesting host-dependent tumor initiation. Additionally, the lack of molecular data and the

uncontrolled genetic base causing transformation in these tumors questions the ability of the chemically induced model to reliably mimic the events leading to generation and evolution of GBM (Huszthy et al., 2012).

Several genetically engineered mouse models have been developed based on the various genetic alterations repeatedly found in GBM. Mouse strains bearing one or a combination of GBM mutations can effectively mimic the genetic alterations found in human tumors within the appropriate brain location and at the appropriate timepoint, avoiding early developmental stages. Such mouse models offer an efficient approach to study tumor initiation, and allow to include the appropriate environment for tumor growth, which helps investigate the role of the microenvironment in GBM progression. Moreover, recent application of the CRISPR-Cas9 genome editing system in mouse models has favored the introduction of specific genetic alterations in NSCs located in the SVZ, using nestin and GFAP promoters, which are activated in GSCs and astrocytes, respectively (Oldrini et al., 2018). Nevertheless, apart from the obvious time and cost limitations, murine tumors also have the disadvantage of failing to fully replicate the complexity of human GBM and the extent of spontaneous ITH found in humans.

Xenotransplantation of established GBM cell lines, either in the brain or in flanks of mice, allows easy and straightforward assessment of changes in tumorigenicity or response to treatment. However, as cell lines may have been extensively passaged *in vitro*, robustness of observations may be dubious on the account of potential genetic drift. Thus, using primary samples is key to maintaining tumor heterogeneity in study models, both between and within samples, based on the knowledge that GSCs adequately replicate the tumor of origin upon injection *in vivo*. Indeed, orthotopic injection of GSCs from patient-derived xenograft (PDX) into immunodeficient mice produces fast growing invasive tumors and accurately replicates the ITH observed in patients. PDX also offers a better approach compared to primary *in vitro* organoid sphere culture, taking into account the BBB, which mimics possible challenges for drug delivery, and the physiological environment in the brain, which provides a suitable microenvironment for GSC preservation. Moreover, it facilitates drug testing in different samples, as possible disparate responses between samples can be addressed as needed by further characterization of the samples to identify specific factors that may influence drug response. Therefore, as our lab has access to many well characterized patient-derived GBM samples, we favored the orthotopic PDX approach for the different *in vivo* studies presented later in this chapter.

2.1.6 Non-coding RNAs in GBM

Following tumor dissociation and surface marker selection, GSCs can be grown and expanded as organoid spheres, and their CSC properties must be confirmed. Importantly, there is compelling evidence highlighting the role of epigenetic pathways for the maintenance of the tumorigenic properties of GSCs, suggesting that the superimposed effects of genetic alterations and epigenetic modulation work together to support GSC aggressiveness (Stricker et al., 2013; Rheinbay et al., 2013; Suvà et al., 2014; Flavahan et al., 2016). Indeed, GSCs require specific serum-free culture conditions and the presence of distinct growth factors to proliferate and maintain their properties (Lee et al., 2006). Upon exposure to serum in the culture medium, GSCs lose their tumorigenic potential and mimic the more differentiated tumor bulk, thus profoundly changing the cell identity (Degrauwe et al., 2016a). It is currently unknown why exposure to serum leads to such profound changes in the cell behavior and expression profile, but this undeniably reiterates the notion that epigenetic changes are a key component of cell plasticity and maintenance of the stem cell phenotype in GSCs. Identifying the epigenetic pathways involved in stemness maintenance could thereby help find interesting approaches to eradicate the tumor effectively. The central role of ncRNAs as regulators of broad gene expression networks places these transcripts under the spotlight as potentially important mediators of the identity of GSCs.

As mentioned previously, the involvement of miRNAs in oncogenesis is now widely recognized. In GBM particularly, miRNA microarrays have uncovered patterns of miRNA expression that are specific to GSCs, with both tumor-initiating and tumor suppressive miRNAs. Indeed, several common up-regulated miRNAs can target transcripts involved in the p53 tumor suppressive pathway, thereby appearing to function as oncomiRs. Conversely, identified down-regulated miRNAs mainly target transcripts of proteins involved in the IGF signaling pathway, involved in cellular growth and proliferation (Lang et al., 2012) (Figure 2.4). In all these studies, Targetscan has provided a valuable tool in bringing light into the pathways downstream of miRNAs. Indeed, this database regroups the seed region of miRNAs and identifies possible binding sites in the 3'UTR of target mRNAs, allowing to further test this interaction in the cancer model of interest (Agarwal et al., 2015). For example, miR-10b, which is strongly over-expressed in GSCs, was found to repress several targets in cell cycle and apoptotic regulating pathways in GBM and its inhibition can block tumor growth *in vivo* (Gabriely et al., 2011). Similarly, miR-21 was found to downregulate IGFBP3, thereby stimulating the IGF pathway and promoting GBM growth (Yang et al., 2014). On the other hand, miR-340 is down-regulated in GSCs and its reactivation

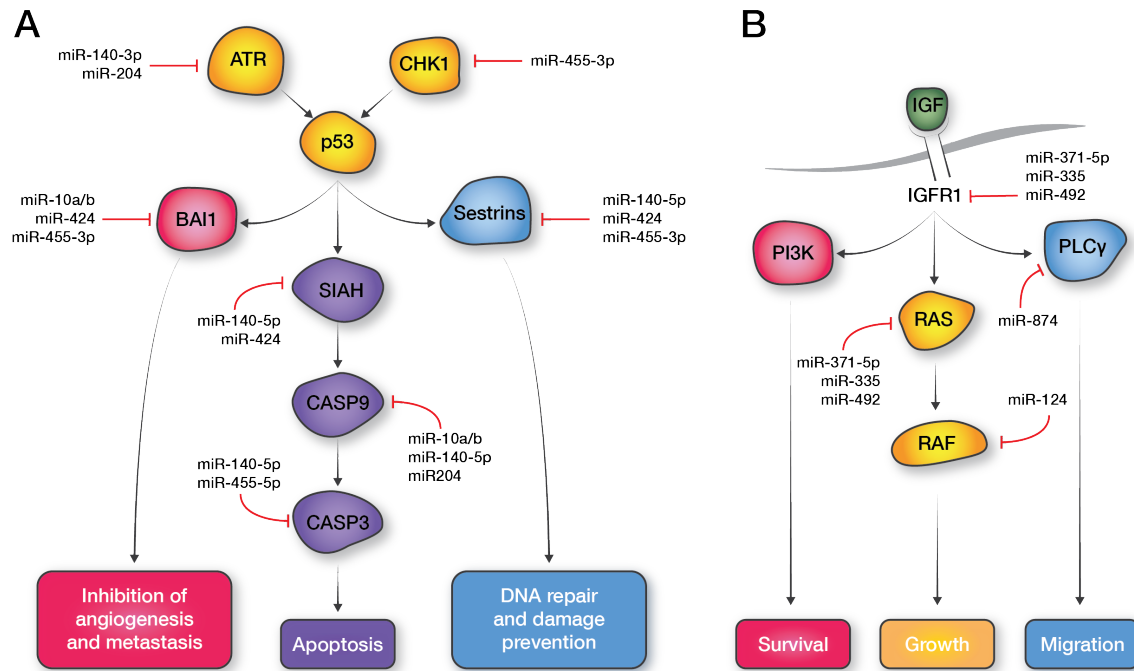


Figure 2.4: Dysregulated miRNAs and targeted pathways in GBM. (A) Up-regulated miRNAs targeting the p53 signaling cascade, thereby down-regulating key factors involved in inhibition of angiogenesis and metastasis, apoptosis and DNA repair pathways. (B) Down-regulated miRNAs targeting the IGF pathway. Failure to inhibit this cascade promotes survival, growth and migration. Adapted from Lang et al. (2012).

induces cell differentiation and decreased invasion and proliferation by restoring repression of a serine/ threonine kinase (Huang et al., 2015).

These observations lead to a central question: what are the mechanisms contributing to the observed changes in the miRNA repertoire and their impaired function? It was first reported that the loci of many dysregulated miRNAs are often located at fragile sites, prone to genetic aberrations (Calin et al., 2004). Interestingly though, the genes encoding the miRNAs whose expression change the most in GBM are not located in such regions, suggesting epigenetic regulation of their expression in tumor cells, either at the transcriptional level, or post-transcriptionally (Ciafre et al., 2005). Little is known about the exact mechanisms responsible for shifting miRNA expression in malignant cells, and this issue needs to be addressed to better exploit the mechanisms in place that regulate the miRNA profile proper to GSCs.

As exemplified by the important impact of the *MGMT* promoter methylation, the DNA methylome can strongly impact the cell machinery and significantly alter the transcriptome. Thus, it is likely involved, at least in part, in the silencing of tumor-suppressive miRNAs. Expression of various TFs may also influence transcription of miRNAs, and impaired miRNA maturation also contributes to malignant transformation (Kumar et al., 2007). In particular, function of miRNAs of the let-7 family is disrupted post-transcriptionally in GSCs, as they are actively

transcribed in GSCs, but their target transcripts, such as *HMGA2* and *IMP2*, do not undergo silencing or degradation (Degrauwe et al., 2016a). Therefore, restoring let-7 function in GSCs could constitute a potentially attractive therapeutic approach to abrogate the stemness mechanisms in place.

In the projects presented here, we first aimed to reverse the stemness phenotype of GSCs by attempting to increase let-7 levels, which may restore their tumor suppressive function. Next, we explored another post-transcriptional pathway involved in let-7 regulation, by investigating the role of H19 in GSCs, a lncRNA that can sequester let-7 miRNAs.

2.2 Targeting glioma stem cells using a small molecule

2.2.1 Background

Expression of let-7 miRNA family is decreased in many tumor types, and global changes in the miRNA repertoire are widely associated with maintenance of stemness features. However, no significant difference in let-7 expression is found between the tumorigenic neurospheres and the more differentiated adherent GBM-derived cells. Nevertheless, levels of let-7 target mRNAs are significantly higher in GSCs than in adherent GBM cells, despite the lack of LIN28B expression, which is a common post-maturation repressor of let-7 miRNAs (Degrauwe et al., 2016a). Previous work from the lab has shown that let-7 target silencing in GSCs is prevented by IMP2, an RBP essential for GSC survival (Janiszewska et al., 2012). Indeed, IMP2 binds let-7 mRNA targets and protects them from let-7 mediated decay, thereby contributing to GSC maintenance (Degrauwe et al., 2016a).

In EwS, miRNA maturation was found to be disrupted through partial reversible repression of TRBP2 activity in CSCs, causing downregulation of miRNA expression and boosting cell tumorigenicity (De Vito et al., 2012). Stimulation of TRBP2, an integral component of a DICER complex involved in miRNA maturation, by the fluoroquinolone enoxacin, a well tolerated fluoroquinolone used in the treatment of urinary tract infections, showed significant upregulation of miRNAs, restoring the cell miRNA repertoire (Shan et al., 2008; Melo and Esteller, 2011). Previously, our lab showed that enoxacin in combination with doxorubicin, a chemotherapeutic agent commonly used in current EwS treatment, could markedly reduce tumorigenicity of EwS in xenotransplanted mice and improve their survival (Cornaz-Buros et al., 2014).

Based on the data generated with EwS, and having a drug in our hands that showed significant

reduction of EwS tumorigenicity, we were prompted to test whether this small molecule could also be effective in other tumors with deregulated miRNA function. As opposed to findings in EwS, the let-7 miRNA expression levels in GSCs are similar to those in their non-tumorigenic counterparts (Degrauwe et al., 2016a). However, increasing the activity of TRBP2 could lead to increased expression of these miRNAs, thus overriding the regulatory effect of IMP2 in GSCs. For this reason, GBM appears as an interesting candidate to assess the possible application of enoxacin to other tumor types as a means to target CSCs that present a deregulated miRNA expression profile. By increasing mature miRNA levels in GSCs, target mRNA silencing may be restored, shifting cells to a more differentiated state and rendering them more sensitive to therapy.

Here, we assessed the efficacy of enoxacin in primary GSCs as a means to decrease the tumorigenic potential of these cells, both in *in vitro* and *in vivo* settings. To potentiate its efficacy, we considered the possibility of using enoxacin in combination with TMZ in the treatment of GBM.

2.2.2 Results

Enoxacin inhibits GSC organoid growth *in vitro*

We first tested sensitivity to enoxacin of five GBM samples obtained from patient tumors, namely MGH 4, 8, 26, 28 and 31, which were isolated following tumor resection and maintained in culture in serum-free conditions as organoid sphere suspensions (Rheinbay et al., 2013; Wakimoto et al., 2011; Patel et al., 2014; Suvà et al., 2014). To assess the effects of enoxacin on GSC cell clonogenicity, single-cell clonogenic assays were performed in organoid culture medium supplemented with different concentrations of enoxacin (10 $\mu\text{g}/\text{mL}$ or 40 $\mu\text{g}/\text{mL}$), and compared to a control condition containing the maximum equivalent volume of 20 mM NaOH. As MGH8S (S, organoid spheres) was more difficult to grow and did not show any organoid growth when plated at low density, even in control conditions, we plated cells from this sample at a higher density of 25 cells per well. Overall, we observed a general decrease and inhibition of clonogenicity in the presence of enoxacin, which was concentration-dependent for all samples (Figure 2.5 A). Sphere formation assays were performed with the same medium conditions and showed overall concentration-dependent organoid growth inhibition in all primary GBM samples tested (Figure 2.5 B).

Characterization of GSC expression profile after incubation with enoxacin

Based on the fact that enoxacin increases affinity of TRBP2 for miRNAs leading to increased miRNA maturation, we looked at the miRNA expression profile of cells after one week of exposure to enoxacin or control medium. Specifically, we first checked whether levels of the let-7 family members were increased using quantitative real-time PCR (qRT-PCR), as these miRNAs are known to be key players in stemness regulation. We also looked at expression levels of miR-143 and miR-145, as this cluster of miRNAs has been shown to be downregulated in GSCs and represses essential transcription factors involved in embryonic stem cell maintenance (Lee et al., 2013; Xu et al., 2009b). MGH4S tends to show an increase in miRNAs at low enoxacin concentrations, whereas MGH8S displays an increase in miRNAs in response to enoxacin in a concentration-dependent manner.

In order to confirm that loss of clonogenicity in cells was linked to increased miRNA levels after enoxacin incubation, we compared the expression levels of various miRNA targets. Contrary to what we expected, transcript levels of miRNA targets, including IMP2, HMGA paralogs and RRM2, were not negatively regulated but instead remained stable or were increased upon drug exposure (Figure 2.5 D).

Analysis of protein expression in MGH28S following exposure to enoxacin confirmed that TRBP2 expression was unaffected, as expected from previous work (De Vito et al., 2012). Also, expression of the let-7 target transcript IMP2 remained unchanged. However, HMGA2 expression was discreetly lower in cells treated with higher doses of enoxacin. Expression of stemness genes such as *SOX2*, which are downregulated in the presence of miR-145, remained unchanged after treatment (Figure 2.5 E). Thus, we need to further explore the mechanisms that cause enoxacin to induce the reduced spherogenicity of organoid-derived cells observed *in vitro*.

Assessment the effect of enoxacin *in vivo*

Upon observing the effect of enoxacin on GSC clonogenicity *in vitro*, we interrogated the impact of enoxacin treatment on GSC tumorigenicity *in vivo*. We injected 15'000 MGH4S or 10'000 MGH28S cells into the brains of NOD-SCID gamma mice and allowed the tumors to engraft for four weeks, after which mice were divided into four groups (five mice per group), and treated either with a control 20 % DMSO solution, enoxacin alone (50 mg/kg/day), TMZ alone (40 mg/kg/day), or a combination of both enoxacin and TMZ, for a total period of three weeks with daily intraperitoneal injections (five injections per week). At the end of the treatment,

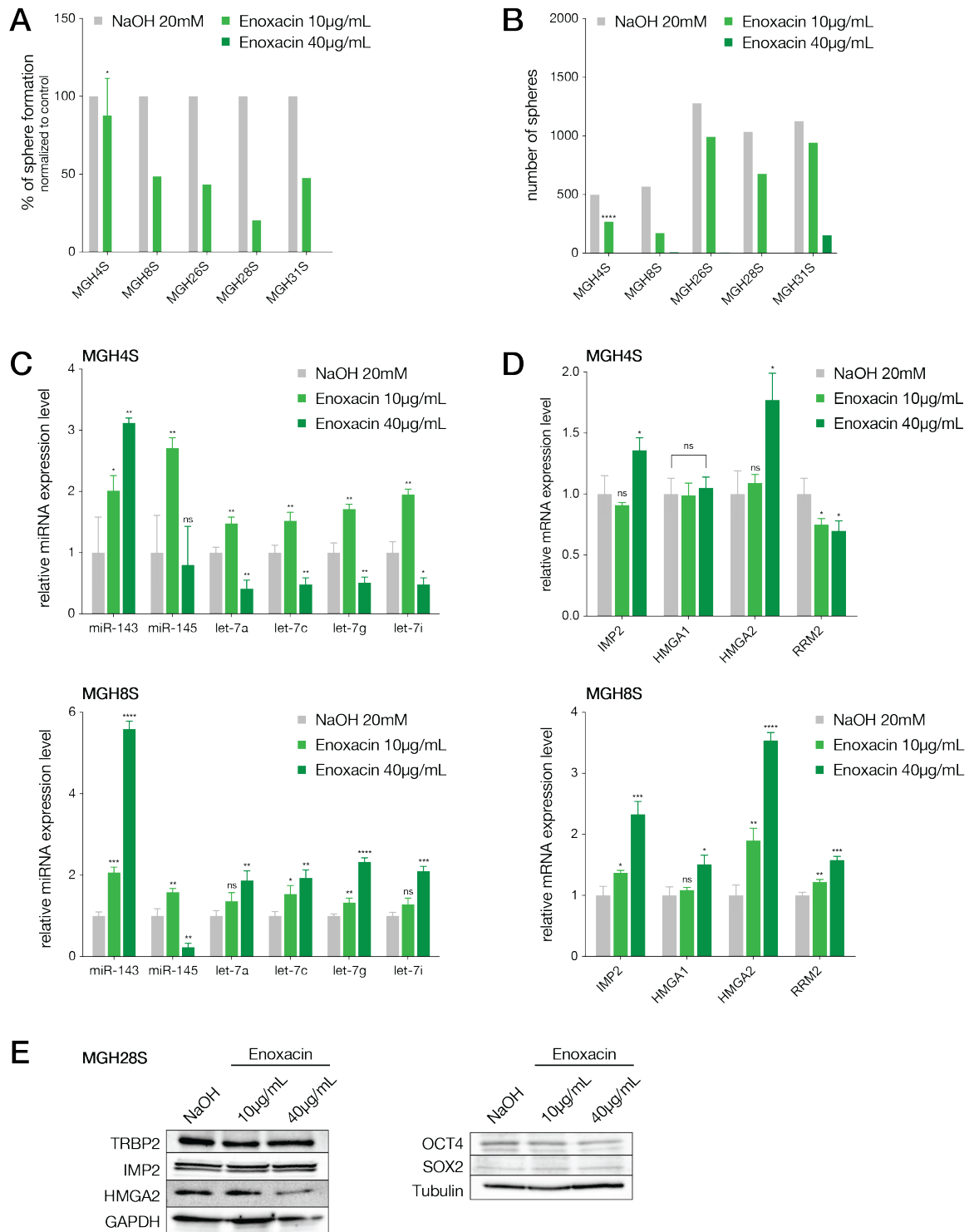


Figure 2.5: Effects of enoxacin on GBM organoids *in vitro*. (A) Clonogenic assays using single cells (MGH4S, MGH26S, MGH28S, MGH31S) or 25 cells (MGH8S) per well. Results are shown as percentage of organoid formation after three weeks in control medium containing NaOH 20 mM (reference value), or in medium supplemented with enoxacin (10 µg/mL or 40 µg/mL). One-way ANOVA was used for statistical analysis. (B) Sphere formation assay. Results are shown as the total number of spheres counted in each 96-well plate after three weeks in control medium with NaOH 20 mM, or in medium supplemented with enoxacin (10 µg/mL or 40 µg/mL). One-way ANOVA was used for statistical analysis. (C) Expression of miRNA in tumors MGH4S and MGH8S after enoxacin exposure for seven days, assessed by qRT-PCR, normalized to control medium containing NaOH 20 mM. Data are presented as mean ± SD. Two-way ANOVA was used for statistical analysis. (D) Expression of let-7 mRNA targets in tumors MGH4S and MGH8S after enoxacin exposure for seven days, assessed by qRT-PCR, normalized to control medium containing NaOH 20 mM. Data are presented as mean ± SD. Two-way ANOVA was used for statistical analysis. (E) Western blot of MGH28S in control (NaOH 20 mM) or enoxacin-containing medium after seven days. Tubulin and GAPDH were used as loading controls. * $P < .05$, ** $P < .01$, *** $P < .001$, **** $P < .0001$.

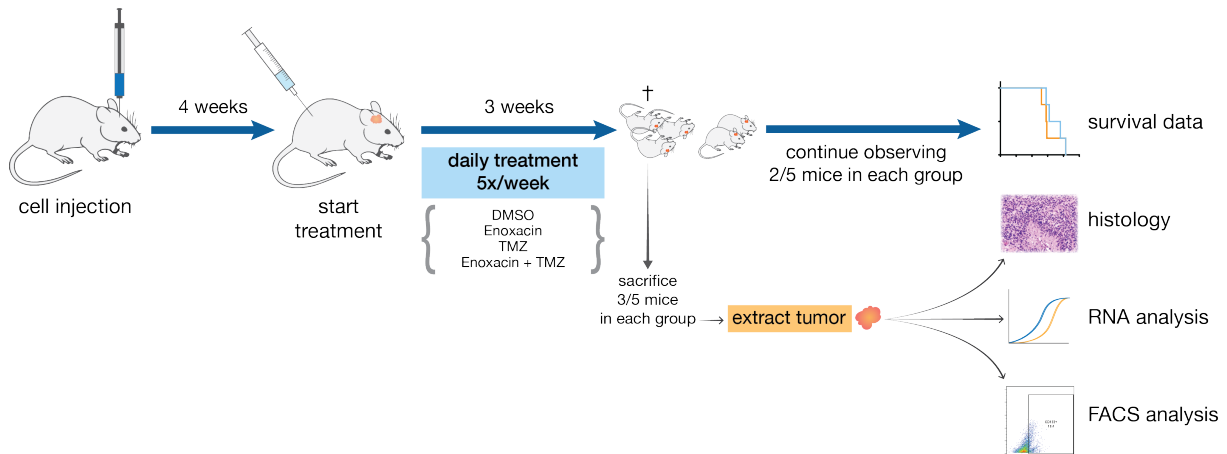


Figure 2.6: Experimental design for *in vivo* drug testing. Treatment was initiated four weeks following orthotopic injection of primary GBM. Mice were separated into four groups and underwent four different treatment regimens for three weeks: DMSO as a control, enoxacin, TMZ, or combination of enoxacin and TMZ. Following treatment, three mice per group would be randomly chosen for tumor extraction and immediate subsequent analysis, while two other mice would be kept for a first estimation for survival.

three mice were sacrificed. Brain tumor tissue was then extracted for histological analysis, RNA extraction and fluorescence-activated cell sorting (FACS) analysis for detection of CD133⁺ cells. The two remaining mice were left for first estimative survival data (Figure 2.6).

Mice from the control group and the enoxacin treatment group had to be sacrificed before the end of the therapy, as they started exhibiting signs of tumor growth before the scheduled date of euthanasia. Brain autopsy confirmed the presence of a tumor in these mice. Mice from the TMZ and combination groups did not exhibit any symptoms at the time of sacrifice and no tumor was visible upon brain dissection. Overall, survival of mice in the control group was similar to that in the group treated with enoxacin. In contrast, survival of mice treated with TMZ or combination therapy was significantly improved (Figure 2.7 A).

We proceeded to tumor dissociation and used flow cytometry to assess the proportion of CD133⁺ cells within the tumor bulk, and to determine whether tumors treated with enoxacin, alone or in combination, may display a reduced proportion of CD133⁺ cells. Enoxacin treatment caused an important decrease in CD133⁺ cells from MGH28S-derived xenografts, but displayed no advantage when used in combination with TMZ compared to treatment with TMZ alone. However, the absolute number of cells sorted from enoxacin-treated MGH28S xenograft was notably lower than in other samples (data not shown). In MGH4S xenografts, control-treated samples showed low initial numbers of CD133⁺ cells. The proportion of GSC-like cells was increased in the enoxacin and/or TMZ treated samples. This result contradicted our hypothesis, especially as TMZ-treated samples, alone or in combination, showed no visible tumor upon dissection, so that we went on to perform analysis from brain parenchyma located near the area

of tumor cell injection. Therefore, samples from these groups possibly consisted essentially of mouse cells, while the antibody used was directed against human CD133 (Figure 2.7 B and C).

According to the CSC paradigm and current definitions, GSCs that are isolated based on expression of cell surface markers such as CD133 are able to recreate organoids *in vitro* (Singh et al., 2003). In order to confirm our flow cytometry results, we kept a fraction of the cells extracted from MGH4S-derived brain tumors from all four treatment conditions, to assess the clonogenic potential of xenograft-derived cells. After 10 days of culture in neurosphere medium, only the cells from control or enoxacin treated xenografts continued to proliferate, while those treated with TMZ, alone or in combination, showed no signs of growth (Figure 2.7 E). Thus, whereas TMZ seemed to have successfully eradicated GSCs from the tumor, enoxacin appears to have not impacted GSC survival and maintenance *in vivo*.

Exposure of organoids derived from xenografts to enoxacin after treatment

We assessed whether the effect previously seen *in vitro* would still be seen on organoids derived from the xenografts, which would suggest the limited effect of enoxacin *in vivo* was possibly due to the delivery method of enoxacin treatment. We repeated sphere formation assay on cells from xenografts treated with DMSO or enoxacin alone. Surprisingly, lower concentration of enoxacin (10 $\mu\text{g}/\text{mL}$) had no effect on organoid formation this time, whereas cell proliferation was completely suppressed upon exposure to higher concentrations of enoxacin (40 $\mu\text{g}/\text{mL}$) (Figure 2.7 D).

Testing toxicity of enoxacin on GBM-derived adherent cells

Based on our observations, enoxacin may in fact exhibit a general toxicity to cells that leads to the inhibition of clonogenicity observed in our first set of experiments *in vitro* (Figure 2.5). To test this, we compared proliferation of spheroids and GBM-derived adherent cells in the presence of enoxacin at different concentrations. Because miRNA pathways are restored in the non-tumor-initiating adherent GBM-derived cells, the TRBP2-mediated effect of enoxacin is expected to have little to no effect on adherent cell proliferation. Surprisingly, while there was no decrease in cell proliferation at lower doses, proliferation seemed to be similarly impaired in both spheroids and adherent cells with higher levels of enoxacin, suggesting that enoxacin does not affect tumor initiating GBM cells specifically. Therefore, the decrease of clonogenicity in organoids detected initially may have resulted from general toxicity of the drug at higher doses (Figure 2.8).

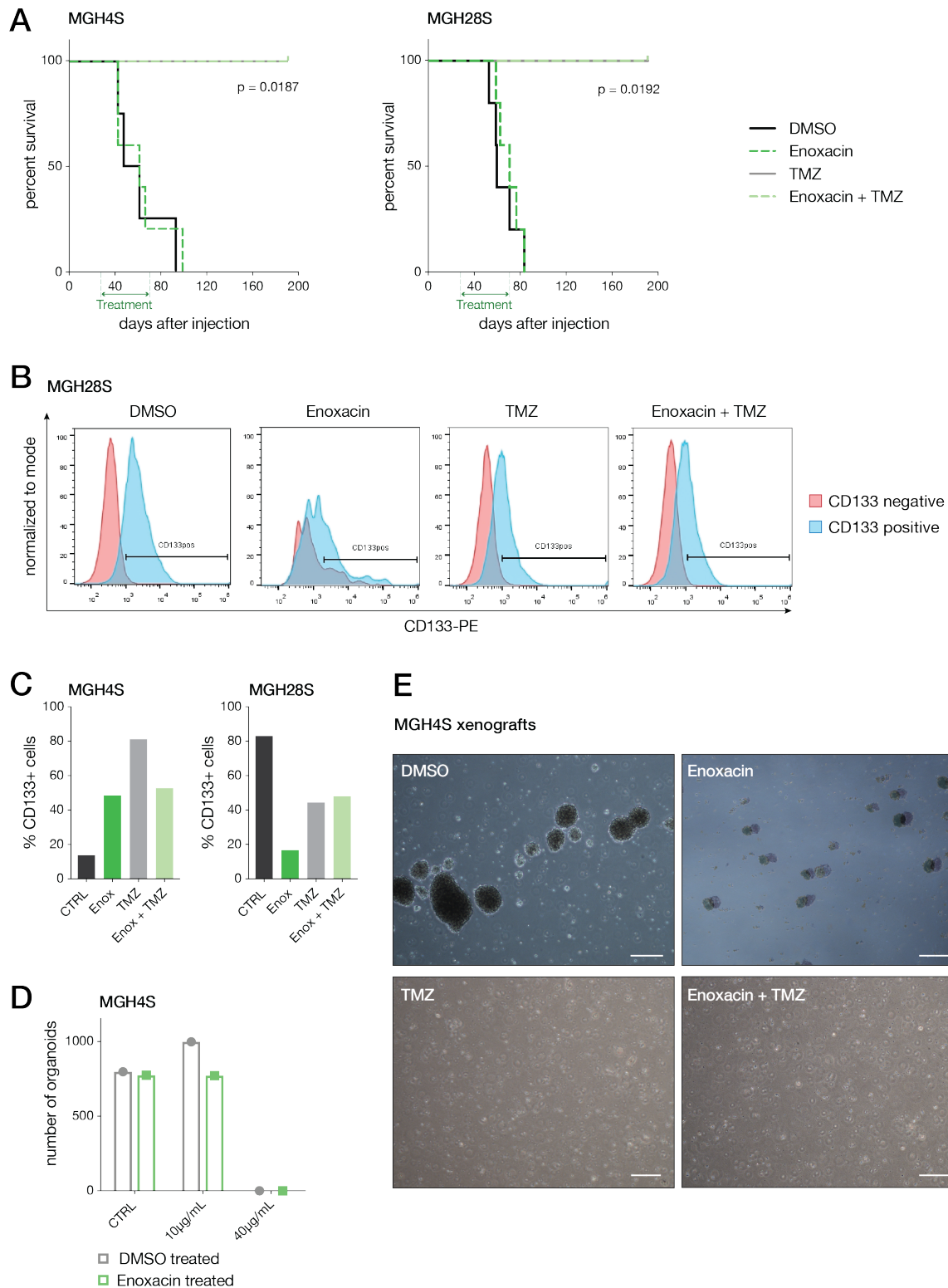


Figure 2.7: Effects of enoxacin on primary GBM organoids *in vivo*. (A) Kaplan-Meier survival curves of mice injected with 15'000 MGH4S or 10'000 MGH28S, subsequently treated with 20% DMSO control solution, enoxacin (50 mg/kg/day), TMZ (40 mg/kg/day) or combination of enoxacin and TMZ. The treatment window is indicated on the x axis. Five mice per group; except for MGH4S 20% DMSO, four mice in group. P -values were calculated using log-rank test. (B) FACS analysis of CD133⁺ cells (blue) from MGH28S tumor after dissociation of tumor xenograft from mice treated with 20% DMSO, enoxacin, TMZ or combination therapy. (C) Percentage of CD133⁺ cells in the live cell population in MGH28S and MGH4S tumors after dissociation of the tumor xenograft. CTRL, DMSO treatment; Enox, enoxacin treatment alone; TMZ, TMZ treatment alone; Enox + TMZ, combination therapy. (D) Organoid sphere formation assay of MGH4S cells after brain tumor dissociation from mice treated with 20% DMSO or enoxacin. Cells were incubated in control medium with 20 mM NaOH (CTRL) or re-exposed to enoxacin at 10 μ g/mL or 40 μ g/mL. (E) Representative images of MGH4S cells grown in normal organoid culture conditions for 10 days after brain tumor dissociation from mice treated with 20% DMSO, enoxacin, TMZ or combination therapy. The scale bars represent 200 μ m.

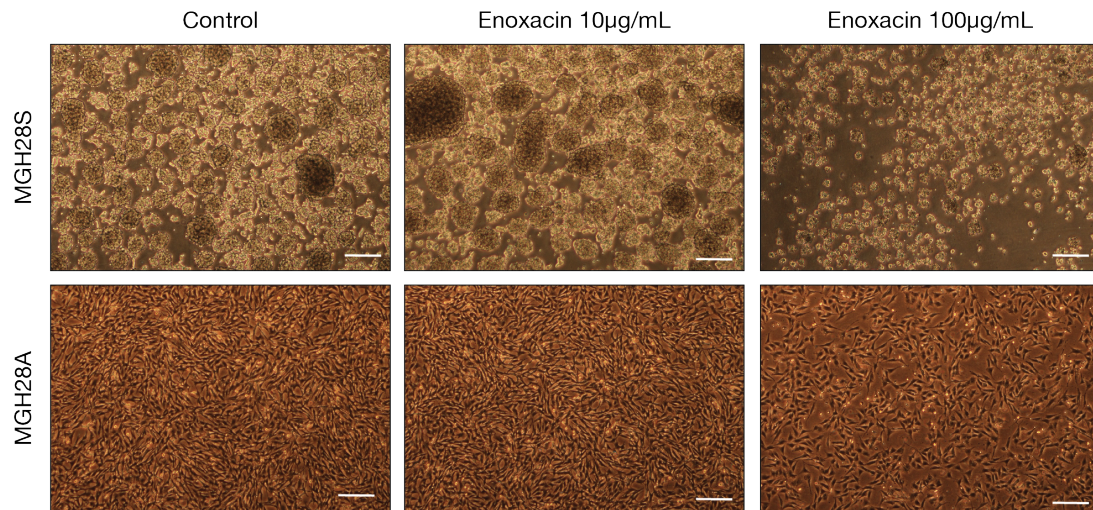


Figure 2.8: Toxicity of enoxacin *in vitro* in organoids versus adherent GBM-derived cells. Representative images of organoid spheres (MGH28S, top) and their adherent counterparts (MGH28A, bottom) after exposure to control medium or enoxacin for three days. The scale bars represent 100 μm .

2.2.3 Discussion

GSCs eradication is a central challenge in the treatment of GBM. Characterization of this tumorigenic subpopulation of cells revealed that, despite maintaining active expression of miRNAs, target transcripts involved in stemness pathways are not downregulated (Degrauwe et al., 2016a). Thus, we hypothesized that by further boosting the expression of miRNAs, we would restore their function and repress essential tumorigenic pathways of GSCs. To do this, we tested a small molecule, enoxacin, which can stimulate TRBP2 activity and the miRNA biogenesis pathway, as shown previously in EwS (De Vito et al., 2012; Cornaz-Buros et al., 2014). We used exclusively primary GBM samples, as they better represent the heterogeneous and complex behavior of human tumors.

We first noted an important effect of enoxacin on organoid clonogenicity, but the mechanisms of this change in cell behavior were not related to variations in let-7 target transcripts levels, as shown by mRNA expression analysis and Western blotting. More importantly, no change in tumorigenicity was seen *in vivo*. It can be argued that the delivery method of the drug was not ideal. However, a paper showed intraperitoneal injections of enoxacin in rats increased overall miRNA levels in the brain after one week of treatment, thus proving enoxacin administered peripherally can pass the blood-brain barrier sufficiently to have a local effect (Smalheiser et al., 2014). Furthermore, we used doses almost twice as high as in the aforementioned study, suggesting our method of enoxacin delivery was most likely adequate.

In patients, TMZ dosage is calculated based on body surface, aiming a range of 70 to

200 mg/m² depending on the therapy regimen. In mice, however, the dose is calculated based on weight. Thus, *in vivo* drug assays use a range of 25 to 50 mg/kg, which best reflect the doses used in humans (Middlemas et al., 2000). We chose a dosage of 40 mg/kg/day in our study, which is consistent with current *in vivo* applications. By selecting a slightly lower dose than the maximum 50 mg/kg/day, we aimed at adjusting the experimental conditions to detect a synergetic effect of TMZ when used in combination, in line with the general goal of reducing chemotherapy doses in patients to lower the morbidity associated with the treatment. However, the remarkable efficiency of TMZ in completely annihilating tumor growth in our experiments came as a surprise. Indeed, response to TMZ largely depends on methylation of the *MGMT* promoter. The *MGMT* promoter is unmethylated in MGH28S, as opposed to MGH4S, which has a methylated promoter (Supplementary Table S1.1) (Wakimoto et al., 2011). Surprisingly, both samples displayed a strong response to TMZ therapy, independently of their methylation status. This unexpected observation highlights the limitations of *in vitro* and *in vivo* studies for drug testing, and demonstrates the importance of translational medicine in effectively building the bridge from bench to bedside.

Adherent cells derived from GBM lack tumorigenic potential and display a shift in their expression profile, with the repression of several miRNA target transcripts. Thus, these cells are theoretically insusceptible to enoxacin exposure. Nonetheless, when comparing toxicity of enoxacin in spheroids and in non-tumorigenic GBM-derived cells, it appeared that enoxacin had a general toxic effect at a high concentration on cells, rendering our first observations *in vitro* unspecific.

Whereas enoxacin gave very promising results in EwS (Cornaz-Buros et al., 2014), our results speak against a potential therapeutic role of this small molecule in GBM. As miRNA levels are conserved in GBM, unlike in EwS, it may be more difficult to simply increase their expression by increasing the affinity of TRBP2, and other mechanisms may already counteract miRNA activity in a strong manner. Arguably, TRBP2 activity may have already reached its peak in GSCs, as levels of let-7 miRNAs are indeed elevated in GBM, as opposed to EwS. Thus, as enoxacin increases TRBP2 activity, but not its expression level, further TRBP2 stimulation may not be possible. Therefore, stimulation of TRBP2 may not represent a good approach to restore function of miRNAs in GSCs. For these reasons, we decided to not further explore the application of enoxacin to GBM, as our observations point to inefficacy of this small molecule as a means to eradicate GSCs. This prompted us to investigate other let-7 regulatory mechanisms in GBM.

2.3 The role of long-non-coding RNA H19 in GBM

2.3.1 Background

The role of epigenetic alterations and mutations in non-coding genes and regulatory DNA sequences are being increasingly linked to oncogenic events in various cancer types, by affecting transcription and the resulting cell phenotype. A growing body of evidence points to lncRNAs as putative mediators of cancer development, contributing to the six initial hallmarks of cancer (Hanahan and Weinberg, 2000), and their expression patterns have in some cases been linked to prognosis (Schmitt and Chang, 2016).

Testing enoxacin as a means to increase levels of let-7 and other miRNAs in GSCs failed to restore miRNA activity. Therefore, we should explore another approach to reestablish let-7 function. We previously mentioned the implication of IMP2 in GBM. While IMP2 was first reported to maintain oxidative phosphorylation in GSCs, its function as an RBP, by binding to let-7 target mRNA transcripts, was also determinant for GSC maintenance (Janiszewska et al., 2012; Degrauwe et al., 2016a). From the data collected in our lab, PAR-CLIP revealed that IMP2 binds several lncRNAs in GSCs, exclusively in organoids. Among these lncRNAs, H19 was the most abundant.

H19, a 2.3 kbp-long ncRNA, which undergoes splicing and adenylation, is a highly conserved maternally expressed gene and belongs to an imprinted cluster on chromosome 11, where it is reciprocally expressed with the paternal allele insulin-like growth factor 2 (IGF2), with which *H19* shares common enhancers. Alterations in the regulation of the chromosome 11p15.5 locus lead to various disorders and increased risk of cancer. Loss of H19 expression and biallelic expression of IGF2 are responsible for the Beckwith-Wiedemann syndrome, associated with overgrowth and predisposition to malignancies, whereas loss of IGF2 expression and biallelic expression of H19 is associated with Silver-Russel syndrome, defined as restriction and retardation of growth, with facial dysmorphia (Angrand et al., 2015). Furthermore, H19 expression tightly regulates hematopoietic stem cell renewal (Venkatraman et al., 2013). Similar to several oncofetal proteins, H19 is highly expressed in embryogenesis, is repressed after birth and remains silenced in differentiated cells, but is often reactivated in cancers (Kallen et al., 2013).

Mechanistically, H19 may act in multiple ways. Histone modifying proteins, such as the Polycomb histone methyltransferase EZH2, can be recruited by H19 in order to induce target gene silencing (Luo et al., 2013). Other mechanisms of action involve binding to and inactivation

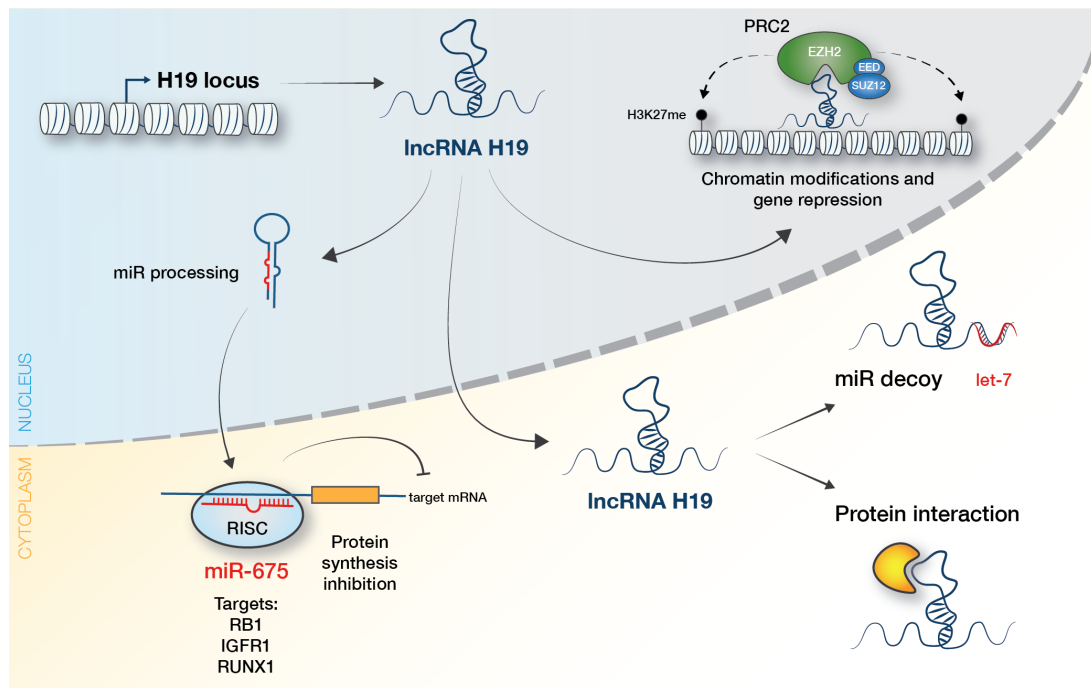


Figure 2.9: The various mechanisms of action of H19. H19 can act both at the transcriptional level, by recruiting PRC2 and other chromatin modifying factors, and at the post-transcriptional level, either by sequestering miRNAs, such as let-7, by binding several proteins and affecting downstream cascades, or by repressing target transcripts through its processing into miR-675. Adapted from Angrand et al. (2015).

of the tumor-suppressor *TP53* (Yang et al., 2012). To add to the complexity of the role of H19, this lncRNA can be processed into a miRNA from the first exon, namely miR-675, involved in skeletal muscle differentiation and regeneration (Dey et al., 2014). Several studies showed that the tumor promoting function of H19 is mediated by miR-675 itself, such as in breast cancer (Vennin et al., 2015) and GBM (Zhang et al., 2016b). Most importantly, H19 contains several let-7 binding sites and can exert a sponge effect on let-7 miRNAs, limiting their availability in the cell (Kallen et al., 2013).

In this study, to explore the function of H19 in GSCs, we addressed the effects of H19 depletion in tumor-initiating cells. As the CRISPR system allows a much more specific and efficient way to repress gene expression, it is interesting to apply this technology for lncRNA silencing. However, because the traditional CRISPR-Cas9 method introducing local indel mutations relies on copy frameshift or introduction of premature stop codons in protein coding sequences, it is not suited for application to non-coding sequences, as ncRNAs may still conserve some biological function despite point mutations. Thus, the CRISPR-intermediated interference (CRISPRi) system can circumvent this issue (Qi et al., 2013; Gilbert et al., 2013). It uses the same guide RNA (gRNA) strategy to recognize and bind the target of interest, but the CRISPR-associated endonuclease 9 (Cas9) here is inactive (dCas9) and fused to a Krüppel associated box (KRAB)

domain. Binding of the CRISPRi-KRAB complex inhibits gene transcription by recruitment of chromatin modifying complexes and trimethylation of Lysine 9 on histone 3 (H3K9me3), resulting in significant silencing of target transcription. Thus, in order to target H19, we used the CRISPRi tool with a set of top-four gRNAs targeting lncRNA H19 around the transcription start site (TSS), as chosen from the datasets from a CRISPRi Non-Coding Library (CRiNCL) (Liu et al., 2017) and based on predicted scores following the hCRISPRi-v2.1 algorithm (Horlbeck et al., 2016) (Supplementary Table S1.3).

Analysis of transcriptomic data from previous work reported that H19 is uniformly expressed in GBM (Zhang et al., 2015), suggesting a possible role in GSCs. Because H19 can repress let-7 miRNAs by acting as a sponge, and bind IMP2, which also regulates the let-7 pathways, we hypothesized there may be a reciprocal interplay between H19 and IMP2. Therefore, we investigated the nature and biological relevance of the interactions between IMP2 and H19 in GSCs, using the primary GBM samples present in our lab.

2.3.2 Results

H19 expression correlates with poor patient survival

Based on RNA-sequencing data from the TCGA database, we found that elevated H19 expression correlates with poor prognosis in GBM (Figure 2.10 A). In contrast, expression of H19 does not affect prognosis of low-grade gliomas, suggesting involvement of H19 in more aggressive tumors only (Supplementary Figure S1.1 A). Interestingly, although there is no statistical difference in the expression levels of H19 among the four GBM subtypes (data not shown), H19 expression is more strongly correlated with poor survival in the mesenchymal and proneural subtypes (Figure 2.10 B). The other subtypes showed no statistical correlation with survival (data not shown). This apparent contradictory observation could be explained by the fact that H19 activity is context-dependent, and is based on its interaction with other partners, either with RBPs or RNAs. Therefore, we looked at the genes whose expression is upregulated in tumors expressing high levels of H19. We found that IMP2 was among the 100 most upregulated genes, and other known let-7 targets were also found among the top 500 upregulated genes, which is consistent with the known function of H19 as a let-7 sponge (Supplementary Table S1.2).

Characterization of primary GBM samples

We used six primary tumor samples, which can be grown either in serum-free conditions as

organoid spheres, that maintain a tumorigenic potential, or in serum containing medium as adherent non-tumorigenic cells. Most of the primary samples used in this study have been previously described, namely MGH 4, 8, 11, 26, 28, and 31 (Rheinbay et al., 2013; Wakimoto et al., 2011; Patel et al., 2014; Suvà et al., 2014), and some characteristics of most of the samples are listed in Supplementary Table S1.1. Tumorigenicity of organoids *in vivo* has been well characterized for tumors MGH4, 8, and 11, with as few as 500 spheroid-derived cells able to form tumors, whereas as many as 100'000 adherent cells did not show tumor initiating capacity (Degrauwe et al., 2016a). Therefore, we tested tumorigenicity of organoids and adherent cells derived from the three other samples, namely MGH26, 28 and 31. Cells were grown as organoids and a subset of cells was exposed to serum, which generated adherent progeny (Figure 2.10 C). After injection into immunocompromised mice, 1'000 organoid-derived cells from MGH26 and MGH28 formed tumors within three months. In contrast, adherent cells from MGH26 did not form tumors. Adherent cells from MGH28S organoids, however, formed a mass when injected at high numbers, but not when injected at lower density (Figure 2.10 D). Surprisingly, MGH31S did not form any tumors, even after injection of 100'000 spheroids in the mouse brain (data not shown). Therefore, as MGH31S cells seem to lack tumor-initiating capacity, MGH31 was excluded from any further analysis.

Next, we looked at the overall expression levels of the IMP paralogs, as well as a known IMP2 mRNA target, namely HMGA2, and H19, in primary tumor samples, comparing organoids to their corresponding adherent cells. Although IMP1 is more abundant in GSCs than in adherent cells, it was generally detected at late cycles on qRT-PCR, with C_t values around 30-35 cycles. IMP2 and IMP3 were considerably more abundant in all organoid samples than in their adherent counterparts (Figure 2.10 E). We also found that expression of IMP paralogs in cell lines U-87 and U-251 is similar to or lower than in adherent cells, but the expression of the let-7 target HMGA2 varies substantially (Supplementary Figure S1.1 B). Therefore, cell lines do not offer an adequate representative cellular environment to investigate the function of these molecules, and appear to behave following distinct rules compared to organoids enriched in GSCs. Based on our observations, with relatively low expression compared to other IMPs, IMP1 is likely not essential for tumorigenic potential in GSCs. Thus, we decided to focus on IMP2 and IMP3 in subsequent investigations. Interestingly, H19 was virtually undetected in MGH31 (data not shown). Hence, the failure of MGH31S to form tumors upon injection *in vivo* (Figure 2.10 D) is in line with the hypothesis that H19 may be a relevant player in regulating GSCs properties.

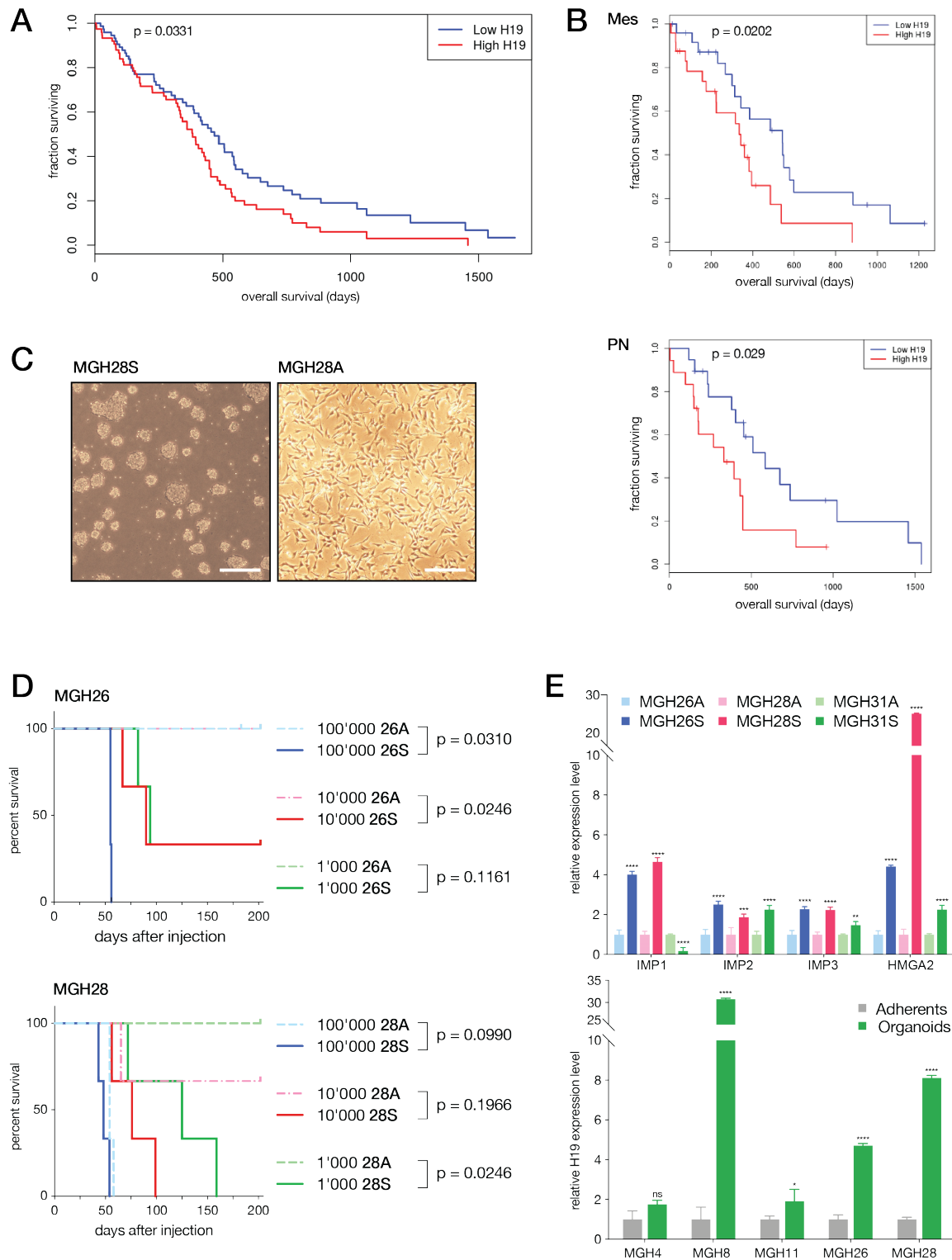


Figure 2.10: H19 is correlated with poor prognosis and is expressed in GSCs. (A) Kaplan-Meier overall survival curves for GBM patients with low (blue) or high (red) H19 expression. Data was obtained from the TCGA database and the curve used RNA-sequencing data from 154 primary GBM. P -value was calculated using log-rank test. (B) Kaplan-Meier overall survival curves for the mesenchymal (Mes) and proneural (PN) GBM subtypes based on low (blue) or high (red) H19 expression. P -values were calculated using log-rank test. (C) Representative image of tumorigenic organoids enriched in GSCs grown in serum-free conditions (S, organoid spheres, left panel) and adherent cells growing as a monolayer following exposure to serum (A, adherent, right panel). The scale bars represent 100 μm . (D) Kaplan-Meier survival curves of mice following injection of organoids (S) and adherent (A) cells (100'000, 10'000 or 1'000 cells) from tumors MGH26 (upper panel) and MGH28 (lower panel). $n = 3$ mice per group. P -values were calculated using log-rank test. (E) mRNA expression profiles of IMPs and their mRNA target HMGA2 in organoids (S) versus adherent (A) cells in five primary GBM samples (upper panel), and expression profile of H19 in organoids versus adherent cells in four primary GBM samples (lower panel), measured by qRT-PCR. Values in adherent cells were used as reference. Results are shown as mean \pm SD. Two-way ANOVA was used for statistical analysis. * $P < .05$, ** $P < .01$, *** $P < .001$, **** $P < .0001$.

Overexpression of H19 increases IMP2 binding and GBM clonogenicity

We next overexpressed H19, cloned into a lentiviral plasmid (pLIV), to determine whether it might increase the tumorigenic potential of GSCs. For this, we used MGH4S, as this sample displayed the lowest detectable expression of H19 (Figure 2.10 E and Figure 2.11 A, left panel). We further confirmed successful induction of H19 in established GBM cell lines U-251 and U-87, in which no endogenous H19 expression was detected (Supplementary Figure S1.1 B and C). Interestingly, we noticed that miR-675, the miRNA product of H19, was also significantly overexpressed, suggesting that the exogenous H19 is intact and can be actively processed by the cell. Based on the panel of genes that are most strongly expressed in high H19-expressing GBM (Supplementary Table S1.2), we observed that their expression was not significantly induced by H19 overexpression, with the marginal exception of IMP2 (Figure 2.11 B, left panel). Western blot analysis, on the other hand, did not show significant increase of IMP2, suggesting that IMP2 levels change only at the transcript level but without a change in its translation into protein. Furthermore, the discrete changes seen in stemness genes *NANOG* and *SOX2* do not reflect a clearly increased stem cell profile. Although let-7 miRNAs were discretely decreased upon H19 overexpression, this reduction was not statistically significant (Figure 2.11 B, right panel). Therefore, it seems that the overall expression profile of the cell remains stable despite a strong induction of H19.

Intriguingly, IMP2 RNA immunoprecipitation (RIP) performed on MGH4S with or without H19 induction shows that IMP2 binds massively more H19 transcripts upon H19 overexpression. Moreover, IMP2 appears to bind other target transcripts more readily in the presence of H19, as exemplified by *HMGA2* (Figure 2.11 C). Knowing that IMP2 protein levels are stable upon overexpression of H19, results from the IMP2 RIP suggest that the amount of H19 transcripts present in the cell strongly influence the relationship with its binding partner IMP2.

Finally, to address whether H19 overexpression may affect the cell phenotype, we first performed single-cell clonogenic assays. Indeed, clonogenicity of MGH4S was significantly increased upon overexpression of H19 (Figure 2.11 D), promptings us to further investigate the behavior of cells upon H19 expression.

Overexpression of H19 *in vivo*

To assess the effect of H19 overexpression *in vivo*, we injected 10'000 MGH4S cells, with or without H19 induction, into the brains of immunosuppressed mice. Surprisingly, H19 did not

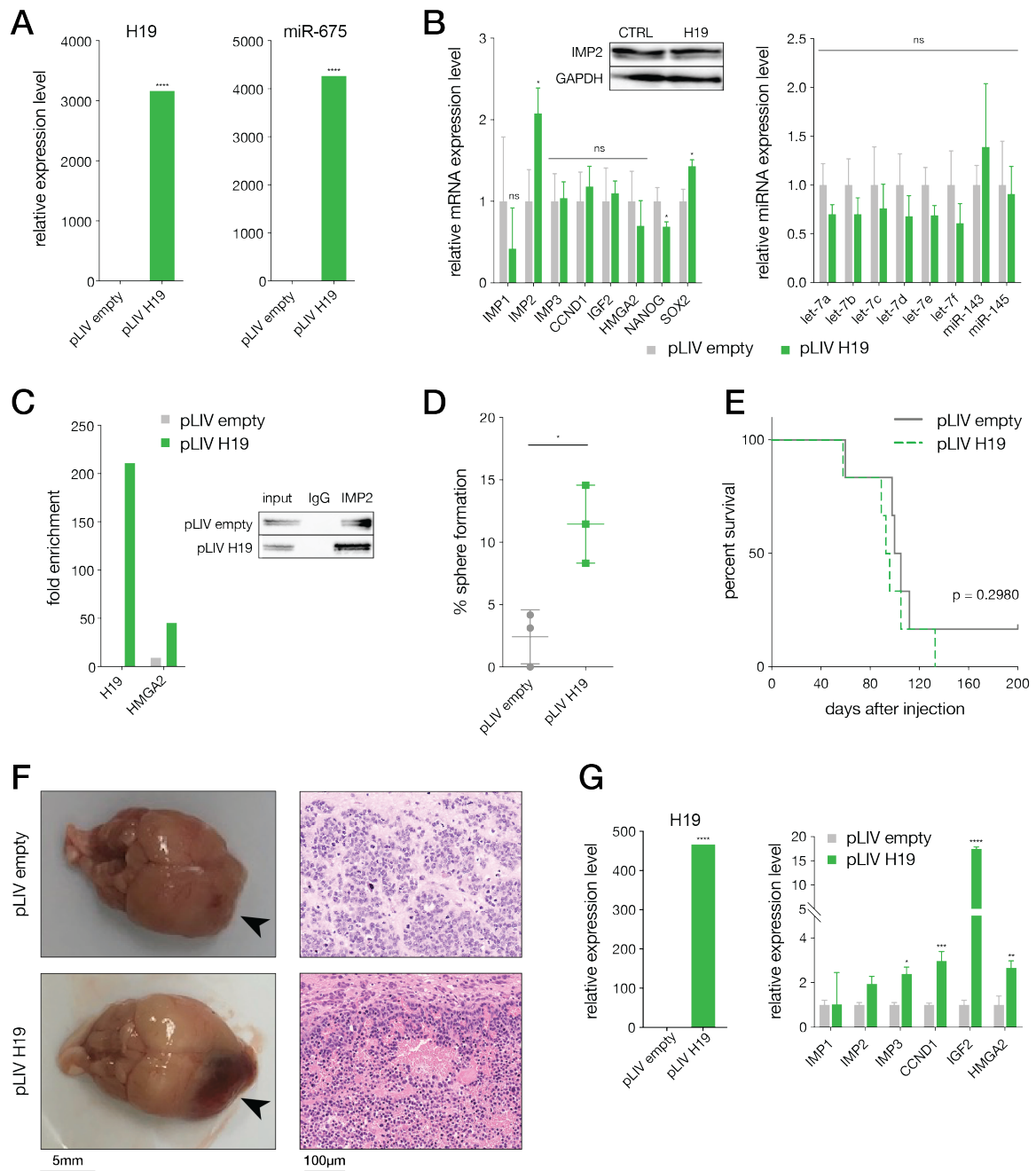


Figure 2.11: H19 overexpression in MGH4S. (A) Overexpression of H19 and its corresponding miRNA, miR-675, in MGH4S. Two-way ANOVA was used for statistical analysis. (B) Expression levels of a panel of genes measured by qRT-PCR. Genes analyzed include mRNA transcripts of the IMP paralogs, a set of genes that are induced in high-H19 GBM, and two stemness genes, *NANOG* and *SOX2* (left panel), and expression levels of miRNAs from the let-7 family, miR-143 and miR-145 (right panel), in control (pLIV empty) and H19-induced cells (pLIV H19). The Western blot image shows levels of IMP2 protein in control (CTRL) or H19 induced (H19) samples. Results are shown as mean \pm SD. Two-way ANOVA was used for statistical analysis. (C) RNA immunoprecipitation of IMP2 and HMGA2 in cells overexpressing H19 (pLIV H19) compared to control cells (pLIV empty), assessed by qRT-PCR (left panel). Western blot images of the corresponding RIP experiment confirms isolation of IMP2 (right panel). (D) Single-cell clonogenic assay in MGH4S control (pLIV empty) or overexpressing H19 (pLIV H19). Student's t-test was used for statistical analysis. (E) Kaplan-Meier survival curves of mice following orthotopic injection of 10'000 MGH4S cells (control, pLIV empty versus H19 overexpression, pLIV H19). $n = 6$ mice per group. P -value was calculated using log-rank test. (F) *Left panels*, Representative pictures of the mouse brain at the time of sacrifice following orthotopic injection of MGH4S control (pLIV empty, top) or overexpressing H19 (pLIV H19, bottom). The tumor is indicated with an arrowhead. *Right panels*, Representative microscopic images of the tumors with H&E staining. (G) Expression levels measured by qRT-PCR of H19 (left panel) and a panel of genes (right panel) in xenografts following tumor dissociation in control tumor (pLIV empty) versus H19 overexpressing tumor (pLIV H19). Results are shown as mean \pm SD. Two-way ANOVA was used for statistical analysis. * $P < .05$, ** $P < .01$, *** $P < .001$, **** $P < .0001$. ns, not significant.

affect the overall survival (Figure 2.11 E). Upon dissection, however, although there was no significant difference in tumor size (data not shown), tumors were much more vascularized in the presence of H19 compared to control samples, a feature that could be expected to correlate with a more aggressive tumor phenotype (Figure 2.11 F). We confirmed that H19 overexpression was maintained after tumor xenograft dissociation and noticed a few genes that appeared to have been upregulated *in vivo*, including CCND1, HMGA2, and mainly IGF2 (Figure 2.11 G), which may translate an imbalance in the imprinting regulation between IGF2 and H19, although post-transcriptional regulation of IGF2 by H19 has also been reported (Li et al., 1998).

In parallel, we carried out the same gain-of-function experiments with GBM cell lines, in which endogenous H19 was undetected (Supplementary Figure S1.1 B). Similar to MGH4S, orthotopic injection of 50'000 U-87 or U-251 cells overexpressing H19 failed to demonstrate increased tumorigenicity of cells *in vivo* compared to control (Supplementary Figure S1.1 C and D). However, we did not see any morphological or histological difference between tumors expressing H19 or not (data not shown). Here as well, we confirmed that H19 overexpression was maintained *in vivo* (Supplementary Figure S1.1 E). Curiously though, U-251 showed tumor growth only after three months, whereas mice injected with U-87 started exhibiting signs of brain tumor progression and had to be sacrificed after a period of only three weeks, showing that these two cell lines display very distinct tumorigenic potential.

2.3.3 Discussion

Many papers have demonstrated the role of H19 in promoting GBM proliferation and invasion, and have well established the role of H19 as a let-7 sponge, but fewer have explored its interaction with RBPs. Taken together, our data suggests that H19 correlates with poor patient survival and binds IMP2, and that overexpression of H19 enhances cell clonogenicity. This observation was however not confirmed *in vivo*. Our first experimental approach focused on the effects of H19 overexpression in GSCs with low endogenous H19 (C_t values averaging 33-34). In gain-of-function experiments, it is reasonable to assume that overexpression can only affect the phenotype to a certain extent. The cells used here, MGH4S, already display strong stemness properties and actively form tumors *in vivo*, which may not be stimulated further. Still, orthotopic brain injection of fewer cells may have more readily shown changes in tumorigenicity *in vivo*. Nevertheless, a strong characterization of the role of H19 at this stage would rely on studying cell changes following depletion of H19.

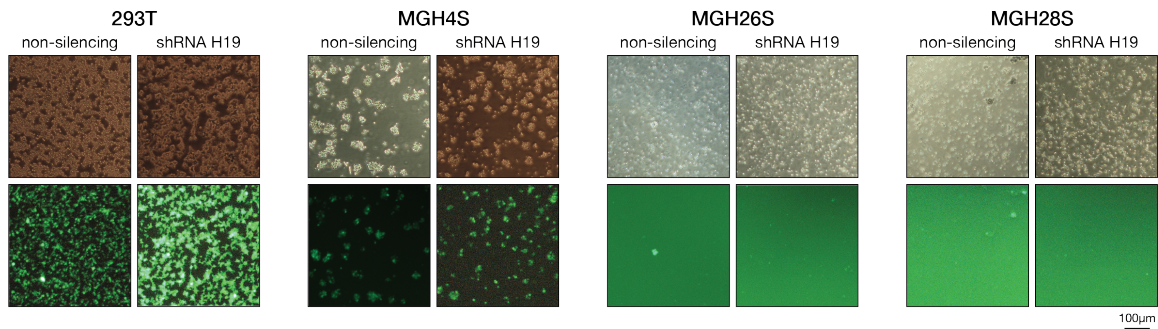


Figure 2.12: Infection efficiency in 293T and in GBM samples. Images show micrographies taken three days after lentiviral infection with a non-silencing shRNA or a shRNA targeting H19, both containing GFP. Cells were exposed to the same amount of virus for a period of 8 h. The lower row shows the fluorescent signal obtained from the corresponding picture in the upper row. The scale bar indicates 100 μm .

For H19 knockdown, we planned on using the CRISPRi silencing system. The already low endogenous level of H19 in MGH4S could not provide adequate conditions for representative results in loss-of-function experiments. Indeed, the remainder of the work would need be performed on a model with high endogenous expression of H19, as seen in MGH8S, MGH26S and MGH28S, to achieve robust knockdown and evaluate the effect on the cell phenotype. Having cloned several oligo sequences into the CRISPR-dCas9-KRAB plasmid, we faced major issues upon lentiviral infection of target cells. We achieved successful infection of 293T cells and of MGH4S, but despite using low amounts of virus, MGH26S and MGH28S stopped growing shortly after exposure to the virus suspension, with or with addition of polybrene in the medium. We excluded the possibility that this may be due to H19 knockdown, as the same phenomenon was seen with the control CRISPRi vector. We questioned whether this could result from toxicity of the CRISPRi vector itself. To address the issue, we used shRNA vectors (shRNA non-silencing and shRNA targeting H19) that expressed to visually follow the infection efficiency. To our surprise, even with the non-silencing control shRNA, cells stopped proliferating and died shortly after infection (Figure 2.12). Extensive attempts to adjust infection conditions bore no fruitful results.

Therefore, the major issue of not having a representative loss-of-function model of H19 or IMP2 made us reconsider the feasibility and completion of the project, as we could no longer address the various questions that remained to be answered, and that required gene editing to provide any constructive conclusion. Consequently, we lack further evidence that H19 is essential for GSC maintenance in our samples, and it is yet unclear why IMP2 binds to H19 transcripts. IMP2 can bind thousands of mRNAs, with a preference for their 3'-UTRs (Conway et al., 2016). The effects of IMP2 binding, however, are broad and depend on the binding partner. Similarly,

H19 can interact with many proteins and transcripts, and can act through various mechanisms.

Interaction between IMP2 and H19 may contribute to either one of the binding partners. In the first scenario, H19 binding may be important for IMP2. In this context, we can hypothesize that H19 localizes IMP2 inside the cell. IMP2 immunohistochemistry and H19 RNA detection on histological tumor slides would allow to see their colocalization in wild-type cells and displacement of IMP2 in cells depleted of H19. Recently, *THOR* was shown to stabilize binding of IMP1 to its targets (Hosono et al., 2017). A similar mechanism between H19 and IMP2 is surely worth investigating. Linked to previous data on the role of IMP2 in GSC maintenance, if observations would confirm that H19 is essential for IMP2 function, it would further support IMP2 as a key RBP in GBM and reinforce its potential for therapeutic targeting. Conversely, in a second scenario, IMP2 binding may be necessary for H19. In light of the implication of IMPs in controlling mRNA fate, IMP2 may participate in the stabilization and transport of H19. Comparing levels and localization of H19 in cells depleted of IMP2 would have provided clues as to this pathway. Transcript stabilization could easily have been tested by measuring and comparing the half-life of H19 in wild-type GSCs and cells depleted of or lacking IMP2. If indeed IMP2-H19 binding is essential primarily for H19, we would need to further investigate its downstream function in our GBM samples.

We can still ask what the main mechanisms of action of H19 could be in GBM. As mentioned previously, lncRNAs can act through various mechanisms. While H19 function was reported to be primarily mediated by its derived miRNA miR-675 (Zhang et al., 2016b), this miRNA was absent from our samples. Notably, this work and most studies on H19 found in the literature mainly use established GBM cell lines, which can explain our divergent observations. Indeed, many studies (Zhang et al., 2016b; Li et al., 2016) used the same two GBM cell lines as we did to explore the role of H19, namely U-251 and U-87, in which we, in contrast, did not detect any H19 expression (Supplementary Figure S1.1 B). Thus, this reflects once more the limitations of research on immortalized cell lines that often tend to display different expression profiles following extensive subculturing, and demonstrates the importance of testing primary samples as well to confirm findings from established cell lines.

The function of H19, in our interest, can be divided into two categories: 1) let-7-dependent pathways, centering the role of H19 around its sponge activity for let-7 miRNAs, and 2) let-7-independent pathways, which would require further characterization. We found that clonogenicity of MGH4S overexpressing H19 is increased, although let-7 target transcripts, such as

HMGA2, were unchanged. RNA profiling of cells depleted of H19 would have been able to further confirm this, by analysis of transcriptome changes and assessing if the let-7 target mRNAs are globally stable. At this point, we assume that increasing levels of H19 do not cause increased sequestering of let-7 miRNAs and postulate that a let-7-independent mechanism is most likely at play in our GBM cells.

Although H19 was initially found to be primarily located in the cytoplasm (Brannan et al., 1990), and association with IMP1 was described to occur exclusively in the cytoplasm (Runge et al., 2000), evidence that H19 binds to EZH2, the methyltransferase of PRC2, and is associated with increased methylation of the E-cadherin promoter suggests that H19 can additionally localize and operate inside the nucleus (Luo et al., 2013). With increasing evidence showing interactions of lncRNAs with chromatin, it would be of interest to perform chromatin isolation by RNA purification sequencing (ChIRP-seq) analysis to investigate direct interactions of H19 with chromatin (Chu et al., 2015). Indeed, from the gain-of-function experiments, it can be believed that increased levels of H19 may not significantly alter the binding sites to chromatin, and would explain the stable phenotype observed. However, taking into account the interaction between IMP2 and H19, we would need to suppress IMP2 in H19-expressing GSCs to observe possible displacement of H19 along the chromatin. Another approach would require a GBM sample that naturally lacks IMP2, which we do not have. Therefore, we again lacked a negative model depleted of IMP2, which would have provided extensive data to compare H19 positions on the chromatin in the presence or absence of its binding partner IMP2.

To conclude, we believe that H19 lncRNA may be a relevant player in GSCs, and further characterization of its role using primary tumor samples can provide valuable new insight for its role in GBM.

2.4 Materials and Methods

Cell culture

GBM tumors were collected at Massachusetts General Hospital and have been characterized in previous works (Supplementary Table S1.1) (Wakimoto et al., 2011; Rheinbay et al., 2013; Suvà et al., 2014). Primary GSCs were grown as organoids in Neurobasal medium (Invitrogen) supplemented with L-glutamine (Gibco), B27 supplement (Invitrogen), N2 supplement (Invitrogen), recombinant human epidermal growth factor (EGF) and basic fibroblast growth factor (bFGF) (PROSPEC) at final concentrations of 20 ng/mL, and 1 % Penicillin-Streptomycin (PenStrep, Gibco). Differentiation of GSC into adherent cells was induced by culturing cells in DMEM medium, supplemented with 10 % fetal bovine serum (FBS, PAN-BIOTECH) and 1 % non-essential amino acids (NeAA, Gibco) in pre-coated plates, which were generated as follows: a 20 μ g/mL solution of poly-L-ornithine (Sigma-Aldrich) was added to plates. After 1 h incubation at 37 °C, the solution was removed and the plates were washed three times with PBS. A 5 μ L/mL solution of laminin (Sigma-Aldrich) in PBS was added to the plates. The plates were then incubated at 37 °C for three hours at least. Cells were grown as a monolayer on the coated plates.

The GBM cell lines U-251 (RRID:CVCL_0021) and U-87 (RRID:CVCL_0022) were purchased from ECACC and ATCC, respectively, and cultured in Dulbecco's MEM (DMEM, Gibco) supplemented with 10 % FBS (PAN-BIOTECH), 1 % NeAA (Gibco) and 1 % PenStrep (Gibco). The LentiX-293T cell line was purchased from Clontech (Cat# 632180) and grown in DMEM (Gibco) supplemented with 10 % FBS (PAN BIOTECH), 1 % NeAA (Gibco) and 1 % PenStrep (Gibco).

Cell cultures were maintained at 37 °C and 5 % CO₂ in humidified culture incubators. Cells were regularly tested to exclude mycoplasma contamination.

Single-cell clonogenic assays

Primary gliomasphere organoids were manually dissociated into a single-cell suspension. Cells were counted and diluted to a final concentration of 100 cells in 10 mL of culture medium. Cells were then plated at single-cell density in low-attachment 96-well plates (Corning) with 100 μ L medium per well. After one week, 100 μ L of fresh medium was added to each well. After a total incubation time of three weeks, the number of organoids was assessed by micrography imaging.

Sphere formation assays

Primary gliomasphere organoids were manually dissociated into a single-cell suspension. Cells were counted and 4'000 cells were added in the first well in a 96-well plate. Serial 1:2 dilutions were performed along the first column and then along each row in the plate. Cells were incubated in 100 μ L for a week and 100 μ L of fresh medium was added to each well after one week. After a final incubation time of three weeks, the total number of organoid spheres was counted. Results are reported as the total number of organoid spheres found in each 96-well plate. Experiments were performed in triplicates.

Stereotactic mouse injections

NOD-SCID gamma mice were given Paracetamol one day prior to surgery. Anaesthesia was obtained by intraperitoneal injection of a solution containing 100 mg/kg Ketamine (Ketasol-100, Graueb AG) and 16 mg/kg Xylazine (Rompun 2%, Provet AG), diluted in PBS. Intracranial injection of cells was performed using a stereotactic apparatus (Kopf Instruments) at coordinates 2.2 mm right lateral relative to the bregma point, and 2.5 mm deep from the dura mater, corresponding to $x = -2.2$ mm, $y = 0$ mm and $z = -2.5$ mm. After surgery, treatment with Cicafalte (Avène) once a day on wound and Paracetamol in water bottle was maintained for seven days. Mice were sacrificed when showing signs of suffering, after which the brain was extracted for further analysis. For survival data, Kaplan-Meier curves and statistical significance using log-rank test were calculated with GraphPad Prism 8 software. Experiments were performed under the licence number VD2488.

Drug delivery

Following stereotactic surgery, the injected tumor cells were allowed to engraft for four weeks. Mice were subsequently treated either with a control 20% DMSO solution, enoxacin (Sigma-Aldrich) alone (50 mg/kg/day), TMZ (Sigma-Aldrich) alone (40 mg/kg/day), or a combination of both enoxacin and TMZ, with five mice per group. The treatment was given by intraperitoneal administration for three weeks, at a rate of five injections per week. After the end of the treatment, three mice from each group were sacrificed for immediate tissue analysis. The two remaining mice from each group were observed for further survival data. For these mice and those that had to be sacrificed before the end of the treatment, Kaplan-Meier curves and statistical significance using log-rank test were calculated with GraphPad Prism 8 software. Experiments were performed under the licence number VD2488.

Lentiviral infection

LentiX-293T (Clontech) packaging cells were transfected using FuGENE[®] 6 Transfection reagent (Promega) for lentivirus production. The envelop and packaging vectors used were pMD2G (Addgene, plasmid # 12259) and pCMV Δ R8.74 (Addgene, plasmid # 12263), respectively. After 72 h, the supernatant was collected, filtered (0.45 μ m) and ultracentrifuged at 4 °C for 2 h at 26'000 RPM with a SW28 rotor. The supernatant was discarded and the virus was left to resuspend overnight at 4 °C. On the following day, 10⁶ cells were incubated for 8 h with the concentrated viral suspension from two LentiX-293T 15 cm dishes and with Polybrene at a final concentration of 6 μ g/mL. Antibiotic selection was initiated three days after infection with puromycin at a final concentration of 2 μ g/mL and maintained until the cells were used for further experiments.

Brain tumor dissociation and flow cytometry

Tumor xenografts were dissociated using the Brain Tumor Dissociation kit (P) (Miltenyi Biotec) according to the manufacturer's instructions. Expression of CSC-associated cell surface marker CD133 was analyzed by FACS with Gallios flow cytometer (Beckman Coulter) and analyzed using FlowJo Software (FlowJo, LLC). Live cell population was selected by DAPI staining, and then sorted using CD133/PE antibody (Miltenyi Biotec).

RNA extraction, cDNA synthesis and quantitative real-time PCR

RNA was extracted using the miRCURY RNA Isolation kit (Exiqon). For cDNA synthesis, 500 ng of RNA were reverse-transcribed using M-MLV Reverse Transcriptase (Promega). qRT-PCR was run by QuantumStudio 5 instrument (ThermoFisher Scientific). Each PCR reaction was performed in triplicates and fold change was calculated using the comparative $\Delta\Delta C_t$ method. For mRNA, PCR was performed with TaqMan Universal PCR mastermix (Applied Biosystems) or PowerUp SYBR Green (Applied Biosystems), and specific PCR probes and primers (Supplementary Table S2.3). Relative gene expression was normalized to endogenous controls GAPDH and TBP. For miRNA, cDNA synthesis was retrotranscribed from 30 ng to 60 ng of RNA using Universal cDNA synthesis kit (Exiqon). PCR was performed using Power SYBR Green (Applied Biosystems) and specific primers designed to recognize mature miRNA (miRNA LNA PCR primer sets, Exiqon). Relative quantification was normalized to endogenous control Snord49A.

Preparation of protein cell lysate and Western blot

Western blot was performed according to standard procedures. Briefly, cells were harvested, centrifuged, washed in ice-cold PBS and lysed in SDS-RIPA buffer (150 mM NaCl, 1 % NP-40, 0.5 % sodium deoxycholate, 0.1 % SDS, 50 mM Tris pH 8.0) and protease inhibitor cocktail (Roche). The lysate was incubated on ice for 20 minutes, sonicated twice for 10 seconds at 35 kHz, and centrifuged at 4 °C for 10 minutes at 13'000 RPM. The supernatant was used for protein sample preparation. Protein concentration was assessed using Bradford Protein Assay Dye (Bio-Rad). An amount of 30 to 40 µg of proteins was loaded per lane for Western Blot and samples underwent electrophoresis through a gradient polyacrylamide gel (6 %-20 %) at 125 mV for 2 h. Transfer was performed with a current of 250 mA for 2 h onto Whatman[®] Protran[®] BA83 nitrocellulose membrane. The membrane was then blocked in 5 % milk in PBS containing 0.5 % tween 20 (TBST) for 1 h, washed with TBST, and hybridized with primary antibody according to the manufacturer's recommendations. Primary antibodies included: anti-IMP2 (MBL International, Cat# RN008P1), anti-IMP3 (MBL International, Cat# RN009P), anti-HMGA2 (Cell Signalling Technologies, Cat# 5269), anti-TRBP2 (Abnova, Cat# MAB0811), anti-OCT3/4 (Santa Cruz, Cat# sc-5279), anti-SOX2 (Sigma, Cat# S9072), anti-GAPDH-HRP (Abcam, Cat# ab9482). Secondary antibodies included: HRP-conjugated sheep anti-mouse (GE Healthcare, Cat# NA931) and goat anti-rabbit (Agilent, Cat# P0448). Bands were visualized and analyzed using Western Bright Sirius (Wiltec AG) detection reagents, according to the manufacturer's instructions, with Fusion Fx software (Vilber Lourmat).

RNA-Immunoprecipitation of IMP2

RIP was performed using the RIP-Assay Kit for miRNA (MBL International) according to the manufacturer's instructions. Approximately 2×10^7 cells were harvested, washed and lysed in Triton-based lysis buffer. After 1 h pre-clear with Protein A agarose beads, the lysate was incubated with 10 µg of anti-IMP2 antibody (MBL International) or 10 µg isotype-matched antibody (MBL International, provided in kit) conjugated with Protein A agarose beads. Beads were then washed with lysis buffer. 10 % of beads were kept for Western blot analysis and RIP RNA was extracted from the remaining beads. For Western blot analysis, beads were incubated in Laemmli sample buffer and boiled for five minutes. The supernatant was collected following centrifugation and subsequently used for Western blot. For qRT-PCR, 500 ng of RNA were retrotranscribed as described above. RIP enrichment of targets was calculated using comparative $\Delta\Delta C_t$ method.

H19 overexpression

H19 cDNA was obtained from Dharmacon (Clone Id: 3449920) and verified by sequencing upon reception. The amplified product from H19 cDNA was cloned onto pENTR/SD/D-TOPO using pENTR Directional TOPO cloning kit (Life Technologies) and onto a Gateway receptor vector using Gateway LR Clonase II kit (Life Technologies). The primers used to amplify cDNA of H19 were: Fwd 5'-CACCGGCAGGGGACACAGGACAG-3' and Rev 5'-GAGTCCAGGGCTCCTGCTGAAG-3'.

CRISPR cloning

The CRISPRv2 plasmid was obtained from Zhang Lab (Addgene plasmid # 52961) (Sanjana et al., 2014). CRISPRv2 was digested with FastDigest Esp3I (ThermoFisher Scientific) at 37 °C for 1 h. The sample was then run on an agarose gel and the 12 kb fragment was extracted using the Monarch DNA Gel Extraction kit (NEB) according to manufacturer's instructions. The forward and reverse oligos were annealed by incubation for five minutes at 95 °C in annealing buffer (10 mM Tris pH 7.5, 1 mM EDTA, 50 mM NaCl) and left to cool down to room temperature. Ligation of the vector with the annealed oligos was performed with T4 DNA ligase (ThermoFisher Scientific) at 16 °C for 16 h, and the enzyme was inactivated at 65 °C for 10 minutes. After butanol precipitation, we electroporated STBL3 bacteria with the ligation reaction product, and subsequently screened and sequenced the resulting clones. The gRNA sequences used in this project were chosen based on the Broad Institute algorithm (<https://portals.broadinstitute.org/gpp/public/analysis-tools/sgrna-design>). For a given gene sequence, the program browses through all possible gRNA sequences adjacent to a protospacer-adjacent motif (PAM) sequence. We kept the top four sequences, ranked from 1 to 4 according to specificity and limited off-target effects. As a general rule, we ensured that our gRNA target the gene of interest between 5-66 % of the target length. The sequences used are listed in Table S1.3. For control conditions, we used a CRISPRv2 vector without a gRNA.

For CRISPRi cloning, we used a vector containing CRISPRv2-dCas9 associated with a KRAB domain, already available in our lab. The same protocol was applied as described above with the oligos listed in Table S1.3, chosen from CRiNCL (Liu et al., 2017) and based on predicted scores following the hCRISPRi-v2.1 algorithm (Horlbeck et al., 2016). For control conditions, we used a CRISPRv2-dCas9 vector without a gRNA.

Survival and expression correlation data

The expression data for GBM in TCGA were obtained from RNA-sequencing. These data refer to 172 samples, of which 154 are primary tumors; for 152 of these we had overall survival information. Dividing the patients into two groups (high- and low- H19, based on median expression), we obtained Kaplan-Meier curves for the two groups. The survival analysis was repeated separately for each molecular subtype (classical, mesenchymal, proneural, neural). The same dataset was used to compute the correlation between H19 expression and the expression of all other genes.

Statistical analyses

GraphPad Prism software 8 was used to generate graphs and to perform the corresponding statistical tests, as indicated in the figure legends.

Chapter 3

Ewing Sarcoma

3.1 Introduction

3.1.1 Pediatric malignancies: a challenging field

Every year, an estimated 250'000 children and adolescents are diagnosed with cancer worldwide (Steliarova-Foucher et al., 2017). Importantly, malignant diseases are the second leading cause of death in children in Switzerland (Arndt et al., 2016). Whereas overall survival of pediatric oncology patients has dramatically improved in the last 50 years, reaching more than 80 % cure in high-income countries (Smith et al., 2014), the prognosis is largely dependant on the tumor type, patient age, and, for solid tumors, metastatic status at diagnosis, with metastatic spread generally associated with dismal outcomes. Indeed, although mortality rates have continued to decline in the last ten years, they have done so at a slower rate and appear to have reached a plateau in the case of solid tumors, especially for high-grade gliomas and metastatic sarcomas (Bosetti et al., 2010; Smith et al., 2014).

Interestingly, the most common sites that undergo transformation vary substantially based on patient age, suggesting that the mechanisms underlying tumorigenesis are primarily age- and organ-dependent (Figure 3.1 A). The incidence of pediatric tumors has remained mostly stable in the past decades. Increased incidence rates of brain tumors and acute lymphoblastic leukemia (ALL) most likely reflect improved diagnostic and imaging techniques (Figure 3.1 B). Indeed, prevention of cancer in the pediatric population remains a major challenge, as there are limited preventable risk factors for these diseases. The few known risk factors for childhood cancer include syndromes resulting from inherited gene mutation (e.g. hereditary retinoblastoma, Li Fraumeni syndrome, Down syndrome), ionizing radiation (e.g. radiation therapy, exposure of

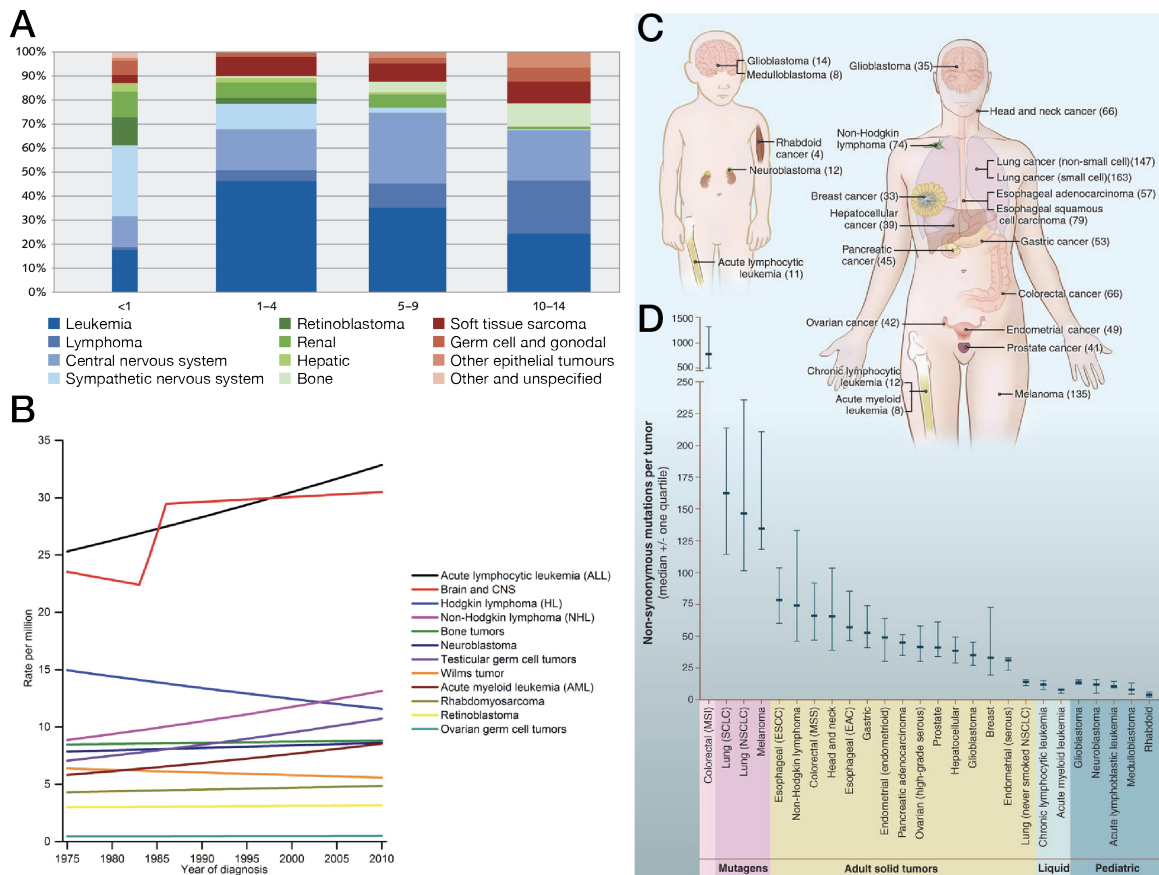


Figure 3.1: Epidemiological and genome-wide data of childhood cancer. (A) Distribution of cancer types by age group from birth to 14 years in Switzerland (2008-2012). Area is proportional to the number of cases. Malignant bone tumors include osteosarcoma and Ewing sarcoma. Adapted from Arndt et al. (2016). (B) Trends in incidence rates of pediatric cancer by site for patients from birth to 19 years, between 1975 and 2010. Lines represent joinpoint fitted trends. Benign and borderline brain tumors are not included. Malignant bone tumors include osteosarcoma and Ewing sarcoma. Reproduced from Ward et al. (2014). (C) Genome-wide sequencing of a diverse group of pediatric (left) and adult (right) cancers reveals strong disparity in mutational load profiles. Numbers in parentheses indicate the median number of non-synonymous mutations per tumor. (D) Number of somatic mutations in adult and pediatric cancers. Median number of non-synonymous mutations per tumor in a variety of adult and pediatric cancers. Horizontal bars indicate the 1st and 3rd quartiles. CNS, central nervous system; MSI, microsatellite instability; SCLC, small cell lung cancers; NSCLC, non-small cell lung cancers; ESCC, esophageal squamous cell carcinomas; MSS, microsatellite stable; EAC, esophageal adenocarcinomas. (C) and (D) reproduced from Vogelstein et al. (2013).

mother during pregnancy, exposure to radiation following the Chernobyl catastrophe), and age of mother at birth (Arndt et al., 2016; Helman and Meltzer, 2003). Certain viruses may also induce malignant transformation (e.g. Kaposi sarcoma, hepatitis, EBV). However, this hardly defends prevention as an effective approach to reduce cancer incidence in children. Thus, the primary goal relies on decreasing morbidity and mortality of children, essentially by developing more targeted, less myeloablative and lower dose therapies that successfully eliminate CSCs.

While cancer is primarily recognized as a genetic disease, adult and pediatric cancers exhibit significant disparity. Indeed, most adult tumors display a high number of mutations, partly due to exposure to numerous stress inducers and pathogenic factors (e.g. sunlight, tobacco smoking, infections). Pediatric cancers, in contrast, carry globally fewer genetic changes in their genome

(Figure 3.1 C and D). Nevertheless, the global expression profile of tumor cells is significantly altered. Thus, cellular transformation may be explained in part by epigenetic events. Some epigenetic changes may result from mutations in epigenetic regulators (Downing et al., 2012), but may also be the consequence of epigenetic modifications resulting from non-random chromosomal rearrangements. As epigenetic alterations can be reversed, they can contribute to explaining the high cellular plasticity observed in tumors.

Although childhood cancers represent a significant burden of disease, their scarcity challenges research opportunities. The small number of cases translates into reduced interest for funding in the biopharmaceutical sector, and the limited number of available participants for phase II trials hinders the statistical power of clinical studies. Also, pharmacological phase I trials are generally limited in children for obvious ethical reasons, which may considerably delay potential testing and use of novel drugs or regimens in the pediatric population. Furthermore, current drugable targets have essentially been identified in adult cancers. Pediatric cancers, in contrast, often lack the same genetic variations, due to their low mutational profile and distinct pathogenesis. Thus, very few drugs used in adult contexts can be applied to pediatric malignancies, and most have limited to no benefit for the pediatric population. Finally, while advanced-age cancer patients may benefit from an improved survival of months to a few years, the goal in treatment of pediatric cancer is no other than complete remission and cure, along with limiting the incidence of secondary tumors in all long-term survivors. This sets the bar at a completely different level for the development of new therapies.

Such challenges in pediatric cancer research highlight the primordial role of using preclinical models that reliably replicate the patients' tumors, including their heterogeneous nature, to identify potential targets. PDX have been found to effectively reproduce the tumor of origin in solid pediatric tumors, preserving the heterogeneous molecular profiles of the initial sample, especially in the case of relapse (Stewart et al., 2017; Nanni et al., 2019). Working with PDX enables drug screening with potential for translation in the clinic. Importantly, a genetic alteration or an activated pathway may be identified and essential to diverse tumor types (Norris and Adamson, 2012), suggesting that subsequent trial design and criteria for patient inclusion should be reshaped accordingly. Genomic sequencing and individualized approach in precision oncology may bear promising results in patient care (Allen et al., 2017; Vo et al., 2020).

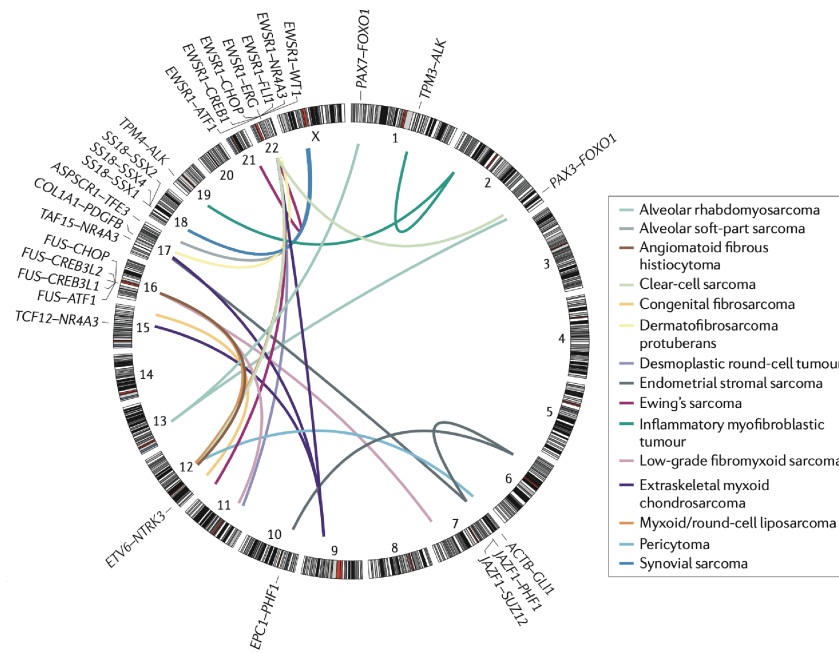


Figure 3.2: Recurrent translocations found in malignant sarcomas. Shared fusion partners are shown according to sarcoma subtypes. The outer ring represents genomic location (as labelled), cytobands are shaded and the centromere is in red, with curves joining fusion partners. Adapted from Taylor et al. (2011).

3.1.2 Sarcomas: a heterogeneous group of tumors

Cancers of the bones and soft tissues fall together in the category of sarcomas. They can emerge from any mesenchymal tissue, including bone, cartilage, muscle, fat or vascular tissue, typically with varying degrees of malignancy. Whereas these tumors are rare in adults, accounting for only 2% of adult cancers, they represent about 20% of pediatric malignancies (Figure 3.1 A). Sarcomas can be divided into two groups based on their karyotype. One group, which comprises 70% of sarcomas, harbors complex karyotypes, linked to perturbed genomic stability, and most commonly affects adults. As may be expected, the signaling pathways of tumor suppressors p53 and retinoblastoma-associated protein (Rb) are frequently disrupted in these sarcomas (Helman and Meltzer, 2003). The second group, which comprises the remaining sarcomas, is characterized by simple karyotypic alterations resulting from non-random chromosomal rearrangements, and arise predominantly in children (Figure 3.2 and Table 3.1). The different translocations result in the expression of an aberrant chimeric proteins that fuse a protein with a DNA binding domain to a protein containing a potent transactivating domain, typically a TET family protein, such as EWS, causing strong transcriptional activation of a new set of targets. Expression of the fusion protein is believed to be the principal trigger event for transformation in a permissive cellular environment. In some cases, the translocation can lead to the overexpression of a growth factor (Riggi et al., 2007).

Table 3.1: Chromosomal translocations in sarcomas.

Tumor type	Translocation	Fusion protein
Ewing sarcoma / ESFT	t(11;22)(q24;q12)	EWSR1-FLI1
	t(21;22)(q22;q12)	EWSR1-ERG
	t(7;22)(p22;q12)	EWSR1-ETV1
	t(2;22)(q33;q12)	EWSR1-FEV
	t(17;22)(q12;q12)	EWSR1-ETV4
	t(16;21)(p11;q22)	FUS-ERG
DSRCT	t(11;22)(p13;q12)	EWSR1-WT1
	t(21;22)(q22;q12)	EWSR1-ERG
Myxoid liposarcoma	t(12;16)(q13;p11)	FUS-DDIT3
	t(12;22)(q13;q12)	EWSR1-DDIT3
Synovial sarcoma	t(X;18)(p11;q11)	SS18-SSX1
	t(X;18)(p11;q11)	SS18-SSX2
	t(X;18)(p11;q11)	SS18-SSX4
	t(X;20)(p11;q13)	SS18L1-SSX1
Alveolar rhabdomyosarcoma	t(2;13)(q35;q14)	PAX3-FKHR
	t(1;13)(p36;q14)	PAX7-FKHR
	t(2;2)(q35;p23)	PAX3-NCOA1
Clear cell sarcoma	t(12;22)(q13;q12)	EWSR1-ATF1
Extraskeletal myxoid chondrosarcoma	t(9;22)(q22;q12)	EWSR1-NR4A3
	t(9;17)(q22;q11)	TAFII68-NR4A3
	t(9;15)(q22;q21)	TCF12-NR4A3
Dermatofibrosarcoma protuberans	t(17;22)(q22;q13)	COL1A1-PDGFB
Alveolar soft-part sarcoma	t(X;17)(p11.2;q25)	ASPL-TFE3

List of the non-random chromosomal translocations found in various bone and soft tissue sarcomas. DSRCT, desmoplastic small round cell tumor. Adapted from Riggi et al. (2007).

Most of the translocations identified in sarcomas involve *Ewing sarcoma breakpoint region 1* (*EWSR1*) on chromosome 22, encoding the RNA binding protein EWS. Nonetheless, *EWSR1* can be found as part of a fusion protein in a variety of sarcomas, including desmoplastic small round cell tumor (DSRCT), myxoid liposarcoma, and clear cell sarcoma of soft tissue (CCS) among others, where the only varying factor is the fusion partner of *EWSR1* (Helman and Meltzer, 2003). Generally, fusion partners of *EWSR1* can be separated into two categories, based on whether they are members of the erythroblastosis transforming virus 1 (ETS) family (such as *FLI1*, found in EwS) or not. Given that the tumors resulting from translocations involving chromosome 22 are distinct entities, it appears that the fusion partner of *EWSR1* is the most determinant factor for the tumor phenotype.

3.1.3 Ewing sarcoma clinical presentation and diagnosis

EwS was first described as a separate entity by James Ewing a century ago, based on observations in a patient who was first diagnosed with osteosarcoma but responded well to radiation therapy. James Ewing later reported similar tumors in other adolescents and initially named the disease “diffuse endothelioma of the bone”, based on the histological morphology of the tumor (Ewing, 1972). It was only 70 years later that the chromosomal translocation was detected. This led to the definition of a new group of malignancies, the Ewing sarcoma family of tumors (ESFT), encompassing Ewing sarcoma (EwS), Askin tumors and peripheral primitive neuroectodermal tumor (PNET). These aggressive tumors of the bone and soft tissue quickly develop distant metastases.

EwS is a highly aggressive sarcoma mostly seen in boys of 10 to 15 years of age, and is the second most common primary bone malignancy in children. The overall 5-year survival rate is around 70% but decreases significantly in the 25% of cases diagnosed with metastatic disease. For those patients and those with relapse, even aggressive multimodal therapy comprising surgery, chemotherapy and radiation therapy fails to increase the long-term survival above 30% (Pishas and Lessnick, 2016). Metastatic dissemination involves mainly the lungs (75%), bones (30%) and the bone marrow (16%) (Worch et al., 2018), and it is suspected that most patients have subclinical metastatic disease at the time of diagnosis (Nesbit et al., 1990).

EwS most commonly presents in the diaphyses of the bone, most frequently in the distal leg bones, and in the pelvis (Figure 3.3 A), but a minority of cases primarily involve soft tissues. At diagnosis, the child may present with localized pain or swelling at the tumor site, with a firm mass appearing over the course of weeks to months. Minor trauma to the involved site may be the first call for attention and reason for pediatric consult. Advanced disease may be accompanied by systemic signs, including fever, fatigue, weight loss or anemia. Imaging of the site of lesion shows destruction of the bone with “moth-eaten” appearance and invasion to the surrounding soft tissues. Periosteal reaction causes formation of reactive bone layers that recall onion-skin, a visible and characteristic imaging feature on radiograms of EwS (Figure 3.3 B, upper panel). Definitive diagnosis is then obtained upon histological analysis of biopsy, which shows typical small blue round cell morphology common to ESFT (Figure 3.3 B, lower panel), detection of the cell surface marker CD99 with immunohistochemistry, and, most importantly, identification by fluorescent *in situ* hybridization (FISH) or qRT-PCR of the fusion protein that is specific for EwS, involving *EWSR1* and a member of the ETS family of TFs.

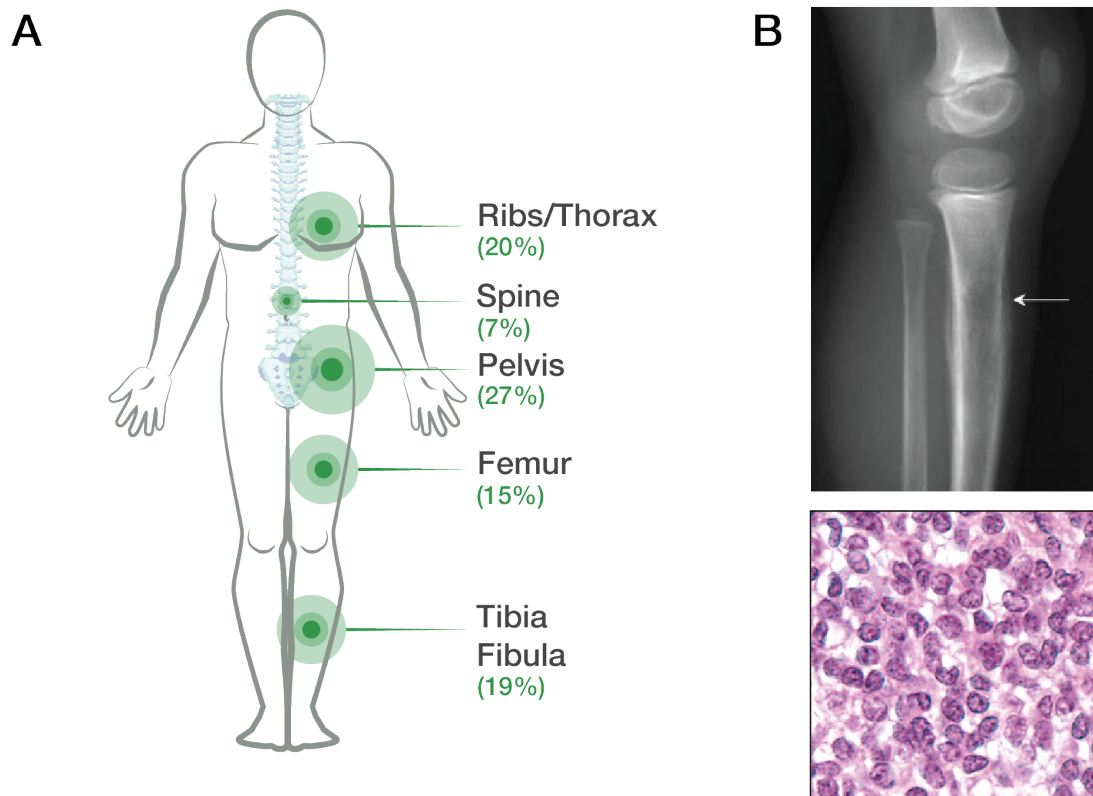


Figure 3.3: Clinical presentation of Ewing sarcoma. (A) Frequency of primary EwS sites (Worch et al., 2018). (B) *Upper panel*, radiography image of the tibia (lateral view) of a patient showing onion-skin periosteal reaction of the bone around the EwS tumor site, indicated with an arrow. Image by Michael Richardson, M.D., distributed under a CC BY-SA 3.0 license. *Lower panel*, Histological image of EwS showing small, poorly differentiated, blue round cells. Reproduced from Robbins et al. (2010).

Of note, EwS is consistent with the CSC model. Indeed, a subpopulation of $CD133^+$ cells displays tumor-initiating capacity upon xenotransplantation, self-renews and generates $CD133^-$ clones, and highly expresses stemness genes, including *NANOG* and *OCT4* (Suvà et al., 2009).

3.1.4 The fusion protein EWS-FLI1

Many translocations have been associated with EwS and are all characterized by EWS fusion to one of five members of the ETS family, namely FLI1, ERG, FEV, ETV1 or E1AF (Arvand and Denny, 2001). About 85% of EwS tumors carry the specific translocation $t(11;22)(q12;q24)$, resulting in the expression of the aberrant chimeric transcription factor EWS-FLI1 responsible for malignant transformation (Delattre et al., 1994).

EWSR1, alongside *TLS/FUS* and *TAF15*, is a member of the *TET* gene family, and encodes the ubiquitously expressed protein EWS. TET proteins share a similar structure composed of SYGQ repeats in the N-terminal region, that function as a DNA transactivation domain, and three RGG repeats of different lengths and a 87-amino acid RRM domain at the C-terminal end, which combined ensure binding to RNA (Paronetto, 2013) (Figure 3.4 A). In particular,

EWS can bind directly to RNA polymerase II (RNA PolII), as well as to various transcription activators or repressors, thereby affecting transcription (Figure 3.4C). Moreover, EWS is also involved in mRNA splicing (Tan and Manley, 2009; Selvanathan et al., 2015) and can associate with DROSHA for miRNA processing (Gregory et al., 2004). In studies carried *in vivo*, knock-down of EWS was associated with high post-natal mortality, decreased meiosis and disrupted B-lymphocyte maturation, as well as arrest in hematopoietic stem cell (HSC) growth and renewal (Li et al., 2007; Paronetto, 2013). Interestingly, the transactivation domain encoded by the seven first exons of *EWSR1* is largely silent in the full length wild-type protein, but becomes strongly activated upon translocation of the C-terminal end. Data suggest that EWS activator repression is mediated by the RGG repeats, which is line with gain-of-function of the activator domain in the fusion protein lacking RGG repeats (Alex and Lee, 2005).

Friend leukemia virus integration 1 transcription factor (FLI1) is a member of the ETS family that includes at least 27 TFs. All members share a common DNA binding domain that binds a consensus core 5'-GGAA/T-3' motif, called the ETS binding domain (Seth and Watson, 2005; Wei et al., 2010). In particular, FLI1 contains 3' and 5' ets binding domains, associated with a helix-loop-helix secondary structure with transcriptional activity, and a FLI1 specific domain (FLS) (Figure 3.4B). Together, the 3' ets binding domain and FLS form the amino terminal transactivation domain (ATA), which is much less powerful than the activation domain of EWS and is lost after translocation, explaining the enhanced function of FLI1 in the fusion protein compared to wild-type FLI1 (Truong and Ben-David, 2000). Moreover, after translocation, FLI1 undergoes conformational changes and activates a larger set of genes than its wild-type form, although the DNA binding domain is conserved (Üren and Toretsky, 2005; Tan and Manley, 2009).

In adults, high FLI1 expression is maintained in hematopoietic tissues but only weak expression is found in the lungs and heart (Ben-David et al., 1991). Overexpression of FLI1 demonstrated malignant potential by causing increased growth and self-renewal of erythroid progenitors (Pereira et al., 1999). Moreover, FLI1 can inhibit Rb expression and promote entry into the S phase of the cell cycle. Finally, homozygotic loss of FLI1 disrupts development of T- and B-cells and impairs vascular endothelial differentiation, and is embryonically lethal (Spyropoulos et al., 2000).

The breakpoint region of *EWSR1* is rather small and extends over a length of 8 kb, spanning exons 7 to 11. The majority of fusions found in EwS contain exons 1 to 7, thereby preserving

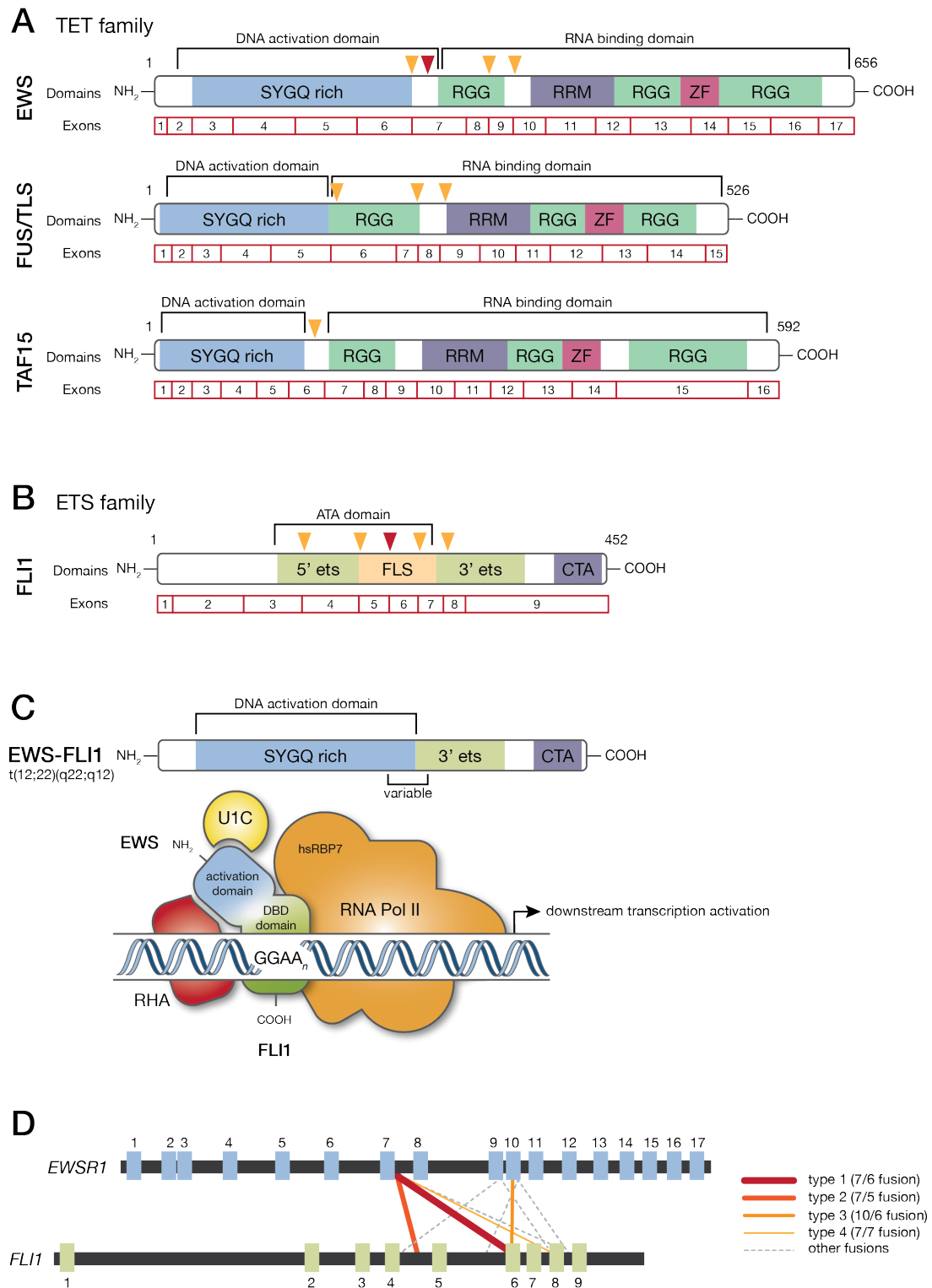


Figure 3.4: Structural features of TET proteins and FLI1, and the EWS-FLI1 fusion protein. The structure of members of the TET family (**A**) and FLI1 (**B**) are shown with the corresponding exons. Common breakpoints are indicated with an arrowhead. The red arrowhead indicates the most frequent breakpoint site. The fusion protein resulting from the t(12;22)(q22;q12) translocation is depicted in (**C**), upper panel, and a schematic representation of EWS-FLI1 and its partners following DNA binding on GGAA repeats is shown in (**C**), lower panel, and regulates changes in target gene expression. (**D**) shows the various fusion types based on exon juxtaposition. The exons are represented as numbered boxes and the lines indicate the breakpoint sites on *EWSR1* and *FLI1*. Adapted from Anderson et al. (2012) and Sankar and Lessnick (2011). RRM, RNA recognition motif; ZF, zinc fingers; FLS, FLI1 specific domain; CTA, C-terminal transcription activating domain; DBD, DNA binding domain; RHA, RNA helicase A; U1C, U1 small nuclear ribonucleoprotein C.

the integrity of the EWS transactivation domain (Zucman-Rossi et al., 1998; Arvand and Denny, 2001; Fisher, 2014). On the other hand, the larger breakpoint region of *FLI1* spans over 35 kb (exons 4 to 9). It occurs most frequently in intron 5, leading to preservation of exons 6 to 9 in the fused product (Zucman-Rossi et al., 1998; Arvand and Denny, 2001). As the breakpoint is quite variable, the fusion protein is classified as type 1 fusion if *EWSR1* exons 1-7 are juxtaposed to *FLI1* exons 6-9, and as type 2 fusion, less prevalent, when *EWSR1* exons 1-7 are fused to *FLI1* exons 5-9 (Figure 3.4D). Of note, it appears that, although some translocations include *EWSR1* exon 8, this exon must be removed during splicing of the EWS-FLI1 transcript for adequate protein expression (Grohar et al., 2016).

3.1.5 EWS-FLI1 and tumorigenesis of EwS

In about one out of five EwS cases, the chromosomal translocation responsible for EWS-FLI1 fusion is the only detected oncogenic event. Thus, EWS-FLI1 is believed to significantly modify the transcriptomic profile of the cell to promote transformation. To understand and characterize the implication of EWS-FLI1 in tumorigenesis, two main approaches have been privileged, one inducing *de novo* expression of the fusion protein in primary cells and cell lines of various origins and differentiation stages, and the other focusing on depleting the fusion protein in EwS primary cells or cell lines.

Evidence that EWS-FLI1 is capable of transforming cells was first reported in NIH3T3 fibroblasts, where expression of the fusion protein promoted cell growth on soft agar (May et al., 1993) and tumor formation *in vivo* with histological similarity to EwS (Thompson et al., 1999). Conversely, inhibition of EWS-FLI1 using either targeted RNA silencing or dominant negative recombinants in cell lines reduced cellular growth and tumorigenesis in mice (Kovar et al., 1996; Tanaka et al., 1997). However, stable expression of EWS-FLI1 in mouse embryonic fibroblasts (MEFs) and human fibroblasts was only possible with a mutated p53 regulatory pathway, allowing cells to overcome growth arrest and apoptosis (Deneen and Denny, 2001). Thus, the cellular context is critical to properly study EWS-FLI1.

To understand how EWS-FLI1 causes transformation, targets that are up- or down-regulated were assessed for their role in oncogenesis. Indeed, EWS-FLI1 can act as both a transcriptional activator and repressor of direct and indirect targets. Several activated genes have been reported, including *c-MYC*, *CCND1*, *ID2*, *EZH2*, *PDGFC*, *DAX1*, *SOX2* and *NKX2.2*, some of which promote cell proliferation and survival. In addition, several targets are repressed with EWS-

FLI1 expression, such as *p21* and *TGF- β RII*, allowing the cell to escape apoptosis and growth arrest (Ordóñez et al., 2009). Notably, EWS-FLI1 strongly induces insulin-like growth factor 1 (IGF1) expression and represses *IGFBP3*. Dependence of EwS and other sarcomas on the IGF1 pathway is supported by the demonstration that IGF1R blockade decreases cell proliferation and tumorigenesis (Scotlandi and Picci, 2008). Moreover, *PTPL1* induction upon EWS-FLI1 expression increases resistance to etoposide (Abaan et al., 2005), and *GSTM4* expression, whose promoter contains a GGAA microsatellite region directly bound by EWS-FLI1, also provides resistance to chemotherapeutic drugs (Luo et al., 2009). Taken together, altered expression of direct and indirect targets dictated by EWS-FLI1 promotes cell survival and proliferation, while also sustaining drug resistance.

Recently, chromatin immunoprecipitation sequencing (ChIP-seq) analyses demonstrated that EWS-FLI1 orchestrates a highly EwS-specific transcriptional program. EWS-FLI1 either represses targets by displacing the regulatory machinery at single GGAA repeats, or activates target genes by chromatin remodelling at GGAA repeats at distal regulatory elements. Binding of EWS-FLI1 multimers is alone sufficient for activation of transcription at GGAA microsatellite repeats at distal regulatory elements. Remarkably, targeted epigenome silencing of EWS-FLI1 bound enhancers successfully blocked gene transcription and was associated with decreased tumor formation *in vivo* (Boulay et al., 2018). Thus, using the ChIP-seq approach has allowed the identification of new targets activated by direct EWS-FLI1 binding to chromatin and to attest to their importance for tumorigenesis (Riggi et al., 2014). Moreover, the SYGQ repeats in EWS mediate recruitment of the chromatin remodeling complex BAF and enhancer activation at GGAA repeats, a feature that is unique to the fusion protein, thus explaining the distinct set of targets modulated by EWS-FLI1 and wild-type FLI1 (Boulay et al., 2017) (Figure 3.5 A). Taken together, these data demonstrate that EWS-FLI1 directs epigenetic changes to activate a specific transcriptional program that induces malignant transformation.

Lastly, recent studies using a single-cell approach revealed ITH with cell-to-cell variation of EWS-FLI1 transcriptional activity that reflects onto the cellular profile (Aynaoud et al., 2019). An optimal EWS-FLI1 activity range offers the necessary conditions for proliferation, whereas low EWS-FLI1 activity induces a mesenchymal-like phenotype, resulting in cells with a strong propensity to migrate and develop metastatic dissemination (Franzetti et al., 2017) (Figure 3.5 B and C). The mechanisms that modulate EWS-FLI1 activity, however, still need to be defined. Nevertheless, these observations further support the strong propensity of EWS-FLI1 to consid-

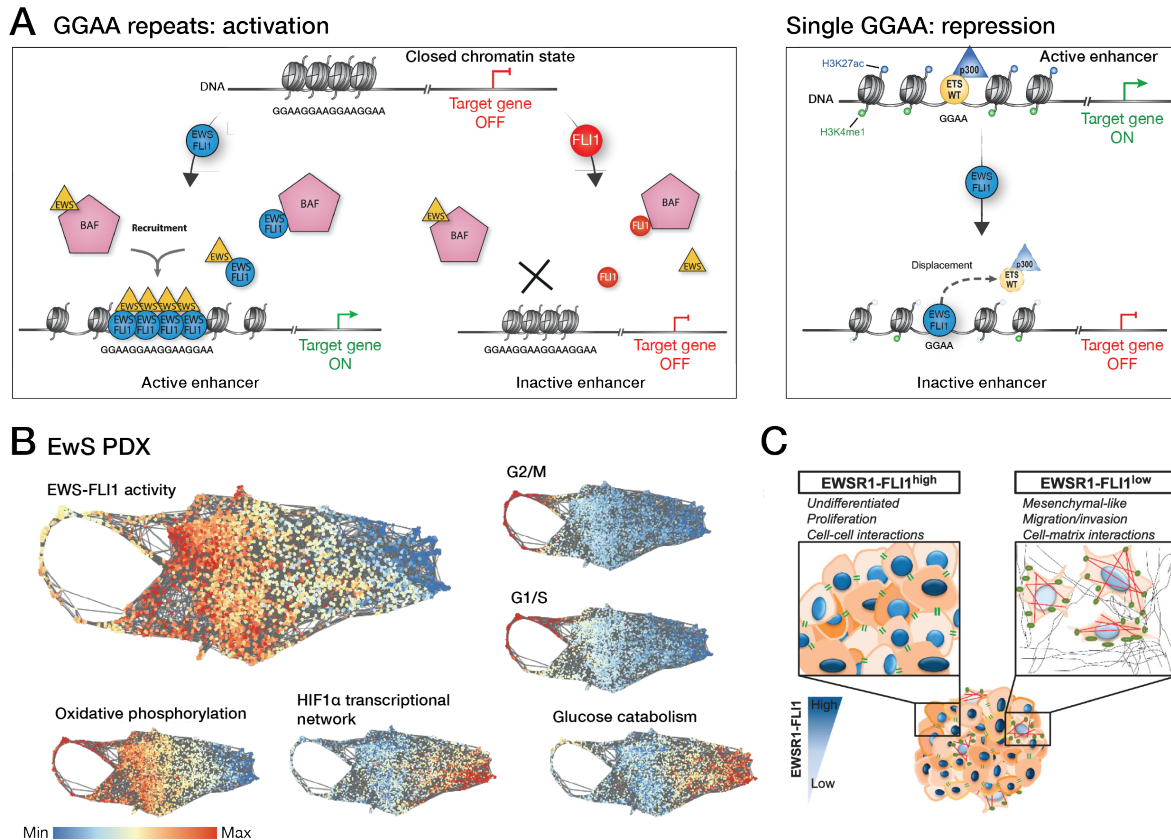


Figure 3.5: EWS-FLI1 modulates chromatin conformation and transcriptional profile in EwS. (A) Schematic depiction of EWS-FLI1 binding at GGAA motifs and chromatin remodeling. *Left*, EWS-FLI1 multimerization permits stable binding at GGAA repeats and recruitment of BAF complexes to enable enhancer activation, whereas wild-type FLI1 cannot stably bind at GGAA repeats and the chromatin remains at a repressed state. *Right*, EWS-FLI1 binds single GGAA motifs in open chromatin and displaces endogenous ETS TFs to repress the enhancer. Adapted from Boulay et al. (2017) and Riggi et al. (2014). (B) Intratumoral heterogeneous activity of EWS-FLI1 illustrated by SPRING representation of the kNN graphs for an EwS PDX dataset. Transcriptional programs of EWS-FLI1 and cell cycle (G2/M and G1/S), as well as scores for gene sets linked to oxidative phosphorylation, hypoxia and glucose metabolism, are shown. Adapted from Aynaud et al. (2019). (C) Schematic representation of cells with low or high EWS-FLI1 transcriptional activity. Adapted from Franzetti et al. (2017).

erably reshape the transcriptional landscape of the cell to support tumor growth, while also showing that ITH complicates the therapeutic approach to EwS.

3.1.6 The cell of origin of EwS

As EwS is a poorly differentiated tumor that bears both mesenchymal and neuroectodermal features, it has been long discussed whether these tumors are of mesenchymal or of neuroectodermal origin. Moreover, because the translocations that characterize sarcomas are found almost exclusively in tissues derived from the mesenchyme, it appears that the cellular state plays a major role in allowing the tumor-initiating cell to effectively express the fusion protein. In line with this, efforts to identify the EwS cell of origin have been long hampered by the toxicity of EWS-FLI1 upon exogenous expression in host cells. As mentioned previously, expression of EWS-FLI1 was achieved in NIH3T3 fibroblasts, but similar attempts in primary mouse MEFs and human

immortalized fibroblasts led to growth arrest and apoptosis. In human fibroblasts, EWS-FLI1 was only expressed upon loss of p53 or p19^{ARF}, a feature that is only found in a minority of tumors (Huang et al., 2005). A permissive environment is therefore required to enable stable EWS-FLI1 expression.

Mesenchymal stem cells (MSCs) are particularly interesting candidates due to their pluripotency and their ability to generate a wide range of differentiated tissues. Indeed, EWS-FLI1 expression induced transformation in mouse bone marrow-derived mesenchymal progenitor cells, which generated tumors with EwS properties (Riggi et al., 2005). Subsequent studies showed that expression of EWS-FLI1 in human MSCs resulted in a change of the transcriptome reminiscent of that of EwS (Riggi et al., 2008), and that this process was even more robust upon transformation of human pediatric mesenchymal stem cells (hpMSCs), with the generation of a subpopulation of CD133⁺ CSCs displaying both mesenchymal and neural features (Riggi et al., 2010). Furthermore, following long-term EWS-FLI1 silencing, EwS cell lines acquired a mesenchymal profile. In particular, neural features were generally lost upon EWS-FLI1 depletion, suggesting that the neuroectodermal features found in EwS likely result from transcriptional reprogramming orchestrated by the fusion protein (Tirode et al., 2007). Taken together, these reports strongly suggest that EwS originates from MSCs, which contain the required permissive state for expression of the fusion protein.

Of note, expression of EWS-FLI1 in hpMSCs induced cell reprogramming toward EwS but also toward a neural crest stem cell (NCSC) phenotype (Riggi et al., 2010). Moreover, human NCSCs have been shown to sustain EWS-FLI1 expression and recapitulate a profile similar to EwS (von Levetzow et al., 2011). Consistent with this notion, MSCs can be derived from NCSCs (Lee et al., 2007). Therefore, these observations may provide a unifying explanation for the initial debate, suggesting that EwS originates from a MSC of mesenchymal or neuroectodermal origin. Importantly, cells maintain strong plasticity following transformation, as shown by the presence of both mesenchymal and neural features in the tumor.

3.1.7 *In vivo* models of EwS

As pediatric sarcomas are mainly driven by a fusion oncogene following chromosomal translocation, possibly early in the developmental stages, it can be assumed that conditional expression of the translocation under the control of a specific promoter and at a specific timepoint will produce accurate transgenic mouse models. Successful models have thus been developed for

rhabdomyosarcoma, myxoid liposarcoma, clear cell sarcoma, and synovial sarcoma (Minas et al., 2017). In EwS, however, the generation of transgenic mice remains a fundamental challenge. This is partly due to the toxicity of EWS-FLI1 in various tissues, as mentioned earlier, with rapid induction of apoptosis, despite addition of the previously reported mutations in p53 or p19^{ARF} (Ordóñez et al., 2009; Minas et al., 2017).

To avoid embryonic lethality, using Prx1-Cre mouse would allow conditional expression of EWS-FLI1 in MSCs, as the *Prx1* gene is expressed specifically in MSC progenitors in limb buds, thereby sparing vital central organs. Nonetheless, the model was associated with high developmental defects of the limbs, as EWS-FLI1 expression blocked differentiation of cells into skeletal muscle and maturation of the bone was impaired. The number of tumors, however, increased with loss of p53, which is consistent with previously reported observations. Nonetheless, this is not representative of the majority of primary EwS, in which this pathway is not affected (Lin et al., 2008).

This study illustrates only one of many attempts at generating an EwS mouse model. Other various complications encountered when creating transgenic EwS models included early development of leukemia and promoter leakiness, all challenged by the absence of additional genetic alterations and the overall high rate of embryonic lethality. Even inducible models remained unsuccessful and lacked progeny (Minas et al., 2017). Furthermore, based on studies from our laboratory, changes in the transcriptional program following EWS-FLI1 expression toward an EwS signature are more important in human MSCs than in mouse cells. Therefore, the inherent permissiveness of cells varies between species, which can also explain the challenges in generating genetically engineered mouse models of EwS. Indeed, regulatory mechanisms and microsatellites are not conserved between humans and mice. As a result, the repertoire of activated and repressed genes upon expression of EWS-FLI1 in mice differs from that in humans, and murine models therefore fail to mimic the epigenetic changes seen in human tumors.

Thus, to date, *in vivo* studies rely exclusively on the use of xenografts, either from cell lines or from primary EwS samples.

3.2 LIN28 and IMP RNA-binding proteins in EwS

As mentioned previously, 25% of the tumors that express LIN28 are childhood malignancies, which is disproportionate in relation to their representation of only 1% of all cancers (Carmel-

Gross et al., 2015). Of the two paralogs, LIN28B appears to be most frequently reactivated in cancer, and can be expressed either alone or in combination with LIN28A (Viswanathan et al., 2009; Carmel-Gross et al., 2015). Because both paralogs are capable of inhibiting the let-7 pathway, albeit by distinct mechanisms, increased prevalence of LIN28B expressing tumors may be explained by LIN28B-specific let-7 independent pathways, consistent with the fact that LIN28B, but not LIN28A, contains a nucleus localizing signal.

In EwS particularly, we recently observed that LIN28B is uniformly re-expressed in a subset of EwS that constitute 10% of cases, and that are associated with a particularly unfavorable prognosis. Essentially, knockdown of LIN28B in LIN28B-expressing (LIN28B⁺) primary EwS organoid cultures, enriched in CSCs, successfully reduced their clonogenic potential and propensity to form tumors *in vivo*. LIN28B⁺ cells displayed decreased let-7 maturation, which could be restored upon testing with the compound 1632, that inhibits LIN28B binding to the terminal loops of pri-let-7 (Roos et al., 2016). Furthermore, we found that the half-life of EWS-FLI1 transcripts is prolonged through direct binding of LIN28B. Importantly, treatment of organoids with the 1632 compound and subsequent injection of treated cells into immunocompromised mice led to inhibition of tumor growth, suggesting a potential approach for clinical application. Therefore, in this particularly aggressive subset of EwS, we showed that LIN28B is essential to stabilize EWS-FLI1 transcripts and maintain the expression of target genes, and is important for establishing the oncogenic program in EwS cells (paper accepted for publication, Figure 3.6 A).

Strikingly, however, let-7 target transcripts were not over-represented among the mRNAs up-regulated following LIN28B depletion. This suggests that other let-7 independent mechanisms may be equally important in the maintenance of a stem-like state. Additionally, stabilization of EWS-FLI1 transcripts by LIN28B did not result in higher EWS-FLI1 protein levels. Indeed, the fusion protein remains stable in LIN28B⁺ and LIN28B⁻ cells. Based on these observations, increased aggressiveness of LIN28B⁺ cells is not due to increased EWS-FLI1 expression, although the chimeric protein constitutes the main tumor drive in EwS. As reported previously, a significant body of data has recently shown that LIN28B regulates target expression at the translational level. We therefore hypothesize that LIN28B orchestrates a series of events that are EWS-FLI1 independent and confer increased malignant potential to CSCs, and still remain to be explored.

Whereas GSCs express IMP2 but not LIN28B (Degrauwe et al., 2016a), EwS can express both families of RBPs. Consistent with this, co-expression of LIN28 and IMPs has been reported in

various cancers (Busch et al., 2016). Through distinct mechanisms, both can negatively regulate the let-7 pathway, giving rise to an elaborate regulatory network in which LIN28 and IMPs sustain the expression of one another and further promote the maintenance of a CSC phenotype (Busch et al., 2016). Additionally, adult hematopoietic progenitor cells can be reprogrammed to acquire fetal-like features following LIN28B induction (Yuan et al., 2012), a process that directly involves interaction of LIN28B and IMP3 independently of let-7 miRNAs, providing supplementary evidence that both RBPs can participate in stemness maintenance (Wang et al., 2019). Interestingly, however, the cellular environment may strongly influence the interplay between IMPs and LIN28B in cancer contexts, as IMP1 expression was shown to result in the negative regulation of LIN28B expression in the intestinal epithelium (Chatterji et al., 2018). In EwS, the role of IMPs has not yet been reported. It remains unclear whether all IMPs or only individual members of the IMP family are involved in CSC maintenance, and we speculate that they may act in a synergistic or complementary manner alongside LIN28B.

Furthermore, our cohort analyses found that 90% of EwS lack the expression of endogenous LIN28B. Therefore, in this subset of EwS, it may be postulated that IMPs participate in CSC maintenance and regulate the let-7 pathway. Of note, the trend seems to be reverted in established EwS cell lines. Indeed, we found that 90% of cell lines are LIN28B⁺, whereas only the remaining 10% are LIN28B⁻. This can either result from *de novo* LIN28B expression, which confers a newly acquired proliferative advantage *in vitro*, or result from the fact that LIN28B⁺ cells are inherently more aggressive and thereby intrinsically fitter and more prone to surviving and proliferating following sustained passaging in *in vitro* cultures. Most likely, both mechanisms may be jointly involved and explain the high proportion of LIN28B⁺ EwS cell lines. Regardless, the discrepant frequency of LIN28B expression in primary cells compared to cell lines further supports LIN28B as a key player in cell tumorigenicity and aggressiveness. Nonetheless, because LIN28B⁻ primary models are particularly challenging to work with in culture conditions with remarkably low proliferation rates, LIN28B⁻ cell lines represent good models to explore the role of IMPs in the absence of LIN28B in EwS.

Therefore, we chose to investigate the biological relevance of IMP expression in EwS and explore a possible interaction with LIN28B in CSC maintenance that may contribute to increased aggressiveness in LIN28B⁺ EwS, using both primary EwS organoids and established EwS cell lines. Subsequently, we questioned which are the EWS-FLI1-independent mechanisms employed by LIN28B to promote cell aggressiveness (Figure 3.6 B).

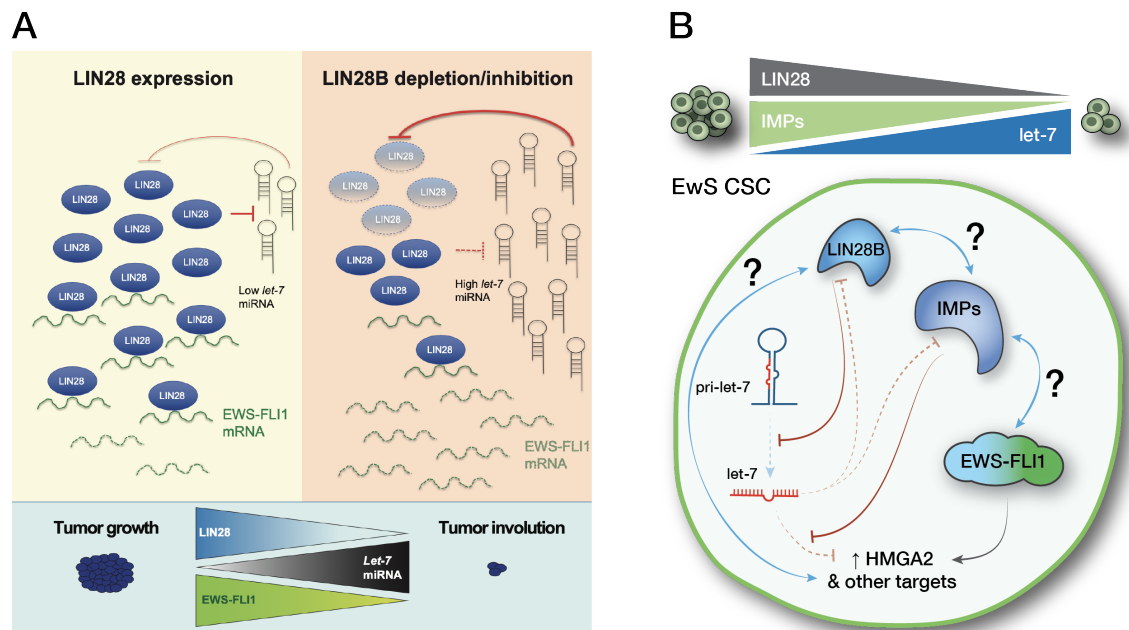


Figure 3.6: The roles of LIN28 and IMPs in EwS CSCs. (A) Schematic depiction of the role of LIN28 in aggressive EwS. LIN28B represses let-7 maturation and stabilizes EWS-FLI1 transcripts, and loss of LIN28B contributes to tumor shrinkage (paper accepted for publication). (B) The first aim of this work is to explore whether IMPs participate in tumorigenesis in LIN28B⁺ EwS and whether they interact with LIN28B. Secondly, we explored LIN28B regulated pathways that promote CSC survival independently of let-7 miRNAs and EWS-FLI1.

3.3 Results

IMP3 expression correlates with poor outcome

To evaluate the putative role of IMPs in promoting EwS progression, we questioned available databases and correlated expression of each IMP paralog with patient survival. We found that IMP3, but neither IMP1 nor IMP2, strongly correlated with poor prognosis when expressed (Figure 3.7A). Additionally, based on public patient datasets from the R2 genomics analysis and visualization platform (<http://r2.amc.nl>), higher IMP3 levels were found in metastatic and relapsed cases compared to newly diagnosed EwS (Figure 3.7B), a trend that was not found for IMP1 and IMP2 (data not shown). Next, based on our previous report that LIN28B is expressed in more aggressive EwS, we looked for a correlation between the expression levels of IMPs. Strikingly, we found that, of the three paralogs, only IMP3 is significantly co-expressed in LIN28B⁺ tumors (Figure 3.7B). Based on these results, it appears that IMP3 may be involved in the tumorigenesis of EwS.

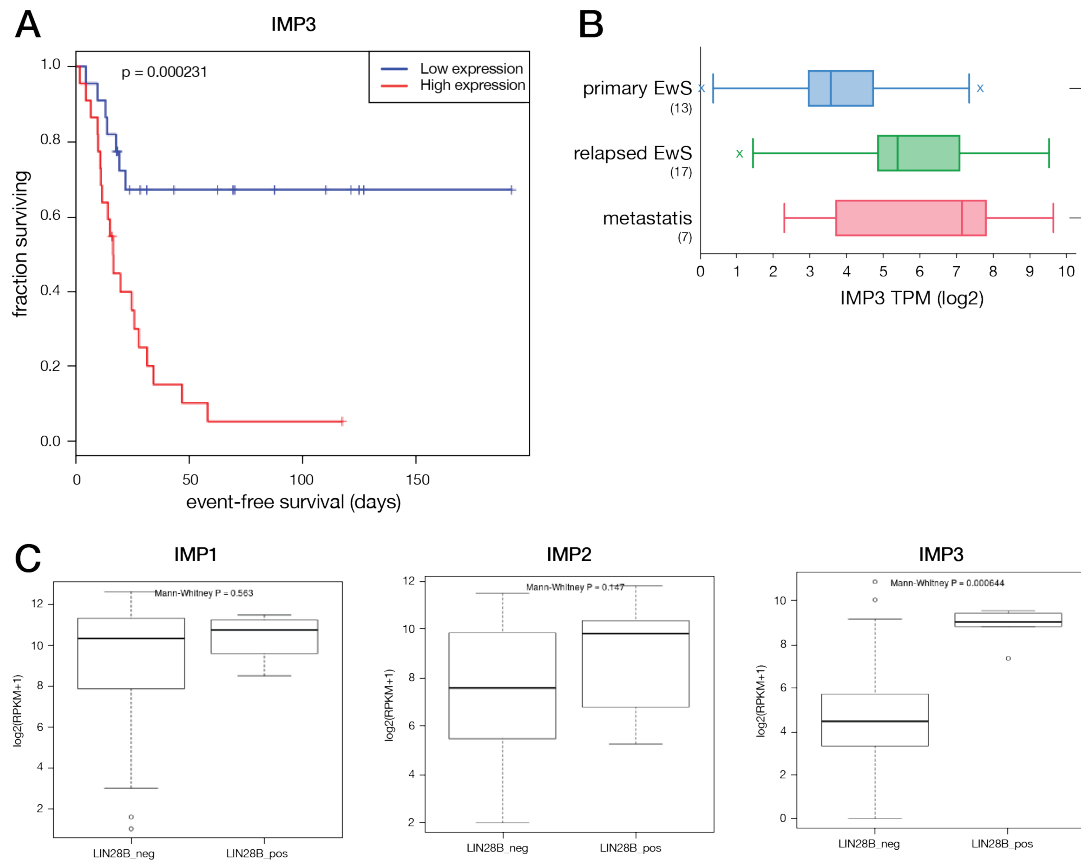


Figure 3.7: IMP3 correlates with poor prognosis and high LIN28B expression. (A) Kaplan-Meier plot of event-free survival where the patients have been divided into high (red) and low (blue) IMP3-expressing based on the median expression of the probe. P -value was calculated using log-rank test. (B) Box-plot showing IMP3 expression in patient samples with newly diagnosed primary EwS with no evidence of previous disease (blue), relapsed EwS (green), or with EwS metastases (red), based on a total of 37 samples. The value in brackets indicates the number of samples in each group. Data generated from the R2 genomics platform. One-way ANOVA was used for statistical analysis. * $P < .05$. (C) The boxplots compare the logarithmic normalized expression of IMP1 (left panel), IMP2 (middle panel) and IMP3 (right panel) in the respective dataset in LIN28B⁺ vs LIN28B⁻ samples, based on the data from 65 primary tumors. Samples were defined as LIN28B⁺ if LIN28B expression was higher than the median expression of all genes over all samples. P -values were calculated used Mann-Whitney U test.

Effect of IMP knockdown in EwS primary cells and cell lines

Next, we assessed the levels of expression of IMPs and LIN28B in two primary samples, namely EwS1 and EwS2, grown as organoid spheres, as well as in three established EwS cell lines, namely A673, SKNMC, and MHHES1, grown as adherent cells. Some of the characteristics of the samples used are listed in Supplementary Table S2.1. Our samples uniformly express all three IMP paralogs. Both primary spheres used are LIN28B⁺. LIN28B is similarly expressed in A673 and SKNMC but is not detected in MHHES1, constituting our only LIN28B⁻ sample (Figure 3.8 A). This is in line with the observation that most EwS cell lines are LIN28B⁺, suggesting reactivation of LIN28B expression may confer a proliferative advantage to the cells when maintained in culture conditions. Thus, throughout this project, we regularly checked expression of LIN28B in MHHES1 cells to ensure that LIN28B remained silenced. Of note,

IMP3 is relatively lower in MHHES1 than in other samples. We compared the mRNA levels of IMPs across samples comparing them to hpMSCs, as they are believed to be the cell of origin of EwS. We found that hpMSCs express very low levels of all IMP paralogs, whereas levels are similar in cell lines and primary EwS. Of note, IMP3 was more highly expressed in primary samples than in cell lines (Figure 3.8 B).

We used the CRISPR/Cas9 technology targeting IMP1, IMP2 and IMP3 to deplete these proteins in our samples (Supplementary Table S2.2). A CRISPR vector encoding the Cas9 sequence but lacking a guide RNA was used as a control (Cas9), and the guide RNA displaying the strongest knockdowns were chosen to target IMP1, IMP2 or IMP3 and are subsequently referred to as sgIMP1, sgIMP2 and sgIMP3, respectively. Following IMP knockdown, cells displayed no significantly visible morphological change (Figure 3.8 C). Based on Western blot analysis, individual knockdown of a member of the IMP family does not affect the expression of other IMPs. Furthermore, we found no remarkable change in LIN28B expression following depletion of IMP, apart from a discrete reduction of LIN28B after knockdown of IMP1 and IMP3 in EwS1 (Figure 3.8 D). Transcript levels of IMPs were strongly reduced following their respective CRISPR-Cas9-mediated knockdown, and were specific to the targeted IMP paralog. However, here we detected upregulation of LIN28B in IMP2 and IMP3 knockdown, in EwS2 only (Figure 3.8 E). In particular, EWS-FLI1 levels remain stable in all samples.

Based on these first results, it is possible that there is some redundancy between IMPs, as downregulation of either one of the paralogs does not seem to affect let-7 target transcripts.

Effects of IMP knockdown on cell viability and proliferation *in vitro*

To assess whether IMP knockdown may affect cell viability, we proceeded to proliferation and metabolic activity assays after knockdown of IMP1, IMP2 or IMP3. We first compared A673 and MHHES1, as the latter lacks LIN28B expression and may therefore display distinct responses to IMP knockdown. However, downregulation of either IMP paralogs resulted in no change of metabolic activity, although discrete reduction of cell proliferation was detected in MHHES1 IMP3 knockdown, as measured by incorporation of BrdU (Figure 3.9 A). Clonogenic assays on these cell lines, in contrast, showed a striking increase in clonogenicity of cells lacking IMP2 (Figure 3.9 B).

In primary EwS organoids, clonogenic assays showed a distinct response to IMP knockdown, as sgIMP2 and sgIMP3 seemed to generally decrease the cell clonogenicity and, in the case of

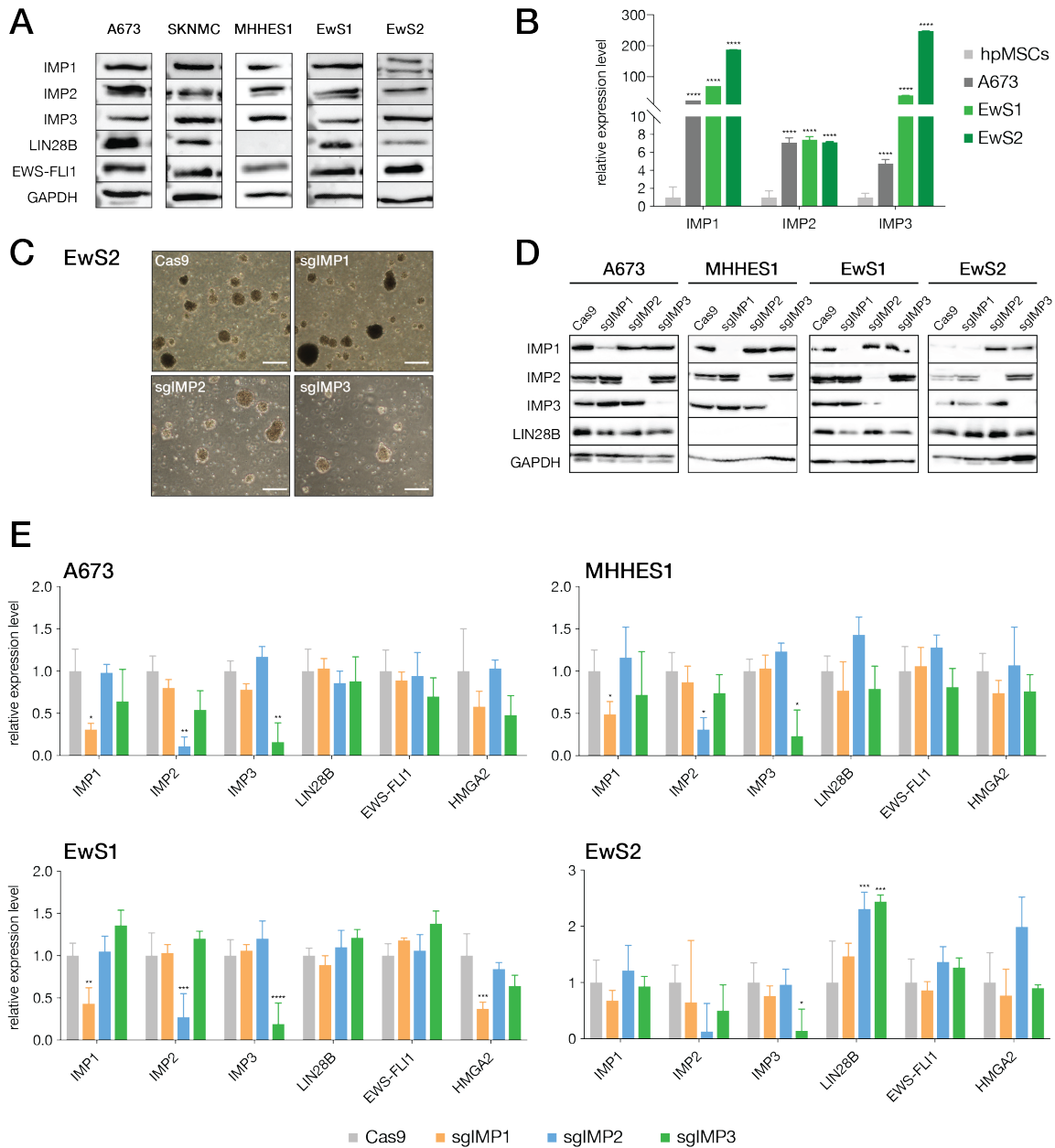


Figure 3.8: IMP expression and CRISPR-mediated knockdown. (A) Western blot showing the levels of IMPs, LIN28B and EWS-FLI1 in cell lines A673, SKNMC and MHHES1, and primary EwS samples (EwS1 and EwS2). MHHES1 is the only sample without LIN28B expression. GAPDH was used as loading control. (B) mRNA expression levels of IMPs in A673, EwS1 and EwS2, compared to hpMSCs, measured by qRT-PCR. Results are shown as mean \pm SD. Two-way ANOVA was used for statistical analysis. (C) Representative micrography images of control (Cas9) or IMP-depleted EwS2 organoids. The scale bar represents 100 μ m. (D) Western blot showing CRISPR-Cas9 mediated knockdown of IMPs. GAPDH was used as loading control. (E) mRNA expression levels of IMPs, LIN28B, EWS-FLI1 and the known let-7 target HMGA2, following CRISPR-Cas9 mediated knockdown of IMPs, measured by qRT-PCR. Results are shown as mean \pm SD. Two-way ANOVA was used for statistical analysis. * $P < .05$, ** $P < .01$, *** $P < .001$, **** $P < .0001$.

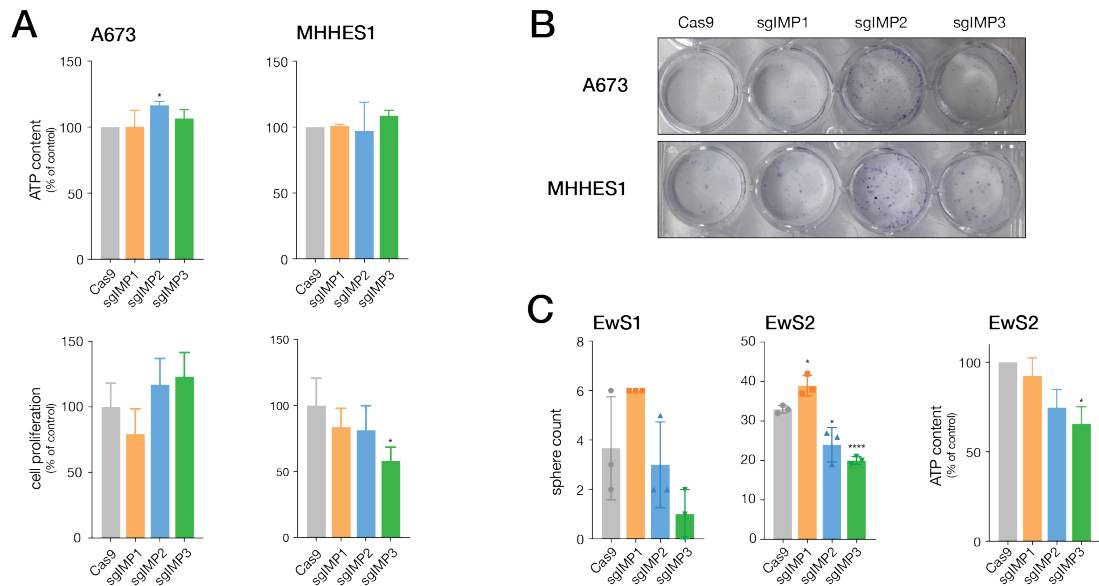


Figure 3.9: Effect of IMP downregulation on proliferation. (A) *Top*, metabolic activity of A673 (left) and MHHES1 (right) following IMP knockdown. *Bottom*, cell proliferation as measured by BrdU incorporation in A673 (left) and MHHES1 (right) following IMP knockdown. The results from two separate experiments on two different cell batches are shown. Results are displayed as mean \pm SD. Two-tailed t-test was used for statistical analysis. (B) Clonogenic assay performed on A673 and MHHES1 infected with control vector or IMP knockdown. Colonies were colored with crystal violet. (C) *Left panels*, single-cell clonogenic assay performed with EwS1 and EwS2 following IMP knockdown. Results are shown as the number of cells counted per 96-well plates. Single values from different experiments are shown. Two-tailed t-test was used for statistical analysis. *Right panel*, metabolic activity of EwS2 following IMP knockdown. The results from two separate experiments on two separate cell batches are shown and displayed as mean \pm SD. Two-tailed t-test was used for statistical analysis. * $P < .05$, ** $P < .01$, *** $P < .001$, **** $P < .0001$.

EwS2, decreased ATP content (Figure 3.9C).

Taken together, our observations indicate that mainly IMP2 and IMP3 may have a putative role in CSC maintenance, although the clonogenic assay performed on A673 and MHHES1 is contradictory to this hypothesis.

Effect of IMP knockdown *in vivo*

Following *in vitro* experiments, we completed our observations by proceeding to *in vivo* injection of cells into immunodeficient mice. For A673 or MHHES1, 10^6 cells were injected bilaterally in the subcutaneous tissue behind the scapula ($n = 5$ mice per group). For EwS1 and EwS2, 10^4 and 2×10^4 cells respectively were injected in the subcapsular compartment of the left kidney, according to usual laboratory practice ($n = 4$ mice per group for EwS1, $n = 5$ mice per group for EwS2). All mice from an experiment were sacrificed at the same timepoint, once the largest tumors had grown to the maximum volume allowed by our experimental license.

The tumorigenic potential of A673 and MHHES1 remained stable in control and IMP depleted cells, as the tumors formed were overall equally large (Figure 3.10 A, left panels). We noted that tumorigenicity of EwS1 organoids was slightly impaired with sgIMP2. However, there was no change in the capacity of EwS2 organoids to form tumors following knockdown of either IMPs

(Figure 3.10 A, right panels). Importantly, we found no significant decrease in the capacity of cells to initiate tumor across our samples following IMP knockdown, as seen by the final proportion of tumors obtained (Figure 3.10 B). Furthermore, for each cell line and primary sample we performed Western blot analyses on cells from dissociated xenografts to confirm that the knockdown remained stable *in vivo* (Supplementary Figure S2.1).

Nevertheless, a trend in IMP3-depleted MHHES1 cells to form less tumors warranted further exploration, as these cells lack LIN28B expression, and represented the most suitable model to explore the role of IMPs independent of LIN28B. Therefore, we repeated MHHES1 injections with 10^5 cells, to see if the trend may become more pronounced when starting with a smaller inoculum ($n = 4$ mice per group). Tumors grew more slowly, as the first ones appeared after six weeks (three weeks when 10^6 cells were injected), and others were only visible after three months. As a result, we decided to assess tumorigenicity of IMP-depleted MHHES1 using a survival curve to measure the duration required for the injected cells to develop a tumor reaching a volume of about 1 cm^3 , at which time the mouse was sacrificed (Figure 3.10 C). The median duration for tumor formation was 62, 52, 83 and 48 days for mice injected with control (Cas9), sg IMP1, sg IMP2 and sg IMP3 cells, respectively. Notably, one mouse injected with IMP2-depleted MHHES1 still had no tumor after nine months. However, the differences were not statistically significant. Therefore, even in cells lacking LIN28B expression, knockdown of individual IMPs is not sufficient to abrogate the tumor-initiating potential of CSCs.

Effect of simultaneous IMP2 and IMP3 knockdown

From our results so far, the knockdown of a member of the IMP family alone failed to affect the cell phenotype in our samples. Nonetheless, we found discrete changes in cell proliferation when IMP2 or IMP3 were depleted. As these two paralogs may share some redundancy, we questioned whether the simultaneous loss of IMP2 and IMP3 could impair CSC proliferation and tumor-initiating capacity. To test this, we infected EwS1 cells with sg IMP2- or sg IMP3-expressing CRISPR vectors alone (sg IMP2 and sg IMP3), or in combination (sg IMP2 + 3). From qRT-PCR results, levels of LIN28B, EWS-FLI1 and the let-7 target HMGA2 remained stable following simultaneous knockdown of IMP2 and IMP3. In addition, Western blot analyses show no changes in the expression levels of either LIN28B or the fusion protein EWS-FLI1 (Figure 3.11 A). Moreover, simultaneous knockdown of IMP2 and IMP3 did not reduce clonogenicity of EwS1 organoid spheres (Figure 3.11 B). Of note, the slight decrease in tumorigenicity suggested from previous

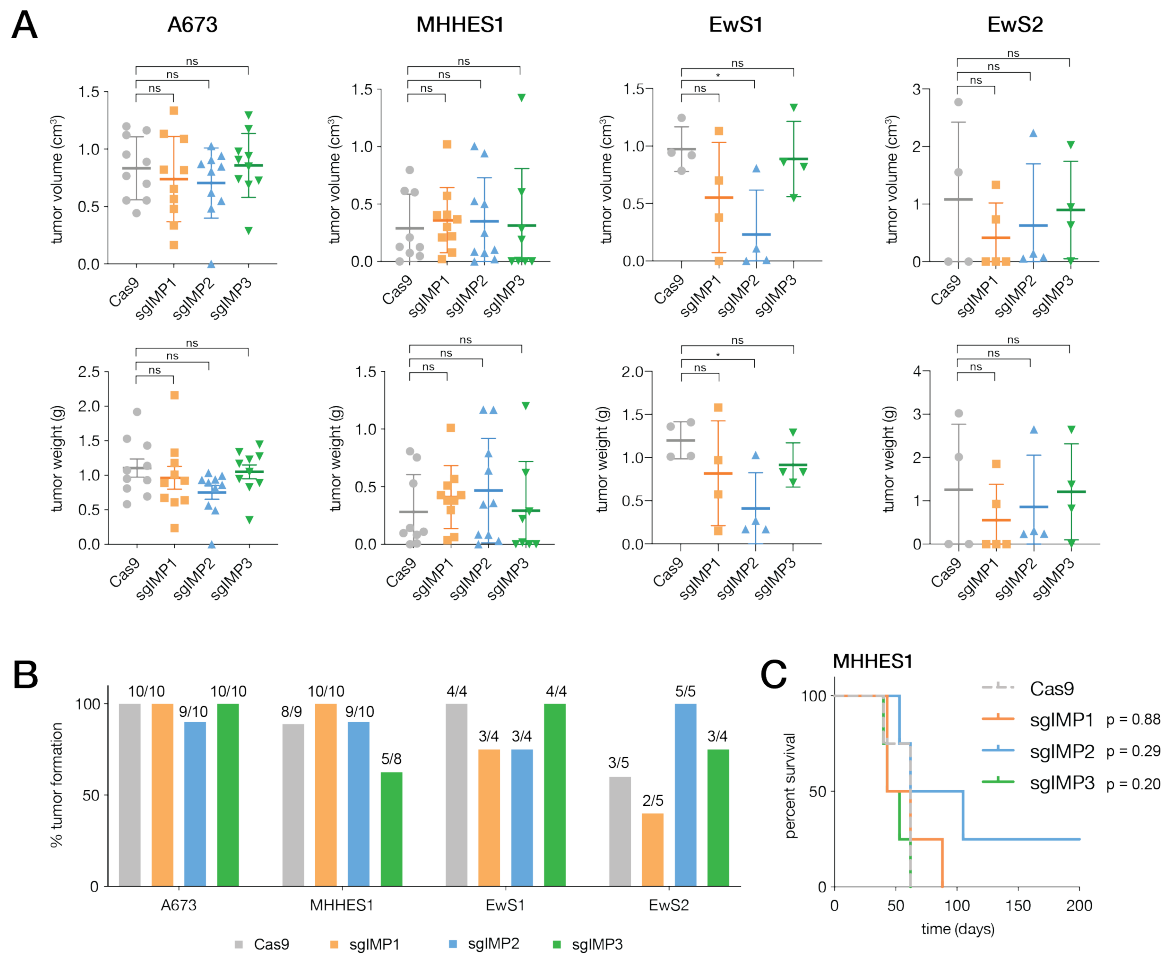


Figure 3.10: IMP knockdown does not impair tumorigenicity *in vivo*. (A) Tumor volume (top panels) and weight (lower panels). The individual values are plotted and the lines show mean \pm SD. Two-tailed t-test was used for statistical analysis. (B) Proportion of tumors formed across the EwS samples injected. The fractions indicate the number of tumors obtained out of the total number of injections. (C) Kaplan-Meier plot showing the time required for tumors to grow to a size of approximately 1 cm³ following injection of 10⁵ MHES1 cells in the subcutaneous tissue of mice ($n = 4$ mice per group). P -values were calculated using log-rank test. * $P < .05$. ns, not significant.

experiments (Figure 3.8 C, left panel) was not replicated here.

Thus, taken together, our observations reject a putative role of IMPs in EwS tumorigenesis, but further support the role of LIN28B as a key driver of CSC maintenance in EwS in LIN28B⁺ tumors.

EWS-FLI1 stability in LIN28B⁺ EwS

Based on the results from tumorigenicity assays, we focused on characterizing the biological functions of LIN28B in EwS. Recent findings from our lab showed that primary LIN28B⁺ EwS have a poorer prognosis (paper accepted for publication). In line with this, based on public patient datasets from R2 genomics analysis and visualization platform (<http://r2.amc.nl>), we found that LIN28B expression is more frequent in relapse (Figure 3.12 A). Additionally, we reported that LIN28B can bind and stabilize EWS-FLI1 transcripts in EwS1 and EwS2. However, EWS-

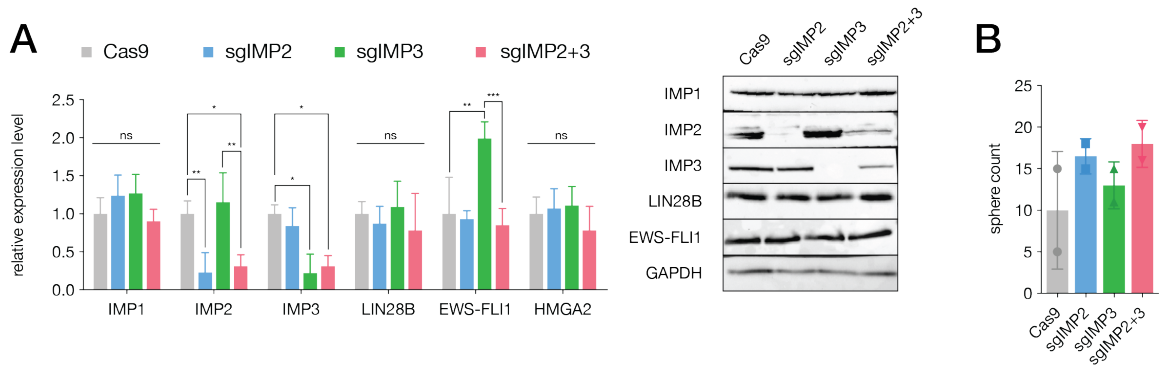


Figure 3.11: Combined knockdown of IMP2 and IMP3 in EwS1 organoids. (A) *Left*, mRNA levels of IMPs, LIN28B, EWS-FLI1 and HMGA2 in EwS1 infected with a control vector (Cas9), depleted from IMP2 (sg IMP2) or IMP3 (sg IMP3) alone or in combination (sg IMP2+3), measured by qRT-PCR. Results are displayed as mean \pm SD. Two-way ANOVA was used for statistical analysis. *Right*, Western blot analysis of samples, showing specific knockdown of the targeted IMP proteins. (B) Single-cell clonogenic assay of EwS1 infected with a control vector (Cas9), depleted from IMP2 (sg IMP2) or IMP3 (sg IMP3) alone or in combination (sg IMP2 + 3), displaying the total number of organoid spheres in a 96-well plate. Two-tailed t-test was used for statistical analysis. * $P < .05$, ** $P < .01$, *** $P < .001$. ns, not significant.

FLI1 protein levels are stable in both LIN28B⁺ and LIN28B⁻ tumors. Furthermore, transcription of EWS-FLI1 was unchanged following depletion of LIN28B, as reported from nuclear run-on assay performed on EwS1, whereas we detected lower levels of nascent transcripts among known EWS-FLI1 targets (paper accepted for publication, Figure 3.12 B). Hence, other mechanisms may be in play that promote an aggressive phenotype in CSCs independently of EWS-FLI1. To explore these, we first determined whether the stabilization of EWS-FLI1 transcripts by LIN28B was common to other LIN28B⁺ cells.

In order to identify other stable or unstable EwS samples, we decided to base our study on other immortalized EwS cell lines. To select the cell lines with the highest dependency to LIN28B, we used the Dependency Map generated by the Broad Institute (Tsherniak et al., 2017). By comparing the expression level of LIN28B and the dependency value (increasing negative values translate a higher degree of dependency), we observed that EwS cell lines follow a trend along which a higher expression of LIN28B appears to correlate with a higher degree of dependency (Figure 3.12 C). While A673 is moderately sensitive to LIN28B knockdown, SKNMC, which expresses the highest LIN28B transcript levels in the corresponding screening, is among the most sensitive cell lines, along with SKNEP1. Thus, we investigated the effect of LIN28B knockdown on EWS-FLI1 stability on A673, SKNMC, and SKNEP1, as well as in SKES1, as it also expresses higher levels of LIN28B.

We then proceeded to LIN28B knockdown using the CRISPR-Cas9 genome editing system. Surprisingly, EWS-FLI1 expression was not reduced upon LIN28B knockdown (Figure 3.12 D and E). Thus, in these cells, LIN28B may not be essential for stabilization of the EWS-FLI1 tran-

scripts. Nonetheless, LIN28B knockdown significantly impaired cellular growth (Figure 3.12 F). In light of recent evidence showing that LIN28B can affect transcription and translation of several targets, we suggest that LIN28B may participate in differential transcription or translation of key pathways that support tumor aggressiveness possibly linked to CSC maintenance.

3.4 Discussion and future perspectives

Despite being rare diseases, childhood cancers are currently the second cause of death in children. Although the emergence of chemotherapy and radiation therapy has significantly improved patient survival, the prognosis remains dismal for some malignancies, particularly in the case of relapse or metastatic disease. Among these, EwS remains a therapeutic challenge. The specific translocation $t(11;22)(q12;q24)$ detected in about 85 % of cases leads to the formation of the aberrant chimeric protein EWS-FLI1, whose expression was found to be sufficient to transform hpMSCs (Delattre et al., 1994; Riggi et al., 2008). Indeed, EWS-FLI1 directly binds the DNA, recruits partners and changes the chromatin conformation, resulting in the activation or repression of target transcription. Thus, substantial epigenetic changes in EwS CSCs dictated by EWS-FLI1 further support the maintenance of an aggressive tumor-driving phenotype, and understanding the key epigenetic pathways affected in these cells is needed to identify putative targets.

Our laboratory previously reported that silencing of miRNAs, including the let-7 family, is essential for CSC maintenance (Riggi et al., 2010; De Vito et al., 2012; Cornaz-Buros et al., 2014). Particularly, we recently reported that LIN28B, capable of repressing let-7 maturation, is reactivated in a subset of highly aggressive EwS. In parallel, IMP2 has been demonstrated to support a CSC phenotype in GBM, in which LIN28B is not expressed, by protecting let-7 target transcripts from degradation (Degrauwe et al., 2016a). Therefore, as LIN28B and IMPs are co-expressed in EwS, we explored whether these RBPs share redundancy in EwS to sustain the growth of the CSC population.

Here, we used the CRISPR-Cas9 gene editing technology to knockdown each IMP paralog in primary EwS and in cell lines. We found that IMP expression is not crucial for CSC proliferation *in vitro* or for tumor growth *in vivo*. Our strategy focused on depleting each IMP paralog separately, and then two paralogs together, based on the hypothesis that IMPs may share some redundancy. We prioritized downregulation of IMP2 and IMP3 over that of IMP1, given that

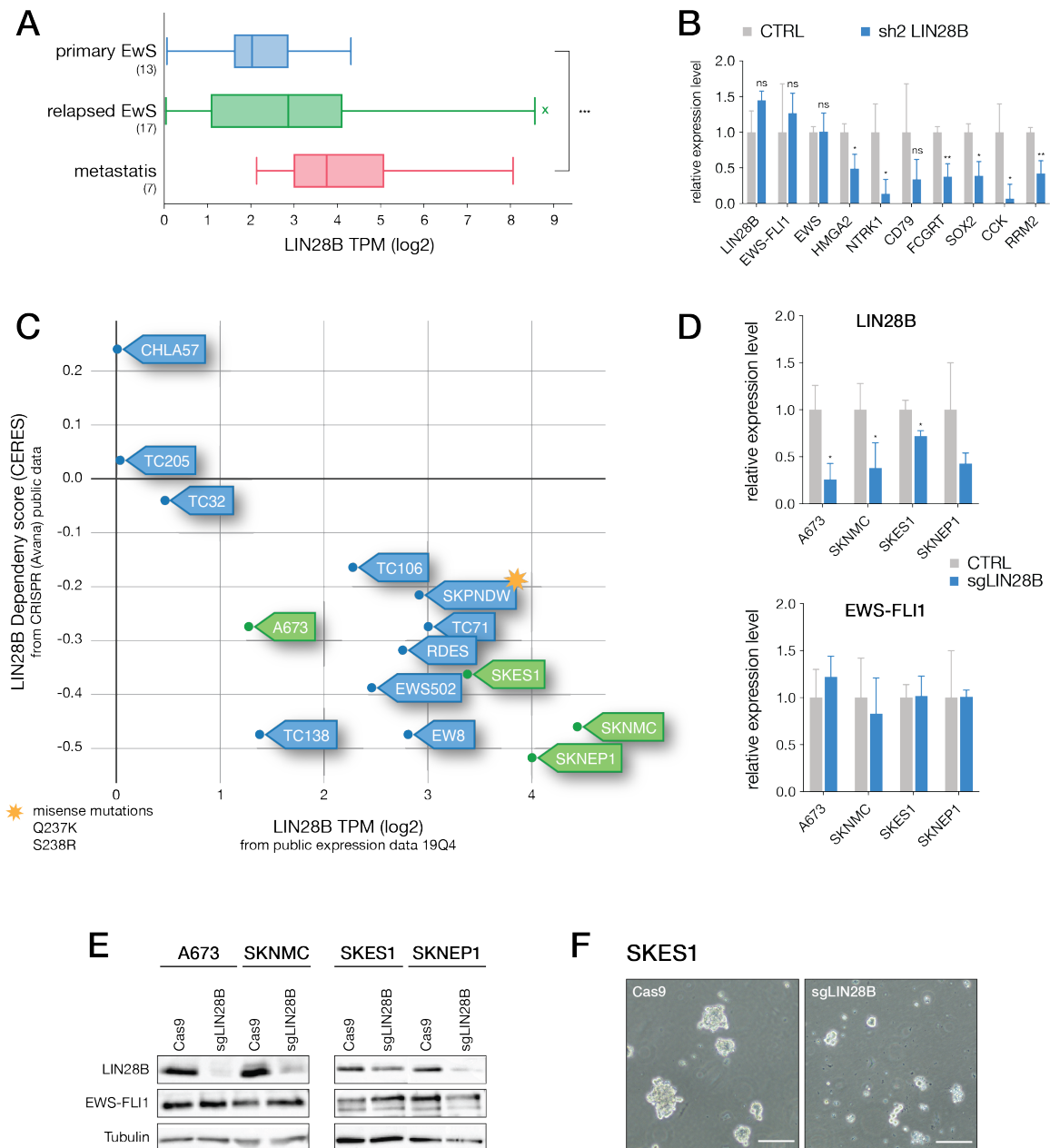


Figure 3.12: LIN28B expression and knockdown in EwS cell lines. (A) Box-plot showing LIN28B expression in patient samples with newly diagnosed primary EwS with no evidence of previous disease (blue), relapsed EwS (green), or with EwS metastases (red), based on a total of 37 samples. The value in brackets indicates the number of samples in each group. Data generated from the R2 genomics platform. One-way ANOVA was used for statistical analysis. (B) Relative nascent RNA levels following LIN28B knockdown using a validated shRNA in EwS1. Results are displayed as mean \pm SD. Multiple t-tests were used for statistical analysis. (C) Dependency map of LIN28B expression is plotted in the x axis (TPM, transcripts per million) and the dependency score is plotted in the y axis. The tags indicate the name of the EwS cell line. The star indicates punctual mutations of LIN28B found in SKPNDW. The cell lines used in this study are indicated in green. (D) Relative levels of mRNA of LIN28B (top panel) and EWS-FLI1 (lower panel) measured by qRT-PCR in different cell lines following CRISPR-mediated knockdown of LIN28B. Results are displayed as mean \pm SD. Multiple t-tests were used for statistical analysis. (E) Western blot analyses of EwS cell lines following CRISPR-mediated knockdown of LIN28B, showing protein expression of LIN28B and EWS-FLI1. Tubulin was used as loading control. (F) Micrography of SKES1 cells infected with a control CRISPR vector (Cas9, left panel) or with LIN28B knockdown (sg LIN28B, right panel). The scale bar represents 50 μ m. * $P < .05$, ** $P < .01$, *** $P < .001$. ns, not significant.

IMP2 strongly affects CSC survival GBM and initial bioinformatic results pointed to a possible role of IMP3. Additionally, our initial *in vitro* results suggested that these two paralogs discretely reduced clonogenicity in EwS organoid spheres (Figure 3.9 A and C). Nonetheless, loss of IMP2 and IMP3 did not further impair cell clonogenicity (Figure 3.11 B). It may have been of interest to see if the absence of all three IMP paralogs successfully impaired cell growth and tumor formation, especially in organoids, as they more adequately mirror the behavior of the original tumors. However, we chose not to proceed to the simultaneous depletion of all three paralogs. Indeed, patient-derived organoids are particularly challenging to work with and are very sensitive to the stress generated during lentiviral infection. Performing three series of infection on these cells would have hardly appropriately reflected the biological changes due the knockdowns only. Furthermore, co-depletion of IMP2 and IMP3 did not affect expression of IMP1, which would have been expected to increase in order to compensate for the lack of the two other paralogs and thereby maintain cell survival and stabilize the cell phenotype. Thus, our observations reinforce the position of LIN28B as a major player in sustaining CSC growth in LIN28B⁺ tumors.

Strikingly, knockdown of each IMP paralog in the MHHES1 cell line, which lacks LIN28B expression, did not impair tumorigenicity *in vivo* and did not affect the expression of let-7 target mRNAs, excluding the hypothesis that IMPs regulate let-7 target expression in the absence of LIN28B in EwS. Thus, it appears that other mechanisms are in place in these cells to promote CSC maintenance through the let-7 pathway. Therefore, the maintained expression of let-7 targets, such as HMGA2 and IMPs themselves, may be controlled by other processes in these cells. As a possible explanation, it was reported that let-7a is a direct EWS-FLI1 target (De Vito et al., 2011). Whether EWS-FLI1-mediated repression of let-7a alone is sufficient to maintain expression of let-7 targets in LIN28B⁻ tumors remains to be explored.

The IMP family of RBPs is known to significantly stabilize transcripts, as evidenced by their ability to increase the half life of mRNPs to more than two hours (Nielsen et al., 2004). Thus, in the LIN28B⁻ MHHES1 cell line, IMPs represented potential candidates involved in EWS-FLI1 mRNA stability. However, our previous study had shown that EWS-FLI1 in LIN28B⁻ organoids had a shorter half-life than in LIN28B⁺ organoids (paper accepted for publication). Here, we found that knockdown of IMPs in MHHES1 indeed failed to affect EWS-FLI1 transcript and protein levels, further rejecting a role of IMP in stabilizing EWS-FLI1 mRNAs.

Furthermore, although bioinformatic data from EwS patient survival and IMP3 levels in tumors indicate a putative role in promoting cancer progression, we did not find that IMP3

directly supports tumorigenicity. On the other hand, of the three paralogs only IMP3 correlated with expression LIN28B. Possibly, the poor outcome observed in high IMP3-expressing tumors results from expression of LIN28B rather than IMP3 itself. Moreover, this is in line with the known effect of LIN28B on the let-7 pathway, which decreases let-7-mediated silencing of IMP3 and other target mRNAs.

Altogether, our results provide additional data to support that LIN28B plays an essential role in EwS CSC maintenance. In addition to stabilizing EWS-FLI1 transcripts, the ability of LIN28B to alter the translational program could also contribute to the aggressive phenotype typical of LIN28B⁺ cancer cells. To explore the effects of LIN28B on the cellular transcriptome and proteome, we first want to compare quantitative proteomic variations in EwS cell lines upon LIN28B knockdown and cross this data with RNA-seq and LIN28B RIP-seq data in the same cells. This will allow us to identify the genes whose protein levels vary while their corresponding transcript levels remain stable. We will then compare the whole cell proteomic and RNA-seq data obtained to the data of primary cells, in which EWS-FLI1 expression was decreased following LIN28B downregulation. By crossing the data together, our goal is to identify specific pathways that are most dependent on LIN28B expression, in an EWS-FLI1-independent manner, and that could mediate an aggressive CSC phenotype (Figure 3.13).

Finally, based on these results, these pathways should be further characterized in EwS. Also, it may be relevant to explore their implication in other pediatric tumors, as many harbor LIN28B reactivation. In conclusion, our results may describe an additional mechanism necessary for CSC maintenance in EwS, and help identify a new potential therapeutic approach for this aggressive tumor. Furthermore, as LIN28B appears to be a central player in many pediatric tumors, this work may help identify a mechanism through which LIN28B increases CSC aggressiveness that may be common to other childhood cancers. Particularly, the potential involvement of LIN28B should be investigated in other childhood sarcomas and cancers that carry specific translocations. Moreover, the existence of a small molecule that prevents LIN28B inhibition of let-7 biogenesis puts this oncofetal RBP in a privileged position as a potential therapeutic target.

It is unclear why or how LIN28B is reactivated in a subset of tumors only. It was first suggested that LIN28B⁺ and LIN28B⁻ tumors may originate from distinct cells, the former originating from NCSCs instead of MSCs. Indeed, whereas normal MSCs lack LIN28B expression, the oncofetal RBP is detected in NCSCs. However, LIN28B appears to be more expressed in relapsed and metastatic disease than in newly diagnosed EwS (Figure 3.12 A). Whether the

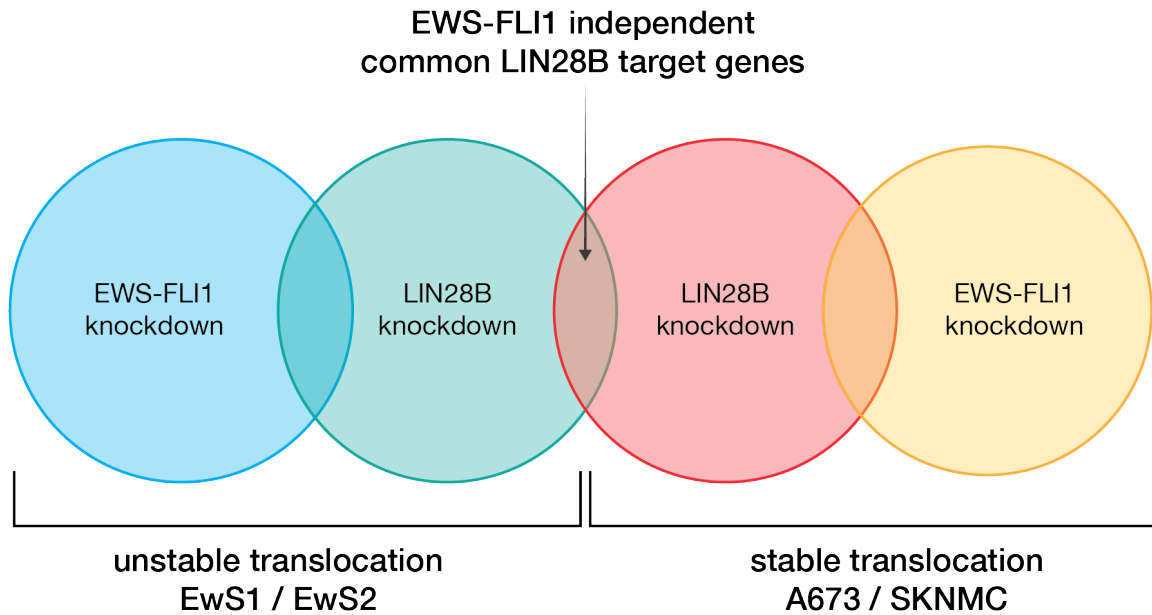


Figure 3.13: Identifying EWS-FLI1 independent genes regulated by LIN28B. Schematic Venn diagram representation of future steps of the project, with analysis of up- or down-regulated genes with knockdown of EWS-FLI1 or LIN28B. Unstable models include EwS1 and EwS2, in which LIN28B knockdown negatively regulates EWS-FLI1 expression, and stable models include A673 and SKNMC, in which EWS-FLI1 remains stable following loss of LIN28B. By excluding genes whose regulation is dictated by EWS-FLI1 and finding genes whose expression changes with LIN28B knockdown only in both models, we will identify a subset of genes whose expression is modulated by LIN28B in both stable and unstable models and in an EWS-FLI1 independent manner.

metastases were diagnosed in recurrent disease only is not specified in this cohort. Nevertheless, we could postulate that LIN28B is secondarily activated in a cell subpopulation following exposure to therapy, in which case LIN28B would constitute a secondary oncogene that appears as a result of epigenetic changes in the CSCs, further contributing to increased tumor heterogeneity and cell survival.

Loss of let-7-mediated repression of LIN28B mRNA by other proteins could activate the negative loop by restoring LIN28B levels. As a result, LIN28B expression would become high enough to continue repressing let-7, activating a positive feedback loop. Thus, we should not exclude IMPs as potential candidates in the first line of lifting the let-7-mediated repression of targets and creating a permissive environment for LIN28B reactivation. Alternatively, a recent study showed that one isoform of the TF CCAAT/enhancer binding protein β (C/EBP- β), namely liver-enriched inhibitory protein (LIP), can repress let-7 transcription (Ackermann et al., 2019), thereby allowing LIN28B expression. Furthermore, a previous study had shown that C/EBP- β transcription is directly activated by EWS-FLI1 (Gardiner et al., 2017). Thus, C/EBP- β transcriptional activation by EWS-FLI1 may be beneficial for CSCs as it results in LIN28B reactivation, a postulation that requires further investigation.

In line with this notion, LIN28B reactivation may result from differential access of EWS-FLI1

to GGAA repeats in the chromatin, which activates or represses transcription of genes that may in turn support expression of LIN28B, as may be the case with C/EBP- β . Among the thousands of GGAA motifs in the genome, only a small fraction is actually open and accessible to EWS-FLI1 (Riggi et al., 2014; Johnson et al., 2017). Thus, each cell may exhibit a different constellation of open GGAA repeats sites. Hence, upon an ideal conformation, reactivation of a gene may occur, that will subsequently activate or repress downstream pathways and promote tumorigenesis. Given the high plasticity CSCs, this process could explain different EWS-FLI1 stabilization mechanisms and, in some cases, reactivation of LIN28B. Nonetheless, the mechanisms that govern differential binding of EWS-FLI1 to DNA still remain to be described.

Of interest, LIN28B stabilizes EWS-FLI1 transcripts in LIN28B⁺ tumors. Still, the EWS-FLI1 protein level is stable between LIN28B⁺ and LIN28B⁻ tumors. Therefore, in the remaining $\sim 90\%$ of EwS, EWS-FLI1 expression is preserved in the absence of LIN28B, either by increased transcription rate, or by protein stability. A study reported that the IGF/PI3K/AKT pathway stimulates EWS-FLI1 transcription (Giorgi et al., 2015), a feature that may be conserved in both LIN28B⁺ and LIN28B⁻ tumors. Alternatively, a study on protein turnover shows that the fusion protein is degraded by the proteasome system upon ubiquitination of a lysine residue at the position 380 (Gierisch et al., 2016). However, to our knowledge no study has identified protein partners that mediate EWS-FLI1 protein stabilization. Thus, in the majority of tumors, EWS-FLI1 may recruit other binding partners to form protein complexes that ensure its constant expression. It would be of interest to characterize these potentially distinct complexes in LIN28B⁺ versus LIN28B⁻ cells to gain a better insight into these mechanisms, by using mass-spectrometry for protein stabilization, and ChIP-seq profiling to identify transcription factors that partner up with EWS-FLI1. This would help identify proteins that ensure EWS-FLI1 protein stabilization or increased EWS-FLI1 transcription in the majority of EwS.

3.5 Materials and Methods

Cell culture

Primary EwS samples were obtained at surgery from Hospital Sant Joan de Déu, Barcelona (EwS1) and from Massachusetts General Hospital, Boston (EwS2), following written informed consent from patients before inclusion of samples in the tumor biobanks. The samples were anonymized prior to analysis and were exempted from informed consent in accordance with the law of the Canton de Vaud. Following mechanical and enzymatic digestion, cells were maintained in culture as organoid spheres in IMDM (Gibco) supplemented with 20 % KO serum (Gibco), human recombinant EGF and bFGF at final concentrations of 10 ng/mL (PROSPEC) and 1 % Penicillin-Streptomycin (PenStrep, Gibco) in ultra-low attachment flasks (Corning), as previously described (Suvà et al., 2009).

The following EwS cell lines used were purchased from ATCC: A673 (RRID:CVCL_0080), SKNMC (RRID:CVCL_0530), SKNEP1 (RRID:CVCL_0631), SKES1 (RRID:CVCL_0627). The MHHES1 cell line (RRID:CVCL_1411) was purchased from DSMZ. The A673, SKNMC and MHHES1 cell lines were cultured in RPMI (Gibco) supplemented with 10 % FBS (PAN BIOTECH) and 1 % PenStrep (Gibco). The SKES1 and SKNEP1 cell lines were cultured in McCoy's 5A Modified Medium (Gibco) supplemented with 15 % FBS (PAN BIOTECH) and 1 % PenStrep (Gibco).

The LentiX-293T cell line was purchased from Clontech (Cat# 632180) and grown in DMEM (Gibco) supplemented with 10 % FBS (PAN BIOTECH), 1 % NeAA (Gibco) and 1 % PenStrep (Gibco).

Cell cultures were maintained at 37 °C and 5 % CO₂ in humidified culture incubators. Cells were regularly tested to exclude mycoplasma contamination.

Lentiviral infection

LentiX-293T (Clontech) packaging cells were transfected using FuGENE[®] 6 Transfection reagent (Promega) for lentivirus production. The envelop and packaging vectors used were pMD2G (Addgene, plasmid # 12259) and pCMVΔR8.74 (Addgene, plasmid # 12263), respectively. After 72 h, the supernatant was collected and filtered (0.45 μm). To transduce primary EwS organoid cells, the supernatant containing the virus suspension was ultracentrifuged at 4 °C for 2 h at 26'000 RPM with a SW28 rotor. The supernatant was discarded and the harvested virus was allowed to resuspend overnight at 4 °C. On the following day, 10⁶ cells were incubated for 8 h with

viral suspension from two LentiX-293T 15 cm dishes, with Polybrene (Sigma-Aldrich) at a final concentration of 6 $\mu\text{g}/\text{mL}$. To transduce EwS cell lines, 10 mL of viral suspension was added to a 60% confluent dish of receiver cells and incubated overnight with Polybrene (Sigma-Aldrich) at a final concentration of 6 $\mu\text{g}/\text{mL}$. The next morning, the medium was changed and completed with 8 mL of the remaining viral suspension and incubated for 8 h with Polybrene (Sigma-Aldrich, 6 $\mu\text{g}/\text{mL}$). Prior to further analysis, antibiotic selection was initiated three days after infection with puromycin at a final concentration of 2 $\mu\text{g}/\text{mL}$ and maintained for 48 h.

Knockdown of IMP1-3 and LIN28B

For stable CRSIPR-mediated knockdown of IMP1-3, we chose gRNA sequences based on the Broad Institute algorithm (<https://portals.broadinstitute.org/gpp/public/analysis-tools/sgrna-design>). For a given gene sequence, the program browses through all possible gRNA sequences adjacent to a PAM sequence. We selected the four top sequences, ranked from 1 to 4 according to specificity and limited off-target effects. As a general rule, we ensured that the gRNAs target the gene of interest between 5-66% of the target length. The sequences listed in Supplementary Table S2.2 were cloned into the CRISPRv2 plasmid (Addgene, plasmid # 52961).

For stable CRISPR-mediated LIN28B knockdown, we used a previously described gRNA that targets exon 2 of LIN28B (Powers et al., 2016). The oligos (Fwd 5'-CACCGCATCGACTGGAAT-ATCCAAG-3'; Rev 5'-AAACCTTGGATATTCCAGTCGATGC-3') were cloned into CRISPRv2 plasmid (Addgene, plasmid # 52961). For CRISPR control conditions, we used a CRISPRv2 vector without a gRNA.

For nascent RNA experiment, shRNA was used for LIN28B silencing. The shRNA inserted in a pLKO.1_puro vector was chosen from the RNAi Consortium and targets the 3'-UTR of LIN28B (TRCN0000122191). In this experiment, we used pLKO.1 shGFP targeting the sequence 5'-GCAAGCTGACCCTGAAGTTCAT-3' as control (Addgene, plasmid # 30323).

CRISPR cloning

The CRISPRv2 plasmid was obtained from Zhang Lab (Addgene plasmid # 52961) (Sanjana et al., 2014). CRISPRv2 was digested with FastDigest Esp3I (ThermoFisher Scientific) at 37 °C for 1 h. The sample was then run on an agarose gel and the 12 kb fragment was extracted with the Monarch DNA Gel Extraction kit (NEB) according to manufacturer's instructions. The forward and reverse oligos were annealed by incubation for five minutes at 95 °C in annealing buffer (10 mM Tris pH 7.5, 1 mM EDTA, 50 mM NaCl) and left to cool down to room temperature.

Ligation of the vector with the annealed oligos was performed with T4 DNA ligase (ThermoFisher Scientific) at 16 °C for 16h, and the enzyme was inactivated at 65 °C for 10 minutes. After butanol precipitation, we electroporated STBL3 bacteria with the ligation reaction product, and subsequently screened and sequenced the resulting clones. For control conditions, we used a CRISPRv2 vector without a gRNA.

Proliferation assays

For single-cell clonogenic assays, primary EwS organoids were manually dissociated into a single-cell suspension. Cells were counted and diluted to a final concentration of 100 cells in 10 mL of culture medium. Cells were then plated at single-cell density in low-attachment 96-well plates (Corning) with 100 μ L medium per well. After one week, 100 μ L of fresh medium was added to each well. After a total incubation time of three weeks, the number of organoid spheres was assessed by micrography imaging.

For metabolic activity assays, CellTiter Glo reagent (Promega) was used according to the manufacturer's instructions. Cells were seeded at a density of 5'000 cells per well in five replicates into black opaque 96-well plates (ThermoFisher Scientific) and incubated for 72 h prior to reading. Luminescence was measured with SynergyMx instrument (BioTek).

Cell proliferation was determined using Cell Proliferation ELISA BrdU colorimetric kit (Roche) according to the manufacturer's instructions. Cells were seeded at a density of 500 cells per well in six replicates into 96-well plates (Corning) and were incubated with BrdU for 2 h 30. Absorbance was measured with SynergyMx instrument (BioTek).

For colony formation assays, cells were seeded at a density of 200 cells per well in six replicates into 24-well plates. After one week, wells were carefully washed with PBS and cells were fixed with 100 % methanol for 20 minutes. Methanol was removed, wells were washed again with PBS and colonies were stained with a 0.5 % crystal violet (Acros Organics) solution for five minutes at room temperature. Plates were washed with water and allowed to dry overnight.

RNA extraction, cDNA synthesis and quantitative real-time PCR

RNA was extracted using the miRNeasy Mini Kit (Qiagen) according the manufacturer's instruction. For cDNA synthesis, 500 ng of RNA template was reverse-transcribed using M-MLV Reverse Transcriptase (Promega). qRT-PCR was performed using PowerUp SYBR Green (Applied Biosystems) with specific primers (Supplementary Table S2.3), and TaqMan Universal PCR Master Mix (Applied Biosystems) with specific probes for *NANOG*, *SOX2* and *H19*. qRT-PCR

was run by QuantumStudio 5 instrument (ThermoFisher Scientific). Each reaction was performed in triplicates and fold expression change was calculated using the comparative $\Delta\Delta C_t$ method, normalized to TBP and 36 β 4 endogenous controls.

Preparation of protein cell lysate and Western blot

For protein extraction, cells were harvested at +4 °C, washed in ice-cold PBS and lysed in SDS-RIPA buffer (150 mM NaCl, 1% NP-40, 0.5% sodium deoxycholate, 0.1% SDS, 50 mM Tris pH 8.0) containing protease inhibitor cocktail (Roche). The lysate was incubated on ice for 20 minutes, sonicated twice for 10 seconds at 35 kHz, and centrifuged at 4 °C for 10 minutes at 13'000 RPM. The supernatant was used for protein sample preparation. Protein concentration was assessed using Bradford Protein Assay Dye (Bio-Rad). Western blot was subsequently performed according to standard procedures. Primary antibodies included: anti-IMP1 (Cell Signalling Technologies, Cat# 2852), anti-IMP2 (MBL International, Cat# RN008P1), anti-IMP3 (MBL International, Cat# RN009P), anti-LIN28B (Cell Signalling Technologies, Cat# 4196), anti-HMGA2 (Cell Signalling Technologies, Cat# 5269), anti-FLI1 (Abcam, Cat# ab15289), anti-GAPDH-HRP (Abcam, Cat# ab9482), and anti-Tubulin (Millipore, Cat# CP06). Secondary antibodies included: HRP-conjugated sheep anti-mouse (GE Healthcare, Cat# NA931) and goat anti-rabbit (Agilent, Cat# P0448). Bands were visualized and analyzed using Western Bright Sirius (Witec AG) detection reagents, according to the manufacturer's instructions, with Fusion Fx software (Vilber Lourmat).

RNA-immunoprecipitation of LIN28B

RIP on EwS cells was performed using the EZ-Magna RIPTM RNA-Binding Protein Immunoprecipitation Kit (MerckMillipore) according to the manufacturer's instructions. Briefly, following lysis of cells at -80 °C, total lysate was incubated overnight with anti-LIN28B (final concentration 1:50, Cell Signalling Technologies, Cat# 4196) pre-bound to magnetic beads provided with the kit. The beads were then washed and the protein-RNA complexes were dissociated by proteinase K digestion for 30 minutes at 55 °C. RNA was subsequently purified using the NucleoSpin[®] RNA isolation kit (Macherey-Nagel). The presence of LIN28B in LIN28B-immunoprecipitated lysate was assessed by Western blot. Isolated RNA was subsequently processed for RNA-seq.

Nascent RNA capture and cDNA synthesis

Nascent RNA capture was performed with a Click-iTTM Nascent RNA Capture Kit (Life Tech-

nologies) according to the manufacturer's instructions. Briefly, cells were incubated with 5-EU at a concentration of 0.5 mM for 30 minutes. Total RNA was isolated using the NucleoSpin® RNA isolation kit (Macherey-Nagel) and biotinylated. Following RNA precipitation, Dynabeads provided with the kit were used to isolate the nascent RNA with incorporated 5-EU. For RNA-seq, the samples were immediately processed for library preparation. For cDNA synthesis from the bound nascent RNA, the bead suspension was heated at 70 °C for five minutes. Random primers (Promega) and dNTP (MP Biomedicals) were immediately added to the mixture. The suspension was left to cool down to room temperature for 30 minutes under constant rotation. M-MLV Reverse Transcriptase (Promega) and RNasin Ribonuclease inhibitor (Promega) were subsequently added to the suspension, which was then warmed to 42 °C for 1 h with gentle vortexing. Finally, the cDNA was collected after heating the solution for five minutes at 85 °C.

***In vivo* mouse injections and tumor dissociation**

NOD-SCID gamma mice were given Paracetamol one day prior to surgery. Anaesthesia was obtained by intraperitoneal injection of a solution containing 100 mg/kg Ketamine (Ketasol-100, Graeb AG) and 16 mg/kg Xylazine (Rompun 2%, Provet AG), diluted in PBS. For EwS cell lines, cells were injected bilaterally in the subcutaneous tissue behind the scapula. For EwS1 and EwS2, cells were injected in the subcapsular compartment of the left kidney. Cells were allowed to engraft for four weeks for the cell lines or eight weeks for the primary cells. Mice from the experiments shown in Figure 3.10 A and B were all sacrificed when a first tumor had reached a volume of about 1 cm³. The tumor volume was calculated as $V = \frac{4}{3} \pi \times \frac{h \times l \times s}{8}$, where h indicates the tumor height, and l and s the dimensions of the tumor on the long and short axes, respectively. Mice from the experiment shown in Figure 3.10 C were sacrificed when their respective tumor reached a size of approximately 1 cm³. Statistical analyses were performed using GraphPad Prism 8 software. Animal experimental protocols were approved by the Veterinary Service of the Canton of Vaud under authorization numbers VD2488 and VD3021.

To assess gene and protein expression in xenografts, tumors were dissociated using the human Tumor Dissociation kit (Miltenyi Biotec) and the gentleMACS™ dissociator (Miltenyi Biotec) according to the manufacturer's instructions. To remove red blood cells, the cell suspension was incubated in ACK buffer (150 mM NH₄Cl, 100 mM KHCO₃, 0.1 mM EDTA-NA₂, pH 7.2) for five minutes on ice. The cells from the xenografts were subsequently cultured in normal conditions until further processing.

Analysis of RNA-sequencing data

RNA-seq library preparation was performed following the Illumina TruSeq or Smarter protocols by the genomics platform at the Institute of Genetics and Genomics of Geneva. Sequencing was performed using HiSeq 4000 Illumina.

Survival and gene expression data

The data presented in Figure 3.7 A was collected from Savola et al. (2011), available as GSE17618, to determine association of IMP expression with survival in EwS. We performed Cox univariate analysis on the 8 probesets of the array associated to the IMP2, thus associating to each gene two z -scores and P -values, for event-free and overall survival. For the data presented in Figure 3.7 C, as LIN28B is not represented in the array used by Savola et al. (2011), we turned to the RNA-seq dataset of Brohl et al. (2014). We retrieved the gene-level normalized data ($\log_2(\text{RPKM})$) from Oncogenomicsdb and limited the analysis to 65 primary tumors (samples with IDs beginning with “EWS” or “NCI”). After defining an expression detection threshold equal to the median expression of all genes across all samples we classified the samples into LIN28B positive (6 samples) and negative (59 samples). We then compared the expression of the IMP paralogs between positive and negative samples, using a Mann-Whitney U-test.

Statistical analyses

GraphPad Prism software 8 was used to generate graphs and to perform the corresponding statistical tests, as indicated in the figure legends.

Chapter 4

Conclusion

Although the cancer hallmarks unify the essential properties of tumor cells across all cancer types, there is extensive heterogeneity not only between different tumors, but also among the cells within a single tumor bulk. Intratumoral heterogeneity is additionally fueled by CSCs, whose discovery in different tumor types suggested that their presence may also constitute a hallmark of cancer. These cells can be isolated by a similar set of markers across multiple tumor types, but maintain distinct profiles. Therefore, it is crucial to identify key regulatory mechanisms that are disrupted in CSCs in different cancers and that contribute to these cells acquiring the same functional phenotype. Despite the fact that CSCs are generated following an array of different biological alterations, it appears that some pathways are almost uniformly altered in several cancers, such as dysregulation of miRNAs expression and reactivation of oncofetal RBPs.

Thus, in this work, we addressed various mechanisms that had been successfully shown to be essential for CSC survival in other tumor types. Ultimately, strategies that we thought would work based on previous results turned out not to be applicable in a different context. Therefore, this work illustrates the challenges in accurately predicting the central cellular mechanisms in cancer and the approaches to use in order to counteract them. Mainly, we noticed that observations in an adult cancer, here GBM, are hardly applicable to the pediatric tumor EwS, and vice-versa. Yet, the initial goal was exactly the opposite, with the idea that enhancing miRNA maturation in GBM would reproduce the phenotype observed in EwS, or that IMPs may be as important for CSCs in EwS as they were in GSCs. This leads us to ask, why did we observe such distinct responses in our models? Much of the answer lies in the complexity and possible redundancies of the mechanisms that govern epigenetic modifications, and their impact in cancer pathogenesis.

In normal cells, epigenetic processes help coordinate the expression of the genes required for development and homeostatic maintenance. Under such control, from the same genome, a population of stem cells within a tissue is maintained and their replication is monitored to generate progenitor and lineage-committed cells, which will in turn be programmed by epigenetic cues to differentiate in an organized fashion. However, this balance can be lost following genetic mutations and/or genomic instability that can lead to aberrant epigenetic control. The resulting deregulated and distorted epigenetic landscape participates in promoting unrestricted cell proliferation, the first step toward tumor initiation and progression. Indeed, changes in the epigenome can result from mutations in genes encoding epigenetic regulators, or in genes with the power to affect downstream transcription of targets. Consequently, cancer cells display modified chromatin conformation, DNA methylation, and/or ncRNA repertoires, leading to an altered transcriptome. As epigenetic modifications are heritable, they participate in selecting subpopulations of cells in the tumor that have proliferative and survival advantage in addition to possibly increased invasive behavior (Tam and Weinberg, 2013; Easwaran et al., 2014). Thus, epigenetic mechanisms have the capacity to orchestrate entire biological networks and rewire the cell entirely, thereby mediating cancer cell plasticity, as exemplified by the successful reprogramming of somatic cells upon *de novo* expression of certain TFs (Yu et al., 2007). Ultimately, these mechanisms can reprogram the cell, reverting its state completely to that of a CSC, displaying a pluripotent and quiescent stem-like state with the capacity to promote local and/or distant invasion. Through its ability to enable altered transcriptional programs to reprogram cells, epigenetics can promote tumorigenesis through the emergence of CSCs and sustain tumor heterogeneity (Mazor et al., 2016).

The cellular context, including the epigenetic state and the surrounding microenvironment, is particularly determinant for cellular transformation. For example, in hereditary retinoblastoma, a first *Rb* allele mutation occurs in the germ line, followed by mutation of the second allele in the fast growing cells of the retina. This leads to bilateral development retinoblastoma before one year of age in most cases. Following treatment, long-term survivors are at high-risk of developing osteosarcoma, as well as soft tissue sarcoma. However, *Rb* is altered in numerous cancers, including ovary, breast, bladder, CML, oesophageal and liver cancers (Burkhart and Sage, 2008; Campbell et al., 2020). In fact, some will argue that the *Rb* pathway is affected in the majority of adult cancers. In contrast, hereditary *Rb* mutations lead almost solely to retinoblastoma as a primary cancer, and does not predispose to all these cancer types equally,

but rather mainly to a restricted panel of tumors (Kleinerman et al., 2007; Dommering et al., 2012). Indeed, the effects of *Rb* loss depend on whether it affects a stem cell, a progenitor cell or a differentiated cell, and on the affected tissue (Burkhart and Sage, 2008). In line with this, we mentioned previously that expression of EWS-FLI1 alone is sufficient to drive tumor formation when expressed in hpMSCs in particular, but not all cells can support its expression, as EWS-FLI1 can be cytotoxic and most cells will undergo apoptosis. Thus, activity of an oncogene is dependent on a permissive environment. Interestingly, such oncogenes can completely rewire the cells so that they become dependent on their expression to survive and proliferate, a phenomenon coined as “oncogene addiction” (Weinstein, 2002). It is particularly striking that, despite genetic instability, the expression of an oncogene can remain crucial for a cell to survive. The importance of a single driver oncogene is best appreciated in cancer cell lines, which can maintain strong oncogene addiction despite undergoing significant genetic drift upon successive passaging and exposure to non-physiological conditions. Thus, identifying such oncogenes is a primary goal in cancer research.

Coming back to the example of EwS, evidence that EWS-FLI1 silencing abrogates cell tumorigenicity strongly suggests that CSCs are “addicted” to this fusion protein. Thus, by targeting EWS-FLI1 directly, a protein that is found only in tumor cells, we could effectively annihilate the cancer cells and cure the patient. It is however unfortunate that such a strategy may not be applied in the case of EwS. This is partly due to the biochemical instability of the molecule and lack of a unique stable conformation of the protein, a result from its low hydrophobicity (Üren et al., 2004). Consequently, lack of a high-resolution 3D structure of EWS-FLI1 challenges the design of specific inhibitors using computer-assisted approaches. Moreover, large-scale screenings and laboratory testing of the molecule alone is hindered, as instability of EWS-FLI1 poses obstacles for its synthesis and purification (Üren and Toretsky, 2005). Currently, screenings mainly focus on testing cells directly. Due to the small size of the patient population and scarcity of tumor samples, such methods require strong collaborations between institutes, and between academia and the industry to efficiently deliver results. Also, delivery of siRNA or antisense oligonucleotides is not yet efficient in humans, but may still bear promises in the future. Therefore, current strategies are focusing on disrupting key protein interactions that affect EWS-FLI1 expression and/or activity. So far, inhibition of RHA, which directly pairs with EWS-FLI1, with the small molecule YK-4-279 successfully disrupted growth of tumor xenografts (Erkizan et al., 2009). The clinical applicability of this approach still remains to be determined. Exploiting the

IGF pathway that is essential for EwS has shown limited results, with only few patients responding well (Olmos et al., 2011). Additionally, epigenetic therapies inhibiting histone deacetylases are also under clinical investigation (Arnaldez and Helman, 2014).

We found that LIN28B may be a secondarily activated oncogene acting as an epigenetic mediator (Feinberg et al., 2016) and participating in the reprogramming of the cell in a subset of highly aggressive EwS. As pediatric tumors generally present a low mutational burden, epigenetic changes play a particularly crucial role in sustaining tumor growth in these cancers. In line with this, re-expression of the oncofetal binding protein LIN28B participates in increasing ITH and CSC maintenance. However, only a minority of EwS appear to express LIN28B, suggesting that other such developmental factors could be involved in EwS tumorigenesis. Because IMP2 is crucial for GSC survival in GBM, and IMPs are involved in normal embryogenesis, we were prompted to assess their possible role in EwS, as they are also expressed in this tumor type and may be equally central in regulating the let-7 pathway. It was striking to find that IMP depletion had no effect on the capacity of EwS CSCs to form tumors. Hence, while a cancer type may be strongly addicted to a gene, as GSCs require IMP2 expression for survival, the same gene may have no role in another tumor type, as EwS cells do not respond to IMP depletion. Intriguingly, GBM is an adult cancer and accordingly has a particularly high mutational load, whereas, in contrast, EwS is a cancer whose emergence and maintenance largely relies on epigenetic mechanisms. Thus, given that the cellular context is highly divergent between these tumors, the specific genetic and epigenetic landscapes of each tumor are indeed determinant for the expression and function of their defined oncogenes, and generate distinct regulatory networks that promote tumor formation and propagation.

In EwS, the chromatin at GGAA repeat motifs is generally tightly packaged, ensuring a closed chromatin conformation, but can become opened when, upon binding to DNA, EWS-FLI1 recruits chromatin remodelling partners, allowing chromatin opening and transcription activation. The mechanisms that allow the initial binding of EWS-FLI1 to occur at these sites are still unknown. Nevertheless, the specific constellation of sites where EWS-FLI1 binds and opens chromatin to modulate gene transcription leads to an altered transcriptome, enabling transformation and tumorigenesis. As a result, secondary oncogenes may appear, as may be the case of LIN28B. Still, as the majority of EwS are LIN28B⁻, and in light of the extensive plasticity of CSCs, other RBPs or other molecules may be recruited by EWS-FLI1. Much investigation is still required to identify putative proteins whose participation with the fusion protein is crucial

for CSC maintenance. By doing so, we may come closer to identifying targetable partners whose downregulation may specifically eradicate CSCs and possibly lead to cure.

Chapter 5

Supplementary Material

5.1 Glioblastoma

Table S1.1: Properties of primary GBM samples.

Tumor sample	Age (years)	Subtype	Stem cell surface markers	IDH	MGMT promoter
MGH4S	N/A	PN	low expression	N/A	methylated
MGH8S	N/A	PN	high expression	N/A	methylated
MGH26S	61	PN	N/A	WT	methylated
MGH28S	60	Mes	nestin +++	WT	unmethylated
MGH31S	70	Mes/N	N/A	WT	unmethylated

List of characteristics of the primary GBM samples used in this work (Wakimoto et al., 2011; Patel et al., 2014). PN, proneural; Mes, mesenchymal; N, neural; WT, wild-type; N/A, not applicable.

Table S1.2: List of upregulated let-7 target genes in high H19 expression GBM.

Gene	Correlation
NID2*	0.381066545
BZW2*	0.379652356
IMP2*	0.378782099
CCND1*	0.358244581
IGF2*	0.357797761
HMGA1*	0.342900201
HMGA2*	0.293640761
IMP3*	0.291511799
CCND2	0.239914434
IMP1	0.224505925

* Genes among the 500 top upregulated genes.

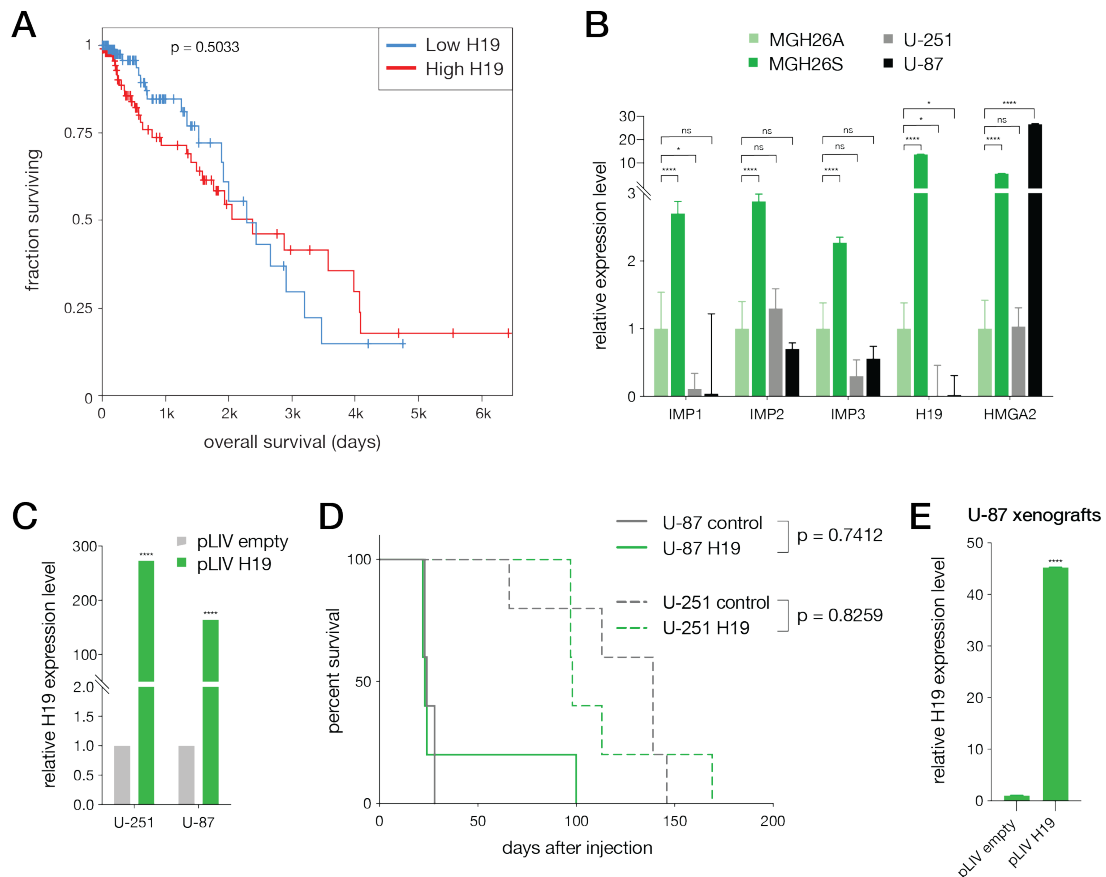


Figure S1.1: H19 overexpression in GBM cell lines. (A) Kaplan-Meier overall survival curves for lower-grade glioma patients with low (blue) or high (red) H19 expression. Data was obtained from the TCGA database and the curve used RNA-sequencing data from 486 brain tumors. *P*-value was calculated using log-rank test. (B) Expression levels of IMPs, H19 and HMGA2 in MGH26 (adherent, A, and spheres, S) and in two GBM cell lines, U-251 and U-87. Two-way ANOVA was used for statistical analysis. (C) Expression of H19 in U-251 and U-87 with the empty control vector (pLIV empty) or H19 overexpression (pLIV H19). Student's *t*-test was used for statistical analysis. (D) Kaplan-Meier survival curves of mice following orthotopic injection of 50'000 U-251 or U-87 cells, infected with an empty vector (control, grey) or with H19 induction (H19, green). *n* = 5 mice per group. *P*-value was calculated using log-rank test. (E) Expression of H19 in U-87 xenografts following dissociation of brain tumors with (pLIV H19) or without (pLIV empty) H19 overexpression. Student's *t*-test was used for statistical analysis. * *p* ≤ .05, ** *p* ≤ .01, *** *p* ≤ .001, **** *p* ≤ .0001. ns, not significant.

Table S1.3: List of oligos used for CRISPRi genome editing.

Target gene	Sequence	
H19 CRISPRi1	Fwd	5'-CACCGGGGAACCGAGGGGCAACCAG-3'
	Rev	5'-AAACCTGGTTGCCCTCGGTTCCCC-3'
H19 CRISPRi2	Fwd	5'-CACCGGGGAACCGAGGGGCAACCAG-3'
	Rev	5'-CACCGGAGATGTCCAAGGTGCTCCT-3'
H19 CRISPRi3	Fwd	5'-CACCGGGGAACCGAGGGGCAACCAG-3'
	Rev	5'-AAACAGGAGCACCTTGGACATCTCC-3'
H19 CRISPRi4	Fwd	5'-CACCGGGGAACCGAGGGGCAACCAG-3'
	Rev	5'-AAACCTGGTTGCCCTCGGTTCCCC-3'

The oligo sequences were chosen from the datasets from CRiNCL (Liu et al., 2017) and based on predicted scores following the hCRISPRi-v2.1 algorithm (Horlbeck et al., 2016).

5.2 Ewing Sarcoma

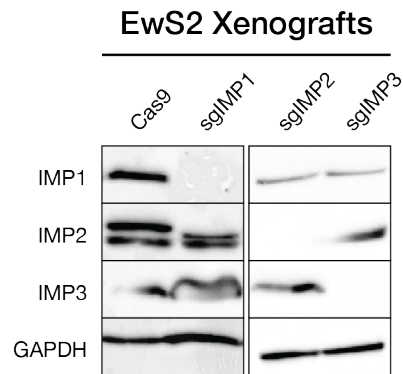


Figure S2.1: Western blot of EwS2 xenografts. GAPDH was used as loading control.

Table S2.1: Characteristics of Ewing sarcoma samples.

Sample	Age (years)	Sex	Site	Staging	EWS-FLI1	LIN28B
EwS1	pediatric	female	scapula	primary	type 1	+
EwS2	pediatric	male	lung	metastatic	type 2	+
A673	15	female	skeletal muscle	primary	type 1	+
SKNMC	14	female	brain	metastatic	type 1	+
MHHES1	12	male	ascites	metastatic	type 2	-
SKES1	18	male	bone	primary	type 2	+
SKNEP1	25	female	pleural effusion	metastatic	type 2	+

List of characteristics of the EwS primary samples (EwS1 and EwS2) and cell lines used in this work.

Table S2.2: List of oligos used for CRISPR-Cas9 genome editing.

Target gene	Sequence	Exon	Product size (%)
IMP1 CRISPR 1	Fwd 5'-CACCGCAAGATCATCTTACAAGCGG-3' Rev 5'-AAACCCGCTTGTAAGATGATCTTGC-3'	7	767 (44.2)
IMP1 CRISPR 2	Fwd 5'-CACCGATTCTGGTGCCCAAAAAACAA-3' Rev 5'-AAACTTGTTTTTTGGGCACCGAATC-3'	2	232 (13.4)
IMP1 CRISPR 3 *	Fwd 5'-CACCGGGCCATCGAGAATTGTTGCA-3' Rev 5'-AAACTGCAACAATTCTCGATGGCCC-3'	9	1010 (58.2)
IMP1 CRISPR 4	Fwd 5'-CACCGGAATGTCACCTATTCCAACC-3' Rev 5'-AAACGGTTGGAATAGGTGACATTCC-3'	5	383 (22.1)
IMP2 CRISPR 1	Fwd 5'-CACCGTGCATATGTGACGTTGACAA-3' Rev 5'-AAACTTGTCAACGTCACATATGCAC-3'	5	366 (20.3)
IMP2 CRISPR 2	Fwd 5'-CACCGAAAAGATGCCAAGTGCGCTG-3' Rev 5'-AAACCAGCGCACTTGGCATCTTTTC-3'	10	1105 (61.4)
IMP2 CRISPR 3 *	Fwd 5'-CACCGGTGGGGACCAGGATCCGCAG-3' Rev 5'-AAACCTGCGGATCCTGGTCCCCACC-3'	6	587 (32.6)
IMP2 CRISPR 4	Fwd 5'-CACCGTGCATATGTGACGTTGACAA-3' Rev 5'-AAACTTGTCAACGTCACATATGCAC-3'	5	366 (20.3)
IMP3 CRISPR 1 *	Fwd 5'-CACCGTATCCCGCCTCATTTACAGT-3' Rev 5'-AAACACTGTAAATGAGGCGGGATAC-3'	3	276 (15.9)
IMP3 CRISPR 2	Fwd 5'-CACCGCCATCGAGGCGCTTTCAGGT-3' Rev 5'-AACACCTGAAAGCGCCTCGATGGC-3'	6	173 (9.9)
IMP3 CRISPR 3	Fwd 5'-CACCGCCACCGTAAAGAAAATGCGG-3' Rev 5'-AACCCGCATTTTCTTTACGGTGGC-3'	5	366 (20.3)
IMP3 CRISPR 4	Fwd 5'-CACCGAGGCGCAGAGGCAAATCACA-3' Rev 5'-AAACTGTGATTTGCCTCTGCGCCTC-3'	10	1105 (61.4)

The oligo sequences were chosen for application of the Zhang Lab protocol using CRISPRv2 according to Shalem et al. (2014). The last two columns indicate the number of the targeted exon, and the expected transcript length following cleavage by Cas9 in bp, and as the percentage length relative to the original transcript (in brackets). * indicates the sequences that were associated with the strongest knockdown and that were subsequently used in described experiments, unless specified otherwise.

Table S2.3: List of primers used for qRT-PCR.

Gene	Forward primer	Reverse primer
<i>IMP1</i>	5'-GGCCATCGACAATTGTTGCAG-3'	5'-CCAGGGATCAGGTGAGACTG-3'
<i>IMP2</i>	5'-AGCTAAGCGGGCATCAGTTTG-3'	5'-CCGCAGCGGGAATCAATCT-3'
<i>IMP3</i>	5'-TATATCGGAAACCTCAGCGAGA-3'	5'-GGACCGAGTGCTCAACTTCT-3'
<i>LIN28B</i>	5'-CCTGTTTAGGAAGTGAAAGAAGAC-3'	5'-CACTTCTTTGGCTGAGGAGGTAG-3'
<i>EWS-FLI1</i>	5'-AGCAGCCTCCCACTAGTTAC-3'	5'-CCAAGTCTCTCTTCTGACTG-3'
<i>HMGA1</i>	5'-CGAAGTGCCAACTAAGAG-3'	5'-TGGTGGTTTTCCGGGTCTTG-3'
<i>HMGA2</i>	5'-GCGCCTCAGAAGAGAGGAC-3'	5'-GTCTTCCCCTGGGTCTCTTAG-3'
<i>RRM2</i>	5'-CACGGAGCCGAAAACCTAAAGC-3'	5'-TCTGCCTTCTTATACATCTGCCA-3'
<i>CCND1</i>	5'-GCTGCGAAGTGGAACCATC-3'	5'-CCTCCTTCTGCACACATTTGAA-3'
<i>NTRK1</i>	5'-GGGCCTCTCCTTACAGGAAC-3'	5'-AGCTTCTGTTTCAGGCACTCC-3'
<i>CD79A</i>	5'-CAAGAACCGAATCATCACAGC-3'	5'-CGTTCTGCCATCGTTTCC-3'
<i>FCGRT</i>	5'-TGGCGATGAGCACCCTACTAC-3'	5'-GATTCCCACCACGAGCAC-3'
<i>CCK</i>	5'-GCCCTGCTGGCAAGATAC-3'	5'-GCAGGTTCTTAACGATGGACA-3'
<i>IGF2</i>	5'-CGATGCTGGTGCTTCTCACC-3'	5'-GTCACAGCTGCGGAAACAGC-3'
<i>TBP</i>	5'-CGGCTGTTTAACTTCGCTTC-3'	5'-CACACGCCAAGAAACAGTGA-3'
<i>36β4</i>	5'-GCAATGTTGCCAGTGTCTGT-3'	5'-GCCTTGACCTTTTCAGCAAG-3'
<i>GAPDH</i>	5'-GGTCTCCTCTGACTTCAACA-3'	5'-GTGAGGGTCTCTCTCTTCCT-3'

Chapter 6

Publications

1 Manuscript I: LIN28B control of EWS-FLI1 stability

The core of the work presented in the thesis manuscript is based on the results collected in our laboratory, showing that LIN28B was re-expressed in a subset of highly aggressive EwS, and that LIN28B binding prolonged the half-life of EWS-FLI1. Furthermore, the putative role of LIN28B could be targeted using the 1632 compound, which reduced the tumor size *in vivo*. My contributions include nascent RNA isolation (Figure 6 B), several Western blots (Figure S3 D and Figure S5 C) and survival assays (Figure S5 B). I analyzed and interpreted the data, reviewed the paper and contributed to its intellectual content. The paper has been accepted for publication in the journal *Cell Reports*.

Title: LIN28B underlies the pathogenesis of a subclass of Ewing sarcoma.

Authors: Tugba Keskin^{1*}, Arnaud Bakaric^{1*}, Patricia Waszyk^{1*}, Gaylor Boulay^{2,13*}, Matteo Torsello^{1,7}, Sandrine Cornaz-Buros^{1,3}, Nadja Chevalier^{1,3}, Thibaud Geiser¹, Patricia Martin¹, Angela Volorio^{1,2}, Sowmya Iyer², Anupriya Kulkarni², Igor Letovanec⁴, Stéphane Cherix⁵, Gregory M Cote⁶, Edwin Choy⁶, Antonia Digkila⁷, Michael Montemurro⁷, Ivan Chebib⁸, Petur G Nielsen⁸, Angel M Carcaboso⁹, Jaume Mora⁹, Raffaele Renella¹⁰, Mario L Suvà², Carlo Fusco¹, Paolo Provero^{11,12}, Miguel N Rivera^{2,13**}, Nicolò Riggi^{1**} and Ivan Stamenkovic^{1**#}

¹ Experimental Pathology Service, Centre Hospitalier Universitaire Vaudois, University of Lausanne, 1011 Lausanne, Switzerland

² Department of Pathology and Center for Cancer Research, Massachusetts General Hospital and Harvard Medical School, Boston, 02114 MA, USA

³ Department of Woman-Mother-Child, Division of Pediatrics, Centre Hospitalier Universitaire Vaudois, University of Lausanne, 1011 Lausanne, Switzerland

⁴ Department of Pathology, Centre Hospitalier Universitaire Vaudois, University of Lausanne, 1011 Lausanne, Switzerland

⁵ Department of Orthopaedics and Traumatology, Centre Hospitalier Universitaire Vaudois, University of Lausanne, 1011 Lausanne, Switzerland

⁶ Center for Sarcoma and Connective Tissue Oncology, Massachusetts General Hospital, Boston, 02114 MA, USA

⁷ Department of Oncology, Centre Hospitalier Universitaire Vaudois, University of Lausanne, 1011 Lausanne, Switzerland

⁸ Department of Pathology, Massachusetts General Hospital and Harvard Medical School, Boston, 02114 MA, USA

⁹ Department of Pediatric Hematology and Oncology, Hospital Sant Joan de Déu, 08950 Barcelona, Spain

¹¹ Center for Translational Genomics and Bioinformatics, San Raffaele Scientific Institute, 20132 Milan, Italy

¹² Dept. of Molecular Biotechnology and Health Sciences, University of Turin, 10124 Turin, Italy

¹³ Broad Institute of Harvard and MIT, Cambridge, 02142 MA, USA

* These authors contributed equally to the work

** These authors share senior authorship

Lead Contact

Corresponding author e-mail address: ivan.stamenkovic@chuv.ch

Conflict of interest statement: The authors declare no conflict of interest.

Abstract

Ewing sarcoma (EwS) is associated with poor prognosis despite current multimodal therapy. Targeting of EWS-FLI1, the fusion protein responsible for its pathogenesis, and its principal downstream targets has not yet produced satisfactory therapeutic options, fuelling the search for alternative approaches. Here, we show that the oncofetal RNA-binding protein LIN28B regulates the stability of EWS-FLI1 mRNA in about 10 % of EwS. LIN28B depletion in these tumours leads to a decrease in expression of EWS-FLI1 and its direct transcriptional network, abrogating EwS cell self-renewal and tumorigenicity. Moreover, pharmacological inhibition of LIN28B mimics the effect of LIN28B depletion, suggesting that LIN28B sustains the emergence of a subset of EwS in which it also serves as an effective therapeutic target.

Significance

We show that a subset (~10%) of Ewing sarcoma (EwS) express the RNA-binding protein LIN28B. Depletion of LIN28B in cells derived from these tumours reduces EWS-FLI1 expression, alters the transcriptional program associated with EwS and decreases their tumorigenic properties. Using a compound that blocks LIN28 function, we demonstrate that inhibition of LIN28B leads to a decrease in EWS-FLI1 expression and the ensuing disruption of its core oncogenic regulatory program, abrogating EwS cell self-renewal and tumour initiation. Our results suggest that LIN28B warrants further investigation as a regulator of the expression of the fusion transcript and as a potential therapeutic target in the tumours that express this oncofetal protein.

Cell Reports, Published March 31, 2020. DOI: 10.1016/j.celrep.2019.12.053

2 Manuscript II: Targeting Haspin for cancer therapy

During my PhD, I was given the opportunity to collaborate on a project led by Johannes C. Melms and Benjamin Izar, from the Dana-Farber Cancer Institute, Boston, focusing on new ways to target RAF/MEK-inhibitor resistant melanoma. A screening of small molecules that inhibit the JAK/STAT pathway revealed that melanoma cells were most sensitive to the drug CX-6258, both *in vitro* and *in vivo*, exhibiting impaired tumor growth upon drug delivery. Among the kinases that bind CX-6258, HASPIN was identified as the main inhibited target and mediator of the drug effect, by induction of type-I interferon (IFN-1). Next, available public data was interrogated to determine whether other neoplasms may respond to HASPIN inhibition. Strikingly, multiple myeloma and EwS expressed high levels of the HASPIN kinase, and cell lines for these two cancers were particularly sensitive to knockdown based on data from the Broad Institute Dependency Map (Tsherniak et al., 2017). Thus, my contribution to this collaboration consisted in exploring the effects of CX-6258 on three EwS cell lines, namely SK-ES-1, SK-NEP-1 and RDES. *In vitro* testing of all three cell lines revealed sensitivity to the drug, as cells treated with CX-6258 displayed a marked reduction of proliferation. Moreover, IFN-1 expression was induced in a dose-dependent fashion in treated EwS cell lines, suggesting that the mechanisms following HASPIN inhibition in EwS are similar to those described in melanoma (Melms et al., 2019). Based on the accumulated results, HASPIN inhibition appears as an interesting approach for melanoma treatment, and could also be extended to other tumor types, such as EwS and multiple myeloma.

Title: Inhibition of Haspin kinase promotes cell-intrinsic and extrinsic anti-tumor activity.

Authors: Johannes C. Melms^{1,2,13,14}, Sreeram Vallabhaneni^{1,2,3,3}, Caitlin E. Mills³, Clarence Yapp³, Jia-Yun Chen³, Eugenio Morelli², Patricia Waszyk⁴, Sushil Kumar^{2,5}, Derrick Deming², Nienke Moret³, Steven Rodriguez³, Kartik Subramanian³, Meri Rogava^{3,13,14}, Adam N. Cartwright², Adrienne Luoma², Shaolin Mei³, Titus J. Brinker^{6,7}, David M. Miller⁸, Alexander Spektor⁹, Dirk Schadendorf¹⁰, Nicolo Riggi⁴, Kai W. Wucherpfennig^{2,5}, Peter K. Sorger^{3,11}, Benjamin Izar^{#,1-3,11-14}

¹ Department of Medical Oncology, Dana-Farber Cancer Institute, Boston, MA

² Department of Cancer Immunology and Virology, Dana-Farber Cancer Institute, Boston, MA

³ Laboratory for Systems Pharmacology, Harvard Medical School, Boston, MA

⁴ Experimental Pathology Service, Centre Hospitalier Universitaire Vaudois, University of Lausanne, Switzerland

⁵ Department of Immunology, Harvard Medical School, Boston, MA

⁶ National Center for Tumor Diseases (NCT), German Cancer Research Center (DKFZ), Heidelberg, Germany

⁷ Department of Dermatology, University Hospital Heidelberg, Heidelberg, Germany

⁸ Department of Dermatology, Massachusetts General Hospital, Boston, MA

⁹ Department of Radiation Oncology, Dana-Farber Cancer Institute, Boston, MA

¹⁰ Department of Dermatology, University Hospital Essen and German Cancer Consortium (DKTK), Germany

¹¹ Ludwig Center for Cancer Research at Harvard, Boston, MA

¹² Broad Institute of MIT and Harvard, Cambridge, MA

¹³ Columbia University Medical Center, Division of Hematology and Oncology, New York, NY

¹⁴ Columbia Center for Translational Immunology, New York, NY

Corresponding author

Benjamin Izar, MD/PhD

The Columbia Center for Translational Immunology (CCTI)

650 West 168th St. Black Building 17th floor

New York, NY 10032

Bi2175@cumc.columbia.edu

(212) 304-5871

Conflict of interest statement:

J.C.M and B.I. filed for a provisional patent on the use of Haspin Kinase inhibitors for cancer therapy. B.I. reports personal fees from Merck & Co. D.S. reports personal fees from Amgen, personal fees from Boehringer Ingelheim, personal fees from Leo Pharma, personal fees and other from Roche, personal fees and other from Novartis, personal fees from Incyte, personal fees and other from Regeneron, personal fees from 4SC, personal fees from AstraZeneca, personal fees and other from BMS, personal fees from Pierre Fabre, personal fees and other from Merck-EMD, personal fees from Pfizer, personal fees and other from Philiogen, personal fees from Array, personal fees and other from MSD, none of which are related to the work presented here. All other authors have no conflict of interest related to the work published in this manuscript.

Abstract

Melanoma patients resistant to RAF/MEK-inhibitors (RMI) are frequently resistant to other therapies, such as immune checkpoint inhibitors (ICI), and individuals succumb to their disease. New drugs that control tumor growth and favorably modulate the immune environment are therefore needed. We report that the small molecule CX-6258 has potent activity against both RMI sensitive (RMS) and resistant (RMR) melanoma cell lines. Haspin Kinase (HASPIN) was identified as a target of CX-6258. HASPIN inhibition resulted in reduced proliferation, frequent formation of micronuclei (MN), recruitment of cGAS and activation of the cGAS-STING-pathway. In murine models, CX-6258 induced a potent cGAS-dependent type-I-interferon response in tumor cells, increased IFN γ -producing CD8⁺ T-cells and reduced Treg frequency *in vivo*. HASPIN was more strongly expressed in malignant compared to healthy tissue and its inhibition by CX-6258 had minimal toxicity in *ex vivo* expanded human tumor-infiltrating lymphocytes (TILs), proliferating TILs and *in vitro* differentiated neurons, suggesting a potential therapeutic index for anti-cancer therapy. Furthermore, the activity of CX-6258 was validated in several Ewing sarcoma and multiple myeloma cell lines. Thus, HASPIN inhibition may overcome drug resistance in melanoma, modulate the immune environment and target a vulnerability in different cancer lineages.

Significance

Haspin Kinase inhibition by CX-6258 is a novel and potent strategy for RAF/MEK-inhibitor resistant melanoma and potentially other tumor types. HASPIN inhibition has direct anti-tumor activity and induces a favorable immune-microenvironment.

Acknowledgements

First and foremost, I would like to thank Prof. Ivan Stamenkovic for his support and for believing in me from day one, for opening the doors of his lab, that eventually became my second home. Thank you for seeing the silver linings and pointing them out to me when I only saw black holes. Thank you for always being available and for constantly pushing me forward.

Next, I want to deeply thank Prof. Nicolò Riggi for his endless availability, humor, trust and support, for the fruitful scientific discussions and for reminding me during the tough times that I can believe in myself. Thank you for giving me the opportunity to work on such exciting projects, some of which taught me patience is the mother of all science.

I would like to express my deep gratitude to Paolo Provero for all the bioinformatic analyses, Mylène Docquier and her team for all the work on RNA-sequencing, and Manfredo Quadroni and his team for the proteomics analyses.

Thanks to all the members of the thesis committee, for investing time on this project, for the constructive discussions and for their precious input on this work.

I want to thank all the present and former members of the Stamenkovic and Riggi labs: Liliane, Tugba, Patricia, Sandrine, Giulia, Nils, Emely, Arnaud, Luisa, Carlo, Sanal, Sabine, Santhosh, Sampath, as well as all the people I have had the chance to meet since I started my journey in research. Thanks to Patricia for her precious help during my time in the lab, especially during our long brain surgery sessions. Thanks to Tugba and Arnaud for their help in our collaboration project. It was a pleasure to work together, and I was very lucky to be part of a team with them. Next, I particularly want to thank Giulia, who introduced me to the work in the lab during my first internship, who closely and patiently supervised and helped me during all the ~~downs~~ ups and downs of my Master thesis, and kept on supporting me during the beginning of my PhD. I will be forever grateful for her support and for all the time that she invested in me. Many, many thanks to Nils for his invaluable help and supervision upon the start of my PhD journey a little over four years ago. My special thanks to Liliane for the aperos, for the

Christmas movie-lunch tradition, for the laughs, for patiently listening, for her tea machine and for her friendship.

Also, I should again thank Liliane, this time for dragging me to that one ADAS meeting on a dark, cold evening, and made me raise my hand at a critical moment. I am incredibly lucky to have met so many exciting people inside the FBM thanks to ADAS. I will always treasure the memories of being part of such a great students' association.

I also wish to express my gratitude to all the people working at the Doctoral School of the FBM for making the administrative part of this journey so smooth all along. Thank you in particular to Alexandra Cassoli, Laura de Santis, Thérèse Liechti and Livia Ioni for all their work. Many thanks to the technical support of the CHUV for making a last-minute videoconference so easy to organise for my private defense.

Thank you to my family for their constant support and for literally putting up with me every second of the way, including in these tough confined corona-times. Particularmente, obrigada à minha mãe. Acho que todos os Waszyk's suíços concordam: tudo sempre foi e sempre será graças a você. Obrigada pelo apoio, os telefonemas, a atenção, os *haja!* compartilhados, etc. Simplesmente obrigada por tudo.

Last but not least, I want to express my deepest gratitude to Peter, my better half, for his unconditional support, his unlimited patience, his profound kindness and care, and for helping me become the best version of myself. Danke für Deine unbeschränkte Unterstützung, Deine Liebenswürdigkeit, Deine Geduld und Deine ständige Aufmerksamkeit. Danke für die Reisen, das Kochen, die Wanderungen mit/ohne Pfifferlingen, die Weihnachtsmärkte, die Shows uuf Schwiizertütsch, die Oktoberfeste in Dirndl und Lederhosen, die Sprüngli Schoggis, und so viel mehr, dass ich hier nie genug Platz haben könnte. Ich bin unendlich glücklich, Dich in meinem Leben haben zu dürfen. Ohne Dich wäre ich nur halb soweit gegangen. Ich freue mich riesig auf die nächsten Schritte in Zürich mit Dir und auf unsere gemeinsame Zukunft.

References

- O. D. Abaan, A. Levenson, O. Khan, P. A. Furth, A. Üren, and J. A. Toretsky. PTPL1 is a direct transcriptional target of EWS-FLI1 and modulates Ewing’s sarcoma tumorigenesis. *Oncogene*, 24(16):2715, 2005.
- T. Ackermann, G. Hartleben, C. Müller, G. Mastrobuoni, M. Groth, B. A. Sterken, M. A. Zaini, S. A. Youssef, H. R. Zuidhof, S. R. Krauss, et al. C/EBP β -LIP induces cancer-type metabolic reprogramming by regulating the let-7/LIN28B circuit in mice. *Commun Biol*, 2(1):1–15, 2019.
- V. Adorno-Cruz, G. Kibria, X. Liu, M. Doherty, D. J. Junk, D. Guan, C. Hubert, M. Venere, E. Mulkearns-Hubert, M. Sinyuk, A. Alvarado, A. I. Caplan, J. Rich, S. L. Gerson, J. Lathia, and H. Liu. Cancer stem cells: targeting the roots of cancer, seeds of metastasis, and sources of therapy resistance. *Cancer Res*, 75(6):924–929, 2015.
- V. Agarwal, G. W. Bell, J.-W. Nam, and D. P. Bartel. Predicting effective microRNA target sites in mammalian mRNAs. *eLife*, 4:e05005, 2015.
- M. Al-Hajj, M. S. Wicha, A. Benito-Hernandez, S. J. Morrison, and M. F. Clarke. Prospective identification of tumorigenic breast cancer cells. *Proc Natl Acad Sci U S A*, 100(7):3983–8, 2003.
- D. Alex and K. A. Lee. RGG-boxes of the EWS oncoprotein repress a range of transcriptional activation domains. *Nucleic Acids Res*, 33(4):1323–1331, 2005.
- L. B. Alexandrov, S. Nik-Zainal, D. C. Wedge, S. A. Aparicio, S. Behjati, A. V. Biankin, G. R. Bignell, N. Bolli, A. Borg, A.-L. Børresen-Dale, et al. Signatures of mutational processes in human cancer. *Nature*, 500(7463):415, 2013.
- C. E. Allen, T. W. Laetsch, R. Mody, M. S. Irwin, M. S. Lim, P. C. Adamson, N. L. Seibel, D. W. Parsons, Y. J. Cho, K. Janeway, et al. Target and agent prioritization for the Children’s Oncology Group—national cancer institute pediatric MATCH trial. *J Natl Cancer I*, 109(5):djw274, 2017.
- V. Ambros and H. R. Horvitz. Heterochronic mutants of the nematode *Caenorhabditis elegans*. *Science*, 226(4673):409–416, 1984.
- D. M. Anderson, K. M. Anderson, C.-L. Chang, C. A. Makarewich, B. R. Nelson, J. R. McAnally, P. Kasaragod, J. M. Shelton, J. Liou, R. Bassel-Duby, et al. A micropeptide encoded by a putative long noncoding RNA regulates muscle performance. *Cell*, 160(4):595–606, 2015.
- J. L. Anderson, C. T. Denny, W. D. Tap, and N. Federman. Pediatric sarcomas: translating molecular pathogenesis of disease to novel therapeutic possibilities. *Pediatr Res*, 72(2):112, 2012.
- K. Anderson, C. Lutz, F. W. Van Delft, C. M. Bateman, Y. Guo, S. M. Colman, H. Kempfski, A. V. Moorman, I. Titley, J. Swansbury, et al. Genetic variegation of clonal architecture and propagating cells in leukaemia. *Nature*, 469(7330):356–361, 2011.
- N. Andor, T. A. Graham, M. Jansen, L. C. Xia, C. A. Aktipis, C. Petritsch, H. P. Ji, and C. C. Maley. Pan-cancer analysis of the extent and consequences of intratumor heterogeneity. *Nat Med*, 22(1):105, 2016.
- P.-O. Angrand, C. Vennin, X. Le Bourhis, and E. Adriaenssens. The role of long non-coding RNAs in genome formatting and expression. *Front Genet*, 6:165, 2015.

- J. Anido, A. Sáez-Borderías, A. González-Juncà, L. Rodón, G. Folch, M. A. Carmona, R. M. Prieto-Sánchez, I. Barba, E. Martínez-Sáez, L. Prudkin, et al. TGF- β receptor inhibitors target the CD44^{high}/Id1^{high} glioma-initiating cell population in human glioblastoma. *Cancer Cell*, 18(6):655–668, 2010.
- F. I. Arnaldez and L. J. Helman. New strategies in Ewing sarcoma: lost in translation? *Clin Cancer Res*, 20(12):3050–3056, 2014.
- V. Arndt, A. Feller, D. Hauri, R. Heusser, C. Junker, C. Kuehni, M. Lorez, V. Pfeiffer, E. Roy, and M. Schindler. Swiss Cancer Report 2015 – Current situation and developments. *Federal Statistical Office (FSO)*, 2016.
- A. Arvand and C. T. Denny. Biology of EWS/ETS fusions in Ewing’s family tumors. *Oncogene*, 20(40):5747, 2001.
- B. Auffinger, D. Spencer, P. Pytel, A. U. Ahmed, and M. S. Lesniak. The role of glioma stem cells in chemotherapy resistance and glioblastoma multiforme recurrence. *Expert Rev Neurother*, 15(7):741–52, 2015.
- M.-M. Aynaud, O. Mirabeau, N. Gruel, S. Grossetete-Lalami, V. Boeva, S. Durand, D. Surdez, O. Saulnier, S. Zaidi, S. Gribkova, et al. Transcriptional programs define intratumoral heterogeneity of Ewing sarcoma at single cell resolution. *BioRxiv*, page 623710, 2019.
- P. Bailey and H. W. Cushing. *A Classification of the Tumors of the Glioma Group on a Histo-genetic Basis, with a Correlated Study of Prognosis... With 108 Illustrations*. JB Lippincott Company, 1926.
- J. Balzeau, M. R. Menezes, S. Cao, and J. P. Hagan. The LIN28/let-7 pathway in cancer. *Front Genet*, 8:31, 2017.
- E. Balzer and E. G. Moss. Localization of the developmental timing regulator Lin28 to mRNP complexes, P-bodies and stress granules. *RNA Biol*, 4(1):16–25, 2007.
- S. Bao, Q. Wu, R. E. McLendon, Y. Hao, Q. Shi, A. B. Hjelmeland, M. W. Dewhirst, D. D. Bigner, and J. N. Rich. Glioma stem cells promote radioresistance by preferential activation of the DNA damage response. *Nature*, 444(7120):756, 2006.
- D. P. Bartel. MicroRNAs: target recognition and regulatory functions. *Cell*, 136:215–233, 2009.
- E. Batlle and H. Clevers. Cancer stem cells revisited. *Nat Med*, 23(10):1124, 2017.
- S. B. Baylin and P. A. Jones. A decade of exploring the cancer epigenome — biological and translational implications. *Nat Rev Cancer*, 11:726–734, 2011.
- B. M. Beckmann, R. Horos, B. Fischer, A. Castello, K. Eichelbaum, A.-M. Alleaume, T. Schwarzl, T. Curk, S. Foehr, W. Huber, et al. The RNA-binding proteomes from yeast to man harbour conserved enigmRBPs. *Nat Commun*, 6:10127, 2015.
- J. L. Bell, K. Wächter, B. Mühleck, N. Pazaitis, M. Köhn, M. Lederer, and S. Hüttelmaier. Insulin-like growth factor 2 mRNA-binding proteins (IGF2BPs): post-transcriptional drivers of cancer progression? *Cell Mol Life Sci*, 70(15):2657–2675, 2013.
- Y. Ben-David, E. Giddens, K. Letwin, and A. Bernstein. Erythroleukemia induction by Friend murine leukemia virus: insertional activation of a new member of the ets gene family, Fli-1, closely linked to c-ets-1. *Genes Dev*, 5(6):908–918, 1991.
- J. H. Bergmann and D. L. Spector. Long non-coding RNAs: modulators of nuclear structure and function. *Curr Opin Cell Biol*, 26:10–8, 2014.
- K. P. Bhat, V. Balasubramaniyan, B. Vaillant, R. Ezhilarasan, K. Hummelink, F. Hollingsworth, K. Wani, L. Heathcock, J. D. James, L. D. Goodman, et al. Mesenchymal differentiation mediated by NF- κ B promotes radiation resistance in glioblastoma. *Cancer Cell*, 24(3):331–346, 2013.

- Y. D. Bhutia, S. W. Hung, M. Krentz, D. Patel, D. Lovin, R. Manoharan, J. M. Thomson, and R. Govindarajan. Differential processing of let-7a precursors influences RRM2 expression and chemosensitivity in pancreatic cancer: role of LIN-28 and SET oncoprotein. *PLoS One*, 8(1):e53436, 2013.
- J. Biswas, V. L. Patel, V. Bhaskar, J. A. Chao, R. H. Singer, and C. Eliscovich. The structural basis for RNA selectivity by the IMP family of RNA-binding proteins. *Nat Commun*, 10(1):4440, 2019. doi: 10.1038/s41467-019-12193-7.
- D. Bonnet and J. E. Dick. Human acute myeloid leukemia is organized as a hierarchy that originates from a primitive hematopoietic cell. *Nature Med*, 3(7):730, 1997.
- T. Borovski, E. M. Felipe De Sousa, L. Vermeulen, and J. P. Medema. Cancer stem cell niche: the place to be. *Cancer Res*, 71(3):634–639, 2011.
- C. Bosetti, P. Bertuccio, L. Chatenoud, E. Negri, F. Levi, and C. La Vecchia. Childhood cancer mortality in Europe, 1970–2007. *Eur J Cancer*, 46(2):384–394, 2010.
- S. Boudoukha, S. Cuvellier, and A. Polesskaya. Role of the RNA-binding protein IMP-2 in muscle cell motility. *Mol Cell Biol*, 30(24):5710–5725, 2010.
- G. Boulay, G. J. Sandoval, N. Riggi, S. Iyer, R. Buisson, B. Naigles, M. E. Awad, S. Rengarajan, A. Volorio, M. J. McBride, et al. Cancer-specific retargeting of BAF complexes by a prion-like domain. *Cell*, 171(1):163–178, 2017.
- G. Boulay, A. Volorio, S. Iyer, L. C. Broye, I. Stamenkovic, N. Riggi, and M. N. Rivera. Epigenome editing of microsatellite repeats defines tumor-specific enhancer functions and dependencies. *Genes Dev*, 32(15-16):1008–1019, 2018.
- C. I. Brannan, E. C. Dees, R. S. Ingram, and S. M. Tilghman. The product of the H19 gene may function as an RNA. *Mol Cell Biol*, 10(1):28–36, 1990.
- J. Brennecke, D. R. Hipfner, A. Stark, R. B. Russell, and S. M. Cohen. bantam encodes a developmentally regulated microRNA that controls cell proliferation and regulates the proapoptotic gene hid in *Drosophila*. *Cell*, 113(1):25–36, 2003.
- A. S. Brohl, D. A. Solomon, W. Chang, J. Wang, Y. Song, S. Sindiri, R. Patidar, L. Hurd, L. Chen, J. F. Shern, et al. The genomic landscape of the Ewing sarcoma family of tumors reveals recurrent STAG2 mutation. *PLoS Genet*, 10(7), 2014.
- D. L. Burkhardt and J. Sage. Cellular mechanisms of tumour suppression by the retinoblastoma gene. *Nat Rev Cancer*, 8(9):671–682, 2008.
- R. A. Burrell, N. McGranahan, J. Bartek, and C. Swanton. The causes and consequences of genetic heterogeneity in cancer evolution. *Nature*, 501(7467):338–345, 2013.
- B. Busch, N. Bley, S. Müller, M. Glaß, D. Misiak, M. Lederer, M. Vetter, H.-G. Strauß, C. Thomssen, and S. Hüttelmaier. The oncogenic triangle of HMGA2, LIN28B and IGF2BP1 antagonizes tumor-suppressive actions of the let-7 family. *Nucleic Acids Res*, 44(8):3845–3864, 2016.
- C. Calabrese, H. Poppleton, M. Kocak, T. L. Hogg, C. Fuller, B. Hamner, E. Y. Oh, M. W. Gaber, D. Finklestein, M. Allen, et al. A perivascular niche for brain tumor stem cells. *Cancer Cell*, 11(1):69–82, 2007.
- J. Calbo, E. van Montfort, N. Proost, E. van Drunen, H. B. Beverloo, R. Meuwissen, and A. Berns. A functional role for tumor cell heterogeneity in a mouse model of small cell lung cancer. *Cancer Cell*, 19(2):244–256, 2011.
- G. A. Calin, C. D. Dumitru, M. Shimizu, R. Bichi, S. Zupo, E. Noch, H. Aldler, S. Rattan, M. Keating, K. Rai, et al. Frequent deletions and down-regulation of micro-RNA genes miR15 and miR16 at 13q14 in chronic lymphocytic leukemia. *Proc Natl Acad Sci U S A*, 99(24):15524–15529, 2002.
- G. A. Calin, C. Sevignani, C. D. Dumitru, T. Hyslop, E. Noch, S. Yendamuri, M. Shimizu, S. Rattan, F. Bullrich, M. Negrini, et al. Human microRNA genes are frequently located at fragile sites and genomic regions involved in cancers. *Proc Natl Acad Sci U S A*, 101(9):2999–3004, 2004.

- P. Campbell, G. Getz, J. Korbel, et al. Pan-cancer analysis of whole genomes. *Nature*, 578(7793):82–93, Feb 2020.
- P. J. Campbell, S. Yachida, L. J. Mudie, P. J. Stephens, E. D. Pleasance, L. A. Stebbings, L. A. Morsberger, C. Latimer, S. McLaren, M.-L. Lin, et al. The patterns and dynamics of genomic instability in metastatic pancreatic cancer. *Nature*, 467(7319):1109–1113, 2010.
- I. Carmel-Gross, N. Bollag, L. Armon, and A. Urbach. LIN28: a stem cell factor with a key role in pediatric tumor formation. *Stem Cells Dev*, 25(5):367–377, 2015.
- P. Carninci, T. Kasukawa, S. Katayama, J. Gough, M. Frith, N. Maeda, R. Oyama, T. Ravasi, B. Lenhard, C. Wells, et al. The transcriptional landscape of the mammalian genome. *Science*, 309(5740):1559–1563, 2005.
- M. S. Carro, W. K. Lim, M. J. Alvarez, R. J. Bollo, X. Zhao, E. Y. Snyder, E. P. Sulman, S. L. Anne, F. Doetsch, H. Colman, et al. The transcriptional network for mesenchymal transformation of brain tumours. *Nature*, 463(7279):318–325, 2010.
- A. Castello, B. Fischer, K. Eichelbaum, R. Horos, B. M. Beckmann, C. Strein, N. E. Davey, D. T. Humphreys, T. Preiss, L. M. Steinmetz, et al. Insights into RNA biology from an atlas of mammalian mRNA-binding proteins. *Cell*, 149(6):1393–1406, 2012.
- A. Castello, B. Fischer, C. K. Frese, R. Horos, A.-M. Alleaume, S. Foehr, T. Curk, J. Krijgsveld, and M. W. Hentze. Comprehensive identification of RNA-binding domains in human cells. *Mol Cell*, 63(4):696–710, 2016.
- S. Cawley, S. Bekiranov, H. H. Ng, P. Kapranov, E. A. Sekinger, D. Kampa, A. Piccolboni, V. Sementchenko, J. Cheng, A. J. Williams, et al. Unbiased mapping of transcription factor binding sites along human chromosomes 21 and 22 points to widespread regulation of noncoding RNAs. *Cell*, 116(4):499–509, 2004.
- A. F. Chambers, A. C. Groom, and I. C. MacDonald. Metastasis: dissemination and growth of cancer cells in metastatic sites. *Nat Rev Cancer*, 2(8):563, 2002.
- J. A. Chao, Y. Patskovsky, V. Patel, M. Levy, S. C. Almo, and R. H. Singer. ZBP1 recognition of β -actin zipcode induces RNA looping. *Genes Dev*, 24(2):148–158, 2010.
- P. Chatterji, K. E. Hamilton, S. Liang, S. F. Andres, H. S. Wijeratne, R. Mizuno, L. A. Simon, P. D. Hicks, S. W. Foley, J. R. Pitarresi, et al. The LIN28B-IMP1 post-transcriptional regulon has opposing effects on oncogenic signaling in the intestine. *Genes Dev*, 32(15-16):1020–1034, 2018.
- J. Chen, Y. Li, T.-S. Yu, R. M. McKay, D. K. Burns, S. G. Kernie, and L. F. Parada. A restricted cell population propagates glioblastoma growth after chemotherapy. *Nature*, 488(7412):522, 2012.
- L. Cheng, Z. Huang, W. Zhou, Q. Wu, S. Donnola, J. K. Liu, X. Fang, A. E. Sloan, Y. Mao, J. D. Lathia, et al. Glioblastoma stem cells generate vascular pericytes to support vessel function and tumor growth. *Cell*, 153(1):139–152, 2013.
- S. H. Choi, S. H. Kim, K.-W. Shim, J. W. Han, J. Choi, D.-S. Kim, C. J. Lyu, J. W. Kim, C.-O. Suh, and J. Cho. Treatment outcome and prognostic molecular markers of supratentorial primitive neuroectodermal tumors. *PloS One*, 11(4):e0153443, 2016.
- J. Christiansen, A. M. Kolte, F. C. Nielsen, et al. IGF2 mRNA-binding protein 2: biological function and putative role in type 2 diabetes. *J Mol Endocrinol*, 43(5):187–195, 2009.
- C. Chu, R. C. Spitale, and H. Y. Chang. Technologies to probe functions and mechanisms of long noncoding RNAs. *Nat Struct Mol Biol*, 22(1):29–35, 2015.
- S. Ciafre, S. Galardi, A. Mangiola, M. Ferracin, C.-G. Liu, G. Sabatino, M. Negrini, G. Maira, C. M. Croce, and M. Farace. Extensive modulation of a set of microRNAs in primary glioblastoma. *Biochem Bioph Res Co*, 334(4):1351–1358, 2005.

- A. E. Conway, E. L. Van Nostrand, G. A. Pratt, S. Aigner, M. L. Wilbert, B. Sundararaman, P. Freese, N. J. Lambert, S. Sathe, T. Y. Liang, et al. Enhanced CLIP uncovers IMP protein-RNA targets in human pluripotent stem cells important for cell adhesion and survival. *Cell Rep*, 15(3):666–679, 2016.
- S. Cornaz-Buros, N. Riggi, C. DeVito, A. Sarre, I. Letovanec, P. Provero, and I. Stamenkovic. Targeting cancer stem-like cells as an approach to defeating cellular heterogeneity in Ewing sarcoma. *Cancer Res*, 74(22):6610–22, 2014.
- C. M. Croce. Causes and consequences of microRNA dysregulation in cancer. *Nat Rev Genet*, 10(10):704–14, 2009.
- G. R. Dagenais, D. P. Leong, S. Rangarajan, F. Lanas, P. Lopez-Jaramillo, R. Gupta, R. Diaz, A. Avezum, G. B. Oliveira, A. Wielgosz, et al. Variations in common diseases, hospital admissions, and deaths in middle-aged adults in 21 countries from five continents (PURE): a prospective cohort study. *Lancet*, 2019.
- I. Dago-Jack and A. T. Shaw. Tumour heterogeneity and resistance to cancer therapies. *Nat Rev Clin Oncol*, 15(2):81, 2018.
- N. Dai, L. Zhao, D. Wrighting, D. Krämer, A. Majithia, Y. Wang, V. Cracan, D. Borges-Rivera, V. K. Mootha, M. Nahrendorf, et al. IGF2BP2/IMP2-deficient mice resist obesity through enhanced translation of Ucp1 mRNA and other mRNAs encoding mitochondrial proteins. *Cell Metab*, 21(4):609–621, 2015.
- S. Darmanis, S. A. Sloan, D. Croote, M. Mignardi, S. Chernikova, P. Samghababi, Y. Zhang, N. Neff, M. Kowarsky, C. Caneda, et al. Single-cell RNA-seq analysis of infiltrating neoplastic cells at the migrating front of human glioblastoma. *Cell Rep*, 21(5):1399–1410, 2017.
- C. De Vito, N. Riggi, M.-L. Suva, M. Janiszewska, J. Horlbeck, K. Baumer, P. Provero, and I. Stamenkovic. Let-7a is a direct EWS-FLI1 target implicated in Ewing’s sarcoma development. *PLoS One*, 6(8):e23592, 2011.
- C. De Vito, N. Riggi, S. Cornaz, M.-L. Suvà, K. Baumer, P. Provero, and I. Stamenkovic. A TARBP2-dependent miRNA expression profile underlies cancer stem cell properties and provides candidate therapeutic reagents in Ewing sarcoma. *Cancer Cell*, 21(6):807–21, 2012.
- N. Degrauwe, T. B. Schlumpf, M. Janiszewska, P. Martin, A. Cauderay, P. Provero, N. Riggi, M.-L. Suvà, R. Paro, and I. Stamenkovic. The RNA binding protein IMP2 preserves glioblastoma stem cells by preventing let-7 target gene silencing. *Cell Rep*, 15(8):1634–47, 2016a.
- N. Degrauwe, M.-L. Suvà, M. Janiszewska, N. Riggi, and I. Stamenkovic. IMPs: an RNA-binding protein family that provides a link between stem cell maintenance in normal development and cancer. *Genes Dev*, 30(22):2459–2474, 2016b.
- O. Delattre, J. Zucman, T. Melot, X. S. Garau, J.-M. Zucker, G. M. Lenoir, P. F. Ambros, D. Sheer, C. Turc-Carel, T. J. Triche, et al. The Ewing family of tumors—a subgroup of small-round-cell tumors defined by specific chimeric transcripts. *New Engl J Med*, 331(5):294–299, 1994.
- B. Deneen and C. T. Denny. Loss of p16 pathways stabilizes EWS/FLI1 expression and complements EWS/FLI1 mediated transformation. *Oncogene*, 20(46):6731, 2001.
- E. T. Dermitzakis, A. Reymond, R. Lyle, N. Scamuffa, C. Ucla, S. Deutsch, B. J. Stevenson, V. Flegel, P. Bucher, C. V. Jongeneel, et al. Numerous potentially functional but non-genic conserved sequences on human chromosome 21. *Nature*, 420(6915):578, 2002.
- T. Derrien, R. Johnson, G. Bussotti, A. Tanzer, S. Djebali, H. Tilgner, G. Guernec, D. Martin, A. Merkel, D. G. Knowles, et al. The GENCODE v7 catalog of human long noncoding RNAs: analysis of their gene structure, evolution, and expression. *Genome Res*, 22(9):1775–1789, 2012.
- R. Derynck and R. A. Weinberg. EMT and cancer: More than meets the eye. *Dev Cell*, 49(3):313–316, 2019.

- B. K. Dey, K. Pfeifer, and A. Dutta. The H19 long noncoding RNA gives rise to microRNAs miR-675-3p and miR-675-5p to promote skeletal muscle differentiation and regeneration. *Genes Dev*, 28(5):491–501, 2014.
- A. Dirkse, A. Golebiewska, T. Buder, P. V. Nazarov, A. Muller, S. Poovathingal, N. H. Brons, S. Leite, N. Sauvageot, D. Sarkisjan, et al. Stem cell-associated heterogeneity in glioblastoma results from intrinsic tumor plasticity shaped by the microenvironment. *Nat Commun*, 10(1):1787, 2019.
- C. J. Dommering, T. Marees, A. H. van der Hout, S. M. Imhof, H. Meijers-Heijboer, P. J. Ringens, F. E. van Leeuwen, and A. C. Moll. RB1 mutations and second primary malignancies after hereditary retinoblastoma. *Fam Cancer*, 11(2):225–233, 2012.
- J. R. Downing, R. K. Wilson, J. Zhang, E. R. Mardis, C.-H. Pui, L. Ding, T. J. Ley, and W. E. Evans. The pediatric cancer genome project. *Nat Genet*, 44(6):619, 2012.
- B. J. Druker. STI571 (GleevecTM) as a paradigm for cancer therapy. *Trends Mol Med*, 8(4):S14–S18, 2002.
- I. Dunham, A. Kundaje, S. Aldred, P. Collins, C. Davis, F. Doyle, C. Epstein, S. Frietze, J. Harrow, R. Kaul, J. Khatun, B. Lajoie, S. Landt, b.-k. Lee, F. Pauli Behn, K. Rosenbloom, P. Sabo, A. Safi, A. Sanyal, and E. Birney. The ENCODE Project Consortium: An integrated encyclopedia of DNA elements in the human genome. *Nature*, 489:57–74, 2012.
- G. P. Dunn, M. L. Rinne, J. Wykosky, G. Genovese, S. N. Quayle, I. F. Dunn, P. K. Agarwalla, M. G. Chheda, B. Campos, A. Wang, et al. Emerging insights into the molecular and cellular basis of glioblastoma. *Genes Dev*, 26(8):756–784, 2012.
- H. Easwaran, H.-C. Tsai, and S. B. Baylin. Cancer epigenetics: tumor heterogeneity, plasticity of stem-like states, and drug resistance. *Mol Cell*, 54(5):716–727, 2014.
- K. Eder and B. Kalman. Molecular heterogeneity of glioblastoma and its clinical relevance. *Pathol Oncol Res*, 20(4):777–787, 2014.
- H. V. Erkizan, Y. Kong, M. Merchant, S. Schlottmann, J. S. Barber-Rotenberg, L. Yuan, O. D. Abaan, T.-h. Chou, S. Dakshanamurthy, M. L. Brown, et al. A small molecule blocking oncogenic protein EWS-FLI1 interaction with RNA helicase A inhibits growth of Ewing’s sarcoma. *Nat Med*, 15(7):750, 2009.
- J. Ewing. Classics in oncology. Diffuse endothelioma of bone. James Ewing. Proceedings of the New York Pathological Society, 1921. *CA Cancer J Clin*, 22(2):95–8, 1972.
- M. Fabbri. TLRs as miRNA receptors. *Cancer Research*, 72(24):6333–6337, 2012.
- M. Fabbri, A. Paone, F. Calore, R. Galli, E. Gaudio, R. Santhanam, F. Lovat, P. Fadda, C. Mao, G. J. Nuovo, et al. MicroRNAs bind to toll-like receptors to induce prometastatic inflammatory response. *Proc Natl Acad Sci U S A*, 109(31):E2110–E2116, 2012.
- A. Fatica and I. Bozzoni. Long non-coding RNAs: new players in cell differentiation and development. *Nat Rev Genet*, 15(1):7, 2014.
- A. P. Feinberg, M. A. Koldobskiy, and A. Göndör. Epigenetic modulators, modifiers and mediators in cancer aetiology and progression. *Nat Rev Genet*, 17(5):284, 2016.
- C. Fisher. The diversity of soft tissue tumours with EWSR 1 gene rearrangements: a review. *Histopathology*, 64(1):134–150, 2014.
- W. A. Flavahan, Y. Drier, B. B. Liau, S. M. Gillespie, A. S. Venteicher, A. O. Stemmer-Rachamimov, M. L. Suvà, and B. E. Bernstein. Insulator dysfunction and oncogene activation in IDH mutant gliomas. *Nature*, 529(7584):110, 2016.
- S. A. Frank and M. A. Nowak. Cell biology: Developmental predisposition to cancer. *Nature*, 422(6931):494, 2003.

- G. Franzetti, K. Laud-Duval, W. Van Der Ent, A. Brisac, M. Irondelle, S. Aubert, U. Dirksen, C. Bouvier, G. de Pinieux, E. Snaar-Jagalska, et al. Cell-to-cell heterogeneity of EWSR1-FLI1 activity determines proliferation/migration choices in ewing sarcoma cells. *Oncogene*, 36(25):3505, 2017.
- G. Gabriely, M. Yi, R. S. Narayan, J. M. Niers, T. Wurdinger, J. Imitola, K. L. Ligon, S. Kesari, C. Esau, R. M. Stephens, et al. Human glioma growth is controlled by microRNA-10b. *Cancer Res*, 71(10):3563–3572, 2011.
- R. Galli, E. Binda, U. Orfanelli, B. Cipelletti, A. Gritti, S. De Vitis, R. Fiocco, C. Foroni, F. Dimeco, and A. Vescovi. Isolation and characterization of tumorigenic, stem-like neural precursors from human glioblastoma. *Cancer research*, 64(19):7011–7021, 2004.
- J. D. Gardiner, L. M. Abegglen, X. Huang, B. E. Carter, E. A. Schackmann, M. Stucki, C. N. Paxton, R. L. Randall, J. F. Amatruda, A. R. Putnam, et al. C/EBP β -1 promotes transformation and chemoresistance in Ewing sarcoma cells. *Oncotarget*, 8(16):26013, 2017.
- L. A. Garraway and E. S. Lander. Lessons from the cancer genome. *Cell*, 153(1):17–37, 2013.
- S. Gerstberger, M. Hafner, and T. Tuschl. A census of human RNA-binding proteins. *Nat Rev Genet*, 15(12):829–845, 2014.
- M. E. Gierisch, F. Pfistner, L. A. Lopez-Garcia, L. Harder, B. W. Schäfer, and F. K. Niggli. Proteasomal degradation of the EWS-FLI1 fusion protein is regulated by a single lysine residue. *J Biol Chem*, 291(52):26922–26933, 2016.
- L. A. Gilbert, M. H. Larson, L. Morsut, Z. Liu, G. A. Brar, S. E. Torres, N. Stern-Ginossar, O. Brandman, E. H. Whitehead, J. A. Doudna, et al. CRISPR-mediated modular RNA-guided regulation of transcription in eukaryotes. *Cell*, 154(2):442–451, 2013.
- R. C. Gimple, S. Bhargava, D. Dixit, and J. N. Rich. Glioblastoma stem cells: lessons from the tumor hierarchy in a lethal cancer. *Genes Dev*, 33(11-12):591–609, 2019.
- C. Giorgi, A. Boro, F. Rechfeld, L. A. Lopez-Garcia, M. E. Gierisch, B. W. Schäfer, and F. K. Niggli. PI3K/AKT signaling modulates transcriptional expression of EWS/FLI1 through specificity protein 1. *Oncotarget*, 6(30):28895, 2015.
- C. L. Gladson, R. A. Prayson, and W. M. Liu. The pathobiology of glioma tumors. *Annu Rev Pathol-Mech*, 5:33–50, 2010.
- T. Glisovic, J. L. Bachorik, J. Yong, and G. Dreyfuss. RNA-binding proteins and post-transcriptional gene regulation. *FEBS Lett*, 582(14):1977–1986, 2008.
- J. M. Goldman and J. V. Melo. Chronic myeloid leukemia—advances in biology and new approaches to treatment. *New Engl J Med*, 349(15):1451–1464, 2003.
- Y. Gong, B. A. Woda, and Z. Jiang. Oncofetal protein IMP3, a new cancer biomarker. *Adv Anat Pathol*, 21(3):191–200, 2014.
- M. M. Gottesman, T. Fojo, and S. E. Bates. Multidrug resistance in cancer: role of ATP-dependent transporters. *Nat Rev Cancer*, 2(1):48, 2002.
- R. Graf, M. Munschauer, G. Mastrobuoni, F. Mayr, U. Heinemann, S. Kempa, N. Rajewsky, and M. Landthaler. Identification of LIN28B-bound mRNAs reveals features of target recognition and regulation. *RNA Biol*, 10(7):1146–1159, 2013.
- M. Greaves and C. C. Maley. Clonal evolution in cancer. *Nature*, 481(7381):306, 2012.
- R. I. Gregory, K.-p. Yan, G. Amuthan, T. Chendrimada, B. Doratotaj, N. Cooch, and R. Shiekhattar. The microprocessor complex mediates the genesis of microRNAs. *Nature*, 432(7014):235, 2004.
- P. J. Grohar, S. Kim, G. O. R. Rivera, N. Sen, S. Haddock, M. L. Harlow, N. K. Maloney, J. Zhu, M. O’Neill, T. L. Jones, et al. Functional genomic screening reveals splicing of the EWS-FLI1 fusion transcript as a vulnerability in Ewing sarcoma. *Cell Rep*, 14(3):598–610, 2016.

- Y. Guo, Y. Chen, H. Ito, A. Watanabe, X. Ge, T. Kodama, and H. Aburatani. Identification and characterization of lin-28 homolog B (LIN28B) in human hepatocellular carcinoma. *Gene*, 384:51–61, 2006.
- P. B. Gupta, C. M. Fillmore, G. Jiang, S. D. Shapira, K. Tao, C. Kuperwasser, and E. S. Lander. Stochastic state transitions give rise to phenotypic equilibrium in populations of cancer cells. *Cell*, 146(4):633–644, 2011.
- R. A. Gupta, N. Shah, K. C. Wang, J. Kim, H. M. Horlings, D. J. Wong, M.-C. Tsai, T. Hung, P. Argani, J. L. Rinn, et al. Long non-coding RNA HOTAIR reprograms chromatin state to promote cancer metastasis. *Nature*, 464(7291):1071, 2010.
- M. Guttman, P. Russell, N. T. Ingolia, J. S. Weissman, and E. S. Lander. Ribosome profiling provides evidence that large noncoding RNAs do not encode proteins. *Cell*, 154(1):240–251, 2013.
- M. Hafner, M. Landthaler, L. Burger, M. Khorshid, J. Hausser, P. Berninger, A. Rothballer, M. Ascano Jr, A.-C. Jungkamp, M. Munschauer, et al. Transcriptome-wide identification of RNA-binding protein and microRNA target sites by PAR-CLIP. *Cell*, 141(1):129–141, 2010.
- M. Hafner, K. E. Max, P. Bandaru, P. Morozov, S. Gerstberger, M. Brown, H. Molina, and T. Tuschl. Identification of mRNAs bound and regulated by human LIN28 proteins and molecular requirements for RNA recognition. *RNA*, 19(5):613–626, 2013.
- D. Hambardzumyan and G. Bergers. Glioblastoma: defining tumor niches. *Trends Cancer*, 1(4):252–265, 2015.
- D. Hanahan and R. A. Weinberg. The hallmarks of cancer. *Cell*, 100(1):57–70, 2000.
- D. Hanahan and R. A. Weinberg. Hallmarks of cancer: the next generation. *Cell*, 144(5):646–674, 2011.
- T. V. Hansen, N. A. Hammer, J. Nielsen, M. Madsen, C. Dalbaeck, U. M. Wewer, J. Christiansen, and F. C. Nielsen. Dwarfism and impaired gut development in insulin-like growth factor II mRNA-binding protein 1-deficient mice. *Mol Cell Biol*, 24(10):4448–4464, 2004.
- S. Hatfield, H. Shcherbata, K. Fischer, K. Nakahara, R. W. Carthew, and H. Ruohola-Baker. Stem cell division is regulated by the microRNA pathway. *Nature*, 435(7044):974, 2005.
- J. M. Heddleston, Z. Li, R. E. McLendon, A. B. Hjelmeland, and J. N. Rich. The hypoxic microenvironment maintains glioblastoma stem cells and promotes reprogramming towards a cancer stem cell phenotype. *Cell Cycle*, 8(20):3274–3284, 2009.
- M. E. Hegi, A.-C. Diserens, T. Gorlia, M.-F. Hamou, N. De Tribolet, M. Weller, J. M. Kros, J. A. Hainfellner, W. Mason, L. Mariani, et al. MGMT gene silencing and benefit from temozolomide in glioblastoma. *New Engl J Med*, 352(10):997–1003, 2005.
- L. J. Helman and P. Meltzer. Mechanisms of sarcoma development. *Nat Rev Cancer*, 3(9):685, 2003.
- M. Henkes, H. van der Kuip, and W. E. Aulitzky. Therapeutic options for chronic myeloid leukemia: focus on imatinib (Glivec®), Gleevec™). *Ther Clin Risk Manag*, 4(1):163, 2008.
- M. Hennchen, J. Stubbusch, I. Abarchan-El Makhfi, M. Kramer, T. Deller, C. Pierre-Eugene, I. Janoueix-Lerosey, O. Delattre, U. Ernberger, J. B. Schulte, et al. Lin28B and let-7 in the control of sympathetic neurogenesis and neuroblastoma development. *J Neurosci*, 35(50):16531–16544, 2015.
- I. Heo, C. Joo, J. Cho, M. Ha, J. Han, and V. N. Kim. Lin28 mediates the terminal uridylation of let-7 precursor MicroRNA. *Mol Cell*, 32(2):276–284, 2008.
- J. M. Hess, A. Bernards, J. Kim, M. Miller, A. Taylor-Weiner, N. J. Haradhvala, M. S. Lawrence, and G. Getz. Passenger hotspot mutations in cancer. *Cancer Cell*, 36(3):288–301, 2019.
- M. A. Horlbeck, L. A. Gilbert, J. E. Villalta, B. Adamson, R. A. Pak, Y. Chen, A. P. Fields, C. Y. Park, J. E. Corn, M. Kampmann, et al. Compact and highly active next-generation libraries for CRISPR-mediated gene repression and activation. *Elife*, 5:e19760, 2016.

- Y. Hosono, Y. S. Niknafs, J. R. Prensner, M. K. Iyer, S. M. Dhanasekaran, R. Mehra, S. Pitchiaya, J. Tien, J. Escara-Wilke, A. Poliakov, et al. Oncogenic role of THOR, a conserved cancer/testis long non-coding RNA. *Cell*, 171(7):1559–1572, 2017.
- D. Huang, S. Qiu, R. Ge, L. He, M. Li, Y. Li, and Y. Peng. miR-340 suppresses glioblastoma multiforme. *Oncotarget*, 6(11):9257, 2015.
- H. Huang, H. Weng, W. Sun, X. Qin, H. Shi, H. Wu, B. S. Zhao, A. Mesquita, C. Liu, C. L. Yuan, et al. Recognition of RNA N 6-methyladenosine by IGF2BP proteins enhances mRNA stability and translation. *Nat Cell Biol*, 20(3):285, 2018.
- H.-Y. Huang, P. B. Illei, Z. Zhao, M. Mazumdar, A. G. Huvos, J. H. Healey, L. H. Wexler, R. Gorlick, P. Meyers, and M. Ladanyi. Ewing sarcomas with p53 mutation or p16/p14ARF homozygous deletion: a highly lethal subset associated with poor chemoresponse. *J Clin Oncol*, 23(3):548–558, 2005.
- J. T. Huse, E. Holland, and L. M. DeAngelis. Glioblastoma: molecular analysis and clinical implications. *Annu Rev Med*, 64:59–70, 2013.
- P. Huszthy, I. Daphu, S. Niclou, D. Stieber, J. Nigro, P. Sakariassen, H. Miletic, F. Thorsen, and R. Bjerkvig. In vivo models of primary brain tumors: Pitfalls and perspectives. *Neuro-Oncology*, 14:979–93, 06 2012.
- C. A. Iacobuzio-Donahue, K. Litchfield, and C. Swanton. Intratumor heterogeneity reflects clinical disease course. *Nat Cancer*, 1(1):3–6, 2020.
- D. Iliopoulos, H. A. Hirsch, G. Wang, and K. Struhl. Inducible formation of breast cancer stem cells and their dynamic equilibrium with non-stem cancer cells via IL6 secretion. *Proc Natl Acad Sci U S A*, 108(4):1397–1402, 2011.
- M. Janiszewska, M. L. Suvà, N. Riggi, R. H. Houtkooper, J. Auwerx, V. Clément-Schatlo, I. Radovanovic, E. Rheinbay, P. Provero, and I. Stamenkovic. Imp2 controls oxidative phosphorylation and is crucial for preserving glioblastoma cancer stem cells. *Genes Dev*, 26(17):1926–44, 2012.
- Y.-M. Jeng, C.-C. Chang, F.-C. Hu, H.-Y. E. Chou, H.-L. Kao, T.-H. Wang, and H.-C. Hsu. RNA-binding protein insulin-like growth factor II mRNA-binding protein 3 expression promotes tumor invasion and predicts early recurrence and poor prognosis in hepatocellular carcinoma. *Hepatology*, 48(4):1118–1127, 2008.
- J. Jin, W. Jing, X.-X. Lei, C. Feng, S. Peng, K. Boris-Lawrie, and Y. Huang. Evidence that Lin28 stimulates translation by recruiting RNA helicase A to polysomes. *Nucleic Acids Res*, 39(9):3724–3734, 2011.
- B. E. Johnson, T. Mazor, C. Hong, M. Barnes, K. Aihara, C. Y. McLean, S. D. Fouse, S. Yamamoto, H. Ueda, K. Tatsuno, et al. Mutational analysis reveals the origin and therapy-driven evolution of recurrent glioma. *Science*, 343(6167):189–193, 2014.
- J. M. Johnson, S. Edwards, D. Shoemaker, and E. E. Schadt. Dark matter in the genome: evidence of widespread transcription detected by microarray tiling experiments. *Trends Genet*, 21(2):93–102, 2005.
- K. M. Johnson, C. Taslim, R. S. Saund, and S. L. Lessnick. Identification of two types of GGAA-microsatellites and their roles in EWS/FLI binding and gene regulation in Ewing sarcoma. *PLoS One*, 12(11), 2017.
- L. Jønson, J. Christiansen, T. V. Hansen, J. Vikeså, Y. Yamamoto, and F. C. Nielsen. IMP3 RNP safe houses prevent miRNA-directed HMGA2 mRNA decay in cancer and development. *Cell Rep*, 7(2):539–551, 2014.
- A. N. Kallen, X.-B. Zhou, J. Xu, C. Qiao, J. Ma, L. Yan, L. Lu, C. Liu, J.-S. Yi, H. Zhang, et al. The imprinted H19 lncRNA antagonizes let-7 microRNAs. *Mol Cell*, 52(1):101–112, 2013.

- P. Kapranov, J. Cheng, S. Dike, D. A. Nix, R. Duttagupta, A. T. Willingham, P. F. Stadler, J. Hertel, J. Hackermüller, I. L. Hofacker, et al. RNA maps reveal new RNA classes and a possible function for pervasive transcription. *Science*, 316(5830):1484–1488, 2007.
- O. Kent and J. Mendell. A small piece in the cancer puzzle: microRNAs as tumor suppressors and oncogenes. *Oncogene*, 25(46):6188, 2006.
- H. H. Kim, Y. Kuwano, S. Srikantan, E. K. Lee, J. L. Martindale, and M. Gorospe. HuR recruits let-7/RISC to repress c-Myc expression. *Genes Dev*, 23(15):1743–8, 2009a.
- J. B. Kim, H. Zaehres, G. Wu, L. Gentile, K. Ko, V. Sebastiano, M. J. Araúzo-Bravo, D. Ruau, D. W. Han, M. Zenke, et al. Pluripotent stem cells induced from adult neural stem cells by reprogramming with two factors. *Nature*, 454(7204):646, 2008.
- V. N. Kim, J. Han, and M. C. Siomi. Biogenesis of small RNAs in animals. *Nat Rev Mol Cell Bio*, 10(2):126, 2009b.
- R. A. Kleinerman, M. A. Tucker, D. H. Abramson, J. M. Seddon, R. E. Tarone, and J. F. Fraumeni Jr. Risk of soft tissue sarcomas by individual subtype in survivors of hereditary retinoblastoma. *J Natl Cancer Inst*, 99(1):24–31, 2007.
- F. Kopp and J. T. Mendell. Functional classification and experimental dissection of long noncoding RNAs. *Cell*, 172(3):393–407, 2018.
- H. Kovar, D. N. Aryee, G. Jug, C. Henockl, M. Schemper, O. Delattre, G. Thomas, and H. Gadner. EWS/FLI-1 antagonists induce growth inhibition of Ewing tumor cells in vitro. *Cell Growth Differ*, 7(4):429–438, 1996.
- A. Kreso and J. E. Dick. Evolution of the cancer stem cell model. *Cell Stem Cell*, 14(3):275–291, 2014.
- A. Kreso, C. A. O’Brien, P. Van Galen, O. I. Gan, F. Notta, A. M. Brown, K. Ng, J. Ma, E. Wienholds, C. Dunant, et al. Variable clonal repopulation dynamics influence chemotherapy response in colorectal cancer. *Science*, 339(6119):543–548, 2013.
- M. S. Kumar, J. Lu, K. L. Mercer, T. R. Golub, and T. Jacks. Impaired microRNA processing enhances cellular transformation and tumorigenesis. *Nat Genet*, 39(5):673, 2007.
- M. Lagos-Quintana, R. Rauhut, W. Lendeckel, and T. Tuschl. Identification of novel genes coding for small expressed RNAs. *Science*, 294(5543):853–858, 2001.
- S. Lamouille, J. Xu, and R. Derynck. Molecular mechanisms of epithelial–mesenchymal transition. *Nat Rev Mol Cell Bio*, 15(3):178–196, 2014.
- M.-F. Lang, S. Yang, C. Zhao, G. Sun, K. Murai, X. Wu, J. Wang, H. Gao, C. E. Brown, X. Liu, et al. Genome-wide profiling identified a set of miRNAs that are differentially expressed in glioblastoma stem cells and normal neural stem cells. *PLoS One*, 7(4):e36248, 2012.
- J. D. Lathia, S. C. Mack, E. E. Mulkearns-Hubert, C. L. Valentim, and J. N. Rich. Cancer stem cells in glioblastoma. *Genes Dev*, 29(12):1203–1217, 2015.
- M. Lederer, N. Bley, C. Schleifer, and S. Hüttelmaier. The role of the oncofetal IGF2 mRNA-binding protein 3 (IGF2BP3) in cancer. In *Seminars in cancer biology*, volume 29, pages 3–12. Elsevier, 2014.
- G. Lee, H. Kim, Y. Elkabetz, G. Al Shamy, G. Panagiotakos, T. Barberi, V. Tabar, and L. Studer. Isolation and directed differentiation of neural crest stem cells derived from human embryonic stem cells. *Nat Biotechnol*, 25(12):1468, 2007.
- H. K. Lee, A. Bier, S. Cazacu, S. Finnis, C. Xiang, H. Twito, L. M. Poisson, T. Mikkelsen, S. Slavin, E. Jacoby, et al. MicroRNA-145 is downregulated in glial tumors and regulates glioma cell migration by targeting connective tissue growth factor. *PLoS One*, 8(2):e54652, 2013.

- J. Lee, S. Kotliarova, Y. Kotliarov, A. Li, Q. Su, N. M. Donin, S. Pastorino, B. W. Purow, N. Christopher, W. Zhang, et al. Tumor stem cells derived from glioblastomas cultured in bFGF and EGF more closely mirror the phenotype and genotype of primary tumors than do serum-cultured cell lines. *Cancer Cell*, 9(5):391–403, 2006.
- J. H. Lee, J. E. Lee, J. Y. Kahng, S. H. Kim, J. S. Park, S. J. Yoon, J.-Y. Um, W. K. Kim, J.-K. Lee, J. Park, et al. Human glioblastoma arises from subventricular zone cells with low-level driver mutations. *Nature*, 560(7717):243, 2018.
- R. C. Lee, R. L. Feinbaum, and V. Ambros. The *C. elegans* heterochronic gene *lin-4* encodes small RNAs with antisense complementarity to *lin-14*. *cell*, 75(5):843–854, 1993.
- Y. S. Lee and A. Dutta. The tumor suppressor microRNA let-7 represses the HMGA2 oncogene. *Genes Dev*, 21(9):1025–30, 2007.
- B. P. Lewis, I. Hung Shih, M. W. Jones-Rhoades, D. P. Bartel, and C. B. Burge. Prediction of mammalian MicroRNA targets. *Cell*, 115(7):787 – 798, 2003.
- B. P. Lewis, C. B. Burge, and D. P. Bartel. Conserved seed pairing, often flanked by adenosines, indicates that thousands of human genes are microRNA targets. *Cell*, 120:15–20, 2005.
- H. Li, W. Watford, C. Li, A. Parmelee, M. A. Bryant, C. Deng, J. O’Shea, and S. B. Lee. Ewing sarcoma gene EWS is essential for meiosis and B lymphocyte development. *J Clin Invest*, 117(5):1314–1323, 2007.
- N. Li, X. Zhong, X. Lin, J. Guo, L. Zou, J. L. Tanyi, Z. Shao, S. Liang, L.-P. Wang, W.-T. Hwang, D. Katsaros, K. Montone, X. Zhao, and L. Zhang. Lin-28 homologue A (LIN28A) promotes cell cycle progression via regulation of cyclin-dependent kinase 2 (CDK2), cyclin D1 (CCND1), and cell division cycle 25 homolog A (CDC25A) expression in cancer. *J Biol Chem*, 287(21):17386–97, 2012.
- W. Li, P. Jiang, X. Sun, S. Xu, X. Ma, and R. Zhan. Suppressing H19 modulates tumorigenicity and stemness in U251 and U87MG glioma cells. *Cell Mol Neurobiol*, 36(8):1219–1227, 2016.
- Y.-M. Li, G. Franklin, H.-M. Cui, K. Svensson, X.-B. He, G. Adam, R. Ohlsson, and S. Pfeifer. The H19 transcript is associated with polysomes and may regulate IGF2 expression intrans. *J Biol Chem*, 273(43):28247–28252, 1998.
- B. B. Liau, C. Sievers, L. K. Donohue, S. M. Gillespie, W. A. Flavahan, T. E. Miller, A. S. Venteicher, C. H. Hebert, C. D. Carey, S. J. Rodig, et al. Adaptive chromatin remodeling drives glioblastoma stem cell plasticity and drug tolerance. *Cell Stem Cell*, 20(2):233–246, 2017.
- P. P. Lin, M. K. Pandey, F. Jin, S. Xiong, M. Deavers, J. M. Parant, and G. Lozano. EWS-FLI1 induces developmental abnormalities and accelerates sarcoma formation in a transgenic mouse model. *Cancer Res*, 68(21):8968–8975, 2008.
- S. J. Liu, M. A. Horlbeck, S. W. Cho, H. S. Birk, M. Malatesta, D. He, F. J. Attenello, J. E. Villalta, M. Y. Cho, Y. Chen, et al. CRISPRi-based genome-scale identification of functional long noncoding RNA loci in human cells. *Science*, 355(6320):eaah7111, 2017.
- M. C. Lloyd, J. J. Cunningham, M. M. Bui, R. J. Gillies, J. S. Brown, and R. A. Gatenby. Darwinian dynamics of intratumoral heterogeneity: not solely random mutations but also variable environmental selection forces. *Cancer Res*, 76(11):3136–3144, 2016.
- D. N. Louis, A. Perry, G. Reifenberger, A. Von Deimling, D. Figarella-Branger, W. K. Cavenee, H. Ohgaki, O. D. Wiestler, P. Kleihues, and D. W. Ellison. The 2016 World Health Organization classification of tumors of the central nervous system: a summary. *Acta Neuropathol*, 131(6):803–820, 2016.
- K. E. Lukong, K.-w. Chang, E. W. Khandjian, and S. Richard. RNA-binding proteins in human genetic disease. *Trends Genet*, 24(8):416–425, 2008.
- M. Luo, Z. Li, W. Wang, Y. Zeng, Z. Liu, and J. Qiu. Long non-coding RNA H19 increases bladder cancer metastasis by associating with EZH2 and inhibiting E-cadherin expression. *Cancer Lett*, 333(2):213–21, Jun 2013.

- W. Luo, K. Gangwal, S. Sankar, K. Boucher, D. Thomas, and S. Lessnick. GSTM4 is a microsatellite-containing EWS/FLI target involved in Ewing's sarcoma oncogenesis and therapeutic resistance. *Oncogene*, 28(46):4126, 2009.
- S. A. Mani, W. Guo, M.-J. Liao, E. N. Eaton, A. Ayyanan, A. Y. Zhou, M. Brooks, F. Reinhard, C. C. Zhang, M. Shipitsin, et al. The epithelial-mesenchymal transition generates cells with properties of stem cells. *Cell*, 133(4):704–715, 2008.
- D. Marchese, N. S. de Groot, N. Lorenzo Gotor, C. M. Livi, and G. G. Tartaglia. Advances in the characterization of RNA-binding proteins. *Wiley Interdiscip Rev RNA*, 7(6):793–810, 2016.
- N. J. Martinez and R. I. Gregory. MicroRNA gene regulatory pathways in the establishment and maintenance of ESC identity. *Cell Stem Cell*, 7(1):31–35, 2010.
- A. Marusyk and K. Polyak. Tumor heterogeneity: causes and consequences. *BBA-Rev Cancer*, 1805(1):105–117, 2010.
- W. A. May, M. L. Gishizky, S. L. Lessnick, L. B. Lunsford, B. C. Lewis, O. Delattre, J. Zucman, G. Thomas, and C. T. Denny. Ewing sarcoma 11; 22 translocation produces a chimeric transcription factor that requires the DNA-binding domain encoded by FLI1 for transformation. *Proc Natl Acad Sci U S A*, 90(12):5752–5756, 1993.
- T. Mazor, A. Pankov, J. S. Song, and J. F. Costello. Intratumoral heterogeneity of the epigenome. *Cancer Cell*, 29(4):440–451, 2016.
- J. C. Melms, S. Vallabhaneni, C. E. Mills, C. Yapp, J.-Y. Chen, E. Morelli, P. Waszyk, S. Kumar, D. Deming, N. Moret, et al. Inhibition of Haspin kinase promotes cell-intrinsic and extrinsic anti-tumor activity. *Cancer Res*, 2019.
- S. A. Melo and M. Esteller. Dysregulation of microRNAs in cancer: playing with fire. *FEBS letters*, 585(13):2087–99, 2011.
- L. M. Merlo, J. W. Pepper, B. J. Reid, and C. C. Maley. Cancer as an evolutionary and ecological process. *Nat Rev Cancer*, 6(12):924–935, 2006.
- D. S. Middlemas, C. F. Stewart, M. N. Kirstein, C. Poquette, H. S. Friedman, P. J. Houghton, and T. P. Brent. Biochemical correlates of temozolomide sensitivity in pediatric solid tumor xenograft models. *Clin Cancer Res*, 6(3):998–1007, 2000.
- T. Z. Minas, D. Surdez, T. Javaheri, M. Tanaka, M. Howarth, H.-J. Kang, J. Han, Z.-Y. Han, B. Sax, B. E. Kream, et al. Combined experience of six independent laboratories attempting to create an Ewing sarcoma mouse model. *Oncotarget*, 8(21):34141, 2017.
- M. Minata, A. Audia, J. Shi, S. Lu, J. Bernstock, M. S. Pavlyukov, A. Das, S.-H. Kim, Y. J. Shin, Y. Lee, et al. Phenotypic plasticity of invasive edge glioma stem-like cells in response to ionizing radiation. *Cell Rep*, 26(7):1893–1905, 2019.
- S. F. Mitchell and R. Parker. Principles and properties of eukaryotic mRNPs. *Mol Cell*, 54(4):547–558, 2014.
- L. G. Morris, N. Riaz, A. Desrichard, Y. Şenbabaoğlu, A. A. Hakimi, V. Makarov, J. S. Reis-Filho, and T. A. Chan. Pan-cancer analysis of intratumor heterogeneity as a prognostic determinant of survival. *Oncotarget*, 7(9):10051, 2016.
- E. G. Moss and L. Tang. Conservation of the heterochronic regulator Lin-28, its developmental expression and microRNA complementary sites. *Dev Biol*, 258(2):432–442, 2003.
- E. A. Mroz, A. M. Tward, R. J. Hammon, Y. Ren, and J. W. Rocco. Intra-tumor genetic heterogeneity and mortality in head and neck cancer: analysis of data from the Cancer Genome Atlas. *PLoS Med*, 12(2):e1001786, 2015.
- F. Mueller-Pillasch, B. Pohl, M. Wilda, U. Lacher, M. Beil, C. Wallrapp, H. Hameister, W. Knöchel, G. Adler, and T. M. Gress. Expression of the highly conserved RNA binding protein KOC in embryogenesis. *Mech Develop*, 88(1):95–99, 1999.

- S. Müller, N. Bley, M. Glaß, B. Busch, V. Rousseau, D. Misiak, T. Fuchs, M. Lederer, and S. Hüttelmaier. IGF2BP1 enhances an aggressive tumor cell phenotype by impairing miRNA-directed downregulation of oncogenic factors. *Nucleic Acids Res*, 46(12):6285–6303, 2018.
- M. Müller-McNicoll and K. M. Neugebauer. How cells get the message: dynamic assembly and function of mRNA–protein complexes. *Nat Rev Genet*, 14(4):275–287, 2013.
- P. Nanni, L. Landuzzi, M. C. Manara, A. Righi, G. Nicoletti, C. Cristalli, M. Pasello, A. Parra, M. Carrabotta, M. Ferracin, et al. Bone sarcoma patient-derived xenografts are faithful and stable preclinical models for molecular and therapeutic investigations. *Sci Rep*, 9(1):1–12, 2019.
- C. Neftel, J. Laffy, M. G. Filbin, T. Hara, M. E. Shore, G. J. Rahme, A. R. Richman, D. Silverbush, M. L. Shaw, C. M. Hebert, et al. An integrative model of cellular states, plasticity, and genetics for glioblastoma. *Cell*, 178(4):835–849, 2019.
- M. E. J. Nesbit, E. A. Gehan, E. O. Burgert Jr, T. J. Vietti, A. Cangir, M. Tefft, R. Evans, P. Thomas, F. B. Askin, and J. Kissane. Multimodal therapy for the management of primary, nonmetastatic Ewing’s sarcoma of bone: a long-term follow-up of the first intergroup study. *J Clin Oncol*, 8(10):1664–1674, 1990.
- D. X. Nguyen, P. D. Bos, and J. Massagué. Metastasis: from dissemination to organ-specific colonization. *Nat Rev Cancer*, 9(4):274, 2009.
- J. Nielsen, J. Christiansen, J. Lykke-Andersen, A. H. Johnsen, U. M. Wewer, and F. C. Nielsen. A family of insulin-like growth factor II mRNA-binding proteins represses translation in late development. *Mol Cell Biol*, 19(2):1262–1270, 1999.
- J. Nielsen, M. A. Kristensen, M. Willemoes, F. C. Nielsen, and J. Christiansen. Sequential dimerization of human zipcode-binding protein IMP1 on RNA: a cooperative mechanism providing RNP stability. *Nucleic Acids Res*, 32(14):4368–4376, 2004.
- M. A. Nieto, R. Y.-J. Huang, R. A. Jackson, and J. P. Thiery. EMT: 2016. *Cell*, 166(1):21–45, 2016.
- J. Nishino, S. Kim, Y. Zhu, H. Zhu, and S. J. Morrison. A network of heterochronic genes including Imp1 regulates temporal changes in stem cell properties. *Elife*, 2:e00924, 2013.
- R. E. Norris and P. C. Adamson. Challenges and opportunities in childhood cancer drug development. *Nat Rev Cancer*, 12(11):776–782, 2012.
- P. C. Nowell. The clonal evolution of tumor cell populations. *Science*, 194(4260):23–8, 1976.
- A. C. Obenauf and J. Massagué. Surviving at a distance: organ-specific metastasis. *Trends in cancer*, 1(1):76–91, 2015.
- C. A. O’Brien, A. Pollett, S. Gallinger, and J. E. Dick. A human colon cancer cell capable of initiating tumour growth in immunodeficient mice. *Nature*, 445(7123):106, 2007.
- H. Ohgaki and P. Kleihues. Population-based studies on incidence, survival rates, and genetic alterations in astrocytic and oligodendroglial gliomas. *J Neuropath Exp Neur*, 64(6):479–489, 2005.
- B. Oldrini, Á. Curiel-García, C. Marques, V. Matia, Ö. Uluçkan, O. Graña-Castro, R. Torres-Ruiz, S. Rodriguez-Perales, J. T. Huse, and M. Squatrito. Somatic genome editing with the RCAS-TVA-CRISPR-Cas9 system for precision tumor modeling. *Nat Commun*, 9(1):1466, 2018.
- D. Olmos, A. S. Martins, R. L. Jones, S. Alam, M. Scurr, and I. R. Judson. Targeting the insulin-like growth factor 1 receptor in Ewing’s sarcoma: reality and expectations. *Sarcoma*, 2011, 2011.
- J. L. Ordóñez, D. Osuna, D. Herrero, E. de Álava, and J. Madoz-Gúrpide. Advances in Ewing’s sarcoma research: where are we now and what lies ahead? *Cancer Res*, 69(18):7140–7150, 2009.
- C. A. Ortmann, D. G. Kent, J. Nangalia, Y. Silber, D. C. Wedge, J. Grinfeld, E. J. Baxter, C. E. Massie, E. Papaemmanuil, S. Menon, et al. Effect of mutation order on myeloproliferative neoplasms. *New Engl J Med*, 372(7):601–612, 2015.

- V. Pachnis, C. Brannan, and S. M. Tilghman. The structure and expression of a novel gene activated in early mouse embryogenesis. *EMBO J*, 7(3):673–681, 1988.
- A. F. Palazzo and E. S. Lee. Non-coding RNA: what is functional and what is junk? *Front Genet*, 6:2, 2015.
- M. P. Paronetto. Ewing sarcoma protein: a key player in human cancer. *Int J Cell Biol*, 2013, 2013.
- D. W. Parsons, S. Jones, X. Zhang, J. C.-H. Lin, R. J. Leary, P. Angenendt, P. Mankoo, H. Carter, I.-M. Siu, G. L. Gallia, et al. An integrated genomic analysis of human glioblastoma multiforme. *Science*, 321(5897):1807–1812, 2008.
- A. E. Pasquinelli, B. J. Reinhart, F. Slack, M. Q. Martindale, M. I. Kuroda, B. Maller, D. C. Hayward, E. E. Ball, B. Degnan, P. Müller, et al. Conservation of the sequence and temporal expression of let-7 heterochronic regulatory RNA. *Nature*, 408(6808):86, 2000.
- A. P. Patel, I. Tirosh, J. J. Trombetta, A. K. Shalek, S. M. Gillespie, H. Wakimoto, D. P. Cahill, B. V. Nahed, W. T. Curry, R. L. Martuza, et al. Single-cell RNA-seq highlights intratumoral heterogeneity in primary glioblastoma. *Science*, 344(6190):1396–1401, 2014.
- S. Peng, L.-L. Chen, X.-X. Lei, L. Yang, H. Lin, G. G. Carmichael, and Y. Huang. Genome-wide studies reveal that Lin28 enhances the translation of genes important for growth and survival of human embryonic stem cells. *Stem Cells*, 29(3):496–504, 2011.
- Y. Peng and C. M. Croce. The role of microRNAs in human cancer. *Signal Transduct Tar*, 1:15004, 2016.
- R. Pereira, C. T. Quang, I. Lesault, H. Dolznig, H. Beug, and J. Ghysdael. FLI-1 inhibits differentiation and induces proliferation of primary erythroblasts. *Oncogene*, 18(8):1597, 1999.
- J. I. Perez-Perri, B. Rogell, T. Schwarzl, F. Stein, Y. Zhou, M. Rettel, A. Brosig, and M. W. Hentze. Discovery of RNA-binding proteins and characterization of their dynamic responses by enhanced RNA interactome capture. *Nature Commun*, 9, 2018.
- H. S. Phillips, S. Kharbanda, R. Chen, W. F. Forrest, R. H. Soriano, T. D. Wu, A. Misra, J. M. Nigro, H. Colman, L. Soroceanu, et al. Molecular subclasses of high-grade glioma predict prognosis, delineate a pattern of disease progression, and resemble stages in neurogenesis. *Cancer Cell*, 9(3):157–173, 2006.
- D. Picard, S. Miller, C. E. Hawkins, E. Bouffet, H. A. Rogers, T. S. Chan, S.-K. Kim, Y.-S. Ra, J. Fangusaro, A. Korshunov, et al. Integrative genomic analyses identify LIN28 and OLIG2 as markers of survival and metastatic potential in childhood central nervous system primitive neuro-ectodermal brain tumours. *Lancet Oncol*, 13(8):838, 2012.
- K. I. Pishas and S. L. Lessnick. Recent advances in targeted therapy for Ewing sarcoma. *F1000*, 5, 2016.
- E. Piskounova, C. Polytaichou, J. E. Thornton, R. J. LaPierre, C. Pothoulakis, J. P. Hagan, D. Iliopoulos, and R. I. Gregory. Lin28A and Lin28B inhibit let-7 microRNA biogenesis by distinct mechanisms. *Cell*, 147(5):1066–1079, 2011.
- A. Poleskaya, S. Cuvellier, I. Naguibneva, A. Duquet, E. G. Moss, and A. Harel-Bellan. Lin-28 binds IGF-2 mRNA and participates in skeletal myogenesis by increasing translation efficiency. *Genes Dev*, 21(9):1125–1138, 2007.
- C. P. Ponting, P. L. Oliver, and W. Reik. Evolution and functions of long noncoding RNAs. *Cell*, 136(4):629–41, 2009.
- J. T. Powers, K. M. Tsanov, D. S. Pearson, F. Roels, C. S. Spina, R. Ebright, M. Seligson, Y. De Soysa, P. Cahan, J. Theissen, et al. Multiple mechanisms disrupt the let-7 microRNA family in neuroblastoma. *Nature*, 535(7611):246, 2016.
- L. S. Qi, M. H. Larson, L. A. Gilbert, J. A. Doudna, J. S. Weissman, A. P. Arkin, and W. A. Lim. Repurposing CRISPR as an RNA-guided platform for sequence-specific control of gene expression. *Cell*, 152(5):1173–1183, 2013.

- J. Qin, X. Liu, B. Laffin, X. Chen, G. Choy, C. R. Jeter, T. Calhoun-Davis, H. Li, G. S. Palapattu, S. Pang, et al. The PSA-/lo prostate cancer cell population harbors self-renewing long-term tumor-propagating cells that resist castration. *Cell Stem Cell*, 10(5):556–569, 2012.
- C. Qiu, Y. Ma, J. Wang, S. Peng, and Y. Huang. Lin28-mediated post-transcriptional regulation of Oct4 expression in human embryonic stem cells. *Nucleic Acids Res*, 38(4):1240–1248, 2009.
- D. F. Quail and J. A. Joyce. Microenvironmental regulation of tumor progression and metastasis. *Nat Med*, 19(11):1423, 2013.
- J. J. Quinn and H. Y. Chang. Unique features of long non-coding RNA biogenesis and function. *Nat Rev Genet*, 17(1):47, 2016.
- M. Ramaswami, J. P. Taylor, and R. Parker. Altered ribostasis: RNA-protein granules in degenerative disorders. *Cell*, 154(4):727–736, 2013.
- T. Reya, S. J. Morrison, M. F. Clarke, and I. L. Weissman. Stem cells, cancer, and cancer stem cells. *Nature*, 414(6859):105, 2001.
- E. Rheinbay, M. L. Suvà, S. M. Gillespie, H. Wakimoto, A. P. Patel, M. Shahid, O. Oksuz, S. D. Rabkin, R. L. Martuza, M. N. Rivera, et al. An aberrant transcription factor network essential for Wnt signaling and stem cell maintenance in glioblastoma. *Cell Rep*, 3(5):1567–1579, 2013.
- E. Rheinbay, M. M. Nielsen, F. Abascal, et al. Analyses of non-coding somatic drivers in 2,658 cancer whole genomes. *Nature*, 578(7793):102–111, Feb 2020.
- N. Riggi, L. Cironi, P. Provero, M.-L. Suvà, K. Kaloulis, C. Garcia-Echeverria, F. Hoffmann, A. Trumpp, and I. Stamenkovic. Development of Ewing’s sarcoma from primary bone marrow-derived mesenchymal progenitor cells. *Cancer Res*, 65(24):11459–11468, 2005.
- N. Riggi, L. Cironi, M.-L. Suvà, and I. Stamenkovic. Sarcomas: genetics, signalling, and cellular origins. Part 1: The fellowship of TET. *J Pathol*, 213(1):4–20, 2007.
- N. Riggi, M.-L. Suvà, D. Suvà, L. Cironi, P. Provero, S. Tercier, J.-M. Joseph, J.-C. Stehle, K. Baumer, V. Kindler, and I. Stamenkovic. EWS-FLI-1 expression triggers a Ewing’s sarcoma initiation program in primary human mesenchymal stem cells. *Cancer Res*, 68(7):2176–85, 2008.
- N. Riggi, M.-L. Suvà, C. De Vito, P. Provero, J.-C. Stehle, K. Baumer, L. Cironi, M. Janiszewska, T. Petricevic, D. Suvà, et al. EWS-FLI-1 modulates miRNA145 and SOX2 expression to initiate mesenchymal stem cell reprogramming toward Ewing sarcoma cancer stem cells. *Genes Dev*, 24(9):916–932, 2010.
- N. Riggi, B. Knoechel, S. M. Gillespie, E. Rheinbay, G. Boulay, M. L. Suvà, N. E. Rossetti, W. E. Boonseng, O. Oksuz, E. B. Cook, A. Formey, A. Patel, M. Gymrek, V. Thapar, V. Deshpande, D. T. Ting, F. J. Hornicek, G. P. Nielsen, I. Stamenkovic, M. J. Aryee, B. E. Bernstein, and M. N. Rivera. EWS-FLI1 utilizes divergent chromatin remodeling mechanisms to directly activate or repress enhancer elements in Ewing sarcoma. *Cancer Cell*, 26(5):668–681, 2014.
- S. L. Robbins, V. Kumar, and R. S. Cotran. *Robbins and Cotran pathologic basis of disease*. Saunders/Elsevier, 2010.
- G. Rodríguez-Hernández, J. Hauer, A. Martín-Lorenzo, D. Schäfer, C. Bartenhagen, I. García-Ramírez, F. Auer, I. Gonzalez-Herrero, L. Ruiz-Roca, M. Gombert, et al. Infection exposure promotes ETV6-RUNX1 precursor B-cell leukemia via impaired H3K4 demethylases. *Cancer Res*, 77(16):4365–4377, 2017.
- M. Roos, U. Pradère, R. P. Ngondo, A. Behera, S. Allegrini, G. Civenni, J. A. Zagalak, J.-R. Marchand, M. Menzi, H. Towbin, et al. A small-molecule inhibitor of Lin28. *ACS Chem Biol*, 11(10):2773–2781, 2016.
- R. Rosenthal, N. McGranahan, J. Herrero, and C. Swanton. Deciphering genetic intratumor heterogeneity and its impact on cancer evolution. *Annu Rev Cancer Biol*, 1:223–240, 2017.

- S. Runge, F. C. Nielsen, J. Nielsen, J. Lykke-Andersen, U. M. Wewer, and J. Christiansen. H19 RNA binds four molecules of insulin-like growth factor II mRNA-binding protein. *J Biol Chem*, 275(38): 29562–29569, 2000.
- N. E. Sanjana, O. Shalem, and F. Zhang. Improved vectors and genome-wide libraries for CRISPR screening. *Nat Methods*, 11(8):783, 2014.
- S. Sankar and S. L. Lessnick. Promiscuous partnerships in Ewing’s sarcoma. *Cancer Genet*, 204(7): 351–365, 2011.
- S. Savola, A. Klami, S. Myllykangas, C. Manara, K. Scotlandi, P. Picci, S. Knuutila, and J. Vakkila. High expression of complement component 5 (C5) at tumor site associates with superior survival in Ewing’s sarcoma family of tumour patients. *ISRN Oncol*, 2011, 2011.
- D. T. Scadden. Nice neighborhood: emerging concepts of the stem cell niche. *Cell*, 157(1):41–50, 2014.
- D. F. Schaeffer, D. R. Owen, H. J. Lim, A. K. Buczkowski, S. W. Chung, C. H. Scudamore, D. G. Huntsman, S. S. Ng, and D. A. Owen. Insulin-like growth factor 2 mRNA binding protein 3 (IGF2BP3) overexpression in pancreatic ductal adenocarcinoma correlates with poor survival. *BMC Cancer*, 10(1):59, 2010.
- A. M. Schmitt and H. Y. Chang. Long noncoding RNAs in cancer pathways. *Cancer Cell*, 29(4):452–463, 2016.
- T. Schneider, L.-H. Hung, M. Aziz, A. Wilmen, S. Thaum, J. Wagner, R. Janowski, S. Müller, S. Schreiner, P. Friedhoff, et al. Combinatorial recognition of clustered RNA elements by the multidomain RNA-binding protein IMP3. *Nat Commun*, 10(1):2266, 2019.
- K. Scotlandi and P. Picci. Targeting insulin-like growth factor 1 receptor in sarcomas. *Curr Opin Oncol*, 20(4):419–427, 2008.
- M. Selbach, B. Schwanhäusser, N. Thierfelder, Z. Fang, R. Khanin, and N. Rajewsky. Widespread changes in protein synthesis induced by microRNAs. *Nature*, 455:58–63, 2008.
- S. P. Selvanathan, G. T. Graham, H. V. Erkizan, U. Dirksen, T. G. Natarajan, A. Dakic, S. Yu, X. Liu, M. T. Paulsen, M. E. Ljungman, et al. Oncogenic fusion protein EWS-FLI1 is a network hub that regulates alternative splicing. *Proc Natl Acad Sci U S A*, 112(11):E1307–E1316, 2015.
- A. Seth and D. K. Watson. ETS transcription factors and their emerging roles in human cancer. *Eur J Cancer*, 41(16):2462–2478, 2005.
- O. Shalem, N. E. Sanjana, E. Hartenian, X. Shi, D. A. Scott, T. S. Mikkelsen, D. Heckl, B. L. Ebert, D. E. Root, J. G. Doench, et al. Genome-scale CRISPR-Cas9 knockout screening in human cells. *Science*, 343(6166):84–87, 2014.
- G. Shan, Y. Li, J. Zhang, W. Li, K. E. Szulwach, R. Duan, M. A. Faghihi, A. M. Khalil, L. Lu, Z. Paroo, et al. A small molecule enhances RNA interference and promotes microRNA processing. *Nat Biotechnol*, 26(8):933, 2008.
- J. R. Shapiro, W.-K. A. Yung, and W. R. Shapiro. Isolation, karyotype, and clonal growth of heterogeneous subpopulations of human malignant gliomas. *Cancer Res*, 41(6):2349–2359, 1981.
- S. V. Sharma, D. Y. Lee, B. Li, M. P. Quinlan, F. Takahashi, S. Maheswaran, U. McDermott, N. Azizian, L. Zou, M. A. Fischbach, et al. A chromatin-mediated reversible drug-tolerant state in cancer cell subpopulations. *Cell*, 141(1):69–80, 2010.
- S. K. Singh, I. D. Clarke, M. Terasaki, V. E. Bonn, C. Hawkins, J. Squire, and P. B. Dirks. Identification of a cancer stem cell in human brain tumors. *Cancer Res*, 63(18):5821–5828, 2003.
- S. K. Singh, C. Hawkins, I. D. Clarke, J. A. Squire, J. Bayani, T. Hide, R. M. Henkelman, M. D. Cusimano, and P. B. Dirks. Identification of human brain tumour initiating cells. *Nature*, 432(7015): 396, 2004.

- N. R. Smalheiser, H. Zhang, and Y. Dwivedi. Enoxacin elevates microRNA levels in rat frontal cortex and prevents learned helplessness. *Front Psychiatry*, 5:6, 2014.
- M. A. Smith, S. F. Altekruze, P. C. Adamson, G. H. Reaman, and N. L. Seibel. Declining childhood and adolescent cancer mortality. *Cancer Soc*, 120(16):2497–2506, 2014.
- M. J. Son, K. Woolard, D.-H. Nam, J. Lee, and H. A. Fine. SSEA-1 is an enrichment marker for tumor-initiating cells in human glioblastoma. *Cell Stem Cell*, 4(5):440–452, 2009.
- D. D. Spyropoulos, P. N. Pharr, K. R. Lavenburg, P. Jackers, T. S. Papas, M. Ogawa, and D. K. Watson. Hemorrhage, impaired hematopoiesis, and lethality in mouse embryos carrying a targeted disruption of the Fli1 transcription factor. *Mol Cell Biol*, 20(15):5643–5652, 2000.
- E. Steliarova-Foucher, M. Colombet, L. A. Ries, F. Moreno, A. Dolya, F. Bray, P. Hesselting, H. Y. Shin, C. A. Stiller, S. Bouzbid, et al. International incidence of childhood cancer, 2001–10: a population-based registry study. *Lancet Oncol*, 18(6):719–731, 2017.
- E. Stewart, S. M. Federico, X. Chen, A. A. Shelat, C. Bradley, B. Gordon, A. Karlstrom, N. R. Twarog, M. R. Clay, A. Bahrami, et al. Orthotopic patient-derived xenografts of paediatric solid tumours. *Nature*, 549(7670):96–100, 2017.
- S. H. Stricker, A. Feber, P. G. Engström, H. Carén, K. M. Kurian, Y. Takashima, C. Watts, M. Way, P. Dirks, P. Bertone, et al. Widespread resetting of DNA methylation in glioblastoma-initiating cells suppresses malignant cellular behavior in a lineage-dependent manner. *Genes Dev*, 27(6):654–669, 2013.
- B. Sundararaman, L. Zhan, S. M. Blue, R. Stanton, K. Elkins, S. Olson, X. Wei, E. L. Van Nostrand, G. A. Pratt, S. C. Huelga, et al. Resources for the comprehensive discovery of functional RNA elements. *Mol Cell*, 61(6):903–913, 2016.
- M.-L. Suvà, N. Riggi, J.-C. Stehle, K. Baumer, S. Tercier, J.-M. Joseph, D. Suvà, V. Clément, P. Provero, L. Cironi, et al. Identification of cancer stem cells in Ewing’s sarcoma. *Cancer Res*, 69(5):1776–1781, 2009.
- M. L. Suvà, E. Rheinbay, S. M. Gillespie, A. P. Patel, H. Wakimoto, S. D. Rabkin, N. Riggi, A. S. Chi, D. P. Cahill, B. V. Nahed, et al. Reconstructing and reprogramming the tumor-propagating potential of glioblastoma stem-like cells. *Cell*, 157(3):580–594, 2014.
- K. Takahashi and S. Yamanaka. Induction of pluripotent stem cells from mouse embryonic and adult fibroblast cultures by defined factors. *Cell*, 126(4):663–676, 2006.
- W. L. Tam and R. A. Weinberg. The epigenetics of epithelial-mesenchymal plasticity in cancer. *Nat Med*, 19(11):1438, 2013.
- A. Y. Tan and J. L. Manley. The TET family of proteins: functions and roles in disease. *J Mol Cell Biol*, 1(2):82–92, 2009.
- F. E. Tan, S. Sathe, E. C. Wheeler, J. K. Nussbacher, S. Peter, and G. W. Yeo. A transcriptome-wide translational program defined by LIN28B expression level. *Mol Cell*, 73(2):304–313, 2019.
- K. Tanaka, T. Iwakuma, K. Harimaya, H. Sato, and Y. Iwamoto. EWS-Fli1 antisense oligodeoxynucleotide inhibits proliferation of human Ewing’s sarcoma and primitive neuroectodermal tumor cells. *J Clin Invest*, 99(2):239–247, 1997.
- P. R. Tata, H. Mou, A. Pardo-Saganta, R. Zhao, M. Prabhu, B. M. Law, V. Vinarsky, J. L. Cho, S. Breton, A. Sahay, et al. Dedifferentiation of committed epithelial cells into stem cells in vivo. *Nature*, 503(7475):218–223, 2013.
- B. S. Taylor, J. Barretina, R. G. Maki, C. R. Antonescu, S. Singer, and M. Ladanyi. Advances in sarcoma genomics and new therapeutic targets. *Nat Rev Cancer*, 11(8):541, 2011.
- J. P. Thakkar, T. A. Dolecek, C. Horbinski, Q. T. Ostrom, D. D. Lightner, J. S. Barnholtz-Sloan, and J. L. Villano. Epidemiologic and molecular prognostic review of glioblastoma. *Cancer Epidemiol Biomarkers Prev*, 23(10):1985–96, 2014.

- The Cancer Genome Atlas Research Network et al. Comprehensive genomic characterization defines human glioblastoma genes and core pathways. *Nature*, 455(7216):1061, 2008.
- J. P. Thiery. Epithelial-mesenchymal transitions in tumour progression. *Nat Rev Cancer*, 2(6):442–54, 2002.
- M. Thomas, J. Lieberman, and A. Lal. Desperately seeking microRNA targets. *Nat Struct Mol Biol*, 17(10):1169, 2010.
- A. D. Thompson, M. A. Teitell, A. Arvand, and C. T. Denny. Divergent Ewing’s sarcoma EWS/ETS fusions confer a common tumorigenic phenotype on NIH3T3 cells. *Oncogene*, 18(40):5506, 1999.
- J. M. Thomson, M. Newman, J. S. Parker, E. M. Morin-Kensicki, T. Wright, and S. M. Hammond. Extensive post-transcriptional regulation of microRNAs and its implications for cancer. *Genes Dev*, 20(16):2202–2207, 2006.
- J. E. Thornton and R. I. Gregory. How does Lin28 let-7 control development and disease? *Trends Cell Biol*, 22(9):474–482, 2012.
- F. Tirode, K. Laud-Duval, A. Prieur, B. Delorme, P. Charbord, and O. Delattre. Mesenchymal stem cell features of Ewing tumors. *Cancer cell*, 11(5):421–429, 2007.
- J. Trendel, T. Schwarzl, R. Horos, A. Prakash, A. Bateman, M. W. Hentze, and J. Krijgsveld. The human RNA-binding proteome and its dynamics during translational arrest. *Cell*, 176(1-2):391–403, 2019.
- A. H. Truong and Y. Ben-David. The role of Fli-1 in normal cell function and malignant transformation. *Oncogene*, 19(55):6482, 2000.
- A. Tsherniak, F. Vazquez, P. G. Montgomery, B. A. Weir, G. Kryukov, G. S. Cowley, S. Gill, W. F. Harrington, S. Pantel, J. M. Krill-Burger, R. M. Meyers, L. Ali, A. Goodale, Y. Lee, G. Jiang, J. Hsiao, W. F. J. Gerath, S. Howell, E. Merkel, M. Ghandi, L. A. Garraway, D. E. Root, T. R. Golub, J. S. Boehm, and W. C. Hahn. Defining a cancer dependency map. *Cell*, 170(3):564–576.e16, 2017.
- A. Urbach, A. Yermalovich, J. Zhang, C. S. Spina, H. Zhu, A. R. Perez-Atayde, R. Shukrun, J. Charlton, N. Sebire, W. Mifsud, et al. Lin28 sustains early renal progenitors and induces Wilms tumor. *Genes Dev*, 28(9):971–982, 2014.
- A. Üren and J. A. Toretsky. Ewing’s sarcoma oncoprotein EWS-FLI1: the perfect target without a therapeutic agent. *Future Oncol*, 1(4):521–528, 2005. PMID: 16556028.
- A. Üren, O. Tcherkasskaya, and J. A. Toretsky. Recombinant EWS-FLI1 oncoprotein activates transcription. *Biochemistry*, 43(42):13579–13589, 2004.
- S. Valastyan and R. A. Weinberg. Tumor metastasis: molecular insights and evolving paradigms. *Cell*, 147(2):275–292, 2011.
- R. J. Vanner, M. Remke, M. Gallo, H. J. Selvadurai, F. Coutinho, L. Lee, M. Kushida, R. Head, S. Morrissey, X. Zhu, et al. Quiescent Sox2+ cells drive hierarchical growth and relapse in sonic hedgehog subgroup medulloblastoma. *Cancer Cell*, 26(1):33–47, 2014.
- A. Venkatraman, X. C. He, J. L. Thorvaldsen, R. Sugimura, J. M. Perry, F. Tao, M. Zhao, M. K. Christenson, R. Sanchez, Y. Y. Jaclyn, et al. Maternal imprinting at the H19-Igf2 locus maintains adult haematopoietic stem cell quiescence. *Nature*, 500(7462):345, 2013.
- C. Vennin, N. Spruyt, F. Dahmani, S. Julien, F. Bertucci, P. Finetti, T. Chassat, R. P. Bourette, X. Le Bourhis, and E. Adriaenssens. H19 non coding RNA-derived miR-675 enhances tumorigenesis and metastasis of breast cancer cells by downregulating c-Cbl and Cbl-b. *Oncotarget*, 6(30):29209, 2015.
- A. Ventura and T. Jacks. MicroRNAs and cancer: short RNAs go a long way. *Cell*, 136(4):586–591, 2009.

- R. G. Verhaak, K. A. Hoadley, E. Purdom, V. Wang, Y. Qi, M. D. Wilkerson, C. R. Miller, L. Ding, T. Golub, J. P. Mesirov, et al. Integrated genomic analysis identifies clinically relevant subtypes of glioblastoma characterized by abnormalities in PDGFRA, IDH1, EGFR, and NF1. *Cancer Cell*, 17(1):98–110, 2010.
- J. E. Visvader and G. J. Lindeman. Cancer stem cells in solid tumours: accumulating evidence and unresolved questions. *Nat Rev Cancer*, 8:755–768, 2008.
- S. R. Viswanathan and G. Q. Daley. Lin28: A microRNA regulator with a macro role. *Cell*, 140(4):445–9, 2010.
- S. R. Viswanathan, G. Q. Daley, and R. I. Gregory. Selective blockade of microRNA processing by Lin28. *Science*, 320(5872):97–100, 2008.
- S. R. Viswanathan, J. T. Powers, W. Einhorn, Y. Hoshida, T. L. Ng, S. Toffanin, M. O’Sullivan, J. Lu, L. A. Phillips, V. L. Lockhart, S. P. Shah, P. S. Tanwar, C. H. Mermel, R. Beroukhi, M. Azam, J. Teixeira, M. Meyerson, T. P. Hughes, J. M. Llovet, J. Radich, C. G. Mullighan, T. R. Golub, P. H. Sorensen, and G. Q. Daley. Lin28 promotes transformation and is associated with advanced human malignancies. *Nat Genet*, 41(7):843–8, 2009.
- K. T. Vo, D. W. Parsons, and N. L. Seibel. Precision medicine in pediatric oncology. *Surg Oncol Clin N Am*, 29(1):63–72, 2020.
- B. Vogelstein, N. Papadopoulos, V. E. Velculescu, S. Zhou, L. A. Diaz, and K. W. Kinzler. Cancer genome landscapes. *Science*, 339(6127):1546–1558, 2013.
- C. von Levetzow, X. Jiang, Y. Gwyne, G. von Levetzow, L. Hung, A. Cooper, J. H.-R. Hsu, and E. R. Lawlor. Modeling initiation of Ewing sarcoma in human neural crest cells. *PLoS One*, 6(4):e19305, 2011.
- H. Wakimoto, S. Kesari, C. J. Farrell, W. T. Curry, C. Zaupa, M. Aghi, T. Kuroda, A. Stemmer-Rachamimov, K. Shah, T.-C. Liu, et al. Human glioblastoma-derived cancer stem cells: establishment of invasive glioma models and treatment with oncolytic herpes simplex virus vectors. *Cancer Res*, 69(8):3472–3481, 2009.
- H. Wakimoto, G. Mohapatra, R. Kanai, W. T. Curry, S. Yip, M. Nitta, A. P. Patel, Z. R. Barnard, A. O. Stemmer-Rachamimov, D. N. Louis, et al. Maintenance of primary tumor phenotype and genotype in glioblastoma stem cells. *Neuro-Oncology*, 14(2):132–144, 2011.
- J. Wang, E. Cazzato, E. Ladewig, V. Frattini, D. I. Rosenbloom, S. Zairis, F. Abate, Z. Liu, O. Elliott, Y.-J. Shin, et al. Clonal evolution of glioblastoma under therapy. *Nat Genet*, 48(7):768, 2016.
- K. C. Wang and H. Y. Chang. Molecular mechanisms of long noncoding RNAs. *Mol Cell*, 43(6):904–14, 2011.
- S. Wang, B. Chim, Y. Su, P. Khil, M. Wong, X. Wang, A. Foroushani, P. T. Smith, X. Liu, R. Li, et al. Enhancement of LIN28B-induced hematopoietic reprogramming by IGF2BP3. *Genes Dev*, 33(15-16):1048–1068, 2019.
- O. Wapinski and H. Y. Chang. Long noncoding RNAs and human disease. *Trends Cell Biol*, 21(6):354–361, 2011.
- E. Ward, C. DeSantis, A. Robbins, B. Kohler, and A. Jemal. Childhood and adolescent cancer statistics, 2014. *CA-Cancer J Clin*, 64(2):83–103, 2014.
- G.-H. Wei, G. Badis, M. F. Berger, T. Kivioja, K. Palin, M. Enge, M. Bonke, A. Jolma, M. Varjosalo, A. R. Gehrke, et al. Genome-wide analysis of ETS-family DNA-binding in vitro and in vivo. *EMBO J*, 29(13):2147–2160, 2010.
- D. Weidensdorfer, N. Stöhr, A. Baude, M. Lederer, M. Köhn, A. Schierhorn, S. Buchmeier, E. Wahle, and S. Hüttelmaier. Control of c-myc mRNA stability by IGF2BP1-associated cytoplasmic RNPs. *RNA*, 15(1):104–115, 2009.

- I. B. Weinstein. Addiction to oncogenes—the Achilles heel of cancer. *Science*, 297(5578):63–64, 2002.
- M. L. Wilbert, S. C. Huelga, K. Kapeli, T. J. Stark, T. Y. Liang, S. X. Chen, B. Y. Yan, J. L. Nathanson, K. R. Hutt, M. T. Lovci, et al. LIN28 binds messenger RNAs at GGAGA motifs and regulates splicing factor abundance. *Mol Cell*, 48(2):195–206, 2012.
- J. Winter, S. Jung, S. Keller, R. I. Gregory, and S. Diederichs. Many roads to maturity: microRNA biogenesis pathways and their regulation. *Nat Cell Biol*, 11:228–234, 2009.
- J. Worch, A. Ranft, S. G. DuBois, M. Paulussen, H. Juergens, and U. Dirksen. Age dependency of primary tumor sites and metastases in patients with Ewing sarcoma. *Pediatr Blood Cancer*, 65(9):e27251, 2018.
- C. Wu, Q. Wei, V. Utomo, P. Nadesan, H. Whetstone, R. Kandel, J. S. Wunder, and B. A. Alman. Side population cells isolated from mesenchymal neoplasms have tumor initiating potential. *Cancer Res*, 67(17):8216–8222, 2007.
- B. Xu, K. Zhang, and Y. Huang. Lin28 modulates cell growth and associates with a subset of cell cycle regulator mRNAs in mouse embryonic stem cells. *RNA*, 15(3):357–361, 2009a.
- N. Xu, T. Papagiannakopoulos, G. Pan, J. A. Thomson, and K. S. Kosik. MicroRNA-145 regulates OCT4, SOX2, and KLF4 and represses pluripotency in human embryonic stem cells. *Cell*, 137(4):647–658, 2009b.
- P. Xu, S. Y. Vernooy, M. Guo, and B. A. Hay. The Drosophila microRNA Mir-14 suppresses cell death and is required for normal fat metabolism. *Curr Biol*, 13(9):790–795, 2003.
- H. Yan, D. W. Parsons, G. Jin, R. McLendon, B. A. Rasheed, W. Yuan, I. Kos, I. Batinic-Haberle, S. Jones, G. J. Riggins, et al. IDH1 and IDH2 mutations in gliomas. *New Engl J Med*, 360(8):765–773, 2009.
- X. Yan, Z. Hu, Y. Feng, X. Hu, J. Yuan, S. D. Zhao, Y. Zhang, L. Yang, W. Shan, Q. He, et al. Comprehensive genomic characterization of long non-coding RNAs across human cancers. *Cancer Cell*, 28(4):529–540, 2015.
- C. H. Yang, J. Yue, S. R. Pfeffer, M. Fan, E. Paulus, A. Hosni-Ahmed, M. Sims, S. Qayyum, A. M. Davidoff, C. R. Handorf, et al. MicroRNA-21 promotes glioblastoma tumorigenesis by down-regulating insulin-like growth factor-binding protein-3 (IGFBP3). *J Biol Chem*, 289(36):25079–25087, 2014.
- F. Yang, J. Bi, X. Xue, L. Zheng, K. Zhi, J. Hua, and G. Fang. Up-regulated long non-coding RNA H19 contributes to proliferation of gastric cancer cells. *FEBS J*, 279(17):3159–3165, 2012.
- J. Yang and R. A. Weinberg. Epithelial-mesenchymal transition: at the crossroads of development and tumor metastasis. *Dev Cell*, 14(6):818–29, 2008.
- J. Yu, M. A. Vodyanik, K. Smuga-Otto, J. Antosiewicz-Bourget, J. L. Frane, S. Tian, J. Nie, G. A. Jonsdottir, V. Ruotti, R. Stewart, et al. Induced pluripotent stem cell lines derived from human somatic cells. *Science*, 318(5858):1917–1920, 2007.
- J. Yuan, C. K. Nguyen, X. Liu, C. Kanellopoulou, and S. A. Muljo. Lin28b reprograms adult bone marrow hematopoietic progenitors to mediate fetal-like lymphopoiesis. *Science*, 335(6073):1195–1200, 2012.
- J. Zhang, S. Ratanasirintraoort, S. Chandrasekaran, Z. Wu, S. B. Ficarro, C. Yu, C. A. Ross, D. Cacciarelli, Q. Xia, M. Seligson, et al. LIN28 regulates stem cell metabolism and conversion to primed pluripotency. *Cell Stem Cell*, 19(1):66–80, 2016a.
- T. Zhang, Y. Wang, F. Zeng, H. Cao, H. Zhou, and Y. Wang. LncRNA H19 is overexpressed in glioma tissue, is negatively associated with patient survival, and promotes tumor growth through its derivative miR-675. *Eur Rev Med Pharmacol Sci*, 20(23):4891–4897, 2016b.
- X. Zhang, K. Kiang, G. Zhang, and G. Leung. Long non-coding RNAs dysregulation and function in glioblastoma stem cells. *Noncoding RNA*, 1(1):69–86, 2015.

- G. X. Y. Zheng, B. T. Do, D. E. Webster, P. A. Khavari, and H. Y. Chang. Dicer-microRNA-Myc circuit promotes transcription of hundreds of long noncoding RNAs. *Nat Struct Mol Biol*, 21(7):585–90, 2014.
- H. Zhu, N. Shyh-Chang, A. V. Segrè, G. Shinoda, S. P. Shah, W. S. Einhorn, A. Takeuchi, J. M. Engreitz, J. P. Hagan, M. G. Kharas, et al. The Lin28/let-7 axis regulates glucose metabolism. *Cell*, 147(1): 81–94, 2011.
- J. Zucman-Rossi, P. Legoix, J.-M. Victor, B. Lopez, and G. Thomas. Chromosome translocation based on illegitimate recombination in human tumors. *Proc Natl Acad Sci U S A*, 95(20):11786–11791, 1998.